EXPLOITING THE ORDER OF MEMBRANE-ASSOCIATING MOLECULES: NMR STUDIES OF ARF1 AND $PIP_2$ AT A MODEL MEMBRANE SURFACE

by

ANITA I. KISHORE

(Under the Direction of James H. Prestegard)

ABSTRACT

Novel nuclear magnetic resonance (NMR) experiments and computational methods have been developed to characterize membrane-associated molecules. The methodology has been applied to the membrane-associating protein Adenosine diphosphate Ribosylation Factor 1 (ARF1) and its ligands when they are organized at the membrane surface. ARF1 is a 21 kDa GDP-GTP switch protein that interacts reversibly with a membrane through the GTP-controlled exposure of its N-myristoyl chain and N-terminal amphipathic helix. Current structural methods have failed to produce ARF1's structure and orientation when associated with the membrane, and new methodology is urgently needed to better understand ARF1's role in vesicle trafficking.

NMR is well suited to the study of membrane-associating systems. By taking advantage of the magnetic properties of liquid crystalline model membranes as both bilayered membrane mimetics and orienting media for molecules dissolved within them, non-myristoylated (non-myr) ARF1 and ARF1's ligands have been uniformly ordered, generating complex NMR spectra rich in structural information. To reduce the complexity, variable angle sample spinning NMR was used to extract phosphorus chemical shift anisotropy offsets from membrane-anchored phosphatidylinositol bisphosphate ($PIP_2$), a signaling lipid believed to promote membrane association of ARF1, yielding the headgroup orientation of $PIP_2$. Nitrogen-proton residual dipolar couplings were also used to ascertain the location and extent of non-myrARF1's interaction with $PIP_2$ in a membrane environment. In anticipation of strong membrane association between $PIP_2$ and ARF1, a novel approach based on the observation of carbon chemical shift anisotropy offsets for ARF1-bound nucleotide cofactors (GDP) was also developed.

My work suggests that $PIP_2$ orients with its inositol headgroup bent toward the membrane and charged phosphate groups exposed, possibly mediating ARF1's membrane-associating ability. When combined in a model membrane with $PIP_2$, non-myrARF1 did show extensive interaction with the lipid, but $PIP_2$ appeared to be extracted

from the membrane, possibly by secluding $PIP_2$'s acyl chains within the hydrophobic pocket normally occupied by ARF1's own myristoyl chain. This work suggests the importance of the myristoyl chain in not only modulating membrane interactions but in regulating more specific interactions with lipid components. The work brings into question many previous conclusions based on studies of the more easily obtained non-myrARF1 and N-terminal truncated forms of ARF1.

INDEX WORDS: Nuclear Magnetic Resonance (NMR), ADP-Ribosylation Factor 1 (ARF1), Variable Angle Sample Spinning (VASS), Chemical Shift Anisotropy (CSA), Residual Dipolar Couplings (RDCs), Phosphatidylinositol bisphosphate ($PI(4,5)P_2$, $PIP_2$)

# EXPLOITING THE ORDER OF MEMBRANE-ASSOCIATING MOLECULES: NMR STUDIES OF ARF1 AND $PIP_2$ AT A MODEL MEMBRANE SURFACE

by

ANITA I. KISHORE

B.S., Yale University, 1999

M.Sc., University of Melbourne, Australia, 2000

A Dissertation Submitted to the Graduate Faculty of The University of Georgia in Partial Fulfillment of the Requirements for the Degree

DOCTOR OF PHILOSOPHY

ATHENS, GEORGIA

2005

EXPLOITING THE ORDER OF MEMBRANE-ASSOCIATING MOLECULES:

NMR STUDIES OF ARF1 AND $PIP_2$ AT A MODEL MEMBRANE SURFACE

by

ANITA I. KISHORE

Major Professor: James H. Prestegard

Committee: Marly K. Eidsness
Jeffrey L. Urbauer

Electronic Version Approved:

Maureen Grasso
Dean of the Graduate School
The University of Georgia
December 2005

# DEDICATION

This dissertation is dedicated to my grandparents and their parents before them, all of whom recognized the importance of education

ACKNOWLEDGEMENTS

This work was supported by a Presidential Fellowship from the University of Georgia. I thank my research advisor, Prof. Jim Prestegard, for his unfailing patience, optimism, and intelligence. He has provided me unique opportunities to write, teach, and travel combined with an ideal environment to do science. I also thank him for his liberal attitude toward education and decision-making. I thank my advisory committee members Prof. Marly Eidsness and Prof. Jeff Urbauer for their guidance, especially Prof. Eidsness for being around from the beginning. I also thank: Prof. Rick Kahn, Juan Carlos Amor, Ron Seidel, and Brett Isreal for providing ARF1 protein and insightful biochemical discussions; my Prestegard labmates, both past and present, for advice, assistance, and friendship; Prof. Pascale Legault and Lisa Jenkins for HPLC training; my merry band of editors Sonal Bansal, Thomas Weldeghiorghis, and John Glushka; Jason Sterling and Greg Wylie for teaching me biochemistry; employees of Varian NMR (Daina Avizonis, Tom Barbara, Sean Burns, Judit Losonczi, Knut Mehr, Dave Rice, and Joe Vance) for assistance with the nanoprobe; John Glushka for keeping the NMR instruments in top shape, regardless of the hour, and for countless conversations about everything and nothing; Denny Warrenfeltz for fixing everything I broke or nearly broke; the administrative staff at the CCRC, especially Beverly Chalk; Quincy Teng for assistance with the chemistry NMR instruments; members of the Boons research group, especially Andre Venot, for their flexibility in scheduling NMR time.

I thank my parents and my sister Drs. Roy, Sheela, and Suchita Kishore for their constant support even in the face of increasing doubt; Prof. Cathy Bougault for her

peerless friendship, scientific advice, and generosity; Sarah Wittkopp for her exquisite sense of humor; Anil Mehta for invaluable scientific discussions and hospitality; my faithful lunchtime partners: Cathy, Sarah, Fang, and Olivia; Prof. Bob Scott, Prof. George Majetich, and especially Prof. Tim Dore for advice and support in my less than academic endeavors; Prof. Frances Separovic for teaching me the things about science that no one ever teaches you; Prof. Gary Brudvig and former Brudvig lab members for teaching me the basics of research; K.V. Lakshmi for encouragement; and my terrific group of friends: Danny Sims, Le'on Willis, Robby Luckett, Brooks & Liz Mendell, Kate Briggman, Iris Tropp, Cari Gervin, Oksana and Tim Sydor for their occasionally successful efforts in getting me out of the lab.

TABLE OF CONTENTS

Page

LIST OF TABLES

Page

LIST OF FIGURES

Page

# CHAPTER 1

# INTRODUCTION AND LITERATURE REVIEW OF NUCLEAR MAGNETIC RESONANCE TECHNIQUES FOR MEMBRANE-ASSOCIATED BIOMOLECULES

## 1.1 STRUCTURAL BIOLOGY OF MEMBRANE PROTEINS

Genomic sequencing efforts have revealed that nearly 30% of all eukaryotic proteins are membrane proteins (1), but most structural efforts to date have focused on characterizing soluble biomolecules. Fewer than 1% of the proteins in the protein data bank (PDB) are membrane proteins (2,3). This seems like a staggering statistic, but it is actually an underestimate of the problem when one considers that it does not count the many proteins that associate with membranes through various forms of lipid anchors (4,5). It is this latter class, membrane-associating molecules, that I target in this thesis with new methods for structural characterization. Biochemical experiments can offer insight into functionality of membrane and membrane-associating proteins, but they cannot provide the details, such as where a protein contacts the membrane surface or how a protein orients relative to the membrane surface, available from a structural approach.

In this dissertation, I investigate the structure and orientation of the membrane-associating protein ARF1 and its ligands through novel nuclear magnetic resonance (NMR) experimental and computational methods developed for characterizing membrane-associating molecules. My specific target is Adenosine diphosphate (ADP) Ribosylation Factor 1 (ARF1), a ubiquitous, eukaryotic 21 kDa, membrane-associating GDP/GTP switch protein that cycles between a cytosolic GDP-bound form and a membrane-associated GTP-bound form during the formation of vesicles that move between the Golgi and the Endoplasmic Reticulum (ER). The exchange of GDP for GTP is believed to activate an N-terminal myristoyl switch (14 carbon fatty acid chain) that enables membrane association, but the sequence of events that controls the exposure of the myristoyl chain is not known. Consequently, details of vesicle formation,

transportation, and docking remain poorly understood. This kind of information is crucial to piecing together a detailed mechanism of membrane-associated, myristoylated (myr) ARF1's involvement in vesicle formation. In this dissertation I have developed NMR experimental and computational methods to address the lack of robust techniques for characterizing membrane-associating molecules, including ARF1 and ARF1 ligands, as they exist in the membrane.

## 1.2 LIMITED TOOLS FOR STRUCTURAL ANALYSIS

### 1.2.1 X-RAY CRYSTALLOGRAPHY: A TOOL FOR SOLUBLE BIOMOLECULES

The bulk of structures deposited in the Protein Data Bank and the BioMagRes Bank to date are of soluble biomolecules. In contrast to the small percentage of membrane protein structures available so far (2,3), 60-70% of pharmaceutical drug targets are membrane proteins (6). (Figure 1.1).

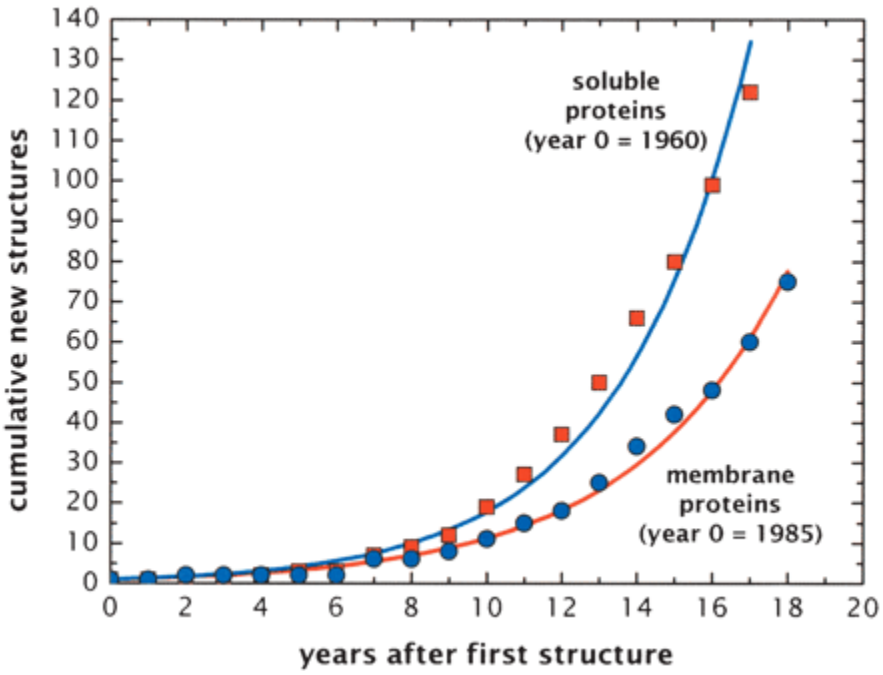


Figure 1.1. Membrane protein structures are few but are increasing at nearly the same rate as soluble protein structures. (Figure used with permission from (3).)

Table 1.1. Protein Data Bank (PDB) Contents as of May 17, 2005 (2)

| | Molecule | | | | |
|---|---|---|---|---|---|
| Experimental Technique | Proteins, Peptides, Viruses | Protein/Nucleic Acid Complexes | Nucleic Acids | Carbohydrates | Total |
| X-Ray + Other (% Total) | 24426 (87) | 1170 (91) | 806 (55) | 11 (85) | 26413 (85) |
| NMR (% Total) | 3782 (13) | 114 (9) | 652 (45) | 2 (15) | 4550 (15) |
| Total | 28208 | 1284 | 1458 | 13 | 30963 |

When available, atomic structural details of soluble biomolecules are most commonly provided by X-ray crystallography (Table 1.1), and soluble mutants of ARF1 are no exception. X-ray crystallography has generated several structures of soluble ARF1 that suggest possible modes of action. The crystal structures of GDP-ARF1 lacking a myristoyl chain (non-myr) and a GTP-loaded ARF1 mutant lacking both the

first 17 amino acid residues (d17) and myristoyl chain have been determined (7,8), and these have been used to suggest a model for the action of the nucleotide-linked conformational switch (Figure 1.2a,b).

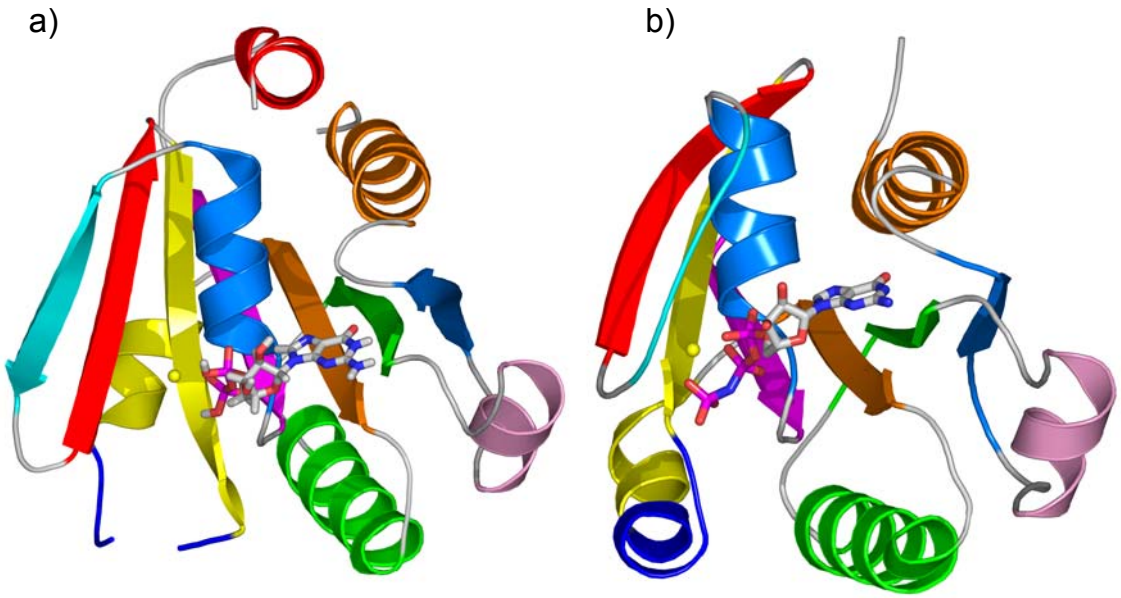


Figure 1.2. X-ray crystal structures show distinct conformational differences between a) wild type-non-myr-ARF1-GDP and b) d17GTP-ARF1.

However, there are many cases in which X-ray crystallography can not provide structures. Some systems - for example, membrane-associating systems such as myr-ARF1 in a membrane, large proteins, membrane proteins, protein-protein or protein-nucleic acid complexes, and even nucleic acids - remain intractable to crystallization due to their large size, surrounding molecules (*i.e.* lipids), or inherent flexibility. The bottleneck in membrane protein crystallography is in growing large, diffraction quality crystals, particularly in the presence of solubilizing lipids. This obstacle to characterization applies as well to many proteins that associate with a lipid membrane, including the myristoylated, GTP-loaded form of ARF1 that is believed to localize to

Golgi trafficking vesicles (more to be described below). This kind of protein is not a true membrane protein - it is a surface-associated protein – but the difficulties associated with it are much the same. In fact, there has been no success to date of crystallizing myr-ARF1 in the presence of a membrane. Missing are details about the orientation of the N-terminal helix and myristoyl chain relative to the rest of the protein.

### 1.2.2 NMR: A TOOL UNIQUELY SUITED FOR MEMBRANE-ASSOCIATED MOLECULES

It is in cases such as myr-ARF1 that NMR can be particularly advantageous. NMR does not require high quality crystals; and provided biomolecules can be produced in high yield, it can be applied to a broad range of systems that have resisted crystallization. For example, recent NMR data on a GDP-loaded, truncated form of ARF1, complementary to the GTP-loaded, truncated form, has brought into question details of the suggested nucleotide-induced switch mechanism and has underscored the possible importance of characterizing full length, myr-ARF1 in a more native environment (9). NMR results from soluble truncated ARF1 confirmed that while the GDP and GTP forms of d17 ARF1 have different conformations, structural differences exist between full length GDP and d17 GDP ARF1 as well, challenging previous assumptions that truncation of N-terminal residues has no effect on ARF1 structure (9).

Past attempts to determine structures of membrane proteins by solution NMR have primarily involved proteins dissolved in micelles, from the first structure of 40 amino acid residues (10) to proteins of nearly 180 residues with aggregate sizes of 50-60 kDa (11-14). These rely chiefly on nuclear Overhauser enhancement (NOE) distance restraints, but the steep distance dependence of the NOE, proportional to $(1/r^6)$ where r is

the internuclear distance, makes it difficult to obtain long-range distance information, something that is crucial for defining extended trans-membrane structures. These studies represent important achievements, but the long correlation times of large, slowly tumbling micelle-bound proteins result in broad signals of low intensity that limit application to smaller proteins. Due to these fundamental limitations of sensitivity, NMR has actually produced very few structures beyond the 25 kDa molecular weight. Nevertheless, there is reason to be optimistic. Over the past 25 years, combined improvements in theoretical understanding, isotopic labeling, probe technology, and magnetic field strength have increased the sensitivity of NMR more than 10,000-fold as shown in Table 1.2. One example of an important NMR development that resulted in breaking the traditional size barrier of solution NMR providing at least resonance assignment information on proteins as large as 900 kDa (15) is Transverse Relaxation Optimized SpectroscopY (TROSY). Though only 5% of the 95 total membrane protein structures deposited into the PDB since 1985 (3) have been derived from NMR, all of those structures have appeared in the last four years. The potential for NMR's future impact in structure determination of membrane proteins is high.

Table 1.2. Sensitivity Enhancement in solution NMR

| Technique | Factor Enhancement |
|---|---|
| Fourier Transform (16) | 10-100 |
| HSQC indirect detection (17-19) | ~30 |
| Magnetic field strength (200-900 MHz) | 9 |
| Cryogenically cooled probes(20) | 2-4 |
| TROSY (21) | 2-5 |
| Total enhancement ($\varepsilon_{TOT}$) | $1.1x10^4$ |

### 1.2.3 SOLID-STATE NMR POSES ADVANTAGES FOR MEMBRANE PROTEIN STRUCTURE DETERMINATION

***Magic angle spinning.*** Solution NMR, however, still faces fundamental limitations such as decreased resolution as molecular size increases; and therefore, confinement to micelle-like models for membrane environment in order to keep particle size under control. Solid-state NMR (SSNMR) offers a principal advantage over solution NMR in that it does not depend on fast molecular tumbling to narrow lines. Except for complexities associated with increasing numbers of resonances, it does not have a size limitation, and extended lipid bilayer assemblies can be used to mimic membrane environments. The two main SSNMR techniques employed in biological systems are magic angle spinning (MAS) and uniform orientation of static samples (Figure 1.3). MAS utilizes spinning at a fixed angle relative to the magnetic field and high power proton decoupling to reduce spectral linewidths to solution-like resolution. Sequential correlation of amino acid residues and distance and torsion angle restraints are available, similar to information obtained through solution NMR experiments, but these have not yet proved as robust as the solution NMR experiments. In the past five years, SSNMR has made impressive strides toward structure determination in the areas of sample preparation, data acquisition, and computational performance (22), but so far only small proteins have been studied because of spectral complexity. Some examples include the alpha spectrin Src-homology 3 (SH3) domain (23) and an amyloid peptide fragment (24). One major disadvantage of MAS, analogous to one of solution NMR, is that all orientational information is lost. Also, SSNMR experiments are typically performed in a

frozen aqueous environment, not the fluid bilayer-like environment believed to be important for correct folding.

***Uniformly oriented samples.*** Samples uniformly oriented in phospholipid bilayers provide a more native environment that can be used to retrieve the orientational information sacrificed in MAS. Hydrophobic peptides are inserted into uniaxially ordered (either mechanically or magnetically) phospholipid membranes. Orientation is determined by relating the anisotropic dipolar coupling or chemical shielding anisotropy tensor of the molecular group of interest to the membrane bilayer normal. Newly developed NMR experiments of oriented samples have resulted in structures of isotopically labeled peptides and proteins (25-29) such as channel lining segments of membrane receptors (30) and HIV peptides (31-34).

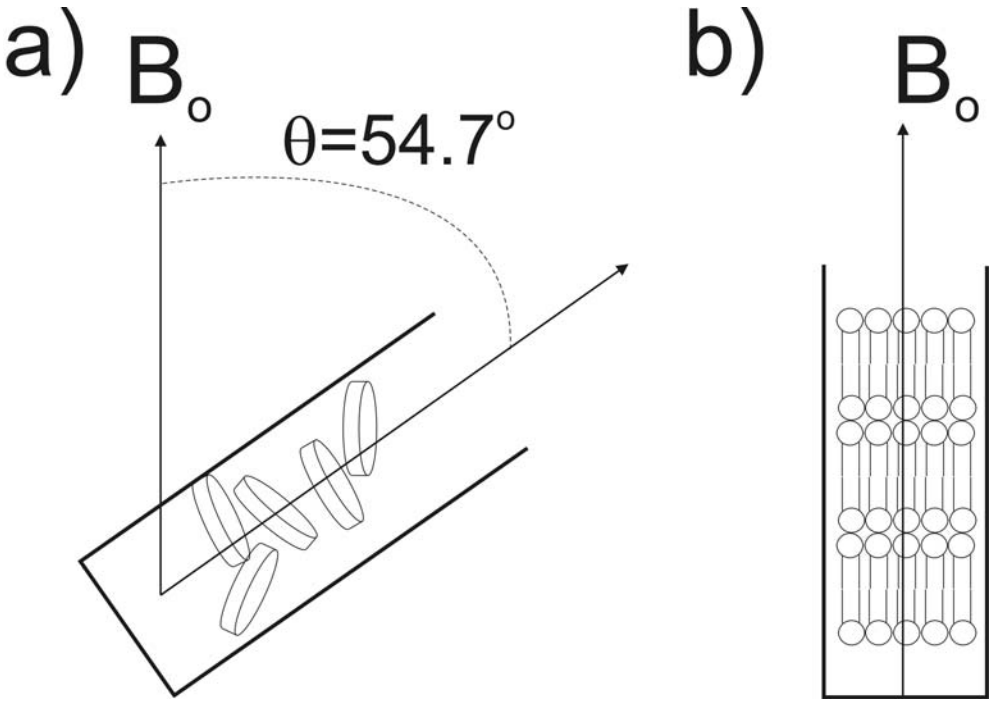


Figure 1.3. The two main techniques of membrane protein structure determination by solid-state NMR (SSNMR) are a) magic angle spinning and b) static, uniform sample orientation. Figure adapted from (31).

## 1.3 EXPLOITING ORDER USING LIQUID CRYSTALS AND NMR

### 1.3.1 COMBINING THE BEST OF SOLIDS AND SOLUTION NMR: ORIENTED LIQUID CRYSTALS

There is a middle ground between solution and solids NMR that may capitalize on some of the best aspects of both, namely the high resolution assignment methods of solution NMR and the bilayer-like environment and orientational data of solids NMR. Nematic (from Greek word for thread) liquid crystals offer long-range orientational information combined with high resolution. A liquid crystal is a unique molecular array that is intermediate between an isotropic liquid and a crystalline lattice. Nematic liquid crystals display cooperative long-range ordering in one dimension, such that their long axes are parallel to each other, but they lack positional ordering in all three dimensions (Figure 1.4a). Saupe and Englert first introduced the use of liquid crystals in NMR in 1963 (35). A molecule oriented in a liquid crystal displays a complex NMR spectrum because the molecule no longer samples all orientations isotropically, and interactions normally averaged to zero introduce additional shifts and splittings of resonances. In their initial application to NMR, the liquid crystals used exhibited strong ordering with the resulting anisotropy greatly complicating spectra.

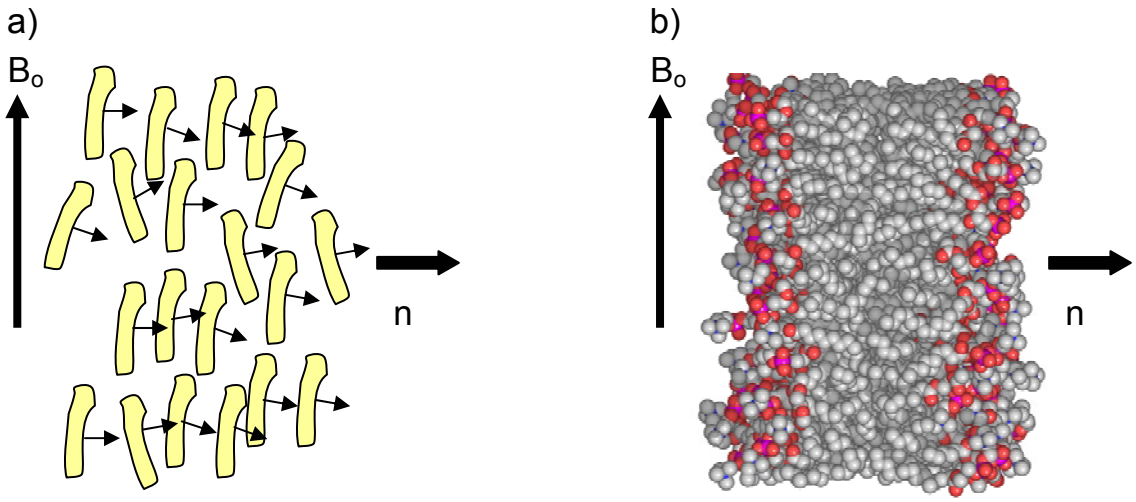


Figure 1.4. Nematic liquid crystals (a) and phospholipid bilayers (b) display similar properties in a magnetic field, $B_o$.

The properties of some model phospholipid membranes and even non-phospholipid bilayered membranes in a magnetic field can make them behave as nematic liquid crystals (Figure 1.4). This recognition fueled numerous NMR studies from 1960 to 1990 and led to advances in the understanding of molecular order and orientation parameters both of membranes (36,37) and of molecules dissolved within them (38-41). A fundamental property of membranes is their unique ability to organize molecules relative to a membrane surface. This is a useful step toward the uniform ordering of ARF1 and its associated ligands at the membrane surface. ARF1 and its ligands, when ordered in a magnetic field by a liquid crystalline membrane mimetic such that they sample only certain orientations, display complex NMR spectra that can be used to determine structure and orientation at the membrane surface. Anisotropic NMR parameters can be exploited to gather long-range constraints and help determine structure. Weakly ordered liquid crystalline membranes allow the collection of high resolution NMR data, while incomplete averaging of the dipolar and CSA tensors

introduces orientation dependence to the spectrum. (Motional averaging in liquid crystal systems, not present in solid-state systems, also reduces line broadening, permitting the application of lower decoupling field strengths.) Improvement upon NOE-based structures can be obtained by incorporating orientation-based restraints into a simulated annealing protocol or by direct determination of structures from orientation data prior to NOE refinement.

Some preliminary work was in fact done with ARF1-derived peptides using similar methods. Myristoylated peptides derived from the N-terminal helix of ARF1 were characterized in uniformly ordered samples and demonstrated alignment with the helix axis parallel to the membrane surface (42). Losonczi *et al*. extended the study of the peptide to a myristoylated and non-myristoylated fragment and found that the myristoyl chain does not greatly affect the peptide's structure (43) but does cause a 180º rotation of the helix relative to the crystal structure (7) (Figure 1.5).

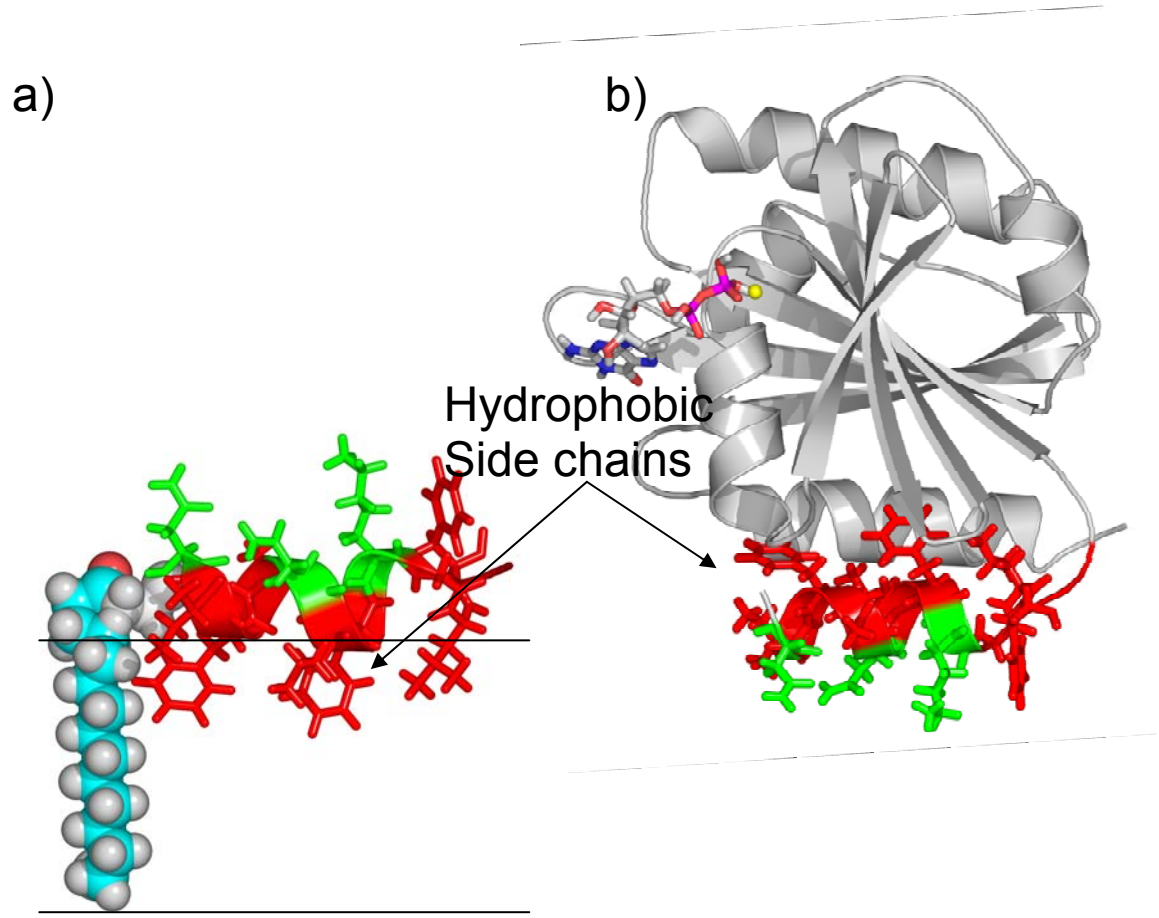


Figure 1.5. The N-terminal helix of a) myristoylated-ARF1 peptide (NMR) is rotated 180º relative to the helix in b) wtARF1-GDP (X-ray, 1HUR.pdb). Hydrophobic side chains shown in red are buried within the bilayer in a) and are tucked in toward ARF1's C-terminus in b).

### 1.3.2 TOOLS NEEDED TO EXPAND THE UTILITY OF LIQUID CRYSTAL NMR

The work of Losonczi and co-workers illustrates the feasibility and necessity of characterizing the full-length protein in a membrane environment. This extends not only to myr-ARF1, but also to other less tightly associating forms and the lipid co-factors that mediate membrane association. However, robust tools for structurally characterizing a fully isotopically labeled protein as large as myr-ARF1 (or related membrane associating species) when oriented in a true membrane environment are currently not available.

Ideally, we would like to observe these molecules in their native, membrane-bound forms. Solubilizing ARF1 and lipid cofactors in amphiphilic micelles, as is becoming common practice for membrane proteins, would not only relegate the study of this system to solution NMR techniques - which represent a serious limitation as they are limited by molecular size – but would also result in an isotropic solution in which orientational information is lost due to the rapid tumbling of spherical micelles. Application of the previously described SSNMR techniques to uniformly oriented myr-ARF1 are as yet unfeasible due to molecular size.

A method of combining the resolution of solution NMR or MAS and the long-range, orientation-based restraints from uniformly ordered myr-ARF1, non-myr-ARF1, or the lipids with which ARF1 associates in the presence of a membrane would yield both structure and orientation of the protein in its natural environment. The level of order that exists in membrane-associated systems is between that of a solution and a membrane-bound system. However, this intermediate ordering regime, $10^{-2}$-$10^{-3}$ or 1 part in 100-1000, remains poorly studied, and strategies for assembling and characterizing molecules in these states are few (44). Variable angle sample spinning (VASS), a specialized NMR technique derived from SSNMR, offers these possibilities when applied to systems uniformly oriented in liquid crystalline model membranes by scaling order and separating overlapping resonances of membrane-anchored molecules. Such studies prove important, not only for membrane proteins, but also for other classes of cell surface molecules such as glycolipids, lipoproteins, transporters, and membrane-associated molecules. To understand how VASS NMR can be used to extract anisotropic NMR parameters and provide both structure and orientation, it is important to review first, the contributions of

anisotropic parameters to NMR spectra and second, how the different liquid crystalline membranes influence NMR spectral properties.

## 1.4 NMR THEORY: ORIGINS OF COMPLEX SPECTRA

In order to successfully take advantage of complex spectral information contained within anisotropically oriented molecules, one needs to understand the origin of its effects. Invented by physicists, hijacked by chemists, and domesticated by biochemists, NMR has become a powerful tool to elucidate structure and dynamics of biomacromolecules. Nuclear spins with nuclear magnetic moments precess in a magnetic field at a characteristic frequency that is related to the gyromagnetic ratio, a fundamental spin property. Strong radiofrequency pulses are applied to induce correlated precession of spins, and weak signals from resonating nuclei are detected by detection coils near the sample. Fourier transformation of the resulting exponentially decaying signals generates unique frequencies that can be used to identify the individual NMR-active nuclei (those with non-zero nuclear magnetic moments) of a given system. Each nucleus that experiences a unique electronic environment gives a distinct resonance frequency (chemical shift). Chemical shift dispersion, the hallmark of a solution NMR spectrum – and what makes NMR useful to chemists - was initially regarded by physicists as a failure of the technique.

The source of all molecular information contained within NMR spectra can be understood by examining the NMR spin Hamiltonian operator, H. The interactions relevant to our discussion are:

$$H = H_Z + H_{CS} + H_J + H_D \quad (1)$$

where

$$H_Z = -\gamma\hbar\mathbf{I}_Z\cdot\mathbf{B}_o \quad \text{(Zeeman interaction)} \quad (2)$$

$$H_{CS} = \gamma\hbar\mathbf{I}_Z[1/3\Sigma(\sigma_{ii}) + 2/3(3\cos^2\theta_i - 1)(\sigma_{ii})] \quad \text{(Chemical shift)} \quad (3)$$

$$H_J = 2\pi J_{ij}\mathbf{I}_{iZ}\cdot\mathbf{S}_{jZ} \quad \text{(Scalar coupling)} \quad (4)$$

$$H_D = -(\mu_o/4\pi)(\gamma_i\gamma_j\hbar)(\mathbf{(I\cdot S)}/r_{ij}^3) - (3\,\mathbf{(I\cdot r)}\,\mathbf{(S\cdot r)}\,)/r_{ij}^5) \quad \text{(Dipolar coupling)} \quad (5)$$

and $\gamma_i$ is the gyromagnetic ratio of nucleus i, $\hbar$ is Planck's constant divided by $2\pi$, $\mathbf{I}_Z$ (or $\mathbf{S}_Z$) is the projection of the nuclear spin angular momentum vector onto the z-axis, $\mathbf{B}_o$ is the magnetic field classically oriented along z, $\sigma_{ij}$ are the elements of the chemical shielding tensor, $\theta_i$ is the angle between the principal axis of the chemical shielding tensor and the magnetic field, $J_{ij}$ is the scalar coupling between nuclei i and j, and $r_{ij}$ is the internuclear distance. In solution, a molecule such as ARF1 solubilized by a micelle randomly samples all orientations on a sphere with respect to the magnetic field, thus reducing the orientation-dependent terms that are proportional to $(3\cos^2\theta_i - 1)$ to zero. In a typical solid, the restricted orientations of molecules result in terms, namely dipolar coupling and chemical shift anisotropy (CSA), that do not average to zero. These anisotropic terms are second rank tensors that vary with orientation, or $\theta_i$. In a disordered sample, the CSA leads to the observation of a powder pattern spectrum, a superposition of resonance positions from all possible molecular orientations; and the dipolar coupling results in broad lines due to abundant long-range homonuclear and heteronuclear couplings. The very interactions that complicate a solid-state spectrum, however, also contain structural and dynamic information. Reducing powder patterns to single lines

and scaling these interactions to a measurable value without eliminating them, as is done in VASS, can provide valuable information on the orientation of molecules.

### 1.4.1 CHEMICAL SHIELDING ANISOTROPY TENSOR

Normally, we think about NMR yielding chemical shifts that vary only with their natural functional groups, but in fact, these functional group dependent shifts are the result of the averaging of chemical shielding tensors that contain orientational information. In this thesis I exploit the orientational dependence of phosphorus ($^{31}P$) and carbon ($^{13}C$) shielding tensors to extract molecular geometry of the ligands that bind ARF1. The terms chemical shift ($\delta$) and chemical shielding ($\sigma$) can be used interchangeably and differ only in sign. Shielding comes from an older convention typically used in solids and is still used today to describe the chemical shielding tensor, represented by the 3 x 3 matrix shown in equation (6).

$$\sigma = \begin{Bmatrix} \sigma_{11} & \sigma_{12} & \sigma_{13} \\ \sigma_{21} & \sigma_{22} & \sigma_{23} \\ \sigma_{31} & \sigma_{32} & \sigma_{33} \end{Bmatrix} \tag{6}$$

Other ways of describing the shielding tensor are through its chemical shielding anisotropy (CSA, $\Delta\sigma$):

$$\Delta\sigma = \sigma_{11} - 0.5(\sigma_{22} + \sigma_{33}) \tag{7}$$

and its isotropic value (typically observed in solution), which is the average of the principal elements of the above tensor, or the trace of the matrix:

$$\sigma_{iso} = 1/3\ (\sigma_{11} + \sigma_{22} + \sigma_{33}) \tag{8}$$

The CSA tensor can be represented as an ellipsoid where the principal axes of the ellipsoid coincide with the principal axes of the tensor. When a frame is defined so that the tensor is diagonal, the tensor is in its principal axis frame (PAF). The orientation of

the PAF for a given molecular group is dictated by its local electronic environment. The PAF orientation for the phosphorus ($^{31}$P) shielding tensor for a typical phosphate group is shown in Figure 1.6. The magnitude and orientation (the set of direction cosines that relates the tensor orientation relative to a molecular reference frame) of the shielding tensor can either be calculated quantum mechanically (45-49) or extracted experimentally from SSNMR of single crystals (50). Principal values (but not orientations) can be determined from a wider variety of other NMR experiments applied to powder samples (51).

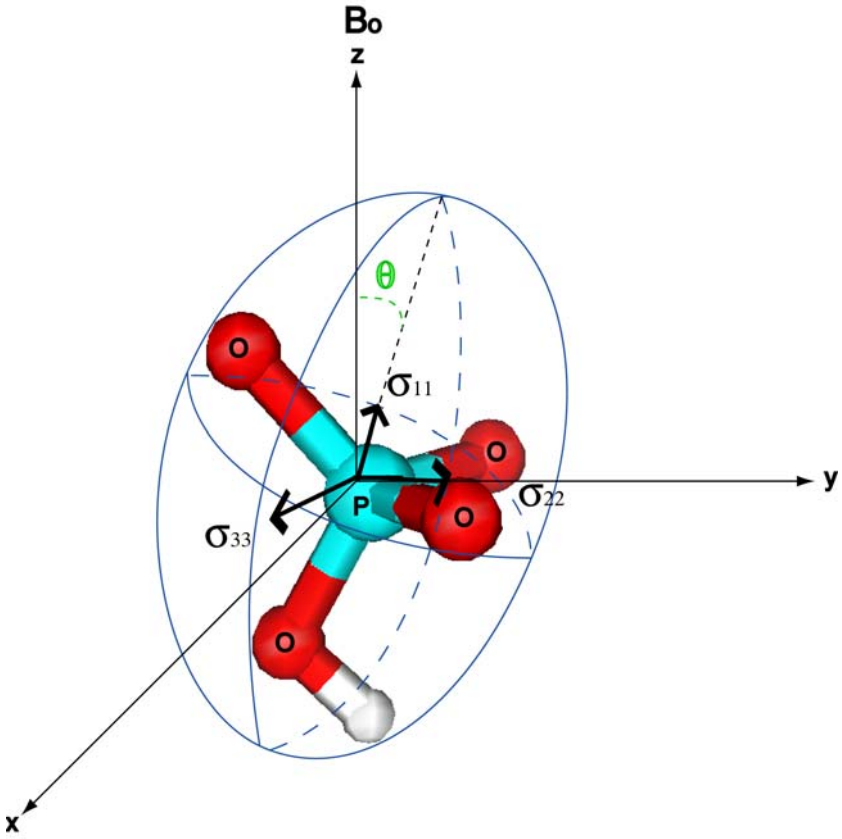


Figure 1.6. The phosphate group $^{31}$P chemical shielding anisotropy tensor.

In one of the simplest NMR experiments, discontinuities in the powder pattern can be taken to represent the principal axes of the shielding tensor (Figure 1.7a). Order with axial symmetry, as might occur in a mechanically or magnetically aligned sample or be imposed by fast rotation about the axis of orientation, reduces the three unique axes of the shielding tensor to an axially symmetric tensor (Figure 1.7b) that can be described by just two values, $\sigma_{\parallel}$ and $\sigma_{\perp}$, where $\sigma_{\parallel}$ is the tensor component along the ordering axis and $\sigma_{\perp}$ is perpendicular to the ordering axis. In an oriented sample, the information contained within the CSA can be used to relate the orientation of the shielding tensor to the molecular alignment frame, and hence to an external reference frame, such as the magnetic field, that might be inducing alignment (Figure 1.8). (When using common

orienting media such as phospholipids, where the diamagnetic anisotropy of susceptibility is negative, the alignment frame is perpendicular to the magnetic field.) One of the challenges to using CSAs is that oriented data often obscure the normal isotropic shift used for resonance assignment. VASS offers a novel way of collecting CSA information that also separates the isotropic and anisotropic components of the chemical shift. The details of this separation are presented in Chapter 2.

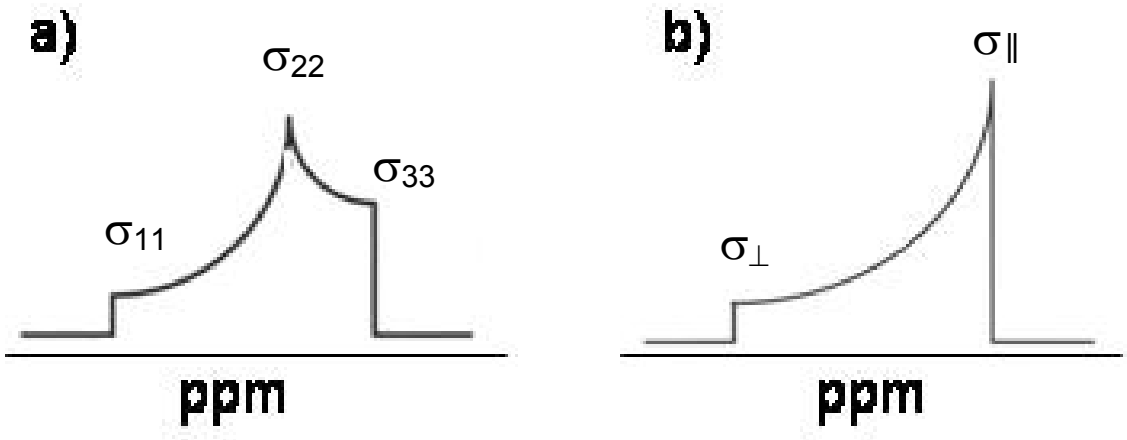


Figure 1.7. SSNMR spectra: a) powder pattern of randomly ordered sample b) powder pattern of sample with axial symmetry. Figure adapted from (52).

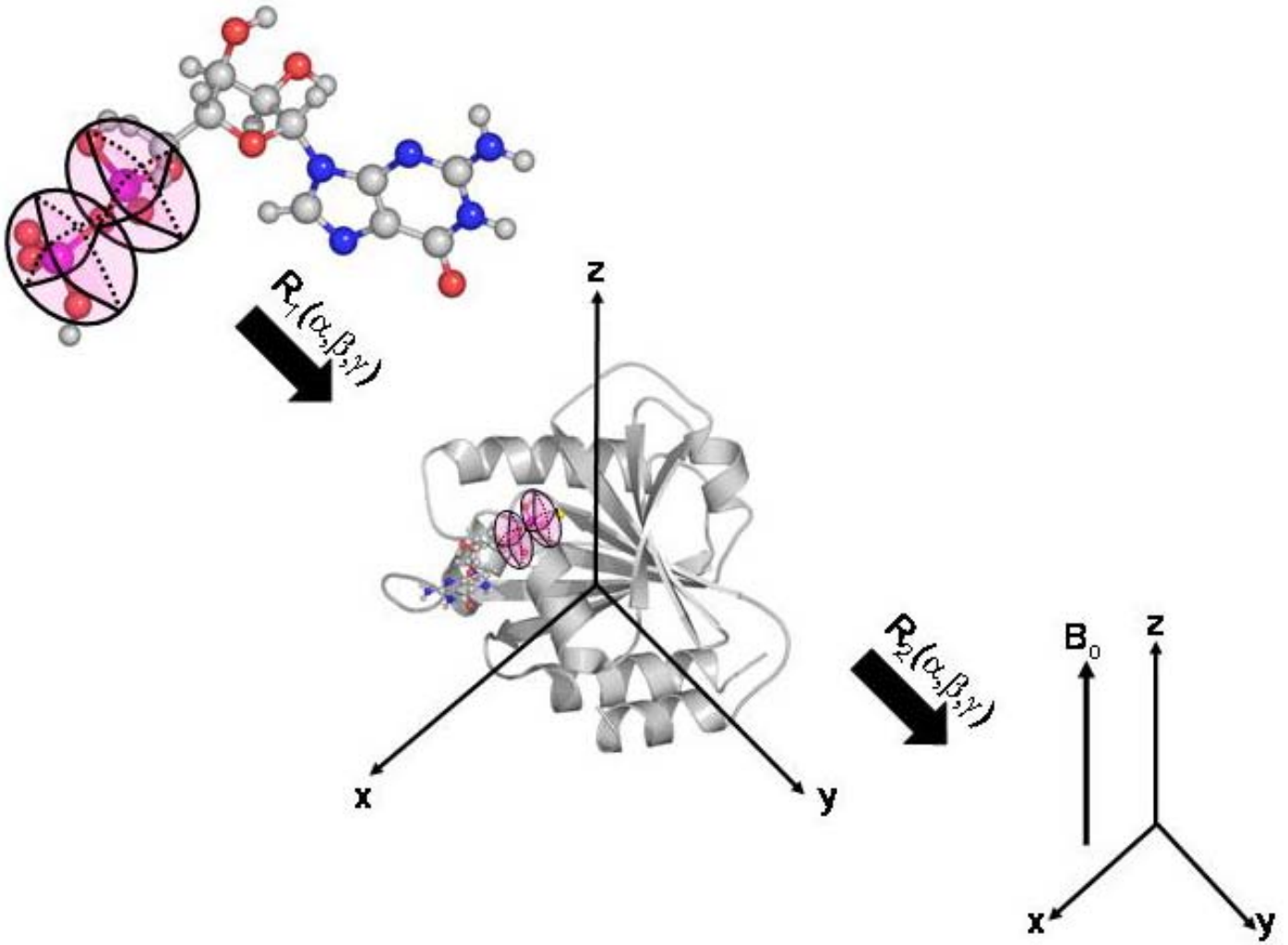


Figure 1.8. The orientation of a molecular group with respect to a common frame can be determined through a series of Euler rotations.

### 1.4.2 DIPOLAR COUPLING TENSOR

The dipolar coupling tensor can also provide long-range molecular orientation. Dipolar couplings have been used in this dissertation to describe ARF1's interaction with the membrane-anchored phospholipid phosphatidylinositol bisphosphate ($PIP_2$) and to assess ARF1's ability to order at a model membrane surface. The internuclear dipolar coupling for two spins I and S is depicted in Figure 1.9.

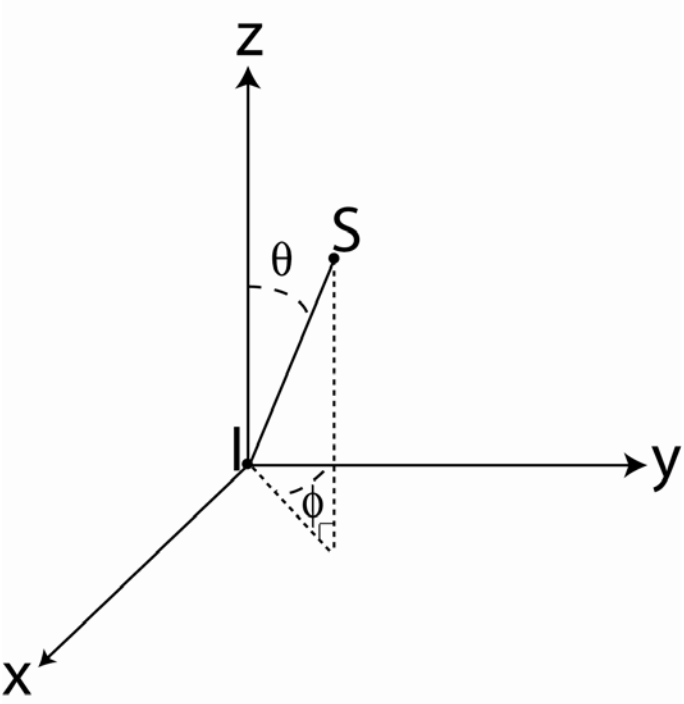


Figure 1.9. The internuclear dipolar coupling vector and polar angles that define its orientation relative to the magnetic field.

The dipolar coupling tensor is assumed to be axially symmetric, and the dipolar interaction Hamiltonian in the high field limit can be approximated as described in equation 9.

$$H_D = -(\mu_o/4\pi)((\gamma_i\gamma_j\hbar)/r_{ij}^3)\,\mathbf{I}_{iZ}\mathbf{S}_{jZ}(3\cos^2\theta - 1) \qquad (9)$$

Note the distance and angular components. The distance between bonded nuclei is assumed fixed and known to high accuracy. Analogous to the CSA, the dipolar coupling tensor relates the orientation of a molecular group to a common alignment frame that is in turn defined relative to the magnetic field. Experimental techniques used to measure and interpret residual dipolar couplings (RDCs) are further discussed in Chapter 3.

It is common practice to minimize the CSA and dipolar couplings in SSNMR by spinning at the magic angle. Transformation of the above interaction terms to the axis of rotation introduces a scaling factor, $<3\cos^2\theta - 1>$, where $\theta$ is the angle between the rotation axis and the magnetic field. This factor goes to zero at $\theta = 54.7°$ ($\theta_m$, the magic angle). When spinning at $\theta_m$ and high RF decoupling powers are applied, narrow linewidths similar to a high resolution isotropic spectrum result. While magic angle spinning (MAS) improves resolution, it simultaneously discards the very orientational information that is structurally useful.

### 1.4.3 NMR SPECTRAL PROPERTIES ARE EXPLOITED THROUGH LIQUID CRYSTALS AND VASS

VASS NMR accomplishes a similar reduction in anisotropy while preserving orientation information by exploiting the directors of liquid crystalline domains. The direction of the liquid crystal director, or main axis of symmetry, is usually fixed for a given liquid crystal as either parallel or perpendicular to the magnetic field, based on the sign of $\Delta\chi$, the anisotropy of magnetic susceptibility. For the liquid crystals used in this dissertation, the director is negative, and thus aligns perpendicular to the field. However, the director's orientation can be manipulated by mechanical spinning in a magnetic field. Domains in the liquid crystal will try to stay ordered with respect to the magnetic field,

but because they reorient slowly, only the average anisotropy dictates the energies for various orientations. Directors realign either parallel or perpendicular to the spinning axis depending on the sign of $\Delta\chi$. Therefore, it becomes possible to change the orientation of the director by spinning at different angles relative to the magnetic field, which scales interactions and simplifies complex, second order spectra without destroying the CSA and dipolar couplings. This is very much like the effects of MAS on a powder sample, but because of averaging about the director axes, the CSA results in single lines that move as a function of the scaling factor, $(3 \cos^2 \theta - 1)$ and dipolar couplings that scale by the same amount.

## 1.5 THE CHOICE OF LIQUID CRYSTAL

### 1.5.1 A VARIETY OF LIQUID CRYSTALS EXISTS

The choice of a liquid crystal as an aligning medium for a biomolecule is critical (53,54). The use of liquid crystals to confer only a very small, but measurable degree of alignment on a molecule of interest was first described in 1997 by Tjandra and Bax (55). These liquid crystals, formed from bilayered micelles or "bicelles," are mixtures of short and long-chain phospholipids dispersed in an aqueous buffer that may form small discs (56). Today, a great many of these weakly ordering alignment media ($10^{-4}$, or 1 part in 10,000) as determined by the anisotropy of the alignment tensor, are available (53). These media are now routinely used in biomolecular structure determination by solution NMR, both to complement more traditional restraints and in *de novo* structure determination (54,55). Those most useful as mimics of membrane environments are described here.

Bicelles are an ideal model membrane because they are similar in composition and structure to a native membrane. The original model for bicelles composed of mixtures of dimyristoylphosphatidylcholine (DMPC) and dihexanoylphosphatidylcholine (DHPC) (3:1) is one of lipid bilayer disks 30-40 nm in diameter, having the shorter chain lipid concentrated at the edges (Figure 1.10).

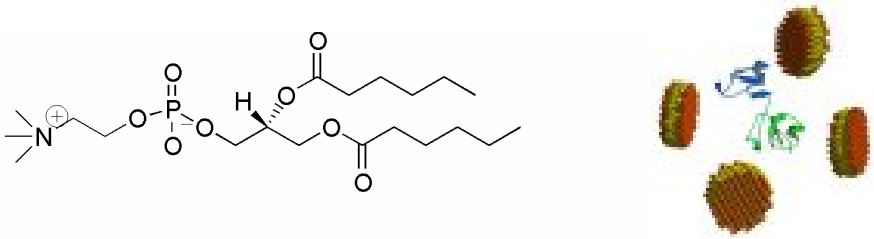

DHPC, dihexanoylphosphatidylcholine; 1,2-dihexanoyl-*sn*-glycero-3-phosphocholine

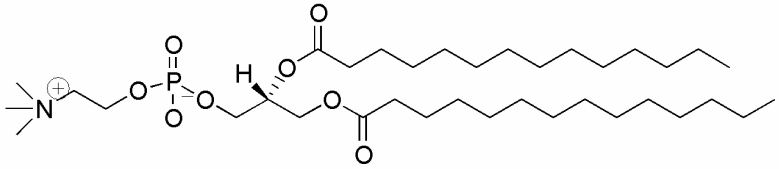

DMPC, dimyristoylphosphatidylcholine; 1,2-dimyristoyl-*sn*-glycero-3-phosphocholine

Figure 1.10. Phospholipid bicelles consisting of DHPC and DMPC are believed to form disk-like shapes and orient molecules (such as proteins) dissolved within them.

The model is supported by a variety of data on closely related systems including low angle X-ray scattering data (57), data on the anisotropic diffusion of solvent about the disks (58), NMR data on the orientation and distribution of the two lipids making up the particles (59,60), as well as electron microscopy, fluorescence, and light scattering data on particle size (60). Nevertheless, it is possible that structures vary with concentration and actual lipid composition. Recently, an alternate "Swiss cheese" model has been proposed for conditions under which much higher resolution NMR data are collected where bilayers are punctuated by holes lined with the shorter lipid (61). Debate about the

actual structures that exist may continue for some time (62,63), but both models share a basic bilayer structure oriented with the normal perpendicular to the magnetic field due to their negative $\Delta\chi$. Both are, therefore, capable of imparting order though collisional (or bilayer association) interactions of soluble, nonspherical molecules with the bilayer surfaces.

Bicelles can also be formed from low molecular weight polyethylene glycol detergents (Figure 1.11). These form bilayers by aggregation of their short alkyl ether chains. In fact, the liquid crystal primarily used for studies in this dissertation is pentaethylene glycol monododecyl ether ($C_{12}E_5$). At certain concentrations in water, pentaethylene glycol monododecyl ether dispersed with small amounts of hexanol spontaneously forms liquid crystalline bilayers that orient in a magnetic field (64). These bilayers are easy to use, low in cost, and particularly advantageous for studying phosphorus-containing biomolecules due to their lack of phosphorus background. Polyethylene glycol bilayers also orient with the bilayer normal perpendicular to the magnetic field due to $\Delta\chi < 0$. Both the original bicelles as well as the $C_{12}E_5$ bicelles can be modified by inclusion of other amphiphiles to manipulate their charge and other properties. Some of these variations, as well as related natural membrane systems are included in the table below.

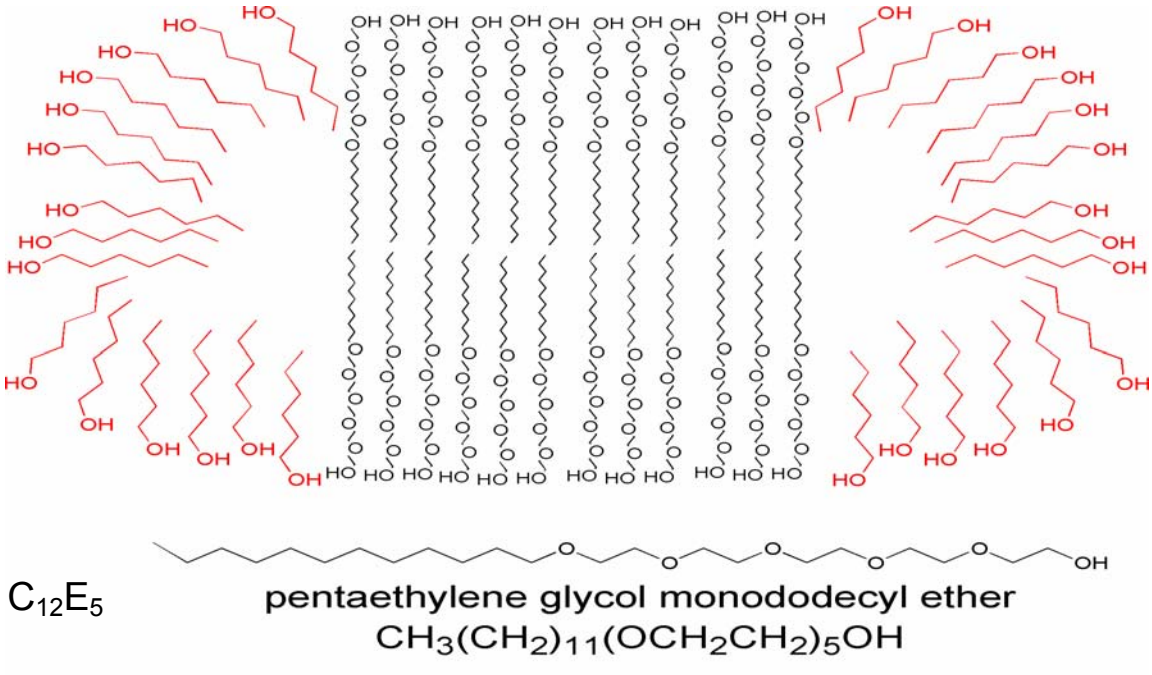


Figure 1.11. Hypothetical structure of pentaethethylene glycol monododecylether ($C_{12}E_5$) bicelles doped with hexanol. Similar bicelles can also be made with pentaethylene glycol monooctyl ether ($C_8E_5$) and octanol.

Another distinctly different alignment medium is based on anisotropically compressed polyacrylamide gels (65,66) in which alignment is independent of the magnetic field direction. Gels do not have a $\Delta\chi$; orientation is based on collisional factors much like the initial bicelle systems, but the collisional barriers are strands of polyacrylamide instead of bilayer surfaces. Strands are given a preferred direction by casting a gel of a diameter larger or smaller than the diameter of an NMR tube and then compressing or stretching the gel inside the tube (67). Dialysis after data collection observation presents a convenient option for sample recovery. Adding a charge to the gel allows somewhat better line shape for signals observed and provides more options for varying alignment properties (68,69).

There is a wide variety of other media in use. Many of them derive from media described above. In Table 1.3 current options for alignment media have been summarized. One of the more intriguing, but relatively unexplored media is the combination of two media to produce field-stabilized, immobilized media. Bacteriophage, for example, aligns with its director parallel to the magnetic field due to its large positive $\Delta\chi$ (70-72). When cast in a polymer substance or polyacrylamide gel and "cured" in a magnetic field, an aligning medium is formed with a mechanically oriented director that can be manipulated by changing the angle relative to the magnetic field but without spinning.

Table 1.3. Alignment media commonly used to measure residual dipolar couplings

| **Medium** | **Molecular Species** | **Charge, ($\Delta\chi$)** | **Temp. range (°C)** | **Features & limitations** | **Ref.** |
|---|---|---|---|---|---|
| Ester-linked phospholipid bicelles | DMPC:DHPC | Neutral, (-) | 27-45 | + Easy preparation, - Expensive, susceptible to hydrolysis | (55,73) |
| Ether-linked phospholipid bicelles | DIODPC:CHAPSO DIODPC:DIHPC | Neutral, (-) | 10-55 | Low pH | (74,75) |
| Phospholipid bicelles doped with charged lipids | DMPC:DHPC: CTAB/SDS | CTAB, positive SDS, negative | 27-40 | | (76) |
| Poly(ethylene) glycol ether bilayers | $C_nE_m$:*n*-alcohol | Neutral (-) | 0-60 | + Easy preparation, inexpensive, highly compatible with biomolecules - Kinetics of alignment *esp.* with dissolved biomolecules unknown | (77) |
| Poly(ethylene) glycol ether bilayers doped with charged lipids | $C_nE_m$:*n*-alcohol:CTAB/SDS | Positive, negative | 0-60 | | (78) |

| Medium | Molecular Species | Charge, ($\Delta\chi$) | Temp. range (°C) | Features & limitations | Ref. |
|---|---|---|---|---|---|
| Bacteriophage | Rod-shaped viruses | Negative (-) | 5-60 | + Easy preparation, sample recovery<br>- Only suitable for negatively charged biomolecules | (70,72,79, 80) |
| Purple membranes | Cooperative anisotropic membranes | Charged | <70 | | (81,82) |
| Stretched or strained polyacrylamide gels | Polyacrylamide gels | Neutral | 5-45 | + Easy sample recovery<br>- Difficult to align homogeneously, strong steric interaction causes broad lines | (65,66) |
| Stretched or strained polyacrylamide gels | Polyacrylamide gels plus detergent | Neutral | 5-45 | + Accomodates larger MW (esp. membrane) proteins<br>+Decreased line broadening | (83,84) |
| Charged polyacrylamide gels | Acrylamide/acrylate | Negative | 5-45 | + High mechanical stability, decreased line broadening<br>- Delicate and easily ruptured | (68,69) |
| Immobilized media | Gel- or polymer-stabilized purple membranes or phage | | | + Director moves with position | (66,85,86) |
| Lanthanide ions/Ln-binding tags | Align by anisotropy of susceptibility | Neutral (+) | | + No compatibility problems<br>- Very small degree of alignment | (87-89) |
| Ln-"flipped" bicelles | DMPC:DHPC:DMPG:DMPE-DTPA-$Yb^{3+}$ | Neutral (+) | 27-45 | + Flips director perpendicular to bicelle<br>+ Suitable for large membrane proteins<br>- Expensive addition to bicelles | (90) |

Abbreviations: DMPC, 1,2-di-tetradecanoyl-*sn*-glycero-3-phosphocholine; DHPC, 1,2-di-hexanoyl-*sn*-glycero-3-phosphocholine; DIODPC, 1,2- di-O-dodecyl-*sn*-glycero-3-phosphocholine; CHAPSO, 3-(chloramidopropyl)dimethylammonio-2-hydroxyl-1-propane sulfonate; DIHPC, 1,2- di-O-hexyl-*sn*-glycero-3-phosphocholine; CTAB, hexadecyltrimethylammonium bromide; SDS, sodium dodecyl sulfate; $C_nE_m$ where n is the number of carbons in a poly(ethylene)glycol headgroup and m refers to the

number of repeating ethylene oxide units; DMPG, 1,2-dimyristoyl-*sn*-glycero-3-phosphoglycerol; DMPE-DTPA, 1,2-Dimyristoyl-*sn*-Glycero-3-PhosphoEthanolamineDiethyleneTriaminePentaAcetate; $Yb^{3+}$, ytterbium.

### 1.5.2 THE NECESSITY OF MULTIPLE ALIGNMENT MEDIA

The identification of suitable media for a particular application is not necessarily trivial. It is not simply sufficient that media do not perturb molecular structures; they must also induce a proper level of alignment. Alignment must be sufficient to give measurable RDCs and chemical shift offsets but, for most applications, not so large as to introduce spectral complexity. For typical solution NMR studies, a principal order parameter of $10^{-3}$ will, for example, give a maximum $^{15}N$-$^{1}H$ RDC splitting for a directly bonded amide pair of about 25 Hz. This is large compared to typical line widths, particularly in the $^{15}N$ dimension of a $^{1}H$-$^{15}N$ HSQC spectrum, but it is not so large that long-range interactions begin to broaden resonances or cause second-order distortions of one bond couplings. Alignment is also weak enough that INEPT transfers optimized for one-bond scalar couplings in TROSY- or HSQC-based experiments do not begin to fail due to mismatch of transfer delays to total couplings. Simple adjustment of media concentration is sometimes enough to scale alignment to a proper level, although the concentration range over which cooperative alignment occurs at all is small for some media. However, in the case of membrane-associated systems, strong alignment is the norm, and lines are already broadened. It is in these cases that techniques such as VASS NMR come in handy to reduce spectral complexity while retaining the orientational information.

It is clear that a number of media are necessary if one is to find media that are compatible with the biomolecule, spectroscopically useful, and convenient to prepare. In

addition to finding a single compatible medium, it is very useful to have the option of using several alignment media in the course of a study to minimize inherent degeneracies in mapping quantities such as RDCs and CSAs to functional group orientations. It is also useful to use two or more alignment media with different alignment tensors to lift the degeneracy of functional group alignment frames determined from order tensors (91). Dipolar couplings (as well as CSAs) suffer from the multivalued nature of the mapping of measured values to fragment orientations. Even after transforming to a principal alignment frame, two different values (in a 0-180° range) can give the same value for the $(3\cos^2\theta\text{-}1)/2$ function. The direction of a single interaction vector in a molecular fragment can, therefore, be defined no better than being on the surface of two opposing cones having these values of $\theta$ as half angles. One approach is to use a set of anisotropic interactions in a rigid fragment to evaluate an order tensor that can in turn define fragment orientations. RDCs (and CSAs) can be redefined in terms of order tensor elements. Equations for RDCs expressed in terms of order parameters have five independent parameters that must be determined before the orientation of a molecular fragment in a principal alignment frame can be determined. The degeneracy problem does not unfortunately stop at this point. Principal order parameters (dependent on $(3\cos^2\theta_{x,y,z} - 1)$) are insensitive to inversion of axis directions. It becomes clear that an order frame can equally well be described by any one of four possible combinations of positive and negative *x*, *y*, and *z* axis directions that yield a right-handed Cartesian coordinate system. One way to lift this degeneracy and determine a unique orientation of a molecular fragment is to anchor the fragment to the alignment medium, *i.e.* bilayer surface, where the direction of the director is known relative to the magnetic field. If the

molecular geometry can be determined relative to the bilayer surface, the unique orientation can be determined. Even in the absence of sufficient data to independently determine a structure, data from orientationally dependent NMR parameters can be used as constraints in modeling, or as filters to eliminate untenable models. I will rely on this latter approach in experiments described in Chapter 2.

A second reason for using multiple media comes from concerns specific to VASS. Depending on the sign of $\Delta\chi$ and the angle the spinning axis makes with respect to the magnetic field (either greater than or less than the magic angle), liquid crystal directors orient either parallel or perpendicular to the spinning axis. Due to sensitivity limitations of our VASS probe, it was more desirable to collect data at angles greater than the magic angle. However, there may be cases where data at additional angles is essential for structure determination. In these cases, the option of using a second aligning medium with perpendicularly orienting directors becomes useful.

Another reason for having multiple alignment media available is for the elimination of the occasional concern about media-induced distortion of molecular geometries. Significant distortions as a direct result of an interaction between the medium and the molecule of interest are unlikely because the energy of interaction required to induce order of one part in $10^3$ is extremely small. However, it is possible to preferentially orient populations of minor states that are in rapid equilibrium with major states. An average state is observed in these cases, and it can be dominated by properties of the minor species (92). Collecting anisotropic data in more than one medium can provide some protection against improper interpretation of measurements skewed by a minority of conformations. It is unlikely that preferential orientation of the same

minority species will occur in all media, and derived conformations will be inconsistent if significant problems of this type occur.

To achieve most of the above advantages, each aligning medium must orient the biomolecule in a significantly different way so that the alignment tensors are not coincident. Simple solutions such as increasing the concentration of a liquid crystal from a lower to a higher percentage, for example, will not work; this will simply scale the dipolar couplings to larger values and will not, in general, provide new orientational restraints for use in structure determination. Use of media with perpendicularly oriented directors also does not yield new information. In alignment media that orient with their directors 90 degrees apart, for example, perpendicular and parallel to the magnetic field, elements of the alignment tensors will simply be scaled by a factor of -1/2. In any event, studies of biomolecular structure or dynamics can benefit greatly from the availability of a number of alignment media. As will be apparent in some of the studies presented here, it will not always be possible to find a sufficient number of media to eliminate all concerns, but for more general studies, following the options described above is important.

## 1.6 APPLICATION TO ADENOSINE DIPHOSPHATE (ADP) RIBOSYLATION FACTOR 1 (ARF1) AND ITS LIGANDS

In this dissertation, I investigate the structure and orientation of membrane-associated ARF1 and its associated ligands through novel nuclear magnetic resonance (NMR) experimental and computational methods developed for characterizing membrane-associated molecules. VASS and liquid crystal NMR techniques combined to characterize oriented, membrane-associated molecules may increase our understanding of

membrane-anchored systems and offer a robust tool for characterizing such systems. The target for the application of the approach outlined above is the ADP Ribosylation Factor, ARF1. A critical step in the secretory pathway is the bidirectional trafficking of cargo-filled vesicles between the endoplasmic reticulum (ER) and the Golgi (Figure 1.12). These vesicles contain proteins, newly folded from the ribosome and processed in the ER, that are transported to the Golgi for further processing and export to the cell surface. Identifying the key players in the assembly of these vesicles has been the subject of much research. Notably, membrane trafficking, assembly of coat proteins, and vesicle budding and fusion all have been attributed to the membrane-associating proteins of the ARF1 family. The family of 21 kDa ARF1 (ADP-Ribosylation Factor) proteins belongs to a superfamily of Ras GTPases that are conserved in both structure and function; members of the family have greater than 60% sequence identity (93). ARFs were first discovered for their ability to stimulate cholera toxin A subunit's ADP-ribosylation of the heterotrimeric G protein, $G_S$ (94). This is the origin of their name; it was only later that their essential role in vesicular trafficking was discovered. A possible mechanism for ARF1's role in vesicle formation is shown in Figure 1.15. A conformational switch between the active GTP-bound and inactive GDP-bound states is a critical factor in the role of ARF1 in transport of vesicles from the Golgi to the ER (9,95). In the active GTP form, the N-terminal myristoyl group (and possibly an amphipathic N-terminal helix), unique to ARF1 among GTPases, is exposed, allowing insertion into the membrane. Membrane associated ARF1 then recruits proteins that coat a localized area causing the membrane surface to deform or bud into vesicles. The interconversion between the GDP (cytosolic) and GTP (membrane-bound) states is slow and is aided by activator and

effector proteins that bind ARF1. ARF1 remains membrane-bound until a GTPase activating protein (GAP) hydrolyzes GTP to GDP, causing the protein to dissociate from the membrane, and allowing the vesicle to fuse with the acceptor membrane. There is little doubt that the exchange of GDP for GTP activates an N-terminal switch involving the N-terminal helix and N-terminal myristoyl chain enabling membrane association, but the actual sequence of events that controls the exposure of these components is not known, and consequently, details of vesicle formation, transportation, and docking, remain poorly understood.

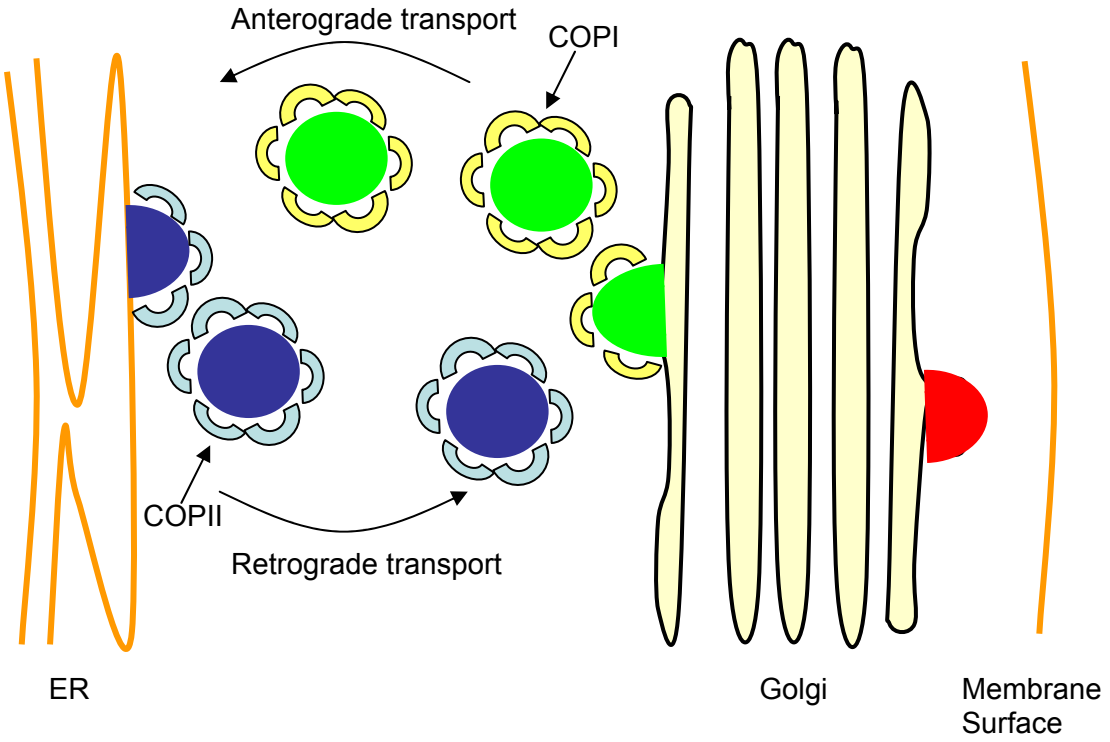


Figure 1.12. Bidirectional trafficking between the endoplasmic reticulum (ER) and the Golgi occurs *via* vesicular transport (Figure adapted from (96)).

Myristoylation (Figure 1.13) certainly facilitates reversible association with the membrane; but, it does not provide sufficient interaction energy on its own to anchor a protein to a membrane (97).

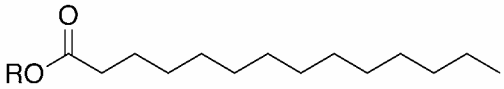


Figure 1.13. The 14-carbon myristoyl group attaches to the N-terminal glycine of ARF1.

In other membrane proteins, hydrophobic and basic patches provide regions that permit otherwise soluble proteins to attach to a membrane. Regions of positive charge in membrane-associated proteins, for example, help localize proteins to negatively charged signaling lipids present in different membrane locations. In the case of ARF1, N-myristoylation, an amphipathic N-terminal helix, a positive patch, and protein-protein interactions with guanine exchange factors (GEFs) and GAPs all could facilitate translocation to the membrane, but mechanistic and structural details on how and if ARF1 uses these components to bind to membranes and regulate the budding of phospholipid membranes are not yet understood. The N-terminal amphipathic helix could associate nonspecifically with the membrane, and the region of positive charge located on the surface of the protein could be a $PIP_2$-binding site. The membrane-anchored lipid $PIP_2$ is a minor component in the plasma membrane that plays a role in intracellular signaling (Figure 1.14).

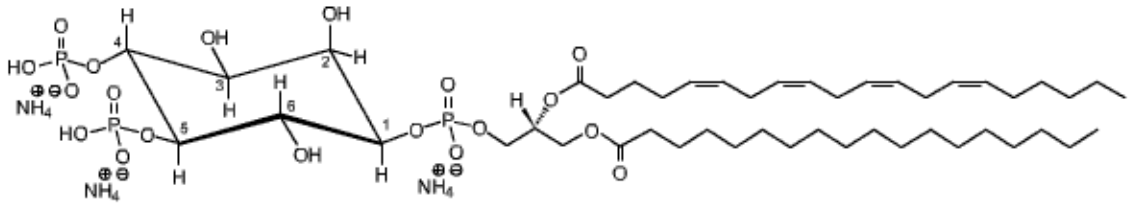

Figure 1.14. Phosphatidylinositol bisphosphate ($PI(4,5)P_2$, or $PIP_2$) may play a role in ARF1 membrane recruitment and function.

There is actually some evidence indicating that $PIP_2$ is important for ARF1's function (98,99). The negatively charged, membrane-anchored $PIP_2$ is believed to be an effector of ARF1 activity that enhances GDP dissociation and stabilizes the nucleotide-free form of ARF1. Understanding the manner in which this happens should begin with information on the structure of both ARF1 and $PIP_2$. $PIP_2$ may bring ARF1 to the membrane, but direct structural evidence for $PIP_2$'s membrane orientation with respect to the bilayer as well as interaction with ARF1 in a membrane is not available. Also, we do not know the extent of structural differences between soluble non-myristoylated (non-myr) and membrane-anchored ARF1. In particular, we know neither how the N-terminal helix of ARF1 orients with respect to the membrane and the rest of the protein when anchored to the membrane surface.

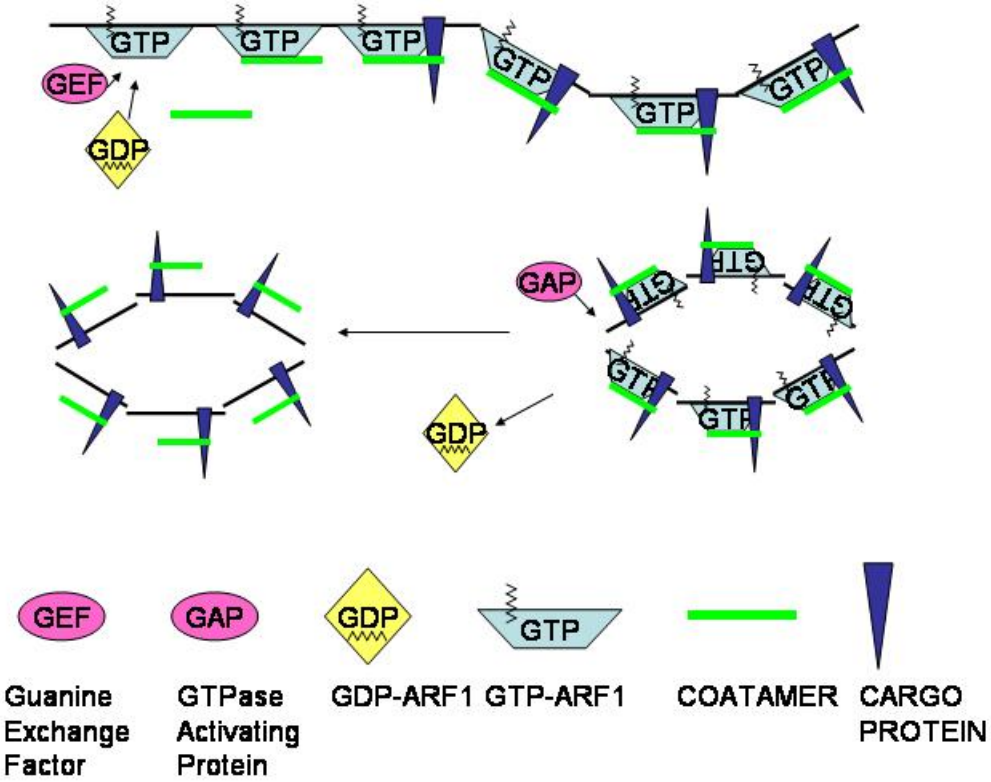


Figure 1.15. Current model of ARF1's activity in the cytosol and at the membrane surface. (Figure adapted from (100).)

In chapter 2, conformations of the phosphoinositides $PIP_2$ and PI(4)P in a polyethylene glycol model membrane are proposed, as determined by constraints from VASS NMR and model structures. Although phospholipid bicelles are now used widely to orient soluble molecules of all types for NMR studies, their application to molecules that associate with a phospholipid bilayer is challenging. Unlike soluble molecules, anisotropic interactions for membrane-associating molecules can be large, and considerable spectral complexity results. One of the challenges of oriented sample NMR is to separate the isotropic chemical shift used for spectral assignment from the anisotropic part used to determine orientation. A compromise between high resolution and orientational information can be achieved by spinning a liquid crystal sample at an

angle other than $\theta_m$ to reintroduce the anisotropic interactions that would be removed by MAS. These enter into the spectrum scaled by $(3 \cos^2 \theta - 1)$ so that complexity is reduced. I have used VASS NMR to record isotropic spectra at the magic angle and to measure chemical shielding anisotropies at other angles. Membrane-anchored phosphoinositides that bind ARF1 are a convenient place to start these studies. $PIP_2$ was chosen as a first step in determining the molecular geometry of a membrane-associated molecule for its functional significance as a putative binding partner of ARF1, and as its three phosphorus atoms shown in Figure 1.14 are readily observed by $^{31}P$ NMR . While spectra are simplified, the small number of phosphorus atoms in $PIP_2$ made a model-free geometry impossible to determine, *a priori*, so we utilized a comparison of experimental chemical shift offsets and offsets calculated for various computational models to determine a viable head group orientation.

In Chapter 3 I explore an alternative approach to collecting chemical shift offsets and RDCs that may be used more widely in biological applications. Magic-angle spinning probes built specifically for high resolution applications can provide more precise data and reduce sample requirements in the collection of RDCs and chemical shift offsets. The applications described here are of techniques suitable for proteins and most commonly depend on observation of $^{15}N$-$^{1}H$ pairs along a polypeptide backbone. These pairs provide for a convenient measurement of a one bond $^{15}N$-$^{1}H$ RDC as well as an $^{15}N$ CSA. Fixed-angle probes sacrifice the ability to scale parameters by spinning off the magic angle, but for weakly aligned systems this may not be necessary. Here the possibilities and current limitations of application of high resolution MAS technology to

measurements of these parameters are addressed using results from an 8 kDa protein in a weakly ordered liquid crystal.

In Chapter 4 I turn to the orientation of $^{15}N$ isotopically labeled, non-myrARF1 in a model membrane using a form of easily acquired data, RDCs, and attempt to increase the membrane association of non-myrARF1 through the use of $PIP_2$ as a membrane-targeting lipid. My work led to identifying the specific molecular interactions between $PIP_2$ and non-myrARF1, but it also led to the surprising finding that the complex is not strongly ordered in the model membrane. $^{31}P$ NMR data on ligands associated with non-myrARF1 (GDP and $PIP_2$) also indicated that non-myrARF1 may actually remove $PIP_2$ from the model membrane, possibly burying the acyl chains of $PIP_2$ in the hydrophobic pocket of non-myrARF1 normally occupied by the myristoyl chain. I also present data on a model for myr-ARF1, an N-terminal hexyl-ARF1 that demonstrates stronger membrane association than either non-myr ARF1-GDP or $PIP_2$-bound ARF1-GDP, but shows significantly weaker binding to $PIP_2$.

In Chapter 5 I have used GDP as a reporter of non-myrARF1's membrane associated state by exploring $^{13}C$ chemical shift anisotropy (CSA) offsets between non-myrARF1 with and without the membrane anchor $PIP_2$. Direct observation of $^{13}C$, when isotopically labeled, will in principle be a more easily observable probe of strongly-ordered $PIP_2$-ARF1 than multidimensional experiments that rely on fast-relaxing $^{1}H$ signals. While true tests of applicability must await availability of strongly associating myr-ARF1 samples, the feasibility of measuring $^{13}C$ chemical shift offsets from well-resolved aromatic carbons is demonstrated using simple one-dimensional NMR techniques. In addition, an alternative method for labeling GDP with a low percentage of

isotopic label (13%) by starting with RNA from *E.coli* grown in a specialized medium is presented. This GDP is shown to provide greater sensitivity and resolution than fully isotopically labeled (98%) GDP, particularly in membrane-associated samples, due to the lack of multiple-bond scalar couplings and long-range dipolar couplings. The use of partially labeled nucleotide cofactors such as GDP is suggested as a feasible route to collecting chemical shift offset data on strongly ordered, membrane-bound systems of other types.

I conclude by considering additional NMR methodology suitable for membrane-associating systems and additional targets for the techniques developed within this dissertation. I also discuss current limitations to myr-ARF1 production. The results contained herein should provide a stepping-stone to characterizing this important system when myr-ARF1 and other more strongly membrane-associated samples become available.

REFERENCES


1. Lehnert, U., Xia, Y., Royce, T.E., Goh, C.S., Liu, Y., Senes, A., Yu, H.Y., Zhang, Z.L., Engelman, D.M. and Gerstein, M. (2004) Computational analysis of membrane proteins: genomic occurrence, structure prediction and helix interactions. *Q Rev Biophys*, **37,** 121-146.
2. Berman, H.M., Westbrook, J., Feng, Z., Gilliland, G., Bhat, T.N., Weissig, H., Shindyalov, I.N. and Bourne, P.E. (2000) The protein data bank. *Nucleic Acids Res*, **28,** 235-242.
3. White, S.H. (2004) The progress of membrane protein structure determination. *Protein Sci*, **13,** 1948-1949.
4. Bijlmakers, M.-J. and Marsh, M. (2003) The on-off story of protein palmitoylation. *Trends Cell Biol*, **13,** 32-42.
5. Maurer-Stroh, S., Gouda, M., Novatchkova, M., Schleiffer, A., Schneider, G., Sirota, F.L., Wildpaner, M., Hayashi, N. and Eisenhaber, F. (2004) MYRbase: analysis of genome-wide glycine myristoylation enlarges the functional spectrum of eukaryotic myristoylated proteins. *Genome Biology*, **5**.
6. Torres, J., Stevens, T.J. and Samso, M. (2003) Membrane proteins: the 'Wild West' of structural biology. *Trends Biochem Sci*, **28,** 137-144.
7. Amor, J.C., Harrison, D.H., Kahn, R.A. and Ringe, D. (1994) Structure of the human ADP-ribosylation factor 1 complexed wtih GDP. *Nature*, **372,** 704-708.
8. Goldberg, J. (1998) Structural Basis for activation of ARF GTPase: mechanisms of guanine nucleotide exchange and GTP-myristoyl switching. *Cell*, **95,** 237-248.
9. Seidel, R.D., Amor, J.C., Kahn, R.A. and Prestegard, J.H. (2004) Conformational changes in human Arf1 on nucleotide exchange and deletion of membrane-binding elements. *J Biol Chem*, **279,** 48307-48318.
10. MacKenzie, K.R., Prestegard, J.H. and Engelman, D.M. (1997) A transmembrane helix dimer: Structure and implications. *Science*, **276,** 131-133.
11. Arora, A., Abildgaard, F., Bushweller, J.H. and Tamm, L.K. (2001) Structure of outer membrane protein A transmembrane domain by NMR spectroscopy. *Nat Struct Biol*, **8,** 334-338.
12. Fernandez, C., Adeishvili, K. and Wuthrich, K. (2001) Transverse relaxation-optimized NMR spectroscopy with the outer membrane protein OmpX in dihexanoyl phosphatidylcholine micelles. *Proc Natl Acad Sci U S A*, **98,** 2358-2363.
13. Hwang, P.M., Choy, W.-Y., Lo, E.I., Chen, L., Forman-Kay, J.D., Raetz, C.R.H., Prive, G.G., Bishop, R.E. and Kay, L.E. (2002) Solution structure and dynamics of the outer membrane enzyme PagP by NMR. *PNAS*, **99,** 13560-13565.
14. Roosild, T.P., Greenwald, J., Vega, M., Castronovo, S., Riek, R. and Choe, S. (2005) NMR structure of Mistic, a membrane-integrating protein for membrane protein expression. *Science*, **307,** 1317-1321.
15. Fiaux, J., Bertelsen, E.B., Horwich, A.L. and Wuthrich, K. (2002) NMR analysis of a 900K GroEL-GroES complex. *Nature*, **418,** 207-211.
16. Kumar, A., Welti, D. and Ernst, R.R. (1975) NMR Fourier zeugmatography. *J Magn Reson*, **18,** 69-83.

17. Muller, L. (1979) High-Sensitivity 2-Dimensional C-13 Nmr-Spectroscopy. *J Magn Reson*, **36,** 301-309.
18. Bax, A., Ikura, M., Kay, L.E., Torchia, D.A. and Tschudin, R. (1990) Comparison of Different Modes of 2-Dimensional Reverse-Correlation Nmr for the Study of Proteins. *J Magn Reson*, **86,** 304-318.
19. Bodenhausen, G. and Ruben, D.J. (1980) Natural Abundance N-15 Nmr by Enhanced Heteronuclear Spectroscopy. *Chem Phys Lett*, **69,** 185-189.
20. Losonczi, J. and Green, I. (2004) Cryogenically cooled NMR probes: More information in less time. *Am Lab*, **36,** 26-+.
21. Pervushin, K., Riek, R., Wider, G. and Wuthrich, K. (1997) Attenuated T-2 relaxation by mutual cancellation of dipole-dipole coupling and chemical shift anisotropy indicates an avenue to NMR structures of very large biological macromolecules in solution. *Proc Natl Acad Sci U S A*, **94,** 12366-12371.
22. McDermott, A.E. (2004) Structural and dynamic studies of proteins by solid-state NMR spectroscopy: rapid movement forward. *Curr Opin Struct Biol*, **14,** 554-561.
23. Castellani, F., van Rossum, B., Diehl, A., Schubert, M., Rehbein, K. and Oschkinat, H. (2002) Structure of a protein determined by solid-state magic-angle-spinning NMR spectroscopy. *Nature*, **420,** 98-102.
24. Jaroniec, C.P., MacPhee, C.E., Bajaj, V.S., McMahon, M.T., Dobson, C.M. and Griffin, R.G. (2004) High-resolution molecular structure of a peptide in an amyloid fibril determined by magic angle spinning NMR spectroscopy. *Proc Natl Acad Sci U S A*, **101,** 711-716.
25. Marassi, F. and Opella, S.J. (1998) NMR structural studies of membrane proteins. *Curr Opin Struct Biol*, **8,** 640-648.
26. Wang, J., Denny, J., Tian, C., Kim, S., Mo, Y., Kovacs, F., Song, Z., Nishimura, K., Gan, Z., Fu, R. *et al.* (2000) Imaging membrane protein helical wheels. *J Magn Reson*, **114,** 162-167.
27. Denny, J.K., Wang, J.F., Cross, T.A. and Quine, J.R. (2001) PISEMA powder patterns and PISA wheels. *J Magn Reson*, **152,** 217-226.
28. Nevzorov, A.A., Mesleh, M.F. and Opella, S.J. (2004) Structure determination of aligned samples of membrane proteins by NMR spectroscopy. *Magn Reson Chem*, **42,** 162-171.
29. Gu, Z.T.T. and Opella, S.J. (1999) Two- and three-dimensional H-1/C-13 PISEMA experiments and their application to backbone and side chain sites of amino acids and peptides. *J Magn Reson*, **140,** 340-346.
30. Opella, S.J., Marassi, F.M., Gesell, J.J., Valente, A.P., Kim, Y., Oblatt-Montal, M. and Montal, M. (1999) Structures of the M2 channel-lining segments from nicotinic acetylcholine and NMDA receptors by NMR spectroscopy. *Nat Struct Biol*, **6,** 374-379.
31. Watts, A. (1998) Solid-state NMR approaches for studying the interaction of peptides and proteins with membranes. *Biochim Biophys Acta*, **1376,** 297-318.
32. Mason, A.J., Grage, S.L., Straus, S.K., Glaubitz, C. and Watts, A. (2004) Identifying anisotropic constraints in multiply labeled bacteriorhodopsin by N-15 MAOSS NMR: A general approach to structural studies of membrane proteins. *Biophys J*, **86,** 1610-1617.

33. Pointer-Keenan, C.D., Lee, D.K., Hallok, K., Tan, A.M., Zand, R. and Ramamoorthy, A. (2004) Investigation of the interaction of myelin basic protein with phospholipid bilayers using solid-state NMR spectroscopy. *Chem Phys Lipids*, **132,** 47-54.
34. Wasniewski, C.M., Parkanzky, P.D., Bodner, M.L. and Weliky, D.P. (2004) Solid-state nuclear magnetic resonance studies of HIV and influenza fusion peptide orientations in membrane bilayers using stacked glass plate samples. *Chem Phys Lipids*, **132,** 89-100.
35. Saupe, A. and Englert, G. (1963) High-resolution nuclear magnetic resonance spectra of orientated molecules. *Phys Rev Lett*, **11,** 462-464.
36. Seelig, J. (1978) $^{31}$P Nuclear magnetic resonance and the head group structure of phospholipids in membranes. *Biochim Biophys Acta*, **515,** 105-140.
37. Seelig, J. and Macdonald, P.M. (1987) Phospholipids and Proteins in Biological-Membranes - H-2 Nmr as a Method to Study Structure, Dynamics, and Interactions. *Acc Chem Res*, **20,** 221-228.
38. Saupe, A. (1968) Recent results in the field of liquid crystals. *Angew Chem Internat Edit*, **7,** 97-&.
39. Bastiaan, E.W., Maclean, C., Van Zilj, P.C.M. and Bothner-by, A.A. (1987) High-resolution NMR of liquids and gases: Effects of magnetic-field-induced molecular alignment. *Annu Rep NMR Spectrosc*, **19,** 35-77.
40. Bothner-By, A.A. (1995) Magnetic field induced alignment of molecules. In Grant, D. M. and Harris, R. K. (eds.), *Encyclopedia of Nuclear Magnetic Resonance*. Wiley, Chichester, pp. 2932-2938.
41. Losonczi, J.A., Andrec, M., Fischer, M.W.F. and Prestegard, J.H. (1999) Order matrix analysis of residual dipolar couplings using singular value decomposition. *J Magn Reson*, **138,** 334-342.
42. Losonczi, J.A. and Prestegard, J.H. (1998) NMR characterization of the myristoylated, N-terminal fragment of ADP-Ribosylation factor 1 in a magnetically oriented membrane array. *Biochemistry*, **37,** 706-716.
43. Losonczi, J.A., Tian, F. and Prestegard, J.H. (2000) Nuclear magnetic resonance studies of the N-terminal fragment of adenosine diphosphate ribosylation factor 1 in micelles and bicelles: Influence of N-myristoylation. *Biochemistry*, **39,** 3804-3816.
44. Zandomeneghi, G. and Meier, B.H. (2004) Adiabatic-passage cross polarization in N-15 NMR spectroscopy of peptides weakly associated to phospholipids: Determination of large RDC. *J Biomol NMR*, **30,** 303-309.
45. Cheeseman, J.R., Trucks, G.W., Keith, T.A. and Frisch, M.J. (1996) A comparison of models for calculating nuclear magnetic resonance shielding tensors. *J Chem Phys*, **104,** 5497-5509.
46. Oldfield, E. (2002) Chemical shifts in amino acids, peptides, and proteins: From quantum chemistry to drug design. *Annu Rev Phys Chem*, **53,** 349-378.
47. deDios, A.C. and Oldfield, E. (1996) Recent progress in understanding chemical shifts. *Solid State Nucl Magn Reson*, **6,** 101-125.
48. Case, D.A. (1998) The use of chemical shifts and their anisotropies in biomolecular structure determination. *Curr Opin Struct Biol*, **8,** 624-630.

49. Sitkoff, D. and Case, D.A. (1998) Theories of chemical shift anisotropies in proteins and nucleic acids. *Prog Nucl Magn Reson Spectrosc*, **32,** 165-190.
50. Herzfeld, J., Griffin, R.G. and Haberkorn, R.A. (1978) Phosphorus-31 chemical shift tensors in barium diethyl phosphate and urea-phosphoric acid: model compounds for phospholipid head-group studies. *Biochemistry*, **17,** 2711-2718.
51. Stueber, D. and Grant, D.M. (2002) C-13 and N-15 chemical shift tensors in adenosine, guanosine dihydrate, 2 '-deoxythymidine, and cytidine. *J Am Chem Soc*, **124,** 10539-10551.
52. Duer, M.J. (2004) *Introduction to solid-state NMR spectroscopy*. Blackwell Publishing, Malden, MA.
53. Prestegard, J.H. and Kishore, A.I. (2001) Partial alignment of biomolecules: an aid to NMR characterization. *Curr Opin Chem Biol*, **5,** 584-590.
54. Prestegard, J.H., Bougault, C.M. and Kishore, A.I. (2004) Residual dipolar couplings in structure determination of biomolecules. *Chem Rev*, **104,** 3519-3540.
55. Tjandra, N. and Bax, A. (1997) Direct measurement of distances and angles in biomolecules by NMR in a dilute liquid crystalline medium. *Science*, **278,** 1111-1114.
56. Sanders, C.R. and Schwonek, J.P. (1992) Characterization of Magnetically Orientable Bilayers in Mixtures of Dihexanoylphosphatidylcholine and Dimyristoylphosphatidylcholine by Solid-State Nmr. *Biochemistry*, **31,** 8898-8905.
57. Hare, B.J., Prestegard, J.H. and Engelman, D.M. (1995) Small angle x-ray scattering studies of magnetically oriented lipid bilayers. *Biophys J*, **69,** 1891-1896.
58. Chung, J. and Prestegard, J.H. (1993) Characterization of Field-Ordered Aqueous Liquid-Crystals by Nmr Diffusion Measurements. *J Phys Chem*, **97,** 9837-9843.
59. Vold, R.R. and Prosser, R.S. (1996) Magnetically oriented phospholipid bilayered micelles for structural studies of polypeptides. Does the ideal bicelle exist? *J Magn Reson Ser B*, **113,** 267-271.
60. Glover, K.J., Whiles, J.A., Wu, G.H., Yu, N.J., Deems, R., Struppe, J.O., Stark, R.E., Komives, E.A. and Vold, R.R. (2001) Structural evaluation of phospholipid bicelles for solution-state studies of membrane-associated biomolecules. *Biophys J*, **81,** 2163-2171.
61. Gaemers, S. and Bax, A. (2001) Morphology of three lyotropic liquid crystalline biological NMR media studied by translational diffusion anisotropy. *J Am Chem Soc*, **123,** 12343-12352.
62. Arnold, A., Labrot, T., Oda, R. and Dufourc, E.J. (2002) Cation modulation of bicelle size and magnetic alignment as revealed by solid-state NMR and electron microscopy. *Biophys J*, **83,** 2667-2680.
63. Nieh, M.P., Glinka, C.J., Krueger, S., Prosser, R.S. and Katsaras, J. (2001) SANS study of the structural phases of magnetically alignable lanthanide-doped phospholipid mixtures. *Langmuir*, **17,** 2629-2638.
64. Jonstromer, M. and Strey, R. (1992) Nonionic bilayers in dilute solutions: effect of additives. *J Phys Chem*, **96,** 5993-6000.

65. Tycko, R., Blanco, F.J. and Ishii, Y. (2000) Alignment of biopolymers in strained gels: A new way to create detectable dipole-dipole couplings in high-resolution biomolecular NMR. *J Am Chem Soc*, **122,** 9340-9341.
66. Sass, H.J., Musco, G., Stahl, S.J., Wingfield, P.T. and Grzesiek, S. (2000) Solution NMR of proteins within polyacrylamide gels: Diffusional properties and residual alignment by mechanical stress or embedding of oriented purple membranes. *J Biomol NMR*, **18,** 303-309.
67. Chou, J.J., Gaemers, S., Howder, B., Louis, J.M. and Bax, A. (2001) A simple apparatus for generating stretched polyacrylamide gels, yielding uniform alignment of proteins and detergent micelles. *J Biomol NMR*, **21,** 377-382.
68. Meier, S., Haussinger, D. and Grzesiek, S. (2002) Charged acrylamide copolymer gels as media for weak alignment. *J Biomol NMR*, **24,** 351-356.
69. Ulmer, T.S., Ramirez, B.E., Delaglio, F. and Bax, A. (2003) Evaluation of Backbone Proton Positions and Dynamics in a Small Portein by Liquid Crystal NMR Spectroscopy. *J Am Chem Soc*, **125,** 9179-9191.
70. Hansen, M.R., Mueller, L. and Pardi, A. (1998) Tunable alignment of macromolecules by filamentous phage yields dipolar coupling interactions. *Nat Struct Biol*, **5,** 1065-1074.
71. Hansen, M.R., Hanson, P. and Pardi, A. (2000) Pf1 filamentous phage as an alignment tool for generating local and global structural information in nucleic acids. *J Biomol Struct Dyn***,** 365-369.
72. Hansen, M.R., Hanson, P. and Pardi, A. (2000) Filamentous bacteriophage for aligning RNA, DNA, and proteins for measurement of nuclear magnetic resonance dipolar coupling interactions. *Methods Enzymol*, **317,** 220-240.
73. Ottiger, M. and Bax, A. (1998) Characterization of magnetically oriented phospholipid micelles for measurement of dipolar couplings in macromolecules. *J Biomol NMR*, **12,** 361-372.
74. Ottiger, M. and Bax, A. (1999) Bicelle-based liquid crystals for NMR-measurement of dipolar couplings at acidic and basic pH values. *J Biomol NMR*, **13,** 187-191.
75. Cavagnero, S., Dyson, H.J. and Wright, P.E. (1999) Improved low pH bicelle system for orienting macromolecules over a wide temperature range. *J Biomol NMR*, **13,** 387-391.
76. Losonczi, J.A. and Prestegard, J.H. (1998) Improved dilute bicelle solutions for high-resolution NMR of biological macromolecules. *J Biomol NMR*, **12,** 447-451.
77. Ruckert, M. and Otting, G. (2000) Alignment of biological macromolecules in novel nonionic liquid crystalline media for NMR experiments. *J Am Chem Soc*, **122,** 7793-7797.
78. Valafar, H., Mayer, K.L., Bougault, C.M., LeBlond, P.D., Jenney, F.E., Jr., Brereton, P.S., Adams, M.W.W. and Prestegard, J.H. (2005) Backbone solution structures of proteins using residual dipolar couplings: Application to a novel structural genomics target. *J Struct Func Genom*, **5,** 241-254.
79. Clore, G.M., Starich, M.R. and Gronenborn, A.M. (1998) Measurement of residual dipolar couplings of macromolecules aligned in the nematic phase of a colloidal suspension of rod-shaped viruses. *J Am Chem Soc*, **120,** 10571-10572.

80. Zweckstetter, M. and Bax, A. (2001) Characterization of molecular alignment in aqueous suspensions of Pf1 bacteriophage. *J Biomol NMR*, **20,** 365-377.
81. Koenig, B.W., Hu, J.-S., Ottiger, M., Bose, S., Hendler, R.W. and Bax, A. (1999) NMR measurement of dipolar couplings in proteins aligned by transient binding to purple membrane fragments. *J Am Chem Soc*, **121,** 1385-1386.
82. Sass, J., Cordier, F., Hoffmann, A., Rogowski, M., Cousin, A., Omichinski, J.G., Lowen, H. and Grzesiek, S. (1999) Purple membrane induced alignment of biological macromolecules in the magnetic field. *J Am Chem Soc*, **121,** 2047-2055.
83. Ishii, Y., Markus, M.A. and Tycko, R. (2001) Controlling residual dipolar couplings in high-resolution NMR of proteins by strain induced alignment in a gel. *J Biomol NMR*, **21,** 141-151.
84. Chou, J., Kaufman, J., Stahl, S.J., Wingfield, P. and Bax, A. (2002) Micelle-induced curvature in a water-insoluble HIV-1 Env peptide revealed by NMR dipolar coupling measurement in stretched polyacrylamide gel. *J Am Chem Soc*, **124,** 2450-2451.
85. Riley, S.A., Giuliani, J.R. and Augustine, M.P. (2002) Capture and manipulation of magnetically aligned Pf1 with an aqueous polymer gel. *J Magn Reson*, **159,** 82-86.
86. Trempe, J.F., Morin, F.G., Xia, Z.C., Marchessault, R.H. and Gehring, K. (2002) Characterization of polyacrylamide-stabilized Pf1 phage liquid crystals for protein NMR spectroscopy. *J Biomol NMR*, **22,** 83-87.
87. Wohnert, J., Franz, K.J., Nitz, M., Imperiali, B. and Schwalbe, H. (2003) Protein alignment by a coexpressed lanthanide-binding tag for the measurement of residual dipolar couplings. *J Am Chem Soc*, **125,** 13338-13339.
88. Ma, C. and Opella, S.J. (2000) Lanthanide ions bind specifically to an added "EF-hand" and orient a membrane protein in micelles for solution NMR spectroscopy. *J Magn Reson*, **146,** 381-384.
89. Bertini, I., Felli, I.C. and Luchinat, C. (2000) Lanthanide induced residual dipolar couplings for the conformational investigation of peripheral (NH2)-N-15 moieties. *J Biomol NMR*, **18,** 347-355.
90. Prosser, R.S., Volkov, V.B. and Shiyanovskaya, I.V. (1998) Novel chelate-induced magnetic alignment of biological membranes. *Biophys J*, **75,** 2163-2169.
91. Al-Hashimi, H.M., Valafar, H., Terrell, M., Zartler, E.R., Eidsness, M.K. and Prestegard, J.H. (2000) Variation of molecular alignment as a means of resolving orientational ambiguities in protein structures from dipolar couplings. *J Magn Reson*, **143,** 402-406.
92. Berthault, P., Jeannerat, D., Camerel, F., Salgado, F.A., Boulard, Y., Gabriel, J.C.P. and Desvaux, H. (2003) Dilute liquid crystals used to enhance residual dipolar couplings may alter conformational equilibrium in oligosaccharides. *Carbohydr Res*, **338,** 1771-1785.
93. Takai, Y., Sasaki, T. and Matozaki, T. (2001) Small GTP-binding proteins. *Physiol Rev*, **81,** 153-208.
94. Kahn, R.A. and Gilman, A.G. (1986) The Protein cofactor necessary for ADP-Ribosylation of GS by cholera toxin is itself a GTP binding-protein. *J Biol Chem*, **261,** 7906-7911.

95. Franco, M., Chardin, P., Chabre, M. and Paris, S. (1996) Myristoylation-facilitated binding of the G protein ARF1(GDP) to membrane phospholipids is required for its activation by a soluble nucleotide exchange factor. *J Biol Chem*, **271,** 1573-1578.
96. Lee, M.C.S., Miller, E.A., Goldberg, J., Orci, L. and Schekman, R. (2004) Bi-directional protein transport between the ER and Golgi. *Annu Rev Cell Dev Biol*, **20,** 87-123.
97. Murray, D., BenTal, N., Honig, B. and McLaughlin, S. (1997) Electrostatic interaction of myristoylated proteins with membranes: simple physics, complicated biology. *Structure*, **5,** 985-989.
98. Randazzo, P.A. (1997) Functional interaction of ADP-ribosylation factor 1 with phosphatidylinositol 4,5-bisphosphate. *J Biol Chem*, **272,** 7688-7692.
99. Seidel, R.D., Amor, J.C., Kahn, R.A. and Prestegard, J.H. (2004) Structural perturbations in human ADP ribosylation factor-1 accompanying the binding of phosphatidylinositides. *Biochemistry*, **43,** 15393-15403.
100. Nie, Z.Z., Hirsch, D.S. and Randazzo, P.A. (2003) Arf and its many interactors. *Curr Opin Cell Biol*, **15,** 396-404.

# CHAPTER 2

# MOLECULAR ORIENTATION AND CONFORMATION OF PHOSPHATIDYLINOSITIDES IN MEMBRANE MIMETICS USING VARIABLE ANGLE SAMPLE SPINNING (VASS) NMR[1]

[1]Kishore, A.I. & J.H. Prestegard. *Biophysical Journal.* 85:3848-3857 (2003).
Reprinted here with permission of publisher.

ABSTRACT

For many biological molecules, determining their geometry as they exist in a membrane environment is a crucial step in understanding their function. Variable angle sample spinning (VASS) NMR provides a new route to obtaining geometry information on membrane-associating molecules; it has been used here to scale and separate anisotropic contributions to phosphorus chemical shifts in NMR spectra of phosphatidylinositol phosphates. The procedure allows spectral assignment via correlation with isotropic chemical shifts and determination of a family of probable headgroup orientations via interpretation of anisotropic shift contributions. The molecules studied include phosphtidylinositol-4-phosphate (PI(4)P) and phosphatidylinositol (4,5)-bisphosphate ($PI(4,5)P_2$). A membrane-like environment is provided by a dispersion of alkyl-poly(ethylene) glycols and *n*-alcohols that forms a field-orienting liquid crystal with a director that can be manipulated by varying the sample spinning axis. The experiments presented indicate that the VASS method will provide a direct approach for assignment and extraction of structural information from membrane-associating biomolecules labeled with a wider variety of NMR active isotopes.

## 2.1 INTRODUCTION TO VASS AND MEMBRANE-ANCHORED MOLECULES

NMR methods of structure determination offer much promise for the study of biomolecules embedded in membrane environments. Among other factors, they do not require the molecules of interest to crystallize, and media resembling native membrane systems can be used. Despite recent advances in both high-resolution solution and solid-state NMR spectroscopy, however, characterizing strongly ordered biomolecules remains a challenging task. Here we present an NMR-based method for the study of membrane-associating systems that allows the integration of high-resolution solution NMR chemical shift assignments with the angular information accessible in oriented systems. The applications presented here are on simple phosphatidylinositol phosphates embedded in membrane arrays, but extension to membrane protein systems is possible.

The approach presented here extracts conformation-dependent offsets from the chemical shift using variable angle sample spinning (VASS). Unlike magic angle spinning in solid-state NMR, in which the sample is fixed at one angle with respect to the magnetic field, in VASS, the rotation axis varies. VASS can be used both to scale and to separate anisotropic contributions to spectra in compounds ordered in liquid crystalline arrays (1). The isotropic contributions can be correlated with solution or high-resolution solids spectra to make resonance assignments, and the anisotropic contributions can be extracted to restrain molecular geometry. The VASS technique can be widely applied to study both liquid crystals themselves (2) as well as biomolecules oriented within such systems without the demands of conventional solid-state experiments. Fast spinning rates, typical of solid-state experiments, are not required to average anisotropy; rapid axially symmetric motion of a molecule oriented in a liquid crystal reduces effective

chemical shift anisotropies (CSAs) and dipolar couplings by more than an order of magnitude such that slow spinning speeds (300-3000 Hz) and low decoupling powers can be employed. VASS has previously been demonstrated to scale the CSA in a small organic molecule (3) and to determine the sign of dipolar couplings in a peptide (4). A recent extension employs two-dimensional switched angle spinning. This technique requires a rapid change in sample orientation with respect to the magnetic field during the experiment; the resulting 2D data has been used to correlate anisotropic contributions to spectra with isotropic resonance positions (5) and to obtain structural information on a peptide oriented in a lipid bilayer (6). In this paper we simply map resonance positions as a function of spinning angle to assign the multiple phosphorus resonances in strongly oriented phosphatidylinositol phosphates and to determine the anisotropic offsets to the chemical shift that can be used to restrict headgroup orientations with respect to the membrane surface.

Phosphatidylinositol phosphates, or phosphatidylinositides, occur at low levels in many biological membranes where they serve as second messengers in the regulation of a wide variety of cellular processes.

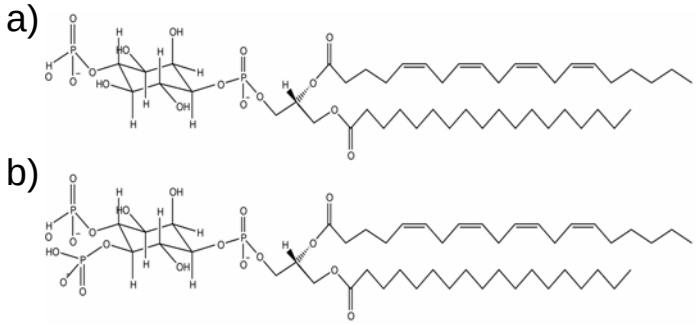


Figure 2.1. Phosphatidylinositol phosphates occur in different phosphorylation states: a) phosphatidylinositol-4-phosphate b) phosphatidylinositol-4,5-bisphosphate.

More recently, their role in recruiting proteins to the membrane, in particular those with pleckstrin homology (PH) domains (7), has been investigated. There is also an interesting hypothesis involving the activation of ADP Ribosylation Factor 1 (ARF1) at the membrane surface. ARF1, a ubiquitous 21 kDa eukaryotic protein involved in membrane trafficking, uses its N-terminal myristoyl group to transiently associate with the cell membrane. It has been suggested that ARF1 specifically interacts with the headgroup of phosphatidylinositol bisphosphate ($PI(4,5)P_2$) (8,9), the major polyphosphatidylinositide found in mammalian cells (10). With its large negative charge and specific phosphorylation sites, $PI(4,5)P_2$ may help recruit ARF1 to the membrane. Knowing phosphatidylinositide headgroup geometry at the membrane surface may help explain exactly how these proteins are targeted to the membrane. Here we use a combination of experimental and computational methods to illustrate how chemical shift offsets obtained from VASS provide orientational restraints on two specific phosphatidylinositides, phosphtidylinositol-4-phosphate (PI(4)P) and phosphatidylinositol bisphosphate ($PI(4,5)P_2$), embedded in a membrane-like bilayer.

The three chemically distinct phosphorus nuclei in $PIP_2$ (Figure 2.1b) make this lipid ideal to study in a liquid crystal as their large CSAs permit the anisotropy offsets to be measured with VASS. CSA offsets combined with molecular models based on phospholipid geometry provide sufficient data to suggest possible membrane-bound conformations of $PIP_2$. When the interaction of ARF with the membrane has been characterized, the orientation of the $PIP_2$ with respect to ARF and the membrane can be determined. This data will report directly on motion and as well as be an indicator of binding to ARF because for axially symmetric order the chemical shift offset or $\Delta\delta$ is

$$\Delta\delta = -2/3\ \Delta\sigma S_{zz}$$

where $\Delta\sigma = \sigma_{II} - \sigma_{\perp}$ and $S_{zz}$ is the order parameter in the principal axis system. The orientation of $PIP_2$ anchored to a membrane and bound to ARF may help explain its role in vesicular trafficking.

## 2.2 VASS THEORY

It is important to understand the connection between anisotropic contributions to phosphorus chemical shifts and molecular geometry constraints. The chemical shift of phosphate esters varies with orientation in a magnetic field due to the anisotropy of the group's electronic distribution; this gives rise to a chemical shift anisotropy (CSA) contribution. If the group tumbles rapidly and samples orientations uniformly, shifts are averaged to the positions observed for resonances in high-resolution solution NMR, $\delta_{iso}$. If the group has a preferred orientation, as it would when anchored to an oriented array of membrane mimetics, resonances are offset by an anisotropic contribution to isotropic chemical shifts, $\Delta\delta_{aniso}$. These offsets are measurable and can be used to place constraints on geometries of molecular models. For the case of an ordered array of bilayer fragments, $\Delta\delta_{aniso}$ can be expressed as

$$\begin{aligned}\Delta\delta_{aniso} &= \delta_{oriented} - \delta_{isotropic} \\ &= 1/3\ S_{bilayer}\ \{(<3\cos^2\theta_1 - 1>) \bullet (\delta_{11} - \delta_{22}) + (<3\cos^2\theta_3 - 1>) \bullet (\delta_{33} - \delta_{22})\} \qquad (1)\end{aligned}$$

where $S_{bilayer}$ is the order parameter of the bilayer (which includes a factor of -1/2 when the bilayer normal is perpendicular to the liquid crystal director axis), $\delta_{ii}$ are the principal values of the static chemical shift tensor, $\theta_i$ are the angles between the bilayer normal and the principal axes of the chemical shift tensor, and the brackets account for additional averaging due to molecular motion. When shift tensors are axially symmetric, these

equations become identical to those relating dipolar couplings to molecular geometry, and procedures similar to those for extracting geometrical information from dipolar couplings can be used to analyze conformational constraints from anisotropic contributions to the chemical shift. The values of $\delta_{ii}$ are well defined in a frame oriented in an individual phosphate ester group. The values and directions of principal axes can, therefore, be taken from suitable model compounds (11). The angles $\theta_i$ of these axes relative to the magnetic field actually depend on molecular geometry through the way in which each phosphate is oriented (Figure 2.1): first, by the phosphate's connection to the inositol ring, second, by the way the ring is oriented in its connection to a diacylglycerol moiety, and third, by the way this moiety is inserted into the membrane. Orientations for phosphate groups allowed by a particular molecular geometry can be used to calculate shift offsets, $\Delta\delta_{aniso}$, and these can be compared to experimental values to eliminate disallowed geometries.

For chemical shift anisotropy data, there is a complication in extracting $\Delta\delta_{aniso}$ from experimental data. This arises because $\Delta\delta_{aniso}$ often dominates resonance positions making it difficult to assign resonances to particular phosphate groups. One way to separate $\Delta\delta_{aniso}$ and $\delta_{iso}$ is to apply VASS to a molecule oriented through its interaction with a liquid crystal. VASS exploits the ability to redefine the direction of principal order relative to the magnetic field by spinning a liquid crystal at particular angles relative to the field (12).

Liquid crystals have been used extensively as solvents in which to determine the CSA of dissolved solute molecules (13). When static, liquid crystals orient in a magnetic field depending on the anisotropy in magnetic susceptibility of a liquid crystal domain,

$\Delta\chi$. In VASS the spinning rate must be fast enough to prevent reorientation of liquid crystal directors during rotation and slow enough to prevent centrifugation of sample. When spinning, the liquid crystal director orients to balance the magnetic and viscous torques on the liquid crystal, ideally aligning either parallel or perpendicular to the spinning axis, depending on the sign of $\Delta\chi$ and the angle the sample makes with respect to the magnetic field (12).

The chemical shift offset under VASS now becomes, in addition, a function of the angle of the spinning axis with respect to the magnetic field, $\beta$, as seen in Eq. 2 and 3. Contributions to spectra are slightly different depending on whether the liquid crystal director is parallel or perpendicular to the spinning axis (1). When the angle $\beta$ is less than the magic angle and $\Delta\chi < 0$, or $\beta$ is more than the magic angle and $\Delta\chi > 0$, the anisotropy is scaled by an additional factor of -½.

$\Delta\chi > 0$: $0° < \beta < 54.7°$
$\Delta\chi < 0$: $54.7° < \beta < 90°$

$$\delta_{exp} = \delta_{iso} + \tfrac{1}{2} ( 3 \cos^2 \beta - 1) \Delta\delta_{aniso} \quad (2)$$

$\Delta\chi > 0$: $54.7° < \beta < 90°$
$\Delta\chi < 0$: $0° < \beta < 54.7°$

$$\delta_{exp} = \delta_{iso} - \tfrac{1}{4} ( 3 \cos^2 \beta - 1) \Delta\delta_{aniso} \quad (3)$$

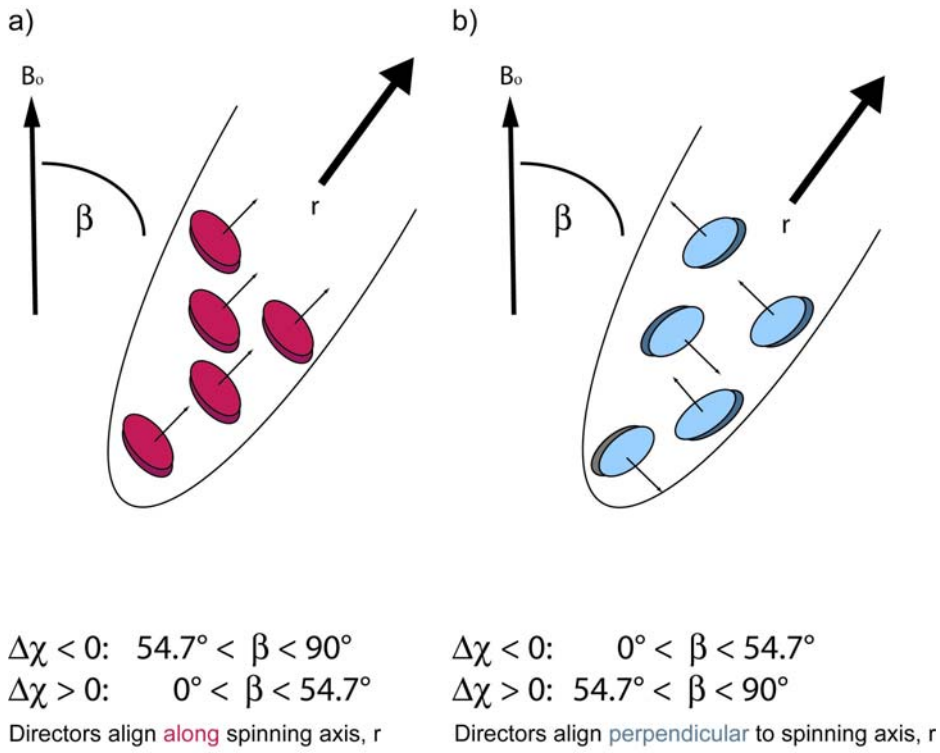


Figure 2.2. Liquid crystalline directors reorient with mechanical spinning in a magnetic field. a) Directors align along the spinning axis for liquid crystals of negative anisotropy of susceptibility ($\Delta\chi<0$) at angles greater than the magic angle and for liquid crystals of positive ($\Delta\chi>0$) at angles less than the magic angle. b) Directors align perpendicular to the spinning axis for liquid crystals with $\Delta\chi<0$ at angles less than the magic angle and for liquid crystals with $\Delta\chi>0$ at angles greater than the magic angle.

In our case we use a liquid crystal of negative anisotropy of susceptibility, or $\Delta\chi<0$, and the liquid crystal director "flips" orientation from being parallel to perpendicular to the spinning axis upon moving from angles greater than the magic angle to angles less than the magic angle (12) as seen in Figure 2.2. From these equations it is clear that a plot of $\delta_{exp}$ versus $(3\cos^2\beta - 1)$ can be used to separate $\delta_{iso}$ and $\Delta\delta_{aniso}$.

### 2.2.1 LIQUID CRYSTALLINE DIRECTOR ALIGNMENT

The choice of a liquid crystal as an aligning medium for a biomolecule is critical (14,15), particularly in the application of VASS. Nematic liquid crystals align

cooperatively along one axis such that their long axes are parallel to each other. Alignment in a magnetic field is based on the interaction of the magnetic dipole moment with the magnetic susceptibility tensor, $\chi$. The energy of interaction with the field:

$$E= (1/\mu) (-½ B_o \cdot \chi \cdot B_o)$$

emphasizes the field-dependency of alignment. A unit vector called the director refers to the preferred orientation of the long axis of the liquid crystal. The direction of the liquid crystal director, or main axis of symmetry, is fixed for a given liquid crystal in a magnetic field, but can be manipulated by mechanical spinning in a magnetic field. Changing the orientation of the director by spinning at different angles, the principle behind VASS NMR, simplifies complex, second order spectra without destroying anisotropic parameters. For example, in a strongly ordered liquid crystal system such as a glycolipid anchored to a liquid crystalline membrane, a proton-coupled carbon spectrum is impossible to analyze due to abundant C-H and H-H dipolar couplings when the director is aligned with the magnetic field. However, when the director aligns along the spinning axis, it is possible to scale these couplings by $(3 \cos^2 \theta - 1)$. The result is well-resolved spectra with a measurable degree of anisotropy of the oriented molecule.

## 2.3 MATERIALS AND METHODS

### 2.3.1 SAMPLE PREPARATION

A number of phospholipid-based liquid crystalline systems exist for orienting biomolecules. For the phosphatidylinositides studied in this preliminary application of the VASS technique, we chose a bilayered liquid crystal (16-18) with no phosphorus atoms in order to reduce problems with background $^{31}P$ signals. When combined in specific ratios with *n*-alcohols, aqueous solutions of poly(ethylene) glycol ethers form

bilayers that align in a magnetic field (16,19). These bilayer systems have a negative anisotropy of susceptibility and orient with their normal perpendicular to the field. Homogenous orientations of a liquid crystalline phase composed of 17.7% (w/w) pentaethylene glycol monododecyl ether ($C_{12}E_5$) and 5.2% hexanol (r = 0.87, where r is the molar ratio of poly(ethylene)glycol:alcohol) in water and of a similar liquid crystalline phase composed of 17.1% (w/v) pentaethylene glycol octyl ether ($C_8E_5$) and 5.5% (w/w) octanol in water (r=1.17) were found to occur in the temperature range from 21-28˚C. All chemicals were purchased from Sigma (Sigma-Aldrich Corp., St. Louis, MO) and used without further purification. Pure PI(4)P (phosphatidylinositol-4-phosphate) and PI(4,5)$P_2$ (phosphatidylinositol 4,5-bisphosphate, both from Avanti Polar Lipids, (Alabaster, AL)) were dried under a stream of nitrogen and dispersed into the bilayers in low molar ratios (where PIP:$C_nE_m$ is 1:100 - 1:200) so that interactions between phosphatidylinositide molecules would be weak and the bilayer order would not be disrupted.

### 2.3.2 INSTRUMENTATION

$^{31}$P VASS spectra were collected at 202.6 MHz on a 500 MHz Varian Inova spectrometer using a Doty Scientific XC5 VASS probe (Doty Scientific, Inc., Columbia, SC) at several angles (90°-20°) of the spinning axis relative to the magnetic field. The angle was adjusted to within 2° of the indicated angle by starting from the magic angle (determined using KBr) and adjusting the angle-controlling dial on the probe, previously calibrated to give a change in 10° for one rotation of the dial. The $^{31}$P 90° pulse length varied from 7 μs at large angles to 12 μs at small angles as expected for the probe's solenoid coil. Waltz $^{1}$H decoupling was applied during acquisition. The recycle time

was 2.0 s, and the number of scans varied for each angle from 1000-12000 depending on the signal-to-noise ratio at a given angle. Spinning speeds from 300-3000 Hz were used, and the spinning rate was controlled to within 2 Hz by a spin rate Probe Controller (Doty Scientific, Inc., Columbia, SC). Initially $^{31}P$ chemical shifts were measured relative to an internal signal from 10 mM inorganic phosphate (pH 7.4) and then referenced to 85% phosphoric acid by subtracting 1.579 ppm. The strong $^{31}P$ signal from inorganic phosphate occasionally obscured resonances from the phosphomonoesters, making assignment difficult in some samples. A non-phosphate buffer (10mM TES, 50mM NaCl, 10% $D_2O$, pH 7.2) aided in assignment of resonances in these samples. Samples without inorganic phosphate were referenced indirectly by correlating the water resonance frequency in these samples to that in a phosphate-containing sample examined immediately before and after the $^{31}P$ observation (20). The degree of sample ordering and homogeneity was monitored through $^{2}H$ quadrupolar splittings from 10% $D_2O$ added to all samples using the VASS probe tuned to $^{2}H$ (76.8 MHz).

### 2.3.3 CHEMICAL SHIFT OFFSET ANALYSIS

To aid in the analysis of experimental data, chemical shift offsets for the phosphomonoesters and diesters were calculated for models of both PI(4)P and PI(4,5)$P_2$. Energy-minimized models were rotated about a pair of torsion angles ($\alpha 1$ and $\alpha 1'$) as defined in Fig. 2 in steps of 10°. For each model produced in this systematic conformational search, chemical shift offsets were calculated. This calculation relies on the successive transformation of the phosphate chemical shift tensor in its principal axis frame first to the local phosphatidylinositide molecular frame, second to an axially averaged bilayer normal frame, and third to the laboratory frame. In order to eliminate

$S_{bilayer}$ and any additional axially symmetric averaging, monoester shifts were scaled relative to the diester shift at each point. A program was written in Maple (Maple 7.0, Waterloo Maple Inc., Waterloo, Ontario) to carry out these transformations and to calculate chemical shifts.

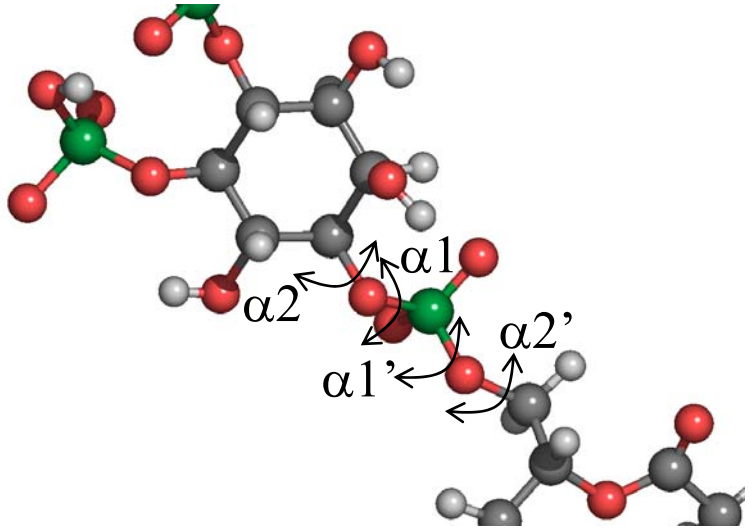


Figure 2.3. $PI(4,5)P_2$ showing the dihedral angles of greatest variability. (Acyl chains and 4-phosphate have been truncated for clarity.) Atoms are color-coded as follows: carbon, gray; oxygen, red; phosphorus, green, hydrogens, white.

The root mean square deviation between the calculated chemical shift offsets and the experimentally observed chemical shift offsets was calculated at each combination of angles and for each phosphate ester under consideration. Structures having rmsd values within estimates of experiment were filtered through steric constraints imposed at normal van der Waals radii. To accomplish this filtering, a systematic conformational search of the phosphatidylinositide structures about selected torsion angles was performed in the molecular modeling program Sybyl (Sybyl 6.7, Tripos Inc., St. Louis, MO), and conformations generated with significant van der Waals radii overlap were eliminated.

Typically in these calculations electrostatic terms were turned off, and an energy cut off of 5 kcal/mol over the minimum conformationally-dependent energy was used.

## 2.4 RESULTS

The stacked plot in Figure 2.4 shows $^{31}P$ NMR spectra of PI(4)P (Figure 2.4A) and PI(4,5)$P_2$ (Figure 2.4B) collected at different spinning angles with respect to the magnetic field; it illustrates how VASS systematically scales the chemical shift offset. One of the first tasks was to assign the resonances to various phosphate sites. This cannot usually be done directly from spectra dominated by anisotropic offsets because they are highly geometry-dependent and can obscure the purely chemical information dominating isotropic shift values. Extrapolation of anisotropic offsets to their isotropic shifts using VASS makes their assignment easier. For PI(4)P and PI(4,5)$P_2$ the difference between the phosphodiester and phosphomonoester signals, both in isotropic and oriented spectra, is large enough to allow the assignment of the upfield shifted resonance to the diester by analogy to other phosphodiesters (21). In Figure 2.4, the diester peak is labeled D. In PI(4,5)$P_2$, distinguishing the two monoesters is more difficult. In detergent micelles, their isotropic chemical shifts are distinct due to their different degrees of ionization at the pH of observation (22). Their assignment is given in Figure 2.4d, the analogous isotropic magic angle spectrum, and this is denoted by the labels M4 and M5 for monoester 4 or 5. In the oriented bilayers, separation in chemical shifts for these two resonances persisted at all angles, but if we were limited to data at only one angle, we could not assume assignments would fall in the same order; the movement of both resonances from 36°-54.7° or 54.7°-90° is, in fact, larger than their chemical shift difference, and an exchange of positions is possible. Following the

movement as a function of angle allows an unambiguous assignment as indicated in Figure 2.4. The large $^{31}P$ signal in all spectra is due to phosphate buffer at pH 7.4. This signal provided a chemical shift reference in oriented spectra, but occasionally obscured the monophosphates' signals. In these cases, a phosphate-free buffer at pH 7.2 was used.

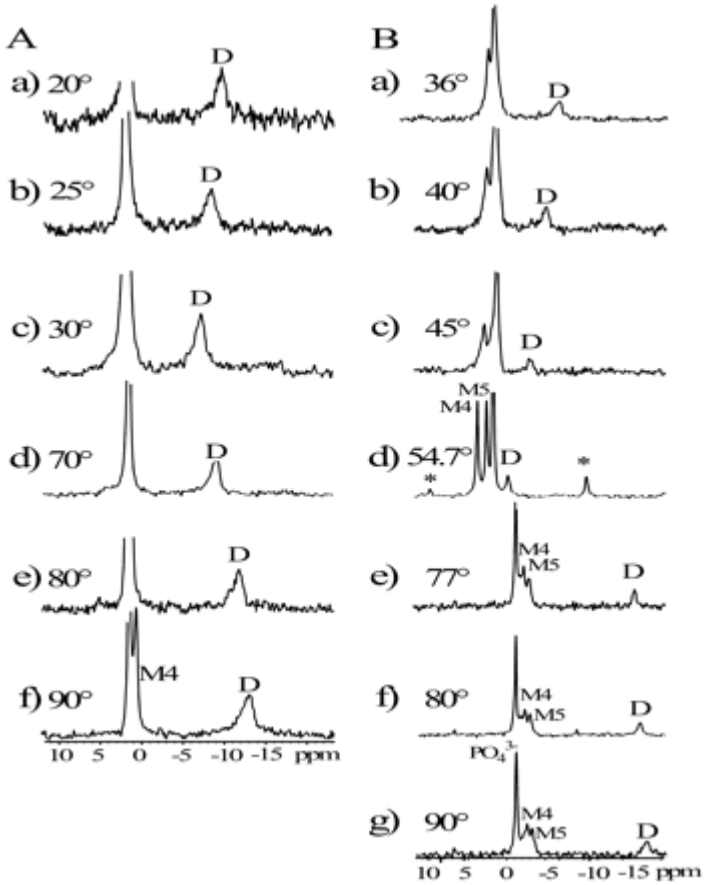


Figure 2.4. $^{31}P$ spectra of A) PI(4)P oriented in 17% (w/w) $C_{12}E_5$/*n*-hexanol (5.5% w/w, 1:200, PI(4)P, $C_{12}E_5$) at 25°C ± 1 at 2000 Hz spinning rate. Phosphomonoester (M) and diester (D) peaks are indicated in the figure and readily identifiable by their distinctive chemical shifts. Spinning sidebands are marked by asterisks. Each spectrum was collected at the angle indicated in the figure. B) PI(4,5)$P_2$ oriented in 17% (w/w) $C_{12}E_5$/*n*-hexanol (5.5%, w/w, 1:200, PI(4,5)$P_2$:$C_{12}E_5$) at 24°C ± 1. Spectra a)-d) were collected at a spinning rate of 2000 Hz, and spectra e)-g) were collected at an 800 Hz spinning rate.

Spectra recorded at angles less than 54.7º (a-c) showed lower signal-to-noise due to the angle of the field relative to the axis of the solenoid coil built into the VASS stator. At these angles the liquid crystal director is oriented perpendicular to the spinning axis and modulation of chemical shift by spinning can further degrade signals. Some loss of signal could also be the result of a mosaic spread of the director orientation (4,23) and the associated appearance of a partial powder pattern; this spread and the appearance of weak sidebands observed at lower spinning rates compromise spectral quality. Significant sidebands also appear when the sample spinning axis is close to the magic angle (54.7° ± 10.0°) due to the disordering of liquid crystal domains; sidebands to the diester peak are shown with an asterisk (*) in Figure 2.4d. Most data points were collected at higher spinning rates and away from the magic angle to avoid effects of disorder. It is interesting to note that the direction of shift, as a function of angle, changes at the magic angle. The diester peak, for example, moves upfield with decreasing angle in the range 0-54.7° but downfield with decreasing angle in the range 54.7-90°. This is a result of a change in liquid crystal director axis from parallel to the spinning axis above 54.7° to perpendicular to the axis below 54.7°.

The predicted angular dependence given in Eq. 2 and 3 can be used to systematically correlate observed chemical shifts to their isotropic shifts. Figure 2.5 shows the linear dependence of the chemical shift on the scaling factor $(3 \cos^2 \beta - 1)$. Using Eq. 2 and 3, the isotropic chemical shifts and chemical shift offsets were evaluated by a least squares fit to the data for PI(4)P and PI(4,5)$P_2$. The extrapolated isotropic chemical shifts calculated from VASS data agree very well within estimated error to the isotropic shifts obtained from magic angle experiments (spinning at 54.7°) or micellar

solution as indicated in Table 1. However, the angular dependence of chemical shift offsets is not always as simple as depicted in Figure 2.5. It has been noted that liquid crystal director alignment can deviate from ideal behavior at certain spinning rates (24,25). In particular, at spinning rates other than those used here, the flip of the director can occur at angles other than the magic angle, and at very fast spinning rates the director may not change direction at all due to centrifugal torque. At the spinning rates employed in this study (300-3000 Hz), we observed the director "flipping" from one side to the other very near the magic angle. However, extrapolated isotropic chemical shifts from the low side of the magic angle did not always agree with chemical shifts from the high side of the magic angle or isotropic chemical shifts observed in micellar spectra. The point at which the theoretical curves for extrapolating isotropic chemical shifts cross in Figure 2.5 is at an angle about 4° off the magic angle. This small uncertainty could be mechanical in origin, due to error in the calibration of the angle, or it could result from this more complicated behavior of the liquid crystal director axis. Additional effects also appeared at lower spinning rates. At the spinning rates given in Figure 2.4-2.5, both the diester and monoester peaks were well resolved, showed minimal spinning sidebands, and yielded acceptable, extrapolated isotropic chemical shifts.

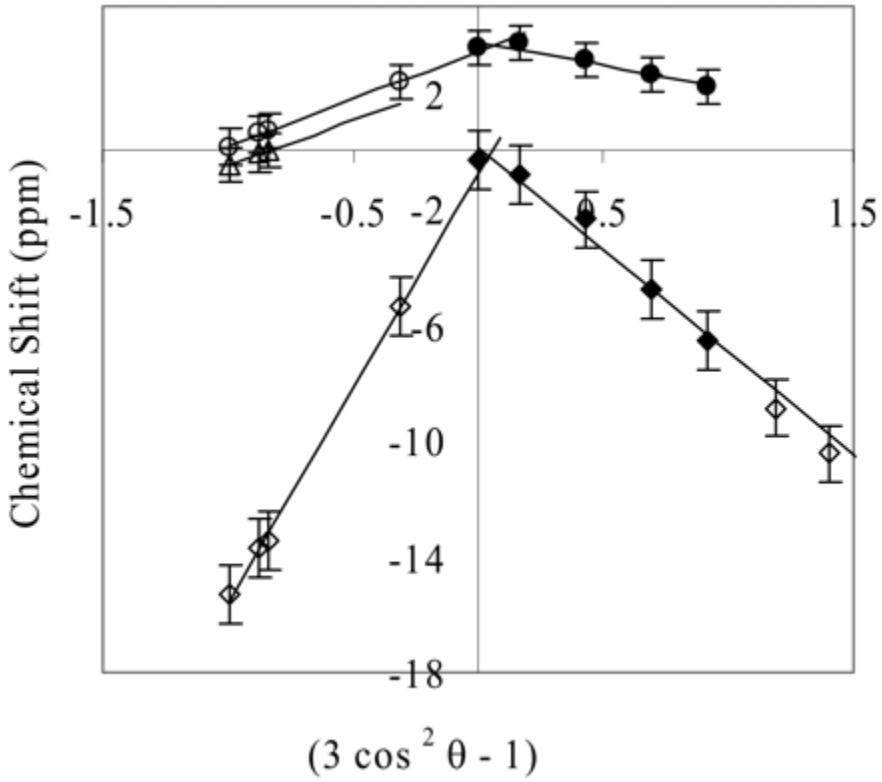


Figure 2.5. $^{31}$P chemical shifts as a function of (3 cos $^2$ β -1). Isotropic chemical shifts of the phosphorus atoms were calculated from the chemical shift offsets by extrapolating their linear dependence on (3 cos $^2$ β -1) to the magic angle. ○ represents the monoester-4 at 800 Hz, • represents the monoester-4 at 2000 Hz, Δ represents the monoester-5 at 800 Hz, ◊ represents the diester at 800 Hz, and ♦ represents the diester at 2000 Hz.

Table 1. Chemical shift offsets and isotropic chemical shifts of phosphatidylinositides[##]

| Phosphate group | Calculated $\delta_{iso}$ (ppm)[*] | Observed $\delta_{iso}$ (ppm)[#] | Observed $\delta_{iso}$ (ppm)[§] | Calculated $\Delta\delta_{aniso}$ (ppm)[¶] | Calculated $\Delta\delta_{aniso}$ (ppm)[**] |
|---|---|---|---|---|---|
| $PI(4,5)P_2$ (monoester-4) | 3.5 ± 0.3 | 3.6 ± 0.1 | 3.5 ± 0.1 | 6.8 ± 0.1 | 8.2 ± 0.2 |
| $PI(4,5)P_2$ (monoester-5) | 2.3 ± 0.1 | 2.4 ± 0.1 | 2.4 ± 0.1 | 5.3 ± 0.5 | -- |
| $PI(4,5)P_2$ (diester) | -0.9 ± 0.4 | -0.3 ± 0.1 | -0.4 ± 0.1 | 29.0 ± 0.5 | 25.4 ± 0.6 |
| PI(4)P (monoester) | 3.3 ± 0.1 | 3.5 ± 0.1 | -- | 5.5 ± 0.1 | 4.9 ± 0.1 |
| PI(4)P (diester) | -0.3 ± 0.2 | -- | -- | 28.3 ± 0.1 | -- |

[*] Isotropic chemical shift calculated from VASS data.
[#] Isotropic chemical shift observed from magic angle spinning spectrum.
[§] Isotropic chemical shift observed from micellar solution.
[¶] VASS-calculated CSA for ($\beta > \beta_m$), where $\beta$ is the angle the sample makes with the magnetic field and $\beta_m$ is the magic angle.
[**] VASS-calculated CSA for ($\beta < \beta_m$).
[##] Errors given for $\delta_{iso}$ and $\Delta\delta_{aniso}$ are standard deviations from a least squares fit of the data to a linear equation; other errors reported are experimental errors estimated from spectral resolution.

## 2.5 DISCUSSION

The limited number of restraints available from the data in Table 1 (two $\Delta\delta_{aniso}$ from PI(4)P and three $\Delta\delta_{aniso}$ from $PI(4,5)P_2$), precludes a direct extraction of molecular geometry. Experimental chemical shift offsets were therefore compared to calculated chemical shift offsets that could be observed, given reasonable geometry restrictions, for a phosphatidylinositide inserted into a membrane. We chose to model the phosphatidylinositides and apply normal van der Waals radius constraints to limit the number of possible solutions to headgroup geometry. We then calculated the chemical

shift offsets as a function of a small set of rotatable torsion angles. Molecular modeling programs were used to construct molecules with an appropriate starting geometry. First, models of PI(4)P and PI(4,5)$P_2$ were generated and minimized in Sybyl and found to yield the idealized phosphatidylinositol geometry, $\alpha 2' = 180°$, $\alpha 1' = 180°$, $\alpha 1 = 180°$, $\alpha 2 = -60°$ (26). Electrostatic charges, both partial and formal, were set to zero in this minimization to eliminate problems that could stem from poor representation of electrostatics in these amphiphilic, membrane-associating molecules. From the starting model described above, a series of molecular models for molecular orientations of the headgroup was generated by performing a systematic conformational search about the three dihedral angles connecting the head group to the bilayer: $\alpha 1$, and $\alpha 1'$, and $\alpha 2$ shown in Fig. 2. $\alpha 2'$ was assumed to be rigid based on a lack of variation in model phospholipids, and its value (180º) was fixed based on the suggested ideal orientation of PI(4)P in a membrane bilayer (26). Other torsion angles of the phosphatidylinositide are likely to be severely restricted due to burial in the bilayer. The search produced a number of possible conformations based on allowable van der Waals contacts. Here we applied a cut off energy of approximately 5 kcal/mol above the minimum energy structure to select a set of sterically allowed conformations.

For the chemical shift offset calculations, another series of models consistent with Sybyl geometry was generated. First, inositol phosphate models of the headgroups were built using the MM2 package in Chem3D (CambridgeSoft Corporation 4.0, Cambridge, MA). Comparison to experimentally determined inositol phosphate crystal structures revealed that the gas phase MM2 force field did not distort the geometry of inositol phosphates significantly (27). Though all bonds may experience some degree of

flexibility, those in the headgroup ring can certainly be assumed to be rigid. The inositol phosphate models were added to one of the diacylglycerol conformers found in the unit cell of dimyristoylphosphatidylcholine (DMPC) (28) to produce the same starting geometry as in the Sybyl structures.

Calculations of chemical shift offsets for each of the models proceeded by first assigning CSA tensors to each phosphate. The principal values of the phosphodiester chemical shift tensor were taken from single crystal, solid-state, NMR studies of dipalmitoylphosphatidylcholine, DPPC (29), and elements of the static monoester chemical shift tensor were taken from serine phosphate (30). In the case of the monoesters, chemical shift tensors were made axially symmetric to mimic rotation about the O-P ester bonds. Chemical shift offsets were then calculated for all models by applying a series of coordinate transformations from the phosphate principal axis frame into the laboratory frame. The time-averaged orientations of the acyl chains are assumed parallel to the bilayer normal, consistent with previous assumptions of membrane-associating species (31).

Calculated chemical shift offsets for each phosphate group in all headgroup orientations were compared to the VASS-determined chemical shift offsets. Since $S_{bilayer}$ in Eq. 1 is not known for the liquid crystals used in these experiments, the ratio of the calculated monoester to calculated diester chemical shift offset for each orientation was compared to the ratio of the experimentally observed monoester to experimentally observed diester chemical shift offset. Root mean square deviation between calculated and observed chemical shift offsets for the monoesters below an estimated error of 5 ppm was used to restrict possible headgroup geometries. This error limit is larger than

experimental error (about 1 ppm), and larger than propagated experimental errors from static model compound tensors (32); it is meant to account for some uncertainty in selection of proper model compounds.

Because calculating chemical shift offsets as a function of multiple torsion angles becomes computationally expensive, we chose to first restrict $\alpha 2$ to one of several representative geometries allowed by van der Waals constraints. The Sybyl systematic conformational search for van der Waals restraints with an energy spread of 5 kcal/mol above the minimum energy conformation yielded a bimodal distribution of $\alpha 2$ values for PI(4)P centered around -80 ± 15° and -145 ± 15° (data not shown). A similar distribution of $\alpha 2$ values for PI(4,5)$P_2$ was also obtained. These values of $\alpha 2$ were used in chemical shift calculations for both PI(4)P and PI(4,5)$P_2$. Points with root mean square deviation between the calculated and observed chemical shift offsets less than 5 ppm are shown for PI(4)P with $\alpha 2$ = -80° in Figure 2.6. No geometries were allowed within the 5.0 ppm rmsd cutoff for $\alpha 2$ = -145°. The allowed geometries shown in Figure 2.6 fall into three families of possible orientations. These are dispersed in conformational space and the angular ranges in two of the families are broad due to the small number of experimental constraints. For PI(4,5)$P_2$ chemical shift calculations as a function of $\alpha 1$ and $\alpha 1'$ at $\alpha 2$ values of -80° and -145° and are shown in Figure 2.7a and 2.7b, respectively. The geometries allowed based on chemical shift offset observation (within a 5.0 ppm cut off) are equally broad in the case of $\alpha 2$ = -145° (Figure 2.7b), but more restrained in the case of $\alpha 2$ = -80° (Fig 2.7a). The latter is in line with the existence of more experimental restraints for the bisphosphate.

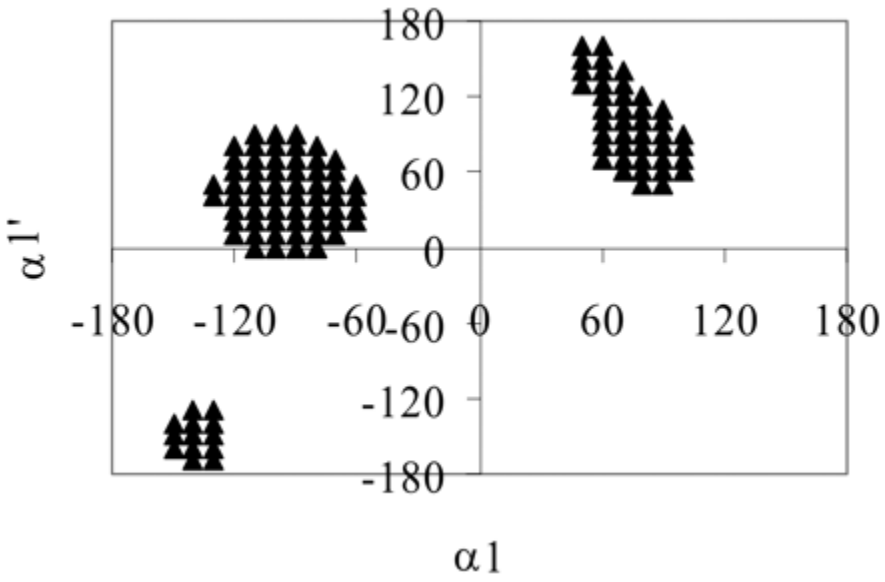


Figure 2.6. PI(4)P conformers as a function of α1 and α1' for fixed α2 = -80° having a root mean square error difference between calculated and observed chemical shift offsets of 5.0 ppm or less. Points have not been filtered by applying van der Waals constraints.

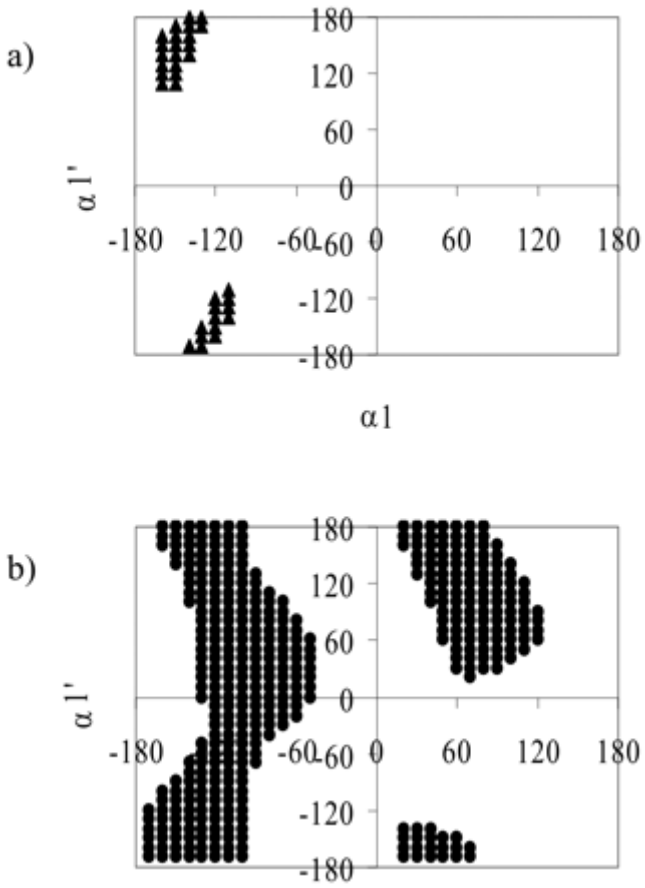


Figure 2.7. PI(4,5)$P_2$ conformers as a function of α1 and α1' having a root mean square error difference between calculated and observed chemical shift offsets of 5.0 ppm or less. a) fixing α2 = -80° and b) fixing α2 = -145°.

Filtering the structures allowed by chemical shift offset data through results from Sybyl energy calculations further restricted geometries and allowed a more precise determination of orientation. Figure 2.8 shows the results of filtering chemical shift offsets allowed for PI(4)P and PI(4,5)$P_2$ structures through the steric filter provided by a 5 kcal/mol energy cut off in Sybyl. For PI(4)P (Figure 2.8a) there are significant reductions in allowed conformational space, but several distinctly different α1, α1' combinations remain. For PI(4,5)$P_2$, there are also reductions in allowed conformational space for both α2 = -80° (Figure 2.8b) and α2 = -145° (Figure 2.8c), and only a few well-defined combinations of α1 and α1' remain.

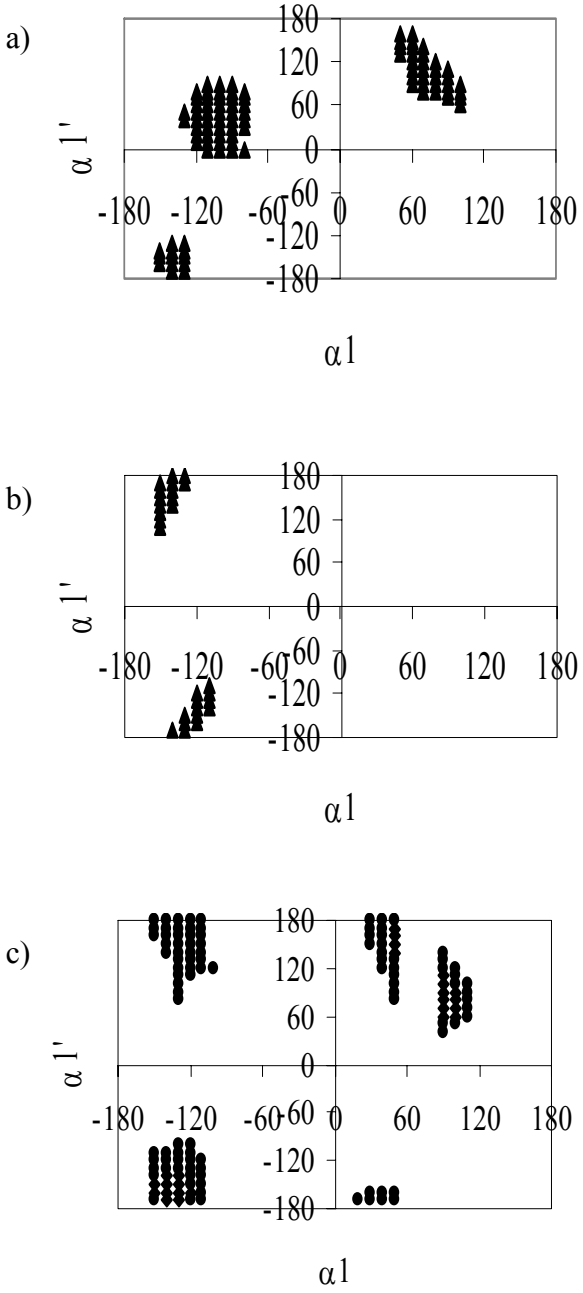


Figure 2.8. Allowed conformers after filtering through van der Waals constraints. a) PI(4)P conformers with rmsd of 5.0 ppm or less are shown as a function of rotating α1 and α1' with α2 = -80°. b) PI(4,5)$P_2$ conformers with rmsd of 5.0 ppm or less are shown as a function of rotating α1 and α1' with α2 = -80° and c) PI(4,5)$P_2$ conformers with rmsd of 5.0 ppm or less are shown as a function of rotating α1 and α1' with α2 = -145°.

It is clear from the range of allowed solutions in Figure 2.8 that we cannot define a unique orientation for either PI(4)P or PI(4,5)$P_2$. However, Figures 2.9 and 2.10 show some representative structures of these phosphatidylinositides. In each case, the structure represents the point with the lowest rmsd of chemical shifts within a given family, and angles differ by no more than 20° from any member of the family. Three possible structures for PI(4)P are shown in Figure 2.9. The energy difference between any two of the structures is no more than 1.3 kcal/mol. The orientation of the PI(4)P headgroup varies substantially as expected for the limited number of restraints in this molecule. Molecular geometries for PI(4,5)$P_2$ are better defined as seen in Figure 2.10. The structures of PI(4,5)$P_2$ in Figure 2.10 feature the inositol phosphate ring bent toward the bilayer surface. The structure in Figure 2.10d differs from those in 2.10a-2.10c by about 1 kcal/mol more in energy.

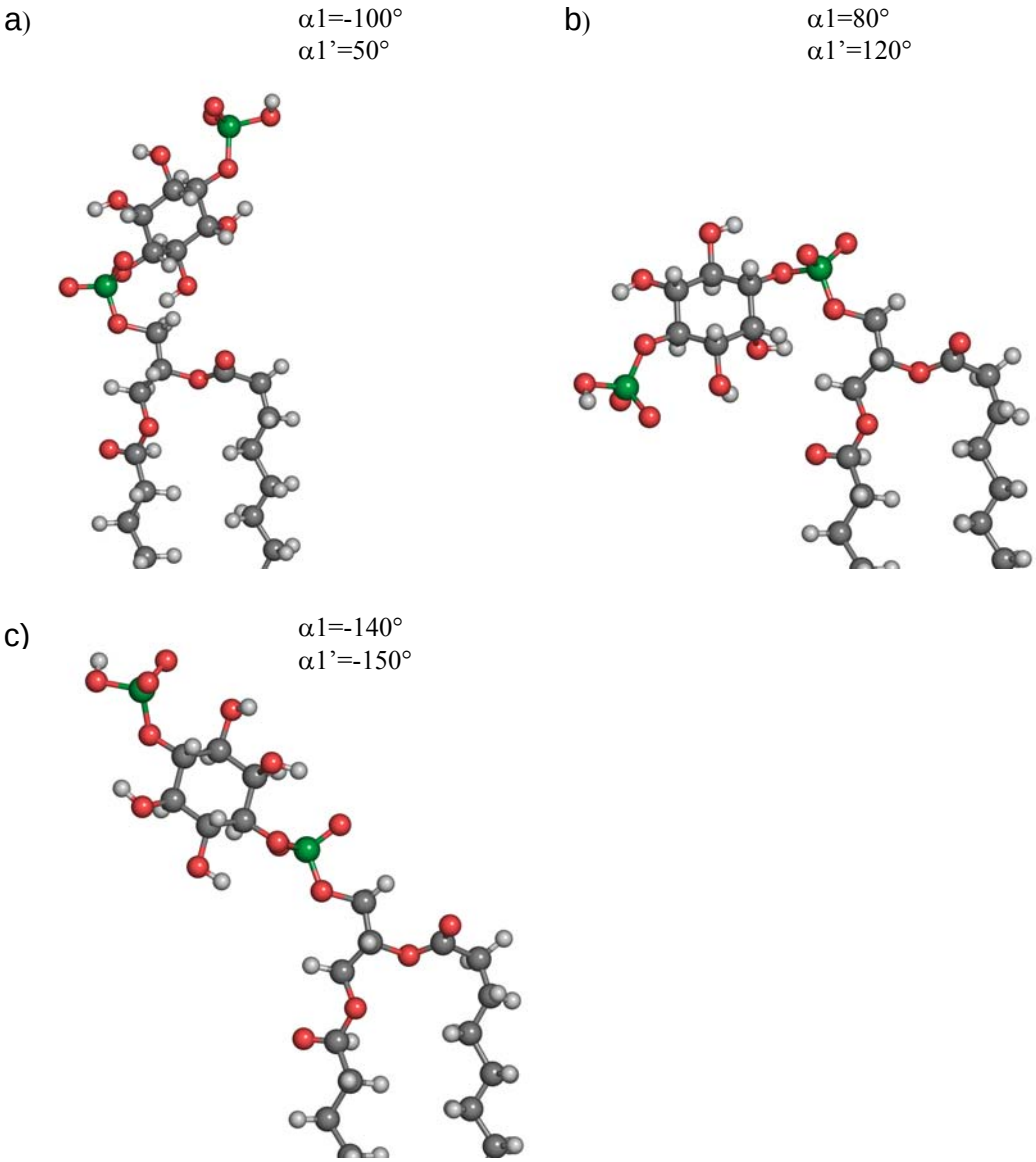


Figure 2.9. Possible conformations of PI(4)P in a bilayer. Dihedral angles α1 and α1' are indicated. (α2= -80°) The conformation shown in b) may be the least probably due to partial burial of monoester in the bilayer. (*All figures were prepared using PyMol (33).)*

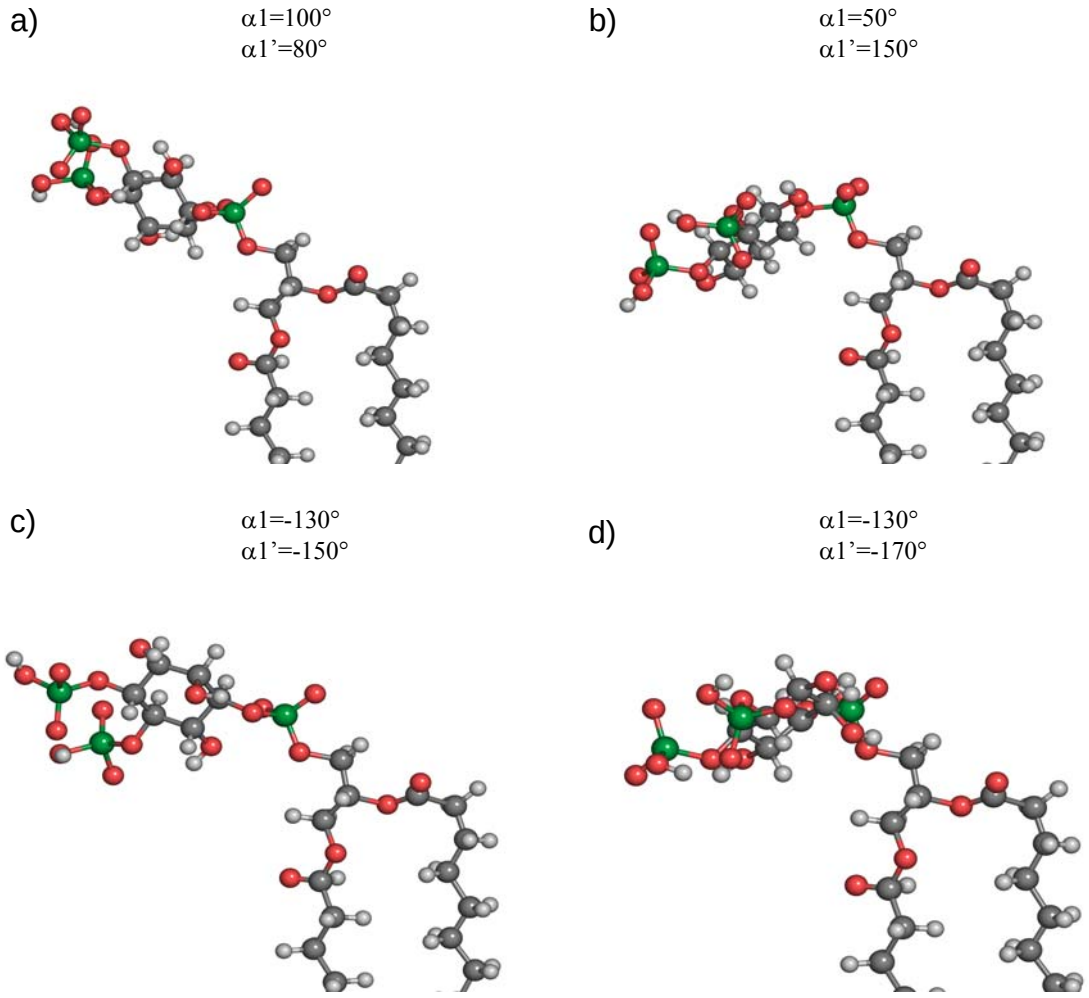


Figure 2.10. Possible conformations of PI(4,5)$P_2$ in a bilayer. a)-c) for α2= -145° and d) for α2=-80°. Dihedral angles α1 and α1' are indicated.

Previous studies of specifically deuterated phosphatidylinositides oriented in DMPC model membranes postulated that the unphosphorylated inositol ring sits nearly perpendicular to the membrane surface to maximize hydrogen bonds with solvent (26), and upon phosphorylation, the ring bends toward the membrane as a result of electrostatic interactions with the positively charged choline headgroups (34-37). Our findings on orientation for the PI(4)P headgroup geometry do encompass previously proposed structures (34) and do show head groups with more extended conformations. The

structure in Figure 2.9b is probably unreasonable in that it would partially bury the head group in the bilayer surface.

We believe our study provides the first experimental report of possible PI(4,5)$P_2$ headgroup geometries. In all cases there is a pronounced tendency for the inositol phosphate ring to bend toward the membrane surface. This cannot arise from specific electrostatic interactions with choline in our case, because we are using bilayers made from neutral alkyl-poly(ethylene)glycol and long-chain alcohols. These interactions may result from more subtle effects such as specific water- or alcohol-mediated hydrogen-bonding that dictates these preferences in our case. In any event, knowing something about the preferred headgroup geometry of phosphatidylinositides could greatly assist in understanding the specific interactions between phosphatidylinositides and the proteins that bind them. This study represents a first step in this direction.

We, unfortunately, cannot be too definitive in our discussion of molecular geometry implications. There are a number of important assumptions underlying the work we have presented. Use of phosphorus chemical shift tensors from model compounds in calculations on more complex systems such as the phosphatidylinositides introduces significant error in the calculation of chemical shift offsets. It is also important to note that we have made assumptions about the lack of internal motion in order to simplify the analysis of chemical shift offset data. Chemical shift offset restraints can only reflect the average orientation of one tensor relative to another, and structures generated are virtual structures in cases where substantial internal motion exists. Finally, the model membrane we have used is far from a true biological membrane in its surface character.

More important than specific information on a set of membrane lipids is the fact that we have illustrated the utility of some important methodology. Using $PI(4,5)P_2$ we have shown the feasibility of chemical shift assignments and extraction of chemical shift offsets using VASS. The high natural abundance of $^{31}P$ and the large chemical shift difference between the monoesters and diester made this technique easy to use on these phospholipids. However, the use of the linear dependence of chemical shift on angle helped in assigning poorly resolved monoester peaks. In more complicated spectra, this technique may become very important. There are also ways of improving geometry definition and relaxing underlying assumptions. Isotopic labeling of strongly oriented biomolecules will provide more data and better definition of geometries, and with more data we may also be able to introduce specific models for internal motion. Introduction and observation of $^{13}C$ would avoid difficulties with phosphorus background in phospholipid-based membrane preparations. Chemical shift restraints from groups with large chemical shift anisotropies, such as $^{13}C$ labeled carbonyl groups or aromatic ribonucleotide bases should prove particularly valuable. For proteins, $^{13}C$ and $^{15}N$ introduction and observation would provide a wealth of information. However, the separation of chemical shift offsets and assignment of 100 or more peaks in a strongly oriented protein spectrum can be a major task. VASS may be particularly advantageous here. Hence, we believe the work we have presented points to some bright prospects for the future.

REFERENCES


1. Courtieu, J., Bayle, J.P. and Fung, B.M. (1994) Variable-angle sample-spinning NMR in liquid-crystals. *Prog NMR Spec*, **26,** 141-169.
2. Grishtein, J., McElheny, D., Frydman, V. and Frydman, L. (2001) A variable-director 13C NMR analysis of lyotropic aramide solutions. *J Chem Phys*, **114,** 5415-5424.
3. Vaananen, T., Jokisaari, J. and Selantaus, M. (1987) A variable-angle spinning system for the determination of NMR parameters of liquid-crystalline samples. *J Magn Reson*, **72,** 414-421.
4. Tian, F., Losonczi, J.A., Fischer, M.W.F. and Prestegard, J.H. (1999) Sign determination of dipolar couplings in field-oriented bicelles by variable angle sample spinning (VASS). *J Biomol NMR*, **15,** 145-150.
5. Havlin, R.H., Park, G.H.J., Mazur, T. and Pines, A. (2003) Using switched angle spinning to simplify NMR spectra of strongly oriented samples. *J Am Chem Soc*, **125,** 7998-8006.
6. Zandomeneghi, G., Williamson, P.T.F., Hunkeler, A. and Meier, B.H. (2003) Switched-angle spinning applied to bicelles containing phospholipid-associated peptides. *J Biomol NMR*, **25,** 125-132.
7. Lemmon, M.A. and Ferguson, K.M. (2000) Signal-dependent membrane targeting by pleckstrin homology (PH) domains. *Biochem J*, **350,** 1-18.
8. Terui, T., Kahn, R.A. and Randazzo, P.A. (1994) Effects of acid phospholipids on nucleotide exchange properties of ADP-Ribosylation Factor-1 - evidence for specific interaction with phosphatidylinositol 4,5-bisphosphate. *J Biol Chem*, **269,** 28130-28135.
9. Seidel, R.D., Amor, J.C., Kahn, R.A. and Prestegard, J.H. (2004) Structural perturbations in human ADP ribosylation factor-1 accompanying the binding of phosphatidylinositides. *Biochemistry*, **43,** 15393-15403.
10. McLaughlin, S., Wang, J.Y., Gambhir, A. and Murray, D. (2002) $PIP_2$ and proteins: Interactions, organization, and information flow. *Annu Rev Biophys Biomolec Struct*, **31,** 151-175.
11. Seelig, J. (1978) $^{31}P$ Nuclear magnetic resonance and the head group structure of phospholipids in membranes. *Biochim Biophys Acta*, **515,** 105-140.
12. Courtieu, J., Alderman, D.W., Grant, D.M. and Bayles, J.P. (1982) Director dynamics and NMR applications of nematic liquid crystals spinning at various angles from the magnetic field. *J Chem Phys*, **77,** 723-730.
13. Lounila, J. and Jokisaari, J. (1982) Anisotropies in spin-spin coupling constants and chemical shifts as determined from the NMR spectra of molecules oriented by liquid crystal solvents. *Prog NMR Spec*, **15,** 249-290.
14. Prestegard, J.H. and Kishore, A.I. (2001) Partial alignment of biomolecules: an aid to NMR characterization. *Curr Opin Chem Biol*, **5,** 584-590.
15. Prestegard, J.H., Bougault, C.M. and Kishore, A.I. (2004) Residual dipolar couplings in structure determination of biomolecules. *Chem Rev*, **104,** 3519-3540.
16. Jonstromer, M. and Strey, R. (1992) Nonionic bilayers in dilute solutions: effect of additives. *J Phys Chem*, **96,** 5993-6000.

17. Freyssingeas, E., Nallet, F. and Roux, D. (1996) Measurement of the membrane flexibility in lamellar and "sponge" phases of the C12E5/hexanol/water system. *Langmuir*, **12,** 6028-6035.
18. Gaemers, S. and Bax, A. (2001) Morphology of three lyotropic liquid crystalline biological NMR media studied by translational diffusion anisotropy. *J Am Chem Soc*, **123,** 12343-12352.
19. Ruckert, M. and Otting, G. (2000) Alignment of biological macromolecules in novel nonionic liquid crystalline media for NMR experiments. *J Am Chem Soc*, **122,** 7793-7797.
20. Maurer, T. and Kalbitzer, H.R. (1996) Indirect referencing of $^{31}$P and $^{19}$F NMR Spectra. *J Magn Res, Ser B*, **113,** 177-178.
21. Tebby, J.C. (ed.) (1991) *Handbook of Phosphorus-31 Nuclear Magnetic Resonance Data*. CRC Press, Boca Raton.
22. van Paridon, P.A., de Kruijff, B., Ouwerkerk, R. and Wirtz, K.W.A. (1986) Polyphosphoinositides undergo charge neutralization in the physiological pH range: a $^{31}$P-NMR study. *Biochim Biophys Acta*, **877,** 216-219.
23. Zandomeneghi, G., Tomaselli, M., Williamson, P.T.F. and Meier, B.H. (2003) NMR of bicelles: orientation and mosaic spread of the liquid- crystal director under sample rotation. *J Biomol NMR*, **25,** 113-123.
24. Bayle, J.P., Perez, F. and Courtieu, J. (1988) Inertial effects in rotating lyotropic liquid crystals. *Liq Cryst*, **3,** 753-758.
25. Vivekanandan, S., Deepak, H.S.V., Gowda, G.A.N., Ramanathan, K.V. and Khetrapal, C.L. (2002) NMR spectra of mixed liquid crystals of opposite diamagnetic susceptibility anisotropies near critical point under variable angle sample spinning. *J Mol Struct*, **602-603,** 485-489.
26. Bradshaw, J.P., Bushby, R.J., Giles, C.C.D. and Saunders, M.R. (1999) Orientation of the headgroup of phosphatidylinositol in a model biomembrane as determined by neutron diffraction. *Biochemistry*, **38,** 8393-8401.
27. Spiers, I.D., Freeman, S. and Schwalbe, C.H. (1995) Crystal structure and modeling studies of myo-inositol 1,2,3-trisphosphate. *J Chem Soc, Chem Commun*, **21,** 2119-2120.
28. Pearson, R.H. and Pascher, I. (1979) The molecular structure of lecithin dihydrate. *Nature*, **281,** 499-501.
29. Herzfeld, J., Griffin, R.G. and Haberkorn, R.A. (1978) Phosphorus-31 chemical shift tensors in barium diethyl phosphate and urea-phosphoric acid: model compounds for phospholipid head-group studies. *Biochemistry*, **17,** 2711-2718.
30. Kohler, S.J. and Klein, M.P. (1977) Phosphorus-31 NMR Chemical Shielding Tensors of L-O-Serine Phosphate and 3'-Cytidine Monophosphate. *J Am Chem Soc*, **99,** 8290-8293.
31. Howard, K.P. and Prestegard, J.H. (1995) Membrane and solution conformations of monogalactosyldiacylglycerol using NMR molecular modeling methods. *J Am Chem Soc*, **117,** 5031-5040.
32. Kohler, S.J. and Klein, M.P. (1977) Orientation and dynamics of phospholipid head groups in bilayers and membranes determined from $^{31}$P nuclear magnetic resonance chemical shielding tensors. *Biochemistry*, **16,** 519-526.

33. DeLano, W.L. (2002) The PyMOL Molecular Graphics System. Delano Scientific, San Carlos, CA.
34. Bradshaw, J.P., Bushby, R.J., Giles, C.C.D., Saunders, M.R. and Saxena, A. (1997) The headgroup orientation of dimyristoylphosphatidylinositol-4-phosphate in mixed lipid bilayers: a neutron diffraction study. *Biochim Biophys Acta*, **1329,** 124-138.
35. Bradshaw, J.P., Bushby, R.J., Giles, C.C.D., Saunders, M.R. and Reid, D.G. (1996) Neutron diffraction reveals the orientation of the headgroup of inositol lipids in model membranes. *Nat Struct Biol*, **3,** 125-127.
36. Bushby, R.J., Byard, S.J., Hansbro, P.M. and Reid, D.G. (1990) The conformational behavior of phosphatidylinositol. *Biochim Biophys Acta*, **1044,** 231-236.
37. Hansbro, P.M., Byard, S.J., Bushby, R.J., Turnbull, P.J.H., Boden, N., Saunders, M.R., Novelli, R. and Reid, D.G. (1992) The conformational behavior of phosphatidylinositol in model membranes - $^{2}$H NMR Studies. *Biochim Biophys Acta*, **1112,** 187-196.

# CHAPTER 3

# ALTERNATIVE METHODS TO COLLECT ANISOTROPIC DATA: MAGIC ANGLE SPINNING PROBES[1]

[1] Kishore, A.I. & J.H. Prestegard. To be submitted to *Journal of Biomolecular NMR*..

ABSTRACT

Magic-angle spinning probes are used here in a novel approach to reintroduce anisotropy to biomolecules weakly aligned in a magnetic field. Residual dipolar couplings (RDCs) were observed separately on a carbohydrate and a small protein when samples were static in the magic angle probe and aligned in the magnetic field. Isotropic data sets were obtained while spinning at the magic angle. Alignment properties of the ordered protein collected during static, magic-angle experiments are similar to properties previously determined using a high resolution, conventional probe. The technique of spinning/static samples to eliminate and reintroduce anisotropy is particularly advantageous in measuring chemical shift offsets since they suffer from a lack of an accurate shift reference. Limitations of current probes are discussed, and applications to novel systems are addressed.

## 3.1 CURRENT APPROACH TO ANISOTROPIC PARAMETER MEASUREMENT

Since its introduction over 10 years ago, the use of anisotropic data such as residual dipolar couplings (RDCs) and chemical shift anisotropy (CSA) offsets has now become routine in NMR structure refinement of biomolecules. RDCs have received the bulk of the attention as constraints in structure determination protocols (1-3), partly for their easy collection and analysis. The techniques for inducing, collecting, and interpreting RDCs have matured to the point that *de novo* NMR structures have recently been determined by RDC methods alone (4-8). The number of alignment media used to induce RDCs has swollen to more than 10 (3,9), and the use of natural or engineered metal-binding sites in proteins has also introduced media-free options for magnetic alignment (10,11). New pulse sequences to collect RDCs appear regularly (3), and applications to dynamics are expanding, although analysis still remains challenging (12-15). Despite impressive advances in alignment media, experimental methodology, and theoretical analysis, all current methods of data collection suffer from one fundamental problem; anisotropic parameters must be separated from isotropic parameters by separately collecting an isotropic reference spectrum. In the case of one-bond RDCs, for example, the splittings measured in aligned media are the sum of an RDC and a scalar coupling. Separate aligned samples and isotropic samples must be prepared in most cases. This can be costly in terms of sample production, particularly in cases such as membrane proteins that are not available in abundant yield. In addition, sample recovery from some aligning media is not always easy. In some cases, when bicelles are used for alignment, for example, an isotropic spectrum can be obtained by dropping the temperature below an aligned-to-isotropic phase transition. However, for chemical shift

anisotropy measurements, even this is problematic because a change in temperature can cause changes in chemical shift that have nothing to due with the phase transition.

### 3.1.1 HIGH-RESOLUTION MAGIC ANGLE SPINNING (HRMAS)

The use of magic angle spinning (MAS) probes may offer solutions to the aforementioned problems of anisotropic data collection by solving the referencing problem. MAS probes are used in conventional solid-state NMR (SSNMR) to average the large anisotropic interactions typical of disordered, solid samples or heterogeneous samples. These second rank tensorial interactions proportional to $(3\cos^2\theta - 1)$ such as dipolar couplings and chemical shift anisotropy can be averaged to zero by rotation in a frame positioned at 54.7°, or the magic angle $\theta_m$, relative to the magnetic field (16,17). More recently, High Resolution MAS (HRMAS) was introduced to provide high resolution $^1$H spectra for less ordered, but still heterogeneous samples (18-20). HRMAS differs from Cross-Polarization Magic Angle Spinning (CPMAS) in that the inherent partial mobility of samples typically studied reduces anisotropic parameters from a fully ordered system, such as a powder, to a more isotropic-like system with much reduced dipolar couplings and CSAs (21). In these systems, slower spinning rates and lower power decoupling schemes than those of typical SSNMR experiments can be used to eliminate residual dipolar couplings and CSA effects. Solution NMR probes are not ideal for these partially ordered samples because their ordered domains often produce large bulk magnetic susceptibilities that can not be removed by shimming alone but can be removed by MAS. Applications of HRMAS are growing in areas as diverse as soluble organic molecules synthesized on solid-support beads (22), tissue samples (23), metabonomic characterization (24), combinatorial chemistry (25), and even food science

(26). $^{1}$H resolution in these probes is typically 0.01 ppm or less (5 Hz at 500 MHz) when spinning. In Table 3.1 the capabilities of currently available 500 MHz NMR probes, including an HRMAS probe (also referred to as a "nanoprobe") are summarized to illustrate that despite small volumes, linewidths are of similar orders of magnitude for spinning samples compared to other high resolution probes. Although a comparison of probe sensitivity is not attempted, it is sufficient to note that sensitivity concerns exist but can often be addressed through efficient coil design (27). In terms of our interest, these probes have the additional advantage that spinning at the magic angle averages the susceptibility anisotropy of liquid crystal samples to zero. This means that the media will not orient and spectra observed will be essentially isotropic, in the same medium, and at the same temperature as a static aligned sample.

Table 3.1. Volumes and resolution of currently available 500 MHz NMR probes

| Probe | Sample Volume in μL | $^{1}$H linewidth in Hz spinning, (non-spinning) |
|---|---|---|
| 5 mM HR [a] | 600 | 0.4, (0.6) [f] |
| 3 mM HR [b] | 140 | 0.4, (0.6) [f] |
| CPMAS [c] | 110 | 30 |
| VASS/SAS [d] | 110 | 4, (25) [g] |
| gH{X} nanoprobe [e] | 40 | 0.4, (25-30) [g] |

[a] Standard 5 mm high-resolution solution probe, Varian
[b] 3 mm high-resolution solution probe, Varian
[c] Cross-Polarization Magic-Angle Spinning solids probe, Varian
[d] Variable Angle Sample Spinning Probe, Doty
[e] Varian high resolution magic angle spinning probe, or Nano-nmr probe
[f] For $CHCl_3$ in acetone-$d_6$
[g] For $H_2O$

### 3.1.2 REINTRODUCING ANISOTROPY THROUGH PROBE TECHNOLOGY

However, the ultimate goal of MAS is to eliminate the anisotropy inherent in inhomogeneous systems. In contrast, my goal is to carefully reintroduce enough anisotropy to extract orientational constraints that reveal molecular orientation of ordered systems. This has typically been done with a variable angle probe, something that is important when the effect of anisotropic parameters on spectra is large. However, in many cases only weak alignment is used and simple comparison of isotropic and aligned conditions is adequate. Data collection can then be simplified to just one angle, for example the magic angle such as in the HR-MAS probe, and still provide a wealth of information. Here, a novel technique to collect and measure RDCs and chemical shift offsets is presented using a high resolution, small volume (40 μL), magic-angle spinning probe on a static sample. Isotropic data sets can be collected on the same sample when spun at the magic angle. Since this probe was not originally designed for data collection of static samples, resolution in these cases suffers compared to anisotropic spectra collected in traditional probes. However, the work described here points to attractive options for data collection when probe technology catches up to demand.

### 3.1.3 MAGIC ANGLE AND LIQUID CRYSTAL THEORY: SPINNING VS. STATIC SAMPLES

Residual anisotropic interactions (namely RDCs and chemical shift offsets) are typically collected in static samples using normal 5 mm NMR tubes positioned with their long axis parallel to the magnetic field for superconducting magnets in high resolution probes (Figure 3.1a). Under these conditions, liquid crystal directors tend to align either parallel or perpendicular to the field, based on the sign of $\Delta\chi$, or their anisotropy of

magnetic susceptibility. In most applications of liquid crystals to biomolecules, $\Delta\chi$ is negative for bicelle and polyethylene glycol ether-samples, and $\Delta\chi$ is positive for bacteriophage-aligned samples. Alignment of a typical liquid crystal with $\Delta\chi < 0$ is shown in Figure 3.1.

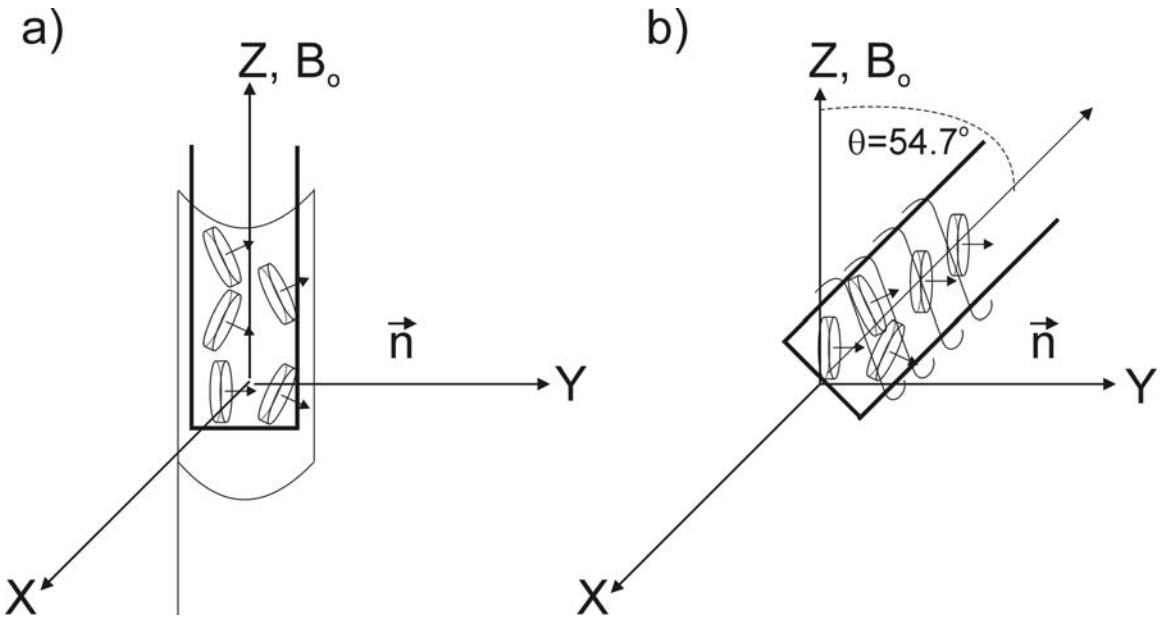


Figure 3.1. Sample positioning in the magnetic field differs between a a) conventional high resolution solution probe and b) high resolution MAS probe. Liquid crystal domains are shown with their directors and net alignment (n) perpendicular to the field in both cases.

In the case of a static liquid crystal sample in a high-resolution magic angle probe where the solenoidal coil surrounds the sample stator (Figure 3.1b), the director still aligns independently of the angle between the stator axis and the magnetic field. Net alignment remains the same. When static and positioned at the magic angle (or any other angle), anisotropic data is still accessible, but static spectra suffer some loss compared to a conventional probe due to 1) a decrease in signal-to-noise ratio from non-optimal sample positioning relative to the magnetic field (scaling by $3\cos^2\theta - 1$) and 2) line broadening from magnetic susceptibility differences not averaged by spinning.

In experiments described here, I have exploited the use of the magic angle for partial magnetic alignment of weakly ordered liquid crystals when static and their averaged disorder into isotropic domains when spinning. From VASS studies of liquid crystals it was demonstrated that when spinning at the magic angle, liquid crystal directors disorder, resulting in a sample that has no preferred order, or an isotropic sample (28). Here I will illustrate the potential of these measurements using primarily $^{15}N$-$^{1}H$ residual dipolar couplings (RDCs) in weakly aligned proteins.

## 3.2 RESIDUAL DIPOLAR COUPLING (RDC) THEORY

In the presence of a strong external magnetic field, through-space coupling of proximate nuclear dipoles can be described as in Eq 1.

$$D_{ij} = -h\gamma_i\gamma_j/(2\pi^2 r_{ij}^3)\langle(3\cos^2(\theta_{ij}) - 1)/2\rangle$$

$$= Dmax_{ij}\langle(3\cos^2(\theta_{ij}) - 1)/2\rangle \quad (1)$$

Where h is Planck's constant, $\gamma_i$ and $\gamma_j$ are the gyromagnetic ratios for spin ½ nuclei, $r_{ij}$ is the internuclear distance between spins i and j, and $\theta_{ij}$ is the angle between the internuclear vector and the external magnetic field. Dmax is the maximum dipolar coupling in Hz for a set of nuclei perfectly aligned along the magnetic field where D is the residual dipolar coupling (RDC) in Hz between nuclei i and j. This time-averaged value, as denoted by brackets, equals zero in an isotropic liquid, where internuclear vectors can sample all possible orientations; hence no RDCs are observed in solution. However, when ordered by a medium that restricts the sampling space (3,29,30), vectors experience preferred orientations and produce measurable RDCs. This anisotropic averaging can be more conveniently represented by a 3 x 3 order matrix where the elements are as follows:

$$S_{kl} = \langle(3\cos(\theta_k)\cos(\theta_l) - k_{kl})/2\rangle \quad (2)$$

Here θ represents the instantaneous angle between the ith molecular axis and the director (whose orientation is typically known relative to the magnetic field) and $k_{kl}$ is the Kronecker delta. The dipolar coupling can be written in terms of elements of this order tensor and a set of direction cosines relating vectors to an arbitrarily chosen fragment frame as follows:

$$D_{ij} = Dmax_{ij} \Sigma S_{kl} \cos(\phi_k)\cos(\phi_l) \quad (3)$$

Here ϕ represents the instantaneous orientation of the ith internuclear vector with respect to the molecular axis (Figure 3.2). The order matrix can be diagonalized using singular value decomposition (SVD) (31), allowing a description of order in terms of just three principal values $S_{xx}$, $S_{yy}$, and $S_{zz}$ and the Euler angles (ϕ, θ, ψ) that relate the principal frame to the initial molecular frame.

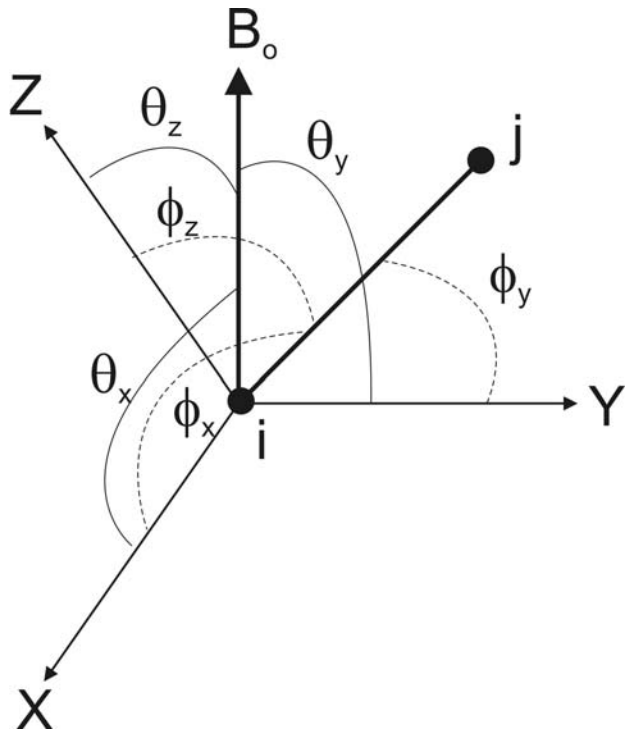


Figure 3.2. Angles ($\phi_{x,y,z}$) define the orientation of the ij interaction vector relative to the molecular frame (X,Y,Z) and angles ($\theta$) define the orientation of the molecular frame relative to the magnetic field, $B_o$.

### 3.2.1 NMR EXPERIMENTS TO COLLECT RDCS

A number of pulse sequences exist to collect homo- and heteronuclear RDCs. Here discussion is limited to some of the simplest experiments to collect N-H RDCs that have become nearly routine in their application to $^{15}$N uniformly labeled proteins. There are two general categories for measuring coupling constants (32): 1) frequency resolved methods where the separation of peak centers is measured in the frequency domain and 2) intensity based methods where the coupling is extracted from the resonance intensity. Only frequency-based experiments were used in this dissertation and will be discussed hereafter. These methods are conceptually simpler and easier to implement and analyze than their intensity-based counterparts. In a fully coupled HSQC spectrum, four peaks are observed for every X-H pair with couplings in both the $^1$H and X dimensions (Figure

3.3a). A fully decoupled HSQC spectrum displays only one peak, represented by the black peak in Figure 3.3a. The easiest way to measure couplings is to remove either the $^{15}N$ decoupling during acquisition (f2-coupled) or the 180° $^{1}H$ pulse in the middle of the $t_1$ evolution period (f1-coupled) of a heteronuclear single quantum coherence (HSQC) sequence (33). Removing the 180° pulse is usually more desirable because couplings can then be measured in the indirect dimension where $T_2$'s are longer than for $^{1}H$ and suffer fewer cross-correlation distortions of peak positions. An example of the RDC contribution to f1-coupled peaks is shown in Figure 3.3b. However, in systems with a high number of cross peaks, the coupled HSQC experiment yields crowded spectra, complicating data analysis.

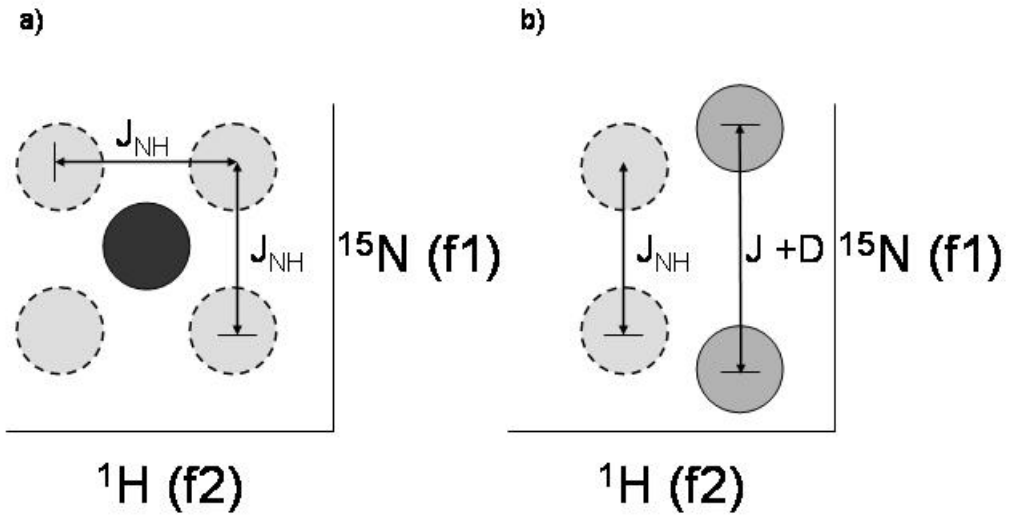


Figure 3.3. Cross peaks are observed in a) fully coupled HSQC spectrum (coupled in both f1 and f2 dimensions) shown in gray with dotted lines compared to a fully decoupled spectrum of just one peak shown in black. b) In an f1-coupled (only) spectrum, the RDC can be measured from the difference in peak splitting between the isotropic (J) and aligned samples (J+D).

An alternative method is to separate the collection of doublets into two experiments. In the in-phase, anti-phase (IPAP) experiment, these two components of

coupling evolution are saved separately. Adding the resulting spectra results in display of one doublet component and subtracting the resulting spectra results in display of the other doublet component (34). Both the coupled HSQC and the IPAP HSQC are robust experiments that provide couplings for weakly ordered systems where the range of RDCs is still relatively small (± 30 Hz). However, both experiments suffer from poor resolution of the upfield component in high molecular weight systems. This results from the same interference between dipolar and CSA interactions that give rise to Transverse Relaxation Optimized SpectroscopY (TROSY) spectra (35) where the narrow downfield component is detected. For RDCs, however, two components must be measured making accurate measurement of RDCs very difficult for large systems.

A simple combination of HSQC experiments incorporates the high sensitivity (all four resonances are detected) of the fully decoupled HSQC and the single sharp peak detection of TROSY-HSQC (35,36). In the decoupled HSQC the observed peak is the center of the four cross peaks normally observed (Figure 3.3a). In the TROSY-HSQC, only the sharpest peak of the four remains due to cancellation or broadening of the other peaks (Figure 3.4).

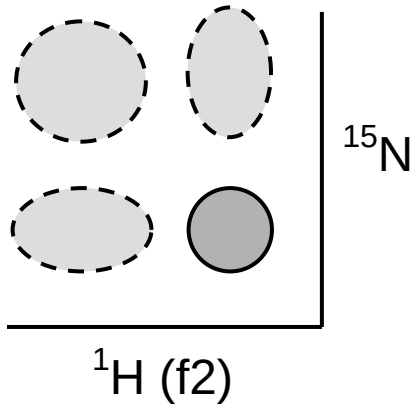


Figure 3.4. Only the sharpest peak (bottom right, dark gray) of the four peaks remains in the TROSY-HSQC.

RDCs can be measured based on peak frequency differences between the fully decoupled HSQC peak (black) and the TROSY peak (dark gray) (37) as shown in Figure 3.5.

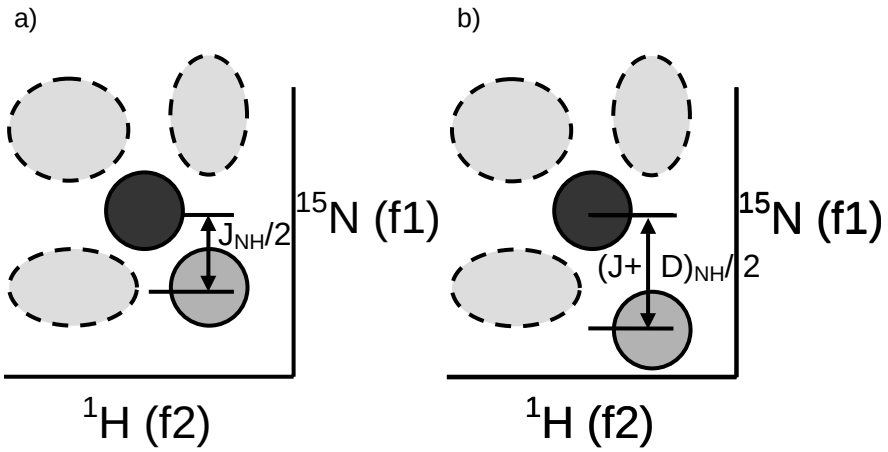


Figure 3.5. The TROSY-HSQC peak (dark gray) is shifted from the decoupled HSQC peak (black) by half the coupling when a) isotropic and b) aligned.

### 3.2.2 INTERPRETATION OF RDCS

RDCs can be added to other restraints in a simulated annealing approach to molecular geometry, or they can be interpreted *a priori* within a given set of molecular coordinates. The discussion here is confined to the latter approach using an order matrix analysis of RDCs. When several RDCs have been measured for a particular fragment or structure, the level of alignment and the orientation of the molecule can be determined. REDCAT, an efficient computational tool for the analysis of RDCs, combines the SVD order matrix analysis with a graphical user interface to simplify the calculation and interpretation of order parameters (15). The diagonalized solutions of the order matrix can be plotted in the form of a Sauson-Flamsteed projection that plots the points at which the axes of principal alignment frames of the solutions pierce the surface of a globe drawn in the molecular frame.

In the experiments described here, we demonstrate the feasibility and challenges of collecting orientational restraints of a weakly ordered carbohydrate and a small, weakly oriented protein (Protein G) using an HRMAS probe positioned at the magic angle while static (aligned) and spinning (isotropic). RDCs of $^{13}C$-$^{1}H$ vectors were measured for the carbohydrate and of $^{15}N$-$^{1}H$ vectors for the protein. The alignment properties and orientation of the protein, Protein G, were determined through an order matrix analysis of N-H RDC vectors and compare favorably to parameters determined using a more conventional approach. A high resolution solid-state variable angle sample spinning probe was also used to collect simple $^{15}N$-$^{1}H$ HSQC experiments of Protein G in solution to further illustrate how variable angle data could be useful in a high resolution probe optimized for $^{1}H$ sensitivity.

## 3.3 MATERIALS & METHODS

### 3.3.1 CARBOHYDRATE SAMPLE PREPARATION

Lactose with a $^{13}C$ label at C-1 of galactose (Omicron Biochemicals, South Bend, IN) was dissolved to 70 mM in $D_2O$ (Cambridge Isotopes Laboratory, Andover, MA). A 4.25% (w/v) solution of liquid crystal sample was prepared by mixing 25 µL pentaethylene glycol monododecyl ether ($C_{12}E_5$), 9 µL hexanol (both from Sigma Aldrich, St. Louis, MO), and 550 µL $D_2O$ (38-40). The sample was carefully inserted into a 40 µL Varian gH{X} nanoprobe tube using a long, flexible, plastic pipette tip so that no air bubble remained in the tube's coil window. The glass tube was sealed with a Teflon plug. Rotors designed for the Varian NanoProbes are available from Varian and Wilmad-Labglass.

### 3.3.2 PROTEIN SAMPLE PREPARATION

The isotopically labeled (98% $^{15}N$) B1 domain of Protein G from Streptococcus was expressed and purified from the University of Georgia BioXpress Laboratories (Athens, GA) on contract synthesis. The liquid crystal sample was prepared as a concentrated stock solution and diluted into a buffer solution containing protein. The 8.8% (w/w) stock solution of pentaethylene glycol monododecyl ether ($C_{12}E_5$) was prepared by mixing 25 μL $C_{12}E_5$, 9 μL hexanol, and 225 μL $D_2O$. After vortexing until the sample was homogenous (about 1 minute), 10 μL of the liquid crystal was added to 30 μL of protein to give a final concentration of 2.2% (w/w) $C_{12}E_5$ and 1.5 mM Protein G in 50 mM phosphate buffer (pH 5.85). The sample was transferred to a 40 μL Varian gH{X} nanoprobe tube and sealed with a Teflon plug.

### 3.3.3 NANOPROBE NMR

NMR data were recorded on a Varian Inova 500 MHz spectrometer (Palo Alto, CA) using a Varian gH{X} nanoprobe with gradients along the z-axis. The gradient-encoded Heteronuclear Single Quantum Coherence (gHSQC) pulse sequence was modified to synchronize gradient coherence coding and decoding pulses with integer multiples of rotor spinning rates (Figure S3.1) and to remove homospoil pulses. To measure X-H couplings, the 180º ($^1H$) pulse during $t_1$ evolution was also removed. Air flow was regulated using a Varian Tachometer/Pneumatics Box. Samples were spun from 500 to 1500 Hz with bearing air flow at 10 psi and drive air flow from 2-10 psi. The spinning rate for lactose was 670 Hz and 1000 Hz for Protein G. Temperature was held constant at 25 ºC for all experiments. Temperature in the static case was regulated by a low, but constant flow of bearing air (1-2 psi for static case) in combination with

Varian's VT regulation heater. Deuterium quadrupolar couplings were observed in the static case at 24 Hz for aligned lactose and 11 Hz for Protein G, both at 25 ºC. The isotropic $^{2}H$ chemical shift was observed during spinning to provide a chemical shift reference. The probe was aligned in the magnet with the magic angle stator axis parallel to the xy shim stack. Samples were shimmed initially with isotropic ($D_2O$) solution, then with $C_{12}E_5$ liquid crystals, and finally with sample. Samples were re-shimmed in between collecting static and spinning spectra. Critical room temperature shims were along z1, x1, y1, xz, and yz. Aligned (static) and isotropic (spinning) spectra were collected under identical experimental conditions with the exception of spinning rates and different shim sets.

HSQC spectra were collected with 2048 points in the direct dimension and 128 complex points in the indirect dimension. A recycle delay of 1.0 s and a delay between gradient pulses (gstab) gave optimal signal to noise at 1.00 ms. A 5.4 ms delay during the INEPT transfer was used, corresponding to a $^{15}N$-$^{1}H$ scalar coupling of -93 Hz. Gradient pulses were used to select coherence. Data were collected in an Echo-Anti Echo fashion. Total acquisition time was 3 h. Data were processed in nmrPipe (41) using a Gaussian multiplier and zero filled to 4096 points in the direct dimension. In the indirect dimension, 256 points of linear prediction, a sine-bell squared apodization function, and zero filling to 2048 points were used. Coupled peaks were picked using nmrPipe and fit using the non-linear lineshape spectral fitting module in nmrPipe (nlinLS). Scalar and dipolar couplings were measured using straightforward modifications of existing nmrPipe scripts.

### 3.3.4 SHIMMING

Narrow line width and symmetric line shape are critical to obtaining good data, and probes at present introduce significant field inhomogeneity problems; it is, therefore, appropriate to provide some practical advice for homogeneity optimization (shimming). Figure 3.6 is used to illustrate the importance of careful shimming in this probe, and $D_2O$ provided a relatively quick standard to implement a shimming protocol.

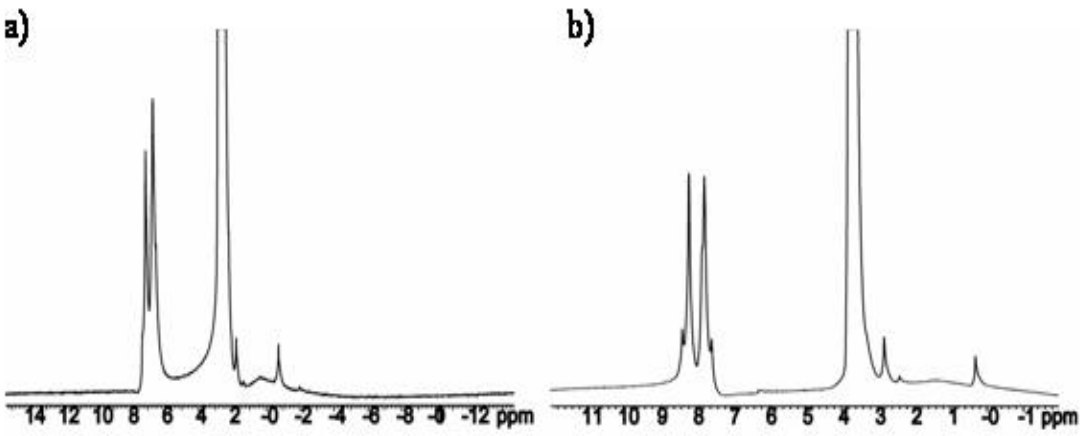


Figure 3.6. $^1$H 1-D NMR spectra of benzamide in DMSO collected in a high resolution solid-state variable angle spinning probe at 90° to the magnetic field after shimming on a) the same sample, linewidth=50 Hz and b) after shimming on $D_2O$, linewidth 28 Hz.

For the HRMAS probe, shimming values change dramatically between static and spinning samples. Several helpful guides to shimming high resolution magic angle probes have been published (42,43). The trick is to line up the MAS spinner axis along the xy shim stack, or the x or y axis of the laboratory frame shim set (visible from underneath the magnet) so that, in principle, either x or y (one or the other) does not change much as the angle is changed. What will change is the projection onto z, so that as the angle becomes smaller, the contribution to z-shims becomes important. If the

stator is correctly positioned along the shim stack, rotation about the x-axis should not affect one of the shim sets, either x or y. Instead of shimming a z-axial centered system, there is a coordinate transformation to a magic-angle centered system, and the interaction between the z-axial shims and x and y becomes important. Shims are more accurately described in the laboratory frame as composed of zonal harmonics, or those that have cylindrical symmetry about the z-axis, and tesseral harmonics, or those that vary azimuthally about the sample (42). For example, when the stator is at 90° to the field, there is no projection of magnetization onto the z-axis so 1) most of the shimming is done in x and y and 2) (incidentally) S/N is at a maximum due to the design of the coil. The spherical harmonic shim terms have been expressed in a magic-angle-tilted frame as linear combinations of laboratory frame shims in Table S3.2 and can be used as a practical guide to shimming. Under static conditions, the field can be shimmed to the third order following the usual protocol for high resolution probes. When spinning, only the zonal shims in the tilted frame contribute, thus simplifying the shimming procedure.

### 3.3.4 VASS PROBE $^{15}$N NMR

Static $^{15}$N-$^{1}$H HSQC (phase selected, no gradients) spectra of 1.3 mM Protein G were collected on a Varian Inova 500 MHz spectrometer (Varian Inc., Palo Alto, CA) using a VASS XC5 probe (Doty Scientific, Columbia, SC) at multiple angles. Initial shimming of the probe was done with a static sample of $D_2O$ in a 5 mM Wilmad 528 glass tube. The minimum $^{1}$H line width observed for $D_2O$ was 21 Hz with a slightly asymmetric lineshape. The Varian pulse sequence HSQC.c, renamed HSQC_d2.c, was modified to run on the $^{15}$N channel. The sequence HSQC_d2.c was further modified to allow coupling in the $t_1$ evolution period by removing the 180º pulse during that period

for coupled HSQC spectra. Data were collected with 2048 points in the direct dimension and 32 complex points in the indirect dimension. Water suppression was accomplished using a low power presaturation pulse of 1.0 s as this probe lacks pulsed field gradients. A recycle rate of 1.0 $s^{-1}$ and a 5.4 ms delay during the INEPT transfer were used, corresponding to a $^{15}N$-$^{1}H$ scalar coupling of -93 Hz. Standard phase cycling from the Varian pulse sequence HSQC was used. Total acquisition time was 28 min. Data were processed in nmrPipe using a Lorentz-to-Gaussian multiplier function and zero filled to 4096 points in the direct dimension. In the indirect dimension, 256 points of linear prediction, a sine-bell squared apodization function, and zero filling to 512 points were used.

## 3.4 RESULTS

### 3.4.1 NMR SPECTRA

For lactose oriented in a 4.25 % (w/w) $C_{12}E_5$ liquid crystal the C1-H1 anomeric resonance is easily resolved in a $^{13}C$-$^{1}H$ HSQC spectrum (Figure 3.7). While differences in splittings are hard to visually discern, fitting of peaks for this sample shows a 7 Hz difference between spinning, isotropic (black) and static, aligned (red) data sets. Aligned data yields broad lines due to inherent magnetic susceptibility effects that are not averaged in a non-spinning sample or due to magnet inhomogeneity effects that could not be removed by shimming.

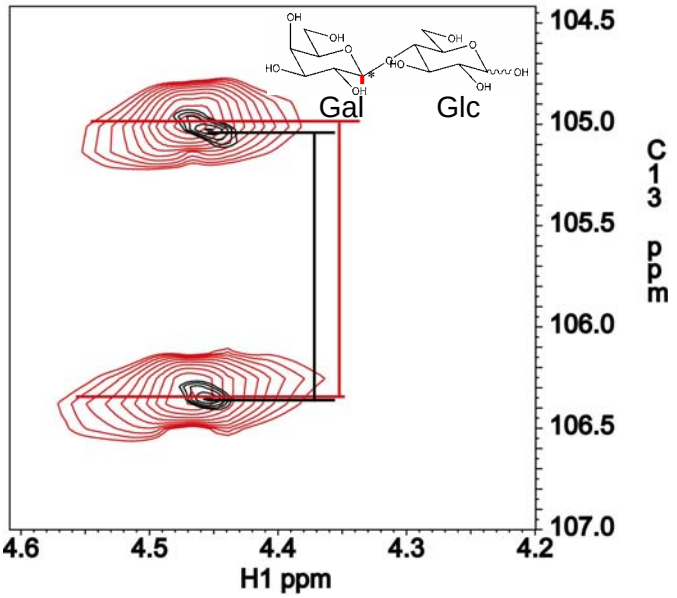


Figure 3.7. $^{13}C$-$^{1}H$ gradient-selected, coupled HSQC spectra of 70mM $^{13}C$-1 lactose in 4.25% $C_{12}E_5$. Isotropic (spinning rate = 670 Hz) data are shown in black, and aligned (static) data are shown in red.

Data for the protein G sample are somewhat more convincing. In Figures 3.8 and 3.9, isotropic (spinning 1000 Hz, black) and aligned (static, red) f1-coupled $^{15}N$-$^{1}H$ HSQC spectra that were collected under identical experimental conditions in a Varian gH{X} nanoprobe (40 µL) are shown. The sample is Protein G and $C_{12}E_5$ combined to a final concentration of 1.5 mM protein and 2.2% (w/w) $C_{12}E_5$ in 50 mM phosphate buffer (pH 5.85). RDCs are still in the range of ± 6 Hz, but the spectral resolution is higher. RDCs were measured for 51 out of 55 amino acid residues in Protein G. Note that in Figure 3.9 some splittings increase and some decrease on alignment. This is characteristic of θ being close to zero or 90° in the $(3\cos^2\theta - 1)$ functional dependence shown by RDCs.

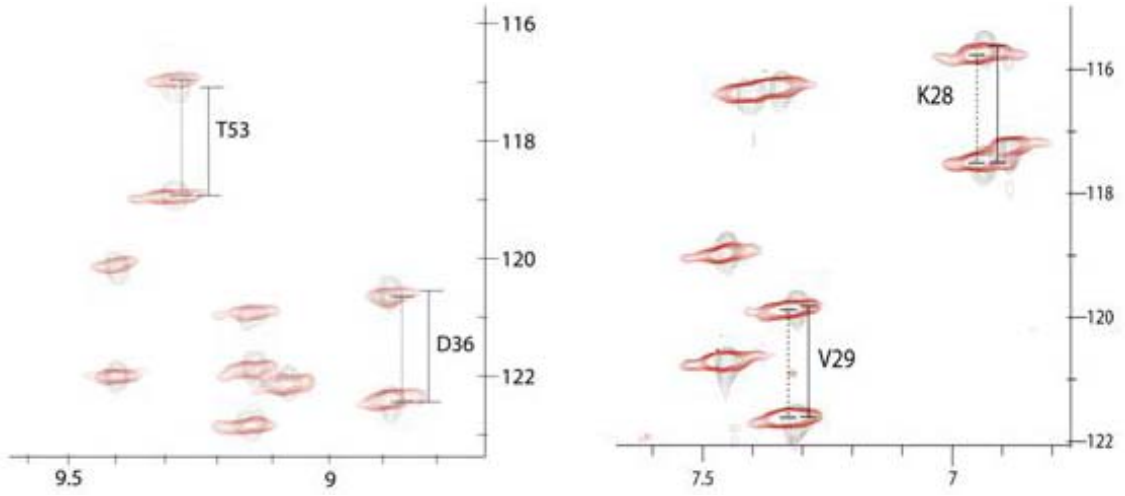


Figure 3.8. $^{15}N$-$^{1}H$ gradient-selected, coupled HSQC spectra of 1.5 mM Protein G in 2.2% $C_{12}E_5$ collected while spinning at 1000 Hz (black) and static (0 Hz, red). Also note that the centers of the doublets seem to be displaced with some being shifted up field and some down field in the aligned sample relative to the isotropic sample.

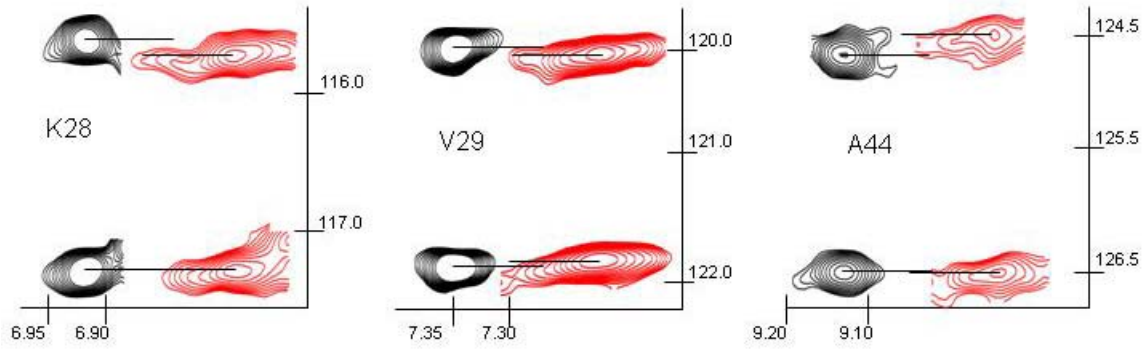


Figure 3.9. Close-up of f1-coupled $^{15}N$-$^{1}H$ HSQC spectra of 1.5 mM Protein G aligned in 2.2% (w/w) $C_{12}E_5$. Isotropic (spinning rate = 1000 Hz) data are shown in black, and aligned (static) data are shown in red. Aligned data are offset in the $^{1}H$ dimension.

## 3.5 DISCUSSION

### 3.5.1 RDC ANALYSIS

Small, nearly isotropic molecules such as mono- and disaccharides orient very weakly in the magnetic field. This weak alignment results in only small values of RDCs (Figure 3.7). The lack of multiple measurable couplings in lactose $^{13}C$ enriched only at

the C1 position prevents order matrix and orientational analysis of this sample, but it does demonstrate the ease and feasibility of measuring $^{13}C$-$^{1}H$ RDCs, useful restraints in carbohydrate analysis (44-47), in the nanoprobe.

We were not able to measure CSA offsets for the carbohydrate. In the case of a more strongly aligned carbohydrate, however, a glycolipid for example, or a sugar ring with an alkyl substituent on the reducing end, chemical shift offsets for a labeled $^{13}C$ group, such as an acetyl carbonyl carbon, could also be measured. The acetyl carbonyl carbon's chemical shift anisotropy of about 110 ppm should be large enough to be readily observed between isotropic and aligned samples. With a principal order parameter of $10^{-3}$, the resonance offset in a 4.7 T magnetic field (500 MHz for proton observation) would be about 14 Hz. Such experiments, however, await suitable samples that exhibit strong interaction with their aligning media in the magnetic field.

For the fully isotopically labeled Protein G sample, 51 RDCs out of 55 total amino acid residues were easily measured (Table S3.1). Chemical shift assignments were transferred from the original assignment at pH 4.34 (48) previously deposited in the Biological Magnetic Resonance Bank (BMRB) (49-51). Hydrogens were added to the pdb molecular structure file 1PGB.pdb (52) using the program Reduce (53) in order to produce a set of $^{15}N$-$^{1}H$ vectors that could be used in an order tensor analysis. Of the 51 couplings measured, 49 were used to determine the molecular orientation using the program REDCAT (15). The direction of the alignment can be plotted as a Sauson-Flaumsteed projection of the principal axis directions from the various order tensor solutions. These are shown in Figure 3.10, and a correlation plot of the experimental and back-calculated RDCs is shown in Figure 3.11a. RDCs measured using the

spinning/static approach of the nanoprobe are comparable to RDCs of Protein G measured in a conventional high resolution solution 5 mm probe operating at 800 MHz for $^{1}H$ (Figure 3.11b). Order parameters calculated using the measured dipolar couplings are summarized for both the HRMAS and the 5 mm probe in Table 3.2. (Peaks were picked and fit in the same way as for data collected in the nanoprobe. Personal communication, T.K. Weldeghiorghis.) It is very hard to reproduce the exact extent of order in different samples, but $S_{xx}$ and $S_{zz}$ are nearly equal in magnitude and opposite in sign for both sets. This is characteristic of a severe departure from axial symmetry, something that is characteristic of the interaction between the particular protein and aligned medium and something that should be seen in both sets of data.

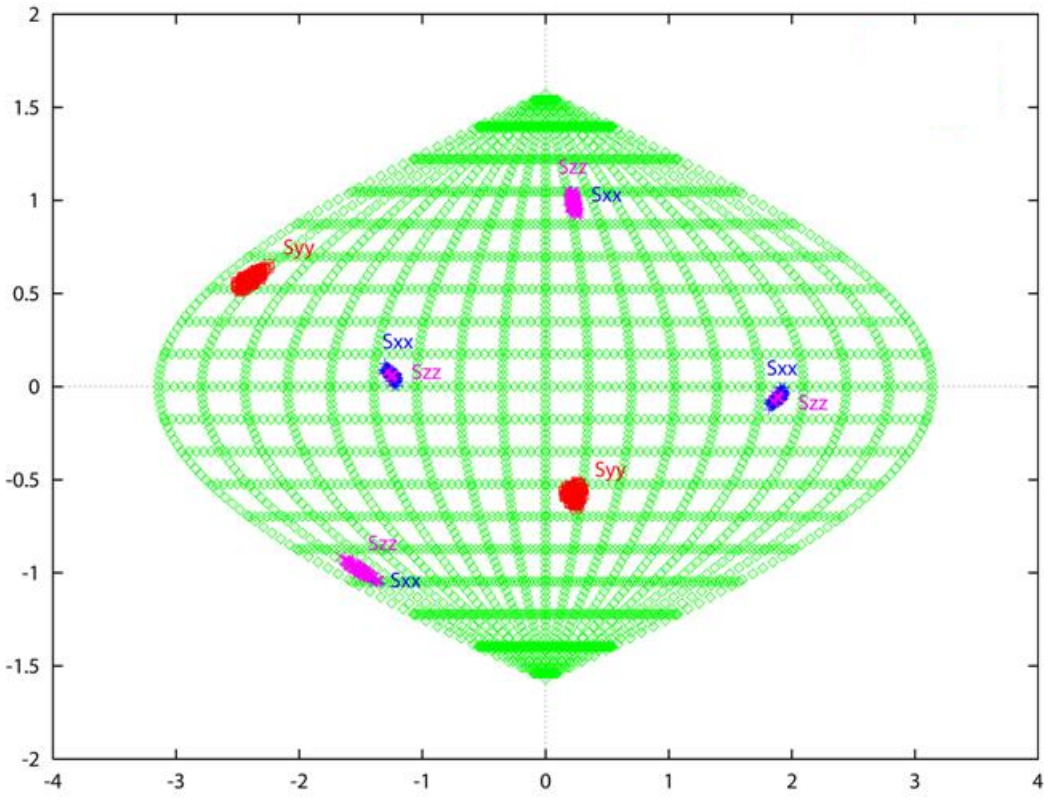


Figure 3.10. Sauson-Flaumsteed Projection of solutions of principal order parameters of the diagonalized matrix based on the 49 RDCs from Protein G.

Table 3.2. RDC parameters for Protein G

| Method | Sxx | Syy | Szz |
|---|---|---|---|
| HRMAS | $2.32e^{-4}$ | $6.29e^{-6}$ | $-2.38e^{-4}$ |
| 5 mm | $-5.46e^{-5}$ | $-2.55e^{-4}$ | $3.10e^{-4}$ |

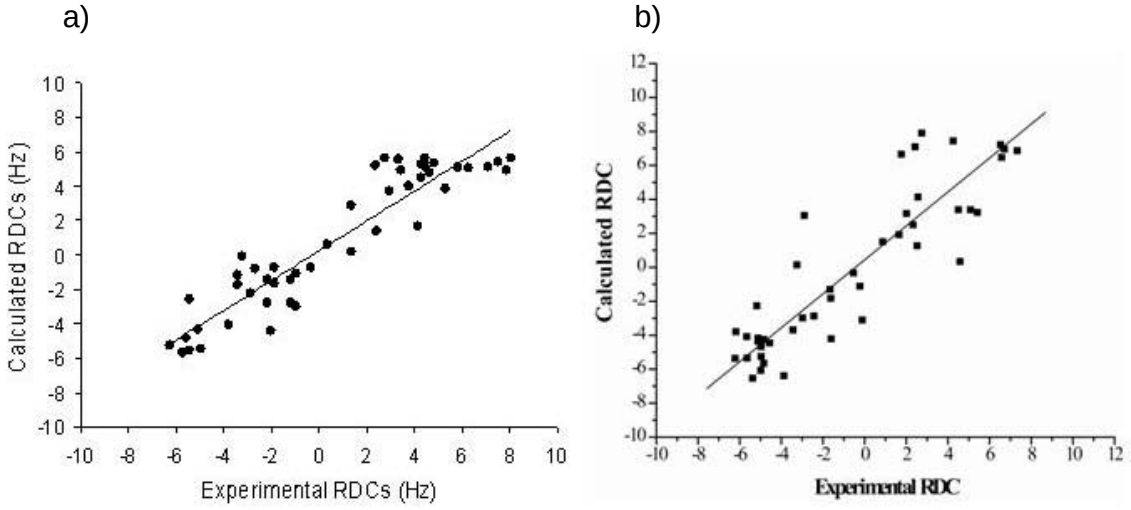


Figure 3.11. Correlation plot of back-calculated versus experimentally collected RDCs using a) spinning/static nanoprobe and best fit order parameters given in Table 3.2 and b) conventional high-resolution 5 mm probe operating at 800 MHz.

The range of RDCs of Protein G are again small in this very weakly ordered sample of 2.2% $C_{12}E_5$ ($10^{-4}$), however, the resolution is somewhat higher. It may also be that we see some of the effects of CSA offsets. The $^{15}N$ CSA is of the order of 100 ppm with the principal tensor axis nearly along the H-N bond. This would mean the CSA offsets would correlate with the increases and decreases of RDCs observed in Figure 3.9. We do see such a correlation with an upfield shift on increasing splittings and a downfield shift on decreasing splittings. The magnitude is expected to be small – on the order of a few Hz – but the correlation may be significant and this could represent useful additional structural information. As the level of order increases, 1 part in 100 for a membrane-associated protein, for example, shifts may be large enough to complicate

assignment of coupled pairs to chemical shift values determined for isotropic samples. A variable angle stator combined with the high resolution and direct $^{1}H$ detection of the HRMAS probe would be very useful in these cases.

### 3.5.2 VASS PROBE YIELDS DATA COMPARABLE TO HIGH RESOLUTION PROBES

In Figures 3.12-3.13 we show that spectra of solution quality can be obtained using a high resolution solid-state variable angle spinning probe. Although the $^{1}H$ resolution of the Doty VASS probe when spinning is expected to be < 4 Hz, static linewidths the $^{1}H$ dimension were 25-30 Hz. Also, note that in the solenoidal coil arrangement in this probe, the maximum signal-to-noise ratio is observed when the sample is at 90º to the magnetic field. More scans must be collected as the angles get smaller in order to maintain the same signal-to-noise. In the coupled HSQC spectra of Protein G in Figures 3.12 and 3.13 not enough points in $t_1$ were collected to provide an accurate measurement of N-H couplings; by our estimate these were roughly -93 ± 7 Hz. Again, reduction in signal-to-noise is apparent in Figures 3.12 and 3.13 as the angle decreases with respect to the magnetic field. These spectra, nevertheless, demonstrate it is possible to obtain data of adequate quality with variable angle probes to measure RDCs and CSA offsets in more strongly ordered samples. The ability to vary RDC by changing the angle is a powerful method of separating scalar coupling from dipolar couplings (54), and the ability to vary CSA offsets is a powerful method of correlating peak positions to chemical shift assignments done in isotropic media (55). The nanoprobe, on the other hand, offers higher resolution and a probe platform that is more available to the NMR and structural biology communities.

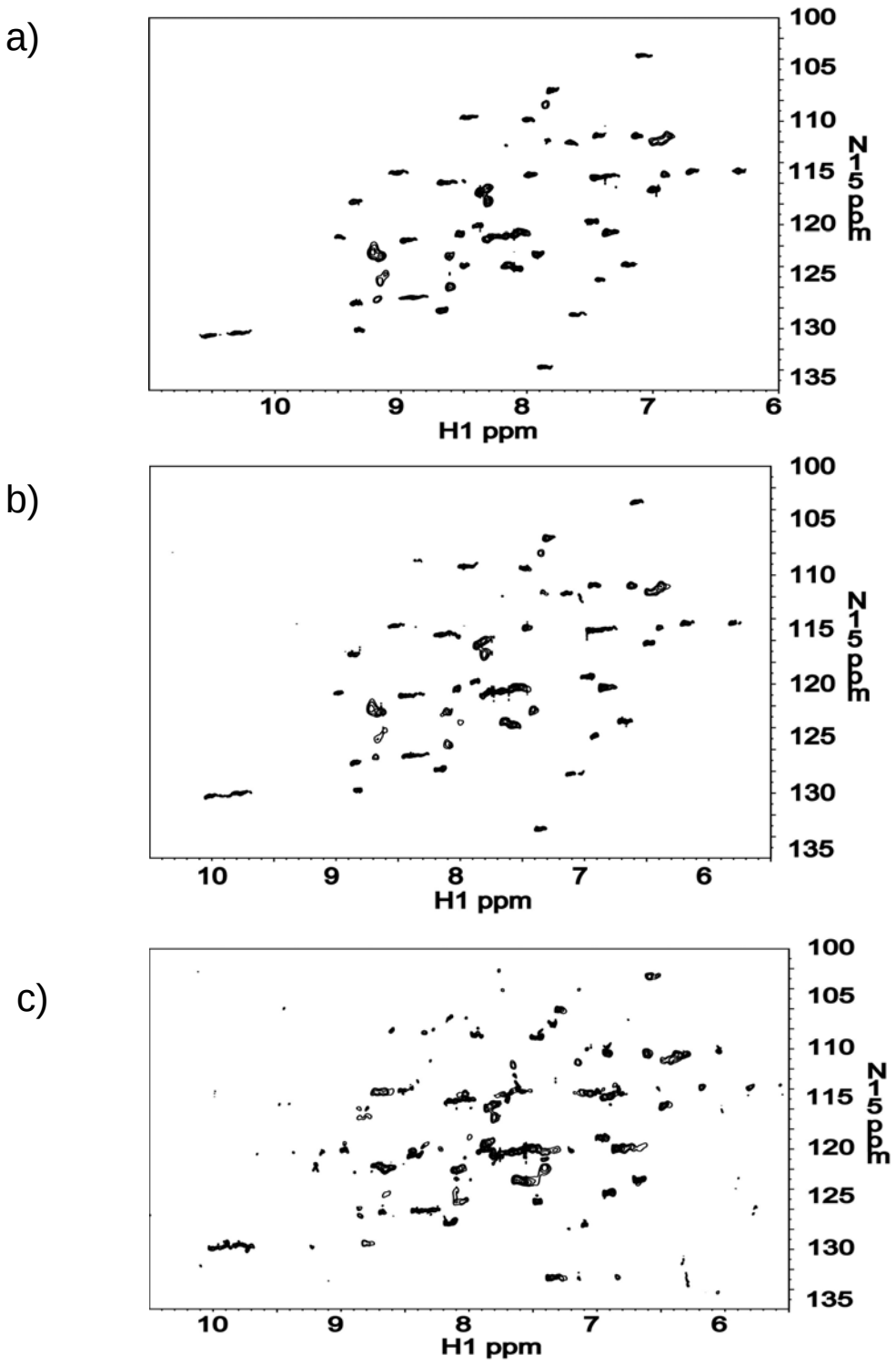


Figure 3.12. $^{15}N$-$^{1}H$ decoupled HSQC NMR spectra of 1.3 mM Protein G collected in a high resolution solid-state variable angle spinning probe at a) 80° b) 70° and c) 60° to $B_o$. Peaks are decoupled in both dimensions.

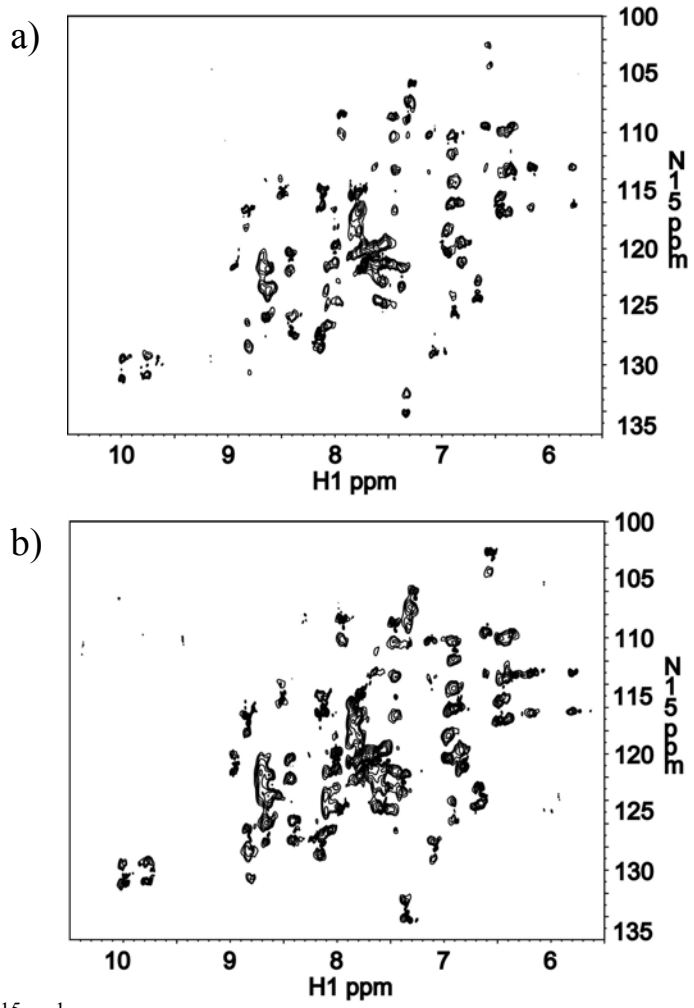


Figure 3.13. $^{15}N$-$^{1}H$ f1-coupled HSQC spectra of 1.3 mM Protein G collected at a) 90º to $B_o$ b) 80º to $B_o$.

There are also improvements to be made. It is clear from Figures 3.6-3.8 and 3.12-3.13 that static spectra collected in these HRMAS and variable angle probes have somewhat distorted lineshapes compared to spectra from more conventional probes. The nanoprobe was designed to collect data while spinning an isotropic liquid (56); hence, its resolution is inherently better for a spinning sample because bulk susceptibility effects are averaged (57). In fact, magnetic susceptibility differences are the dominant contribution to line broadening (22). Magnetic susceptibility jumps between the

sample/rotor interface both along the spinning axis and at each end of the sample give rise to magnetic field gradients that are extremely difficult to remove by shimming alone (21). Improved susceptibility-matched materials designed for non-spinning applications could also help $B_o$ homogeneity, extending the length of the sample beyond the edges of the coil, where the magnetic field is significantly less homogeneous (57). In addition, greater temperature regulation for static experiments is important. Temperature gradients have been observed to affect protein $^{15}N$-$^{1}H$ scalar couplings, and their effect on aligned data is can be as significant. In the current magic-angle spinning probe, the only source of cooling air is the spinning air shaft. In static experiments, however, little air flows into the stator, thus creating possible temperature gradients within the sample. As an example, Kurita and co-workers have determined the CSA of a peptide dissolved in a weakly ordered liquid crystal by collecting the isotropic data set, while spinning at the magic angle, and the aligned data set from a conventional 5 mm probe (58). However, the difference in temperature alone, in addition to shimming, suggests chemical shift offsets could be complicated by a number of additional factors, not just due to induced alignment.

### 3.5.4 FUTURE DIRECTIONS: APPLICATIONS TO BIAXIAL SYSTEMS

High resolution variable angle probes offer another promising application in biomolecular structure determination of samples ordered by biaxial liquid crystals. As early as 1970, deuterated liquid crystals with more than one director were examined using $^{2}H$ NMR (59-63). Many of these liquid crystals were strongly aligned, highly organic systems not amenable to the weak levels of order and solubility constraints required for biomolecular structure and orientation studies. However, the idea of a single medium

that can uniquely orient a dissolved molecule with more than one set of order parameters remains a possibility (64,65). Orientational degeneracy in using one alignment medium precludes absolute determination of orientation in the magnetic field, but finding multiple media that orient the molecule in a significantly different way can be challenging (3). If, for example, a polyacrylamide gel can be prepared such that when stretched and/or compressed, it yields multiple alignment tensors not related by a simple symmetry operation, one may have a biaxial alignment medium. A biaxially ordered liquid crystal or alignment medium could potentially offer significant savings in sample preparation for RDC measurements. One of the limitations of extracting multiple alignment tensors from biaxial systems is that conventional probe technology allows only one director – or its 90° complement – to be sampled. A high resolution variable angle probe could help generate simultaneous RDC measurements from different alignment tensors for subsequent use in structure determination or validation.

### 3.5.6 CONCLUSIONS

Here we have shown that residual dipolar couplings and perhaps CSA offsets can be collected in a magic-angle nanoprobe by comparing spectra under static and spinning conditions. The isotropic scalar couplings are measured on the same sample when spinning. This technique is advantageous for several reasons. First, the small volumes available in the nanoprobe are designed for mass-limited samples. Sensitivity in mass limited situations is higher in this 40 μL active coil volume compared to conventional high resolution probes designed for 5 mm tubes due to the smaller coil with its inherently higher Q-factor. Additionally, the sample couples more strongly to the coil when dimensions are smaller, which greatly enhances signal-to-noise. Second, both isotropic

and dipolar couplings can be measured on the same sample without changing the temperature or introducing additional media to induce alignment. Finally, chemical shift referencing is simplified since sample conditions are identical under both spinning and non-spinning conditions. The limitations of resolution and line width in these small volume HRMAS probes still prevent widespread application of this technique. However, we believe the use of HRMAS probes opens exciting new avenues for collecting anisotropic data that should be explored.

REFERENCES


1. Bax, A., Kontaxis, G. and Tjandra, N. (2001) Dipolar couplings in macromolecular structure determination. *Nuclear Magnetic Resonance of Biological Macromolecules, Pt B*, Vol. 339, pp. 127-174.
2. Bax, A. (2003) Weak alignment offers new NMR opportunities to study protein structure and dynamics. *Protein Sci*, **12,** 1-16.
3. Prestegard, J.H., Bougault, C.M. and Kishore, A.I. (2004) Residual dipolar couplings in structure determination of biomolecules. *Chem Rev*, **104,** 3519-3540.
4. Hus, J.C., Marion, D. and Blackledge, M. (2000) De novo determination of protein structure by NMR using orientational and long-range order restraints. *J Mol Biol*, **298,** 927-936.
5. Hus, J.C., Marion, D. and Blackledge, M. (2001) Determination of protein backbone structure using only residual dipolar couplings. *J Am Chem Soc*, **123,** 1541-1542.
6. Lipsitz, R.S. and Tjandra, N. (2004) Residual dipolar couplings in NMR structure analysis. *Annu Rev Biophys Biomolec Struct*, **33,** 387-413.
7. Valafar, H., Mayer, K.L., Bougault, C.M., LeBlond, P.D., Jenney, F.E., Jr., Brereton, P.S., Adams, M.W.W. and Prestegard, J.H. (2005) Backbone solution structures of proteins using residual dipolar couplings: Application to a novel structural genomics target. *J Struct Func Genom*, **5,** 241-254.
8. Prestegard, J.H., Mayer, K.L., Valafar, H. and Benison, G.C. (2005) Determination of protein backbone structures from residual dipolar couplings. *Nuclear Magnetic Resonance of Biological Macromolecules, Part C*, Vol. 394, pp. 175-+.
9. Griesinger, C., Meiler, J. and Peti, W. (2004) Angular Restraints from Residual Dipolar Couplings for Structure Refinement. In Downing, A. K. (ed.), *Protein NMR Techniques*. Humana Press, Totowa, N.H., Vol. 278.
10. Ma, C. and Opella, S.J. (2000) Lanthanide ions bind specifically to an added "EF-hand" and orient a membrane protein in micelles for solution NMR spectroscopy. *J Magn Reson*, **146,** 381-384.
11. Wohnert, J., Franz, K.J., Nitz, M., Imperiali, B. and Schwalbe, H. (2003) Protein alignment by a coexpressed lanthanide-binding tag for the measurement of residual dipolar couplings. *J Am Chem Soc*, **125,** 13338-13339.
12. Tian, F., Al-Hashimi, H.M., Craighead, J.L. and Prestegard, J.H. (2001) Conformational analysis of a flexible oligosaccharide using residual dipolar couplings. *J Am Chem Soc*, **123,** 485-492.
13. Tolman, J.R., Al-Hashimi, H.M., Kay, L.E. and Prestegard, J.H. (2001) Structural and dynamic analysis of residual dipolar coupling data for proteins. *J Am Chem Soc*, **123,** 1416-1424.
14. Tolman, J.R. (2002) A novel approach to the retrieval of structural and dynamic information from residual dipolar couplings using several oriented media in biomolecular NMR spectroscopy. *J Am Chem Soc*, **124,** 12020-12030.
15. Valafar, H. and Prestegard, J.H. (2004) REDCAT: a residual dipolar coupling analysis tool. *J Magn Reson*, **167,** 228-241.

16. Stejskal, E.O., Schaefer, J. and Waugh, J.S. (1977) Magic-Angle Spinning and Polarization Transfer in Proton-Enhanced Nmr. *J Magn Reson*, **28,** 105-112.
17. Pines, A., Gibby, M.G. and Waugh, J.S. (1973) Proton-Enhanced Nmr of Dilute Spins in Solids. *J Chem Phys*, **59,** 569-590.
18. Maas, W.E., Laukien, F.H. and Cory, D.G. (1996) Gradient, high resolution, magic angle sample spinning NMR. *J Am Chem Soc*, **118,** 13085-13086.
19. Fitch, W.L., Detre, G., Holmes, C.P., Shoolery, J.N. and Keifer, P.A. (1994) High-Resolution H-1-Nmr in Solid-Phase Organic-Synthesis. *J Org Chem*, **59,** 7955-7956.
20. Keifer, P.A. (1999) NMR tools for biotechnology. *Curr Opin Biotechnol*, **10,** 34-41.
21. Elbayed, K., Dillmann, B., Raya, J., Piotto, M. and Engelke, F. (2005) Field modulation effects induced by sample spinning: application to high-resolution magic angle spinning NMR. *J Magn Reson*, **174,** 2-26.
22. Keifer, P.A., Baltusis, L., Rice, D.M., Tymiak, A.A. and Shoolery, J.N. (1996) A comparison of NMR spectra obtained for solid-phase-synthesis resins using conventional high-resolution, magic-angle-spinning, and high-resolution magic-angle-spinning probes. *J Magn Reson Ser A*, **119,** 65-75.
23. Cheng, L.L., Ma, M.J., Becerra, L., Ptak, T., Tracey, I., Lackner, A. and Gonzalez, R.G. (1997) Quantitative neuropathology by high resolution magic angle spinning proton magnetic resonance spectroscopy. *Proc Natl Acad Sci U S A*, **94,** 6408-6413.
24. Griffin, J.L., Walker, L.A., Garrod, S., Holmes, E., Shore, R.F. and Nicholson, J.K. (2000) NMR spectroscopy based metabonomic studies on the comparative biochemistry of the kidney and urine of the bank vole (Clethrionomys glareolus), wood mouse (Apodemus sylvaticus), white toothed shrew (Crocidura suaveolens) and the laboratory rat. *Comparative Biochemistry and Physiology B-Biochemistry & Molecular Biology*, **127,** 357-367.
25. Lippens, G., Warrass, R., Wieruszeski, J.M., Rousselot-Pailley, P. and Chessari, G. (2001) High resolution magic angle spinning NMR in combinatorial chemistry. *Combinatorial Chemistry & High Throughput Screening*, **4,** 333-351.
26. Shintu, L., Ziarelli, F. and Caldarelli, S. (2004) Is high-resolution magic angle spinning NMR a practical speciation tool for cheese samples? Parmigiano Reggiano as a case study. *Magn Reson Chem*, **42,** 396-401.
27. Lacey, M.E., Subramanian, R., Olson, D.L., Webb, A.G. and Sweedler, J.V. (1999) High-resolution NMR spectroscopy of sample volumes from 1 nL to 10 mu L. *Chem Rev*, **99,** 3133-+.
28. Courtieu, J., Bayle, J.P. and Fung, B.M. (1994) Variable-angle sample-spinning NMR in liquid-crystals. *Prog NMR Spec*, **26,** 141-169.
29. Tjandra, N. and Bax, A. (1997) Direct measurement of distances and angles in biomolecules by NMR in a dilute liquid crystalline medium. *Science*, **278,** 1111-1114.
30. Prestegard, J.H. and Kishore, A.I. (2001) Partial alignment of biomolecules: an aid to NMR characterization. *Curr Opin Chem Biol*, **5,** 584-590.

31. Losonczi, J.A., Andrec, M., Fischer, M.W.F. and Prestegard, J.H. (1999) Order matrix analysis of residual dipolar couplings using singular value decomposition. *J Magn Reson*, **138,** 334-342.
32. Prestegard, J.H., Al-Hashimi, H.M. and Tolman, J.R. (2000) NMR structures of biomolecules using field oriented media and residual dipolar couplings. *Q Rev Biophys*, **33,** 371-424.
33. Tolman, J.R. and Prestegard, J.H. (1996) A quantitative J-correlation experiment for the accurate measurement of one-bond amide N-15-H-1 couplings in proteins. *J Magn Reson Ser B*, **112,** 245-252.
34. Ottiger, M., Delaglio, F. and Bax, A. (1998) Measurement of J and dipolar couplings from simplified two-dimensional NMR spectra. *J Magn Reson*, **131,** 373-378.
35. Pervushin, K., Riek, R., Wider, G. and Wuthrich, K. (1997) Attenuated T-2 relaxation by mutual cancellation of dipole-dipole coupling and chemical shift anisotropy indicates an avenue to NMR structures of very large biological macromolecules in solution. *Proc Natl Acad Sci U S A*, **94,** 12366-12371.
36. Riek, R., Wider, G., Pervushin, K. and Wuthrich, K. (1999) Polarization transfer by cross-correlated relaxation in solution NMR with very large molecules. *Proc Natl Acad Sci U S A*, **96,** 4918-4923.
37. Kontaxis, G., Clore, G.M. and Bax, A. (2000) Evaluation of cross-correlation effects and measurement of one-bond couplings in proteins with short transverse relaxation times. *J Magn Reson*, **143,** 184-196.
38. Ruckert, M. and Otting, G. (2000) Alignment of biological macromolecules in novel nonionic liquid crystalline media for NMR experiments. *J Am Chem Soc*, **122,** 7793-7797.
39. Jonstromer, M. and Strey, R. (1992) Nonionic bilayers in dilute solutions: effect of additives. *J Phys Chem*, **96,** 5993-6000.
40. Freyssingeas, E., Nallet, F. and Roux, D. (1996) Measurement of the membrane flexibility in lamellar and "sponge" phases of the C12E5/hexanol/water system. *Langmuir*, **12,** 6028-6035.
41. Delaglio, F., Grzesiek, S., Vuister, G.W., Zhu, G., Pfeifer, J. and Bax, A. (1995) Nmrpipe - a Multidimensional Spectral Processing System Based on Unix Pipes. *J Biomol NMR*, **6,** 277-293.
42. Sodickson, A. and Cory, D.G. (1997) Shimming a high-resolution MAS probe. *J Magn Reson*, **128,** 87-91.
43. Piotto, M., Elbayed, K., Wieruszeski, J.M. and Lippens, G. (2005) Practical aspects of shimming a high resolution magic angle spinning probe. *J Magn Reson*, **173,** 84-89.
44. Martin-Pastor, M. and Bush, C.A. (2000) Conformational studies of human milk oligosaccharides using H-1-C-13 one-bond NMR residual dipolar couplings. *Biochemistry*, **39,** 4674-4683.
45. Martin-Pastor, M. and Bush, C.A. (2000) The use of NMR residual dipolar couplings in aqueous dilute liquid crystalline medium for conformational studies of complex oligosaccharides. *Carbohydr Res*, **323,** 147-155.
46. Martin-Pastor, M. and Bush, C.A. (2001) Refined structure of a flexible heptasaccharide using $^{1}H$-$^{13}C$ and $^{1}H$-$^{1}H$ NMR residual dipolar couplings in

concert with NOE and long range scalar coupling constants. *J Biomol NMR*, **19,** 125-139.

47. Martin-Pastor, M., Canales-Mayordomo, A. and Jimenez-Barbero, J. (2003) NMR experiments for the measurement of proton-proton and carbon-carbon residual dipolar couplings in uniformly labelled oligosaccharides. *J Biomol NMR*, **26,** 345-353.
48. Gronenborn, A.M., Filpula, D.R., Essig, N.Z., Achari, A., Whitlow, M., Wingfield, P.T. and Clore, G.M. (1991) A Novel, Highly Stable Fold of the Immunoglobulin Binding Domain of Streptococcal Protein-G. *Science*, **253,** 657-661.
49. Doreleijers, J.F., Mading, S., Maziuk, D., Sojourner, K., Yin, L., Zhu, J., Markley, J.L. and Ulrich, E.L. (2003) BioMagResBank database with sets of experimental NMR constraints corresponding to the structures of over 1400 biomolecules deposited in the Protein Data Bank. *J Biomol NMR*, **26,** 139-146.
50. Nabuurs, S.B., Nederveen, A.J., Vranken, W., Doreleijers, J.F., Bonvin, A., Vuister, G.W., Vriend, G. and Spronk, C. (2004) DRESS: a database of REfined solution NMR structures. *Proteins: Struct, Function, Bioinform*, **55,** 483-486.
51. Nederveen, A.J., Doreleijers, J.F., Vranken, W., Miller, Z., Spronk, C., Nabuurs, S.B., Guntert, P., Livny, M., Markley, J.L., Nilges, M. *et al.* (2005) RECOORD: A recalculated coordinate database of 500+proteins from the PDB using restraints from the BioMagResBank. *Proteins: Struct, Function, Bioinform*, **59,** 662-672.
52. Gallagher, T., Alexander, P., Bryan, P. and Gilliland, G.L. (1994) 2 Crystal-Structures of the B1 Immunoglobulin-Binding Domain of Streptococcal Protein-G and Comparison with Nmr. *Biochemistry*, **33,** 4721-4729.
53. Word, J.M., Lovell, S.C., Richardson, J.S. and Richardson, D.C. (1999) Asparagine and glutamine: Using hydrogen atom contacts in the choice of side-chain amide orientation. *J Mol Biol*, **285,** 1735-1747.
54. Tian, F., Losonczi, J.A., Fischer, M.W.F. and Prestegard, J.H. (1999) Sign determination of dipolar couplings in field-oriented bicelles by variable angle sample spinning (VASS). *J Biomol NMR*, **15,** 145-150.
55. Kishore, A.I. and Prestegard, J.H. (2003) Molecular orientation and conformation of phosphatidylinositides in membrane mimetics using variable angle sample spinning (VASS) NMR. *Biophys J*, **85,** 3848-3857.
56. Barbara, T.M. and Bronnimann, C.E. (1999) Target field design for magic angle gradient coils. *J Magn Reson*, **140,** 285-288.
57. Barbara, T.M. (1994) Cylindrical Demagnetization Fields and Microprobe Design in High-Resolution Nmr. *J Magn Reson Ser A*, **109,** 265-269.
58. Kurita, J., Shimahara, H., Utsunomiya-Tate, N. and Tate, S. (2003) Measurement of N-15 chemical shift anisotropy in a protein dissolved in a dilute liquid crystalline medium with the application of magic angle sample spinning. *J Magn Reson*, **163,** 163-173.
59. Collings, P.J., Photinos, D.J., Bos, P.J., Ukleja, P. and Doane, J.W. (1979) NMR in spinning samples of biaxial liquid crystals. *Phys Rev Lett*, **42,** 996-999.
60. Doane, J.W. (1983) Deuterium NMR of biaxially ordered liquid crystals. *Isr J Chem*, **23,** 323-328.

61. Luckhurst, G.R. (2001) Biaxial nematic liquid crystals: fact or fiction? *Thin Solid Films*, **393,** 40-52.
62. Taylor, T.R., Fergason, J.L. and Arora, S.L. (1970) Biaxial liquid crystals. *Phys Rev Lett*, **24,** 359-362.
63. Yaniv, A., Doane, J.W., Barbara, T. and Dailey, B.P. (1982) NMR spectral patterns in magneto-aligned biaxial liquid crystals. *Mol Cryst Liq Cryst*, **88,** 311-315.
64. Tolman, J.R. (2001) Dipolar couplings as a probe of molecular dynamics and structure in solution. *Curr Opin Struct Biol*, **11,** 532-539.
65. Riley, S.A., Giuliani, J.R. and Augustine, M.P. (2002) Capture and manipulation of magnetically aligned Pf1 with an aqueous polymer gel. *J Magn Reson*, **159,** 82-86.

SUPPLEMENTARY MATERIAL

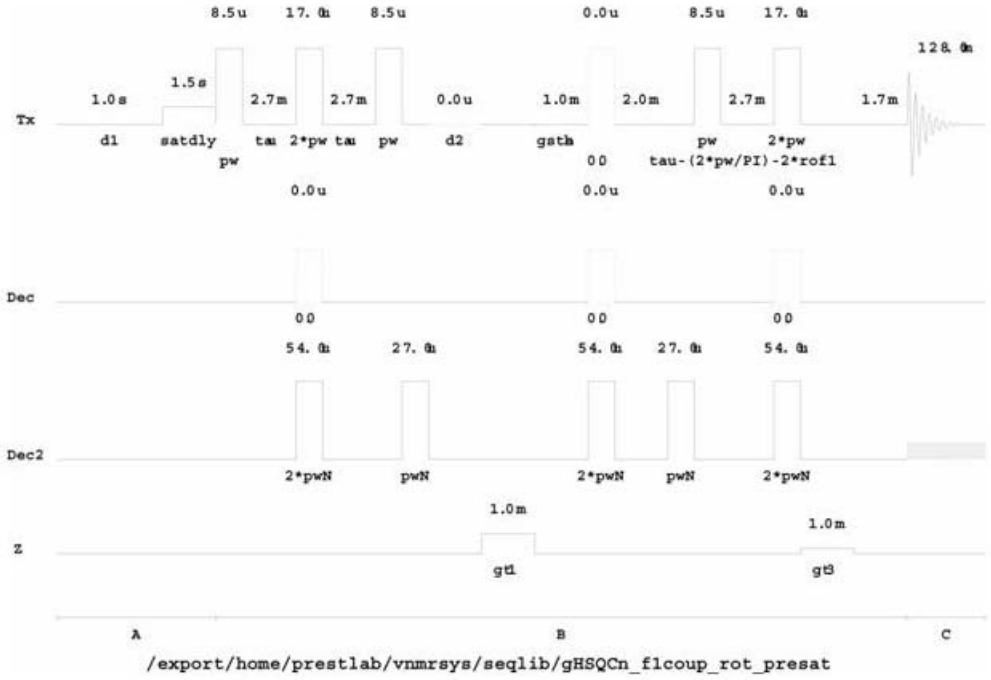


Figure S3.1. Gradient-selected coupled HSQC pulse sequence with gradient selection pulses synchronized with integer multiple of spinning rate. Water suppression was accomplished with a presaturation pulse.

Table S3.1. Scalar and residual dipolar couplings for Protein G measured using the spinning/static nanoprobe approach. All values are reported in Hz.

| Amino Acid[a] | J[b] | J+D[c] | RDCs (exp)[d] | RDCs (calc)[e] |
|---|---|---|---|---|
| Q2 | 95.654 | 90.795 | -4.859 | 0 |
| Y3 | 95.321 | - | - | - |
| K4 | 93.619 | 97.373 | 3.754 | 3.999 |
| L5 | 93.314 | 96.642 | 3.328 | 5.579 |
| A6 | 94.711 | 95.938 | 1.227 | 5.22188 |
| L7 | 94.126 | 99.925 | 5.799 | 5.103 |
| N8 | 93.574 | 98.877 | 5.303 | 3.837 |
| G9 | 94.654 | 96.018 | 1.364 | 2.855 |
| K10 | 93.865 | 96.284 | 2.419 | 1.401 |
| T11 | 93.116 | - | - | - |
| L12 | 92.148 | 94.491 | 2.343 | 5.172 |
| K13 | 92.785 | 97.607 | 4.822 | 5.302 |
| G14 | 93.301 | 99.137 | 5.836 | 5.034 |
| E15 | 92.354 | 95.105 | 2.751 | 5.589 |
| T16 | 93.310 | 97.732 | 4.422 | 5.600 |
| T17 | 94.455 | 98.755 | 4.300 | 4.502 |
| T18 | 93.273 | 93.589 | 0.316 | 0.581 |

| Amino Acid[a] | J[b] | J+D[c] | RDCs (exp)[d] | RDCs (calc)[e] |
|---|---|---|---|---|
| E19 | 93.375 | 97.513 | 4.138 | 1.650 |
| A20 | 95.681 | 94.460 | -1.221 | -1.483 |
| V21 | 92.818 | 89.410 | -3.408 | -1.200 |
| D22 | 93.108 | 92.145 | -0.963 | -2.994 |
| A23 | 94.009 | 95.363 | 1.354 | 0.144 |
| A24 | 94.308 | 89.188 | -5.120 | -4.320 |
| T25 | 92.837 | 87.271 | -5.566 | -4.835 |
| A26 | 94.665 | 91.773 | -2.892 | -2.228 |
| E27 | 93.997 | 91.817 | -2.180 | -1.415 |
| K28 | 94.291 | 88.578 | -5.713 | -5.706 |
| V29 | 93.522 | 88.561 | -4.961 | -5.443 |
| F30 | 95.212 | 98.861 | -1.891 | -1.695 |
| K31 | 94.467 | 92.285 | -2.182 | -2.796 |
| Q32 | 93.063 | 87.648 | -5.415 | -5.579 |
| Y33 | - | - | - | - |
| A34 | 94.646 | 91.976 | -2.670 | -0.816 |
| N35 | 93.871 | 90.071 | -3.800 | -4.070 |
| D36 | 94.573 | 88.337 | -6.236 | -5.243 |
| N37 | 92.723 | 91.75 | -0.973 | -1.094 |
| G38 | 94.845 | 94.493 | -0.352 | -0.743 |
| V39 | 93.522 | 88.068 | -5.454 | -2.591 |
| D40 | 93.618 | 90.223 | -3.395 | -1.744 |
| G41 | 92.725 | 90.685 | -2.040 | -4.423 |
| E42 | 93.446 | 90.23 | -3.216 | -0.121 |
| W43 | 93.598 | 102.013 | 7.837 | 4.936 |
| A44 | 92.925 | 100.941 | 8.016 | 5.604 |
| Y45 | 92.994 | 97.267 | 4.273 | 5.237 |
| D46 | 93.832 | 100.072 | 6.240 | 5.068 |
| D47 | 96.544 | - | - | - |
| A48 | 94.417 | 93.212 | -1.205 | -2.786 |
| T49 | 93.996 | 92.101 | -1.895 | -0.766 |
| K50 | 93.819 | 98.222 | 4.403 | 5.124 |
| T51 | 92.959 | 95.913 | 2.954 | 3.711 |
| F52 | 93.782 | 98.419 | 4.637 | 4.760 |
| T53 | 92.841 | 100.351 | 7.510 | 5.379 |
| V54 | 94.607 | 98.973 | 4.366 | 5.276 |
| T55 | 92.79 | 96.203 | 3.413 | 4.884 |
| E56 | 92.038 | 99.087 | 7.049 | 5.101 |

[a] Amino acid assignment (48)
[b] N-H isotropic scalar coupling
[c] Scalar plus residual dipolar coupling
[d] Experimental RDCs measured ((J+D) – J)
[e] Back-calculated RDCs (based on the best fit alignment tensor reported in Table 3.2)

Table S3.2. Spherical harmonic shims in the tilted frame expressed as linear combinations of laboratory frame shims.[a] (42)

First order:
$B_z^* = 1/\sqrt{3}\ B_z - \sqrt{(2/3)}\ B_x$
$B_x^* = 1/\sqrt{3}\ B_z + \sqrt{(2/3)}\ B_x$
$B_y^* = B_y$

Second order:
$B_{z2}^* = B_{(x2-y2)} - 2\sqrt{2}\ B_{zx}$
$B_{zx}^* = -1/3\ B_{zx} + (1/6)\sqrt{2}\ B_{z2} - (1/6)\sqrt{2}\ B_{(x2-y2)}$
$B_{zy}^* = -1/\sqrt{3}\ B_{zy} - \sqrt{(2/3)}\ B_{xy}$
$B_{(x2-y2)}^* = (2/3)\ \sqrt{2}\ B_{zx} + 1/3\ B_{z2} + 2/3\ B_{(x2-y2)}$
$B_{xy}^* = -1/\sqrt{3}\ B_{xy} + \sqrt{(2/3)}\ B_{zy}$

Third order:
$B_{z3}^* = (-2/3)/\sqrt{3}\ B_{z3} - 1/\sqrt{6}\ B_{z2x} + 5/\sqrt{3}\ B_{z(x2-y2)} - (5/3)/\sqrt{6}\ B_{x3}$
$B_{z2x}^* = (1/3)\sqrt{(2/3)}B_{z3} - (1/2)\sqrt{3}\ B_{z2x} + (5/6)\sqrt{3}\ B_{x3}$
$B_{z2y}^* = (-10/3)\sqrt{2}B_{xyz} + (1/6)\ B_{z2y} + (5/6)\ B_{y3}$
$B_{z(x2-y2)}^* = (1/3)\ \sqrt{3}\ B_{z3} - 1/3\ \sqrt{(2/3)}B_{x3}B_{xyz}^* = -1/3\ B_{xyz} + (1/12)\sqrt{2}\ B_{z2y} - (1/12)\ \sqrt{2}\ B_{y3}$
$B_{x3}^* = (-1/3)\sqrt{(2/3)}\ B_{z3} + 1/2/\sqrt{3}\ B_{z2x} + 2\sqrt{(2/3)}\ B_{z(x2-y2)} + (5/6)/\sqrt{3}\ B_{x3}$
$B_{y3}^* = 2\sqrt{2}\ B_{xyz} + (½)\ B_{z2y} + (1/2)\ B_{y3}$

Fourth order:
$B_{z4}^* = (-7/18)\ B_{z4} + \sum (m=1\ldots4)\ c_m T_{4m}$

Fifth order:
$B_{z5}^* = (-1/6)\ \sqrt{3}\ B_{z5} + \sum (m=1\ldots4)\ c_m T_{5m}$

[a] In this system the MAS frame and the laboratory frame share the same y-axis, and the spinning axis is oriented in the x-z frame.

# CHAPTER 4

# NMR STUDIES OF $PIP_2$-ARF1 INTERACTIONS AT A MEMBRANE SURFACE[1]

[1] Kishore, A.I., R.D. Seidel & J.H. Prestegard. To be submitted to *Biochemistry*.

ABSTRACT

$^{31}$P NMR spectra and $^{15}$N-$^{1}$H residual dipolar couplings (RDCs) were used to assess the extent of protein-lipid binding and level of ordering of the membrane-associating protein ADP Ribosylation Factor 1 (ARF1) at the membrane surface. Phosphatidylinositol bisphosphate ($PIP_2$) and its soluble analog dibutyryl-inositol bisphosphate were incorporated separately into a liquid crystalline model membrane and added to ARF1 to increase the fraction of membrane-associated ARF1. $PIP_2$ was found to bind ARF1 tightly, possibly more tightly than previously reported values (10-45 μM), and some $PIP_2$ appeared to come out of the membrane. Results suggest the surprising finding that ARF1 may extract $PIP_2$ from the membrane, possibly tucking $PIP_2$'s acyl chains into the hydrophobic cleft normally occupied by ARF1's myristoyl chain. NMR data from a model for myristoylated ARF1, hexyl-ARF1, indicate decreased $PIP_2$ binding and membrane association, suggesting hexyl-ARF1 may provide a better understanding of ARF1 structure and function than other non-myristoylated models.

## 4.1 THE ARF1 MEMBRANE ASSOCIATION PROBLEM

Structural characterization of membrane-associated molecules lags behind their biochemical characterization due to a lack of suitable experimental tools. Recent developments in nuclear magnetic resonance (NMR) spectroscopy are making it possible to study membrane-associating molecules in a membrane-like environment through the careful reintroduction of anisotropic data using novel NMR technologies similar to those introduced in the previous chapters. However, the bottleneck in expression and purification of many membrane-associated proteins still restricts the application of these new techniques to more easily obtained, smaller molecules such as membrane-associating peptides (1,2) or lipids (3).

An example of an important target for structural study is the membrane-associating protein ADP Ribosylation Factor 1 (ARF1). ARF1 is a member of a family of Ras-related ~21 kDa guanine nucleotide-binding eukaryotic proteins involved in vesicle trafficking and coatamer formation. Another important aspect of ARF1 is its ability to bind both GDP and GTP through a myristoyl-initiated conformational switch. The sequence of events leading to ARF1's membrane association and functional role in trafficking is not fully understood. Ideally, determining the structure of myrARF1 in a membrane would be an important first step in understanding ARF1's role in vesicle formation. However, myrARF1 expression has not yet been successful in yields sufficient for NMR structural study. Nevertheless, through X-ray structures (4,5) and NMR evidence (6) on the soluble non-myrARF1 and related mutants, several structural regions have been implicated in membrane targeting. The N-terminal myristoyl chain, N-terminal amphipathic helix, and positive patch of basic residues, together, may target

ARF1 to the membrane for subsequent activation. These structural elements are, in fact, common to a number of membrane-associating proteins and are illustrated using myrARF1 in Figure 4.1. Phosphatidylinositol bisphosphate ($PIP_{2)}$, a phospholipid commonly involved in signaling events, is known to interact with positive patches on a number of ARF1 effectors and activators and may aid in membrane association (7,8). Independent studies have also suggested that non-myristoylated ARF1 binds $PIP_2$ with weak affinity (<10-45 μM) both in the presence (9,10) and absence (11) of other lipids. The investigation of $PIP_2$-ARF1 interactions represents an important undertaking that can be pursued in the absence of viable myr-ARF1 samples.

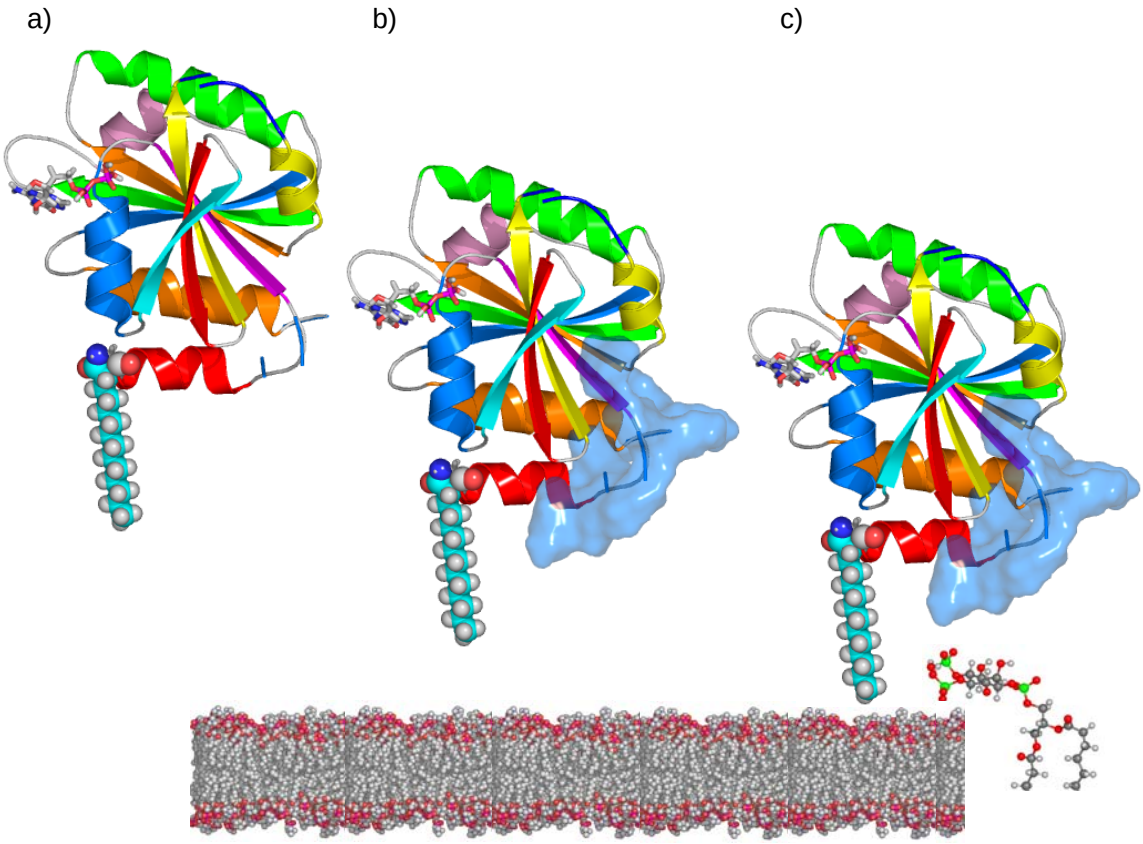


Figure 4.1. ARF1 illustrates the different classes of membrane-associated molecules. a) A single domain with an acyl modification, myristoylation in ARF1's case (spheres) and an amphipathic helix in red b) plus a patch of positively charged amino acid residues (shown as a blue surface) c) plus membrane-anchoring $PIP_2$ also shown.

## 4.2 NMR CHARACTERIZATION OF $PIP_2$-ARF1 INTERACTIONS

NMR is uniquely suited to study this protein-lipid interaction. First, perturbations in chemical shift resonances in a protein upon addition of ligand (or *vice versa*) are indicative of a protein-ligand interaction. The specific molecular interactions can be identified if resonances have been assigned, and binding constants in the μM to mM range can be determined by quantifying these interactions. Most importantly, the degree of order and orientation of a molecule, such as membrane-associated ARF1, can be determined by NMR. Since their introduction in 1963, liquid crystals have been used to orient molecules within a magnetic field (12). Alignment of biomolecules in the magnetic field has produced a wealth of information on their structures and orientations. The kind of data available from ordered molecules, namely residual dipolar couplings (RDCs) and chemical shift offsets, can be analyzed with order matrix analysis to determine the amount of ordering a molecule has along each of the three axes in an alignment frame (13,14). This information can also provide the orientation of the molecule relative to the alignment frame by placing constraints on the geometries of molecular models.

Perhaps the closest example of RDCs being used to characterize the interaction of a protein with a membrane is a recent study of the photo-initiated interaction of the transducin peptide bound to its membrane-bound receptor rhodoposin (15,16). This interaction is not strong and the effects of interaction with the membrane bound rhodopsin must be separated from the non-specific interaction of soluble peptide with membrane surfaces.

### 4.2.1 PROPOSED STUDY OF ARF1-$PIP_2$

In this work, I have attempted to study the alignment of unmyristoylated (non-myr) ARF1 upon interaction with $PIP_2$ (17). This association also proves to be weak. Two forms of $PIP_2$ with differing acyl chain lengths were tested. Dibutyryl $PIP_2$ was used to compare its behavior with ARF1 in solution (from previously collected data) to ARF1 in the presence of a model membrane. Diacyl $PIP_2$ (with acyl chains on the order of 18-20 carbons) was then tested as a naturally occurring lipid that is more readily incorporated into a membrane than dibutryl-$PIP_2$. Specific changes in chemical shift of resonances from $^{15}N$-labeled non-myrARF1 were observed upon addition of both forms of $PIP_2$, indicating $PIP_2$ binds non-myrARF1 in the presence of a model membrane on a timescale that yields averaged NMR signals. The degree of ordering of non-myrARF1 was assessed using a form of easily acquired data, $^{15}N$-$^{1}H$ (RDCs) in the presence and absence of $PIP_2$. $PIP_2$ and phosphates of the GDP-bound ARF1 were also monitored *via* $^{31}P$ NMR. The results suggest the surprising finding that the $PIP_2$-non-myrARF1 complex in a membrane binds $PIP_2$ with sufficient strength to change the equilibrium of $PIP_2$ in the model membrane compared to $PIP_2$ alone in a membrane. A model for myrARF1, hexylated ARF1, was also tested for $PIP_2$ binding and membrane association. Biochemical implications of the findings are also discussed.

## 4.3 MATERIALS & METHODS

### 4.3.1 SAMPLE PREPARATION

ARF1 samples with three different isotopic labeling schemes were prepared exactly according to the previously published protocol (18), and the second sample, $^{2}H$, $^{15}N$-ARF1, was prepared by the same methods using $D_2O$ in place of $H_2O$ with a

subsequent exchange into protonated Tris buffer (20 mM Tris, 100 mM NaCl, 2 mM $MgCl_2$, pH 7.6). The third sample, $^{13}C$, $^{15}N$-ARF1, was prepared similarly to the first sample but using a mixture of C1 and C2 $^{13}C_1$-glucose in place of unlabeled glucose; it was exchanged into protonated potassium phosphate buffer (10 mM, 50 mM NaCl, 1 mM $MgCl_2$, 5 mM $NaN_3$, pH 7.0). Hexyl-ARF1 was prepared by first expressing a mutant form of ARF1 where the N-terminal glycine was mutated to a cysteine (G2C) followed by attachment of a hexyl chain to the terminal cysteine by a disulfide linkage (19). Hexyl-methanethiolsulfonate (HTMS, Toronto Research Chemicals Inc., Toronto, Canada) plus G2C-ARF1 were combined in a 1:1 ratio to yield a stoichiometric hexylation. Hexyl-ARF1 was exchanged into phosphate buffer as described above.

### 4.3.2 ALIGNMENT MEDIUM PREPARATION

$C_{12}E_5$/hexanol has previously been identified as a suitable alignment medium for both ARF1 (6) and $PIP_2$ (20). This medium was prepared as follows: Pentaethylene glycol monododecyl ether $C_{12}E_5$ (Sigma, St. Louis, MO) was combined with hexanol in the ratio 0.88:1 to make a solution of 4.6% (w/w) (21-23). ARF1 constructs were added to reach concentrations of 0.7 to 1.0 mM. Dibutyryl-phosphatidylinositol (4,5)-bisphosphate (Echelon Biosciences Inc., Salt Lake City, UT) (Figure 4.2a) was lyophilized and added directly to the protein-liquid crystal solution to yield a final concentration of 2.0 mM, or about 3:1, $PIP_2$/ARF1 and 1:41 $PIP_2$/lipid. Long-chain $PIP_2$ (phosphatidylinositol 4,5-bisphosphate, Avanti Polar Lipids, (Alabaster, AL)) from here on referred to as diacyl $PIP_2$ (Figure 4.2b), was dried under a stream of nitrogen and added directly to the $C_{12}E_5$ bilayers at a relatively low molar ratio of $PIP_2$ to $C_{12}E_5$ (1:80) so that bilayer order is not disrupted. A stock solution of 25% (w/v) phospholipid ether-

linked bicelles were also prepared in Tris buffer (pH 7.6) in a 3:1 ratio of dimyristoylphosphatidylcholine (DMPC) and dihexanoylphosphatidylcholine (DHPC) (Avanti Polar Lipids, Alabaster, AL). Samples were equilibrated in the magnetic field at 25 °C ($C_{12}E_5$) and 35 ºC (bicelles) for approximately 2 h before beginning NMR acquisition. Liquid crystal alignment in all cases was confirmed by monitoring $^2H$ quadrupolar splitting by NMR.

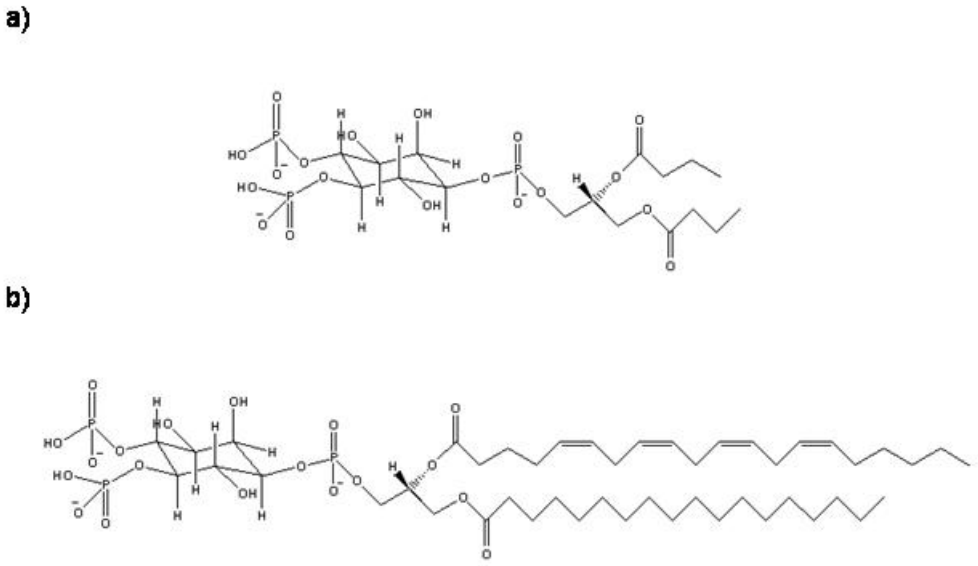


Figure 4.2. Molecular structures of a) dibutyryl $PIP_2$ and b) diacyl $PIP_2$.

4.3.3 NMR EXPERIMENTS

All two dimensional experiments were performed on a Varian Inova spectrometer operating at 800 MHz for proton, and 81.8 MHz for nitrogen. A triple resonance Varian Cold Probe was used to enhance sensitivity. Because of losses associated with high conductivity samples in this type of probe, a 4 mM Shigemi tube was used to decrease the volume of salt in the coil. The heteronuclear single quantum coherence (HSQC) experiment was used to confirm the presence of native-like structures for the protein in the presence of liquid crystal media and to monitor chemical shift perturbations. RDCs

were collected either using the In-Phase/Anti-Phase HSQC experiment (24) or using an interleaved TROSY-HSQC/decoupled HSQC experiment (25-27). For IPAP-HSQC data, 256 complex points were collected in $t_1$ and 2048 points were collected in $t_2$. The total acquisition time was 6 h for the IPAP data and 45 min for decoupled HSQCs. $^{31}P$ spectra were collected on a Varian Inova spectrometer operating at 499 MHz for proton and 202.6 MHz for phosphorus using a 5 mm Varian broadband observe probe. Adiabatic WURST $^{1}H$-decoupling was applied at a $B_1$ field of 7000 Hz.

All data sets were processed with NMRPipe (28). A Lorentz-to-Gaussian function was used for apodization in both dimensions, and 256 points were linear predicted in the indirect dimension. Zero-filling to 4096 in $t_2$ and 512 points in $t_1$ prior to FT were applied in each dimension. Peaks were picked using NMRDraw and fit to a Gaussian lineshape using the non-linear least squares fitting routine (nlinLS) in NMRPipe.

## 4.4 RESULTS

### 4.4.1 CHEMICAL SHIFT PERTURBATIONS IN $^{15}N$-$^{1}H$ HSQC SPECTRA

Chemical shift perturbations in select amino acid resonances were observed between the liquid crystal aligned samples with and without $PIP_2$. Figure 4.3 shows the changes in chemical shifts in both the $^{1}H$ and $^{15}N$ dimensions for the residues undergoing the most change in $C_{12}E_5$-oriented ARF1 with a) dibutyryl and b) diacyl $PIP_2$. Chemical shifts appear to be extensive throughout the protein, but most changes are actually confined to a small number of structural elements. Individual residues experiencing shifts are reported in Table 4.1. Many of these shifts were previously reported for dibutyryl $PIP_2$ binding of ARF1 in solution (6). Line broadening is more noticeable in

diacyl $PIP_2$-ARF1 (Figure 4.3b) due to more abundant long range dipolar couplings that come along with higher levels of ordering. Nevertheless, resolution still permits easy assignment and measurement of chemical shift differences.

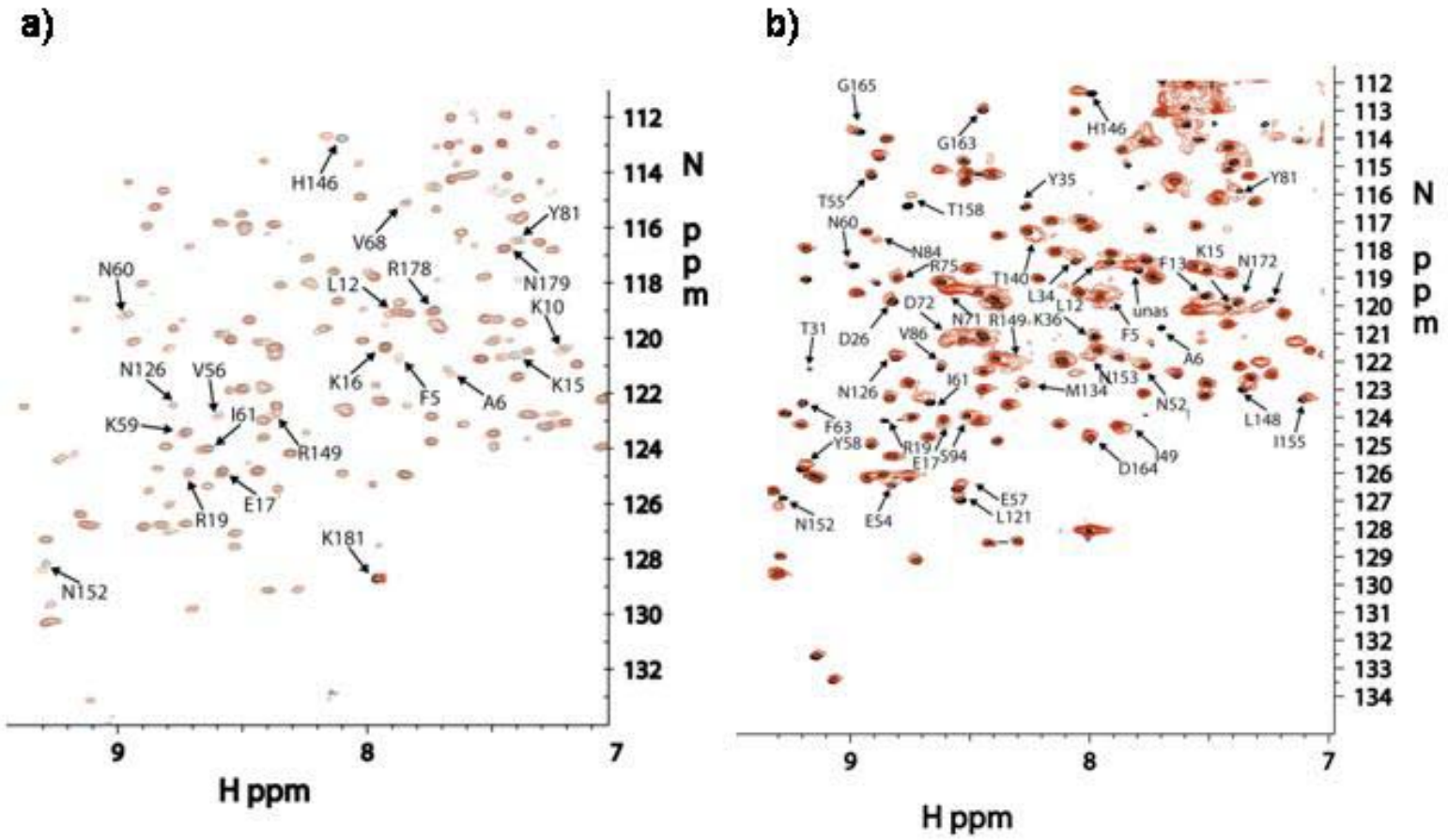


Figure 4.3. $^{15}N$-$^{1}H$ HSQC spectra of $^{15}N$ ARF1 oriented in $C_{12}E_5$ with and without $PIP_2$. a) dibutyryl $PIP_2$: 0.8 mM ARF1 in 2.2% $C_{12}E_5$ with (red) and without (black) 1.4 mM dibutyryl $PIP_2$. b) diacyl $PIP_2$: 1.0 mM ARF1 in 4.6% $C_{12}E_5$ with (red) and without (black) 1.4 mM diacyl $PIP_2$.

### 4.4.2 $PIP_2$ AND GDP CHARACTERIZATION BY PHOSPHORUS NMR

Figure 4.4 shows $^{31}P$ chemical shift differences between the different forms of $PIP_2$ oriented in $C_{12}E_5$ bilayers in the absence of ARF1. In isotropic solution, $^{31}P$ phosphomonoester chemical shifts typically resonate from 0 to 4 ppm and phosphodiesters typically resonate from +1 to -1 ppm at pH 6-8 (Figure 4.4b). When aligned, mono- and diesters are readily identified based on their distinctive chemical shifts, particularly for the diacyl $PIP_2$ diester, whose large chemical shift anisotropy offsets contribute to the large upfield chemical shifts of its resonances (Figure 4.4a).

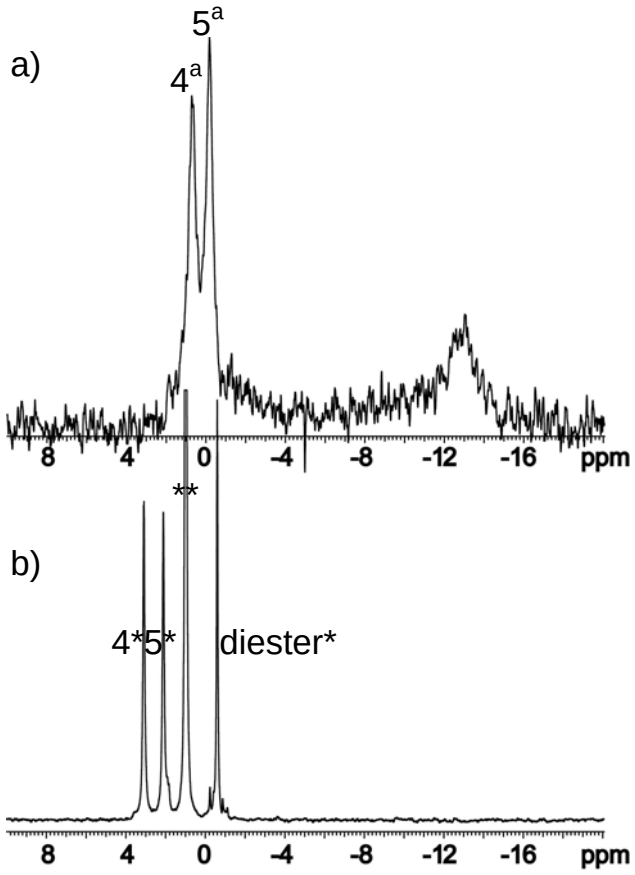


Figure 4.4. $^{31}P$ NMR spectra of $PIP_2$ aligned in $C_{12}E_5$: a) 0.7 mM diacyl $PIP_2$ in 4.6% $C_{12}E_5$ in Tris buffer (pH 7.6) and b) 1.0 mM dibutyryl $PIP_2$ in 2.2% $C_{12}E_5$ in 10 mM phosphate buffer (pH 7.0). $PIP_2$ chemical shift assignments are based on previously recorded spectra in solution (29) and in $C_{12}E_5$ aligned bilayers (20). [a] represents membrane-aligned resonances, * represents isotropic resonances, and ** represents inorganic phosphate.

$^{31}$P spectra in Figure 4.5 of a) dibutyryl- and b) diacyl-$PIP_2$ $C_{12}E_5$ preparations are similar to spectra in Figure 4.4, but now are in the presence of ARF1. Alpha and beta phosphates of GDP which now appear were assigned based on chemical shifts of GDP-bound proteins reported previously (30). At least two species of $PIP_2$ are present in both spectra. In Figure 4.5a additional peaks were attributed to an isotropic $PIP_2$ component. In Figure 4.5b small additional peaks downfield of each major peak were attributed to ARF1-bound dibutyryl $PIP_2$.

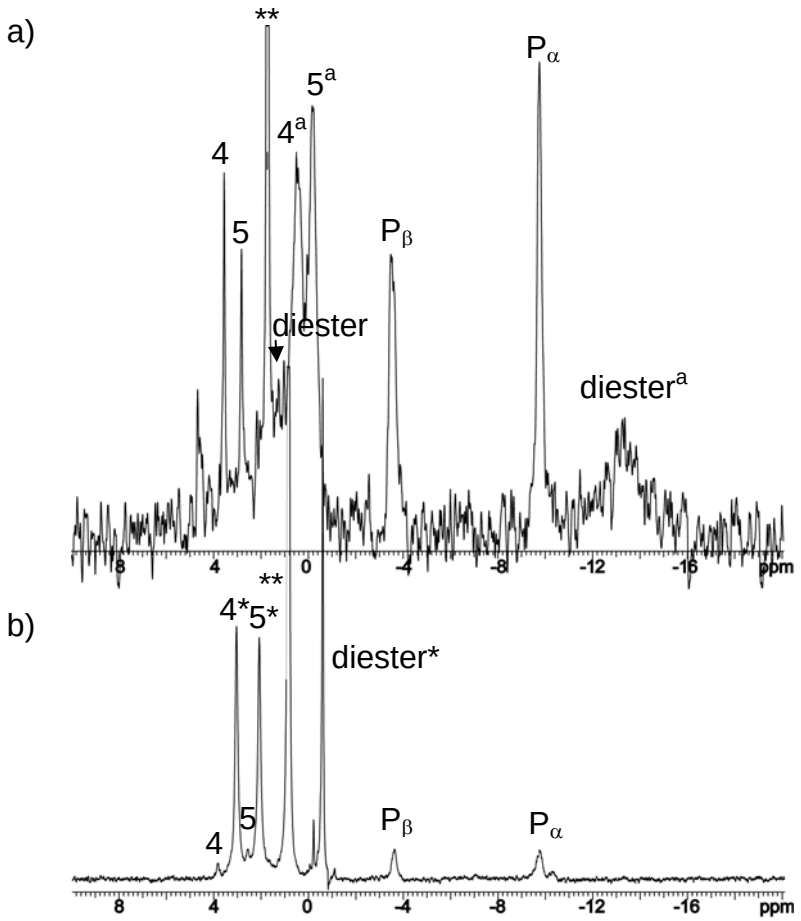


Figure 4.5. $^{31}P$ NMR spectra of ARF1 oriented in $C_{12}E_5$ with a) diacyl $PIP_2$ and b) dibutyryl $PIP_2$. GDP-bound ARF1 shifts are denoted as $P_\alpha$ and $P_\beta$. GDP-bound protein shift assignments are based on previously recorded nucleotide-binding proteins. (31,32) Aligned $PIP_2$ in (a) is identified as [a]. Phosphorus atoms free in solution are indicated by asterisks. Free inorganic phosphorus is denoted **.

In Figure 4.6 $^{31}P$ spectra of hexyl-ARF1 are shown when ordered in 2.2% $C_{12}E_5$ in a) the absence of diacyl $PIP_2$ and b) in the presence of diacyl $PIP_2$. The presence of free GMP and GDP are also observed, both with and without $PIP_2$. Only the free $P_\beta$ resonance is seen due to nearly degenerate chemical shifts for free and ARF1-bound $P_\alpha$. A single population of $PIP_2$ is observed in Figure 4.6b.

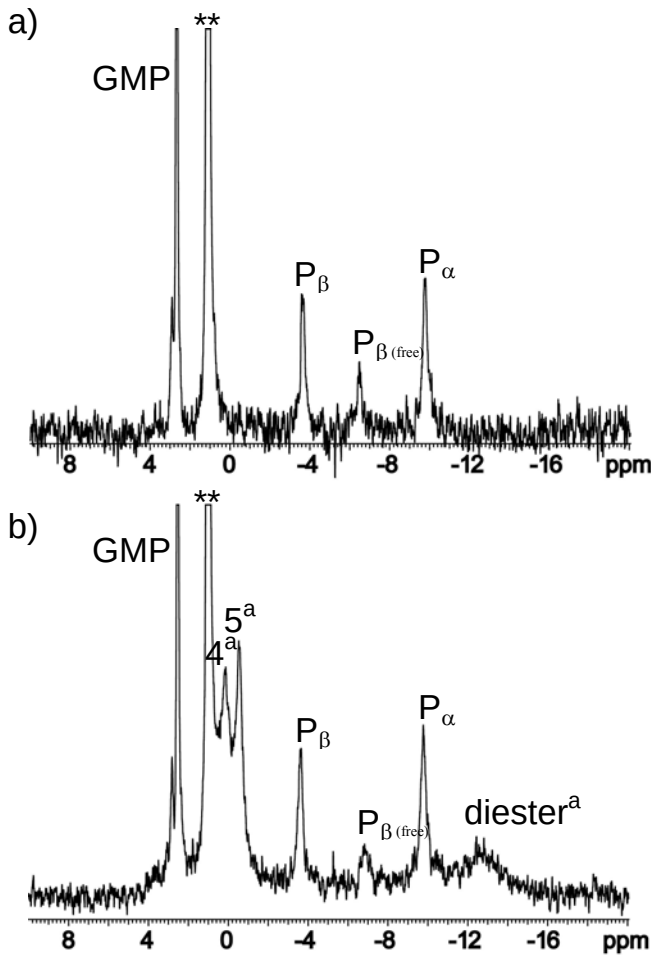


Figure 4.6. $^{31}$P NMR spectra of a) hexyl-ARF1 aligned in 2.2% $C_{12}E_5$ in the absence of diacyl $PIP_2$ and b) in the presence of diacyl $PIP_2$. Aligned $PIP_2$ in (b) is identified as [a]. Free inorganic phosphate is denoted **. Excess GDP and GMP (hydrolysis product of GDP) peaks are also observed.

### 4.4.3 ORDER AND ORIENTATION DETERMINATION BY N-H RDCS

$^{15}$N-$^{1}$H RDCs were measured and compared with values predicted from ARF1's X-ray structure. The degree of alignment of the protein was determined from the one bond couplings. Small changes in RDCs were observed between IPAP-HSQC peaks of ARF1 oriented in $C_{12}E_5$ alone and with dibutyryl $PIP_2$-doped $C_{12}E_5$ as shown in Figure 4.7a. RDCs were also measured using HSQC-TROSY peak pairs as illustrated for ARF1

ordered with 4.6% $C_{12}E_5$ and diacyl $PIP_2$ in Figure 4.7b. Table 4.3 summarizes the RDCs measured for ARF1 ordered in 4.6% $C_{12}E_5$ and diacyl $PIP_2$.

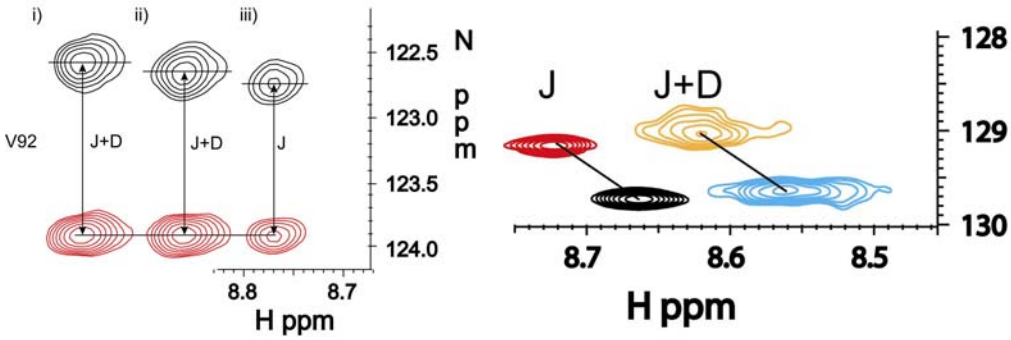


Figure 4.7 Overlay of the $^{15}N$-$^{1}H$ doublet components of select ARF1 residues. a) IPAP-HSQC peaks of Val92 in ARF1 demonstrating $^{15}N$-$^{1}H$ RDCs and scalar couplings in i) 2.2% $C_{12}E_5$ plus dibutyryl $PIP_2$ ii) 2.2% $C_{12}E_5$ alone iii) isotropic buffer solution. b) HSQC-TROSY pairs for A125 in ARF1 showing couplings in isotropic buffer solution (red, black) and aligned in 4.6% $C_{12}E_5$ plus diacyl $PIP_2$ (yellow, blue). Aligned data are offset in the $^{1}H$ dimension.

## 4.5 DISCUSSION

### 4.5.1 CHEMICAL SHIFT PERTURBATIONS SHOW ARF1 BINDS $PIP_2$

$^{15}N$-HSQC data indicate ARF1 interacts with $PIP_2$ in a specific way in these membrane mimetic samples. When mapped onto the protein structure (Figure 4.8), chemical shift perturbations at first appear extensive throughout ARF1, but are localized to regions previously postulated to be important in guanine exchange factor (GEF) binding (11). In the figure, regions where $^{15}N$ and $^{1}H$ combined shifts are greater than 0.06 ppm for dibutyryl $PIP_2$ and 0.18 ppm for diacyl $PIP_2$ are displayed in blue. Shift deviations were measured in Hz and converted to ppm to account for the greater sensitivity of $^{15}N$ shifts (in ppm) to small conformational changes. A more quantitative description of shifts is given in Figure 4.9, where the dotted lines at 0.06 ppm (4.9a) and 0.18 ppm (4.9b) denote the standard deviation observed over all shift deviations. The

perturbed regions agree qualitatively with regions identified in previous studies of dibutyryl $PIP_2$-ARF1 in solution (11). In this case shifts were isolated primarily to three regions: the N-terminal helix and positive patch, the nucleotide binding region (consisting of the P-loop, the G3 motif, and Helix A), and the inter-switch region (Table 4.1). This suggests structural perturbations induced by interaction near the positive patch are propagated through the inter-switch region to the nucleotide binding pocket.

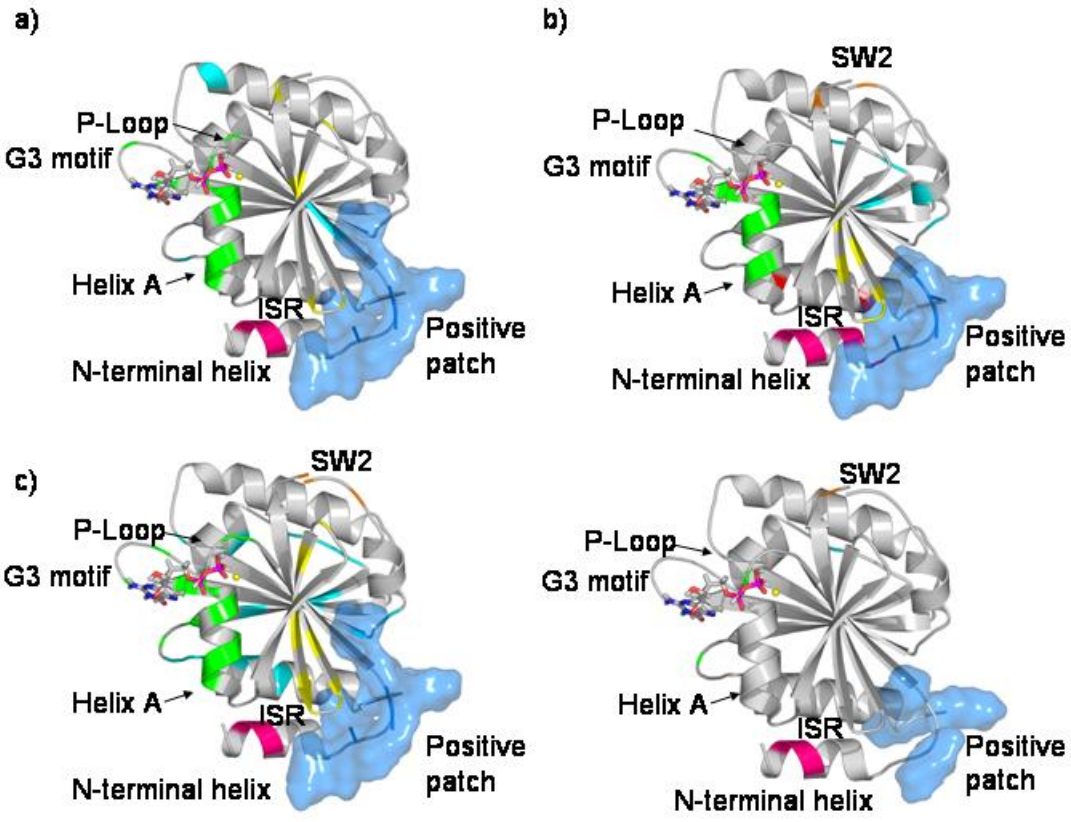


Figure 4.8. Chemical shift changes are mapped onto ARF1's secondary structure in a) solution ARF1-dibutyryl $PIP_2$ b) ARF1-2.2% $C_{12}E_5$-dibutyryl $PIP_2$ c) ARF1-4.6% $C_{12}E_5$-diacyl $PIP_2$. d) hexARF1 2.2% $C_{12}E_5$-diacyl $PIP_2$.

Chemical shift perturbations are similar for the dibutyryl $PIP_2$-bound ARF1 in 2.17% $C_{12}E_5$ and dibutyryl $PIP_2$-bound ARF1 in solution (4.8a,b), but perturbations for diacyl $PIP_2$-bound ARF1 in 4.6% $C_{12}E_5$ are more substantial. Of note are additional changes in Switch 2, the C-terminal helix, and helix A and more extensive shifts in the interswitch and nucleotide-binding regions. In particular, the TCAT box (T158-C159-A160-T161), a region of high guanine binding specificity, is perturbed specifically upon addition of diacyl $PIP_2$. It has previously been suggested that $PIP_2$ binding alters the affinity for guanine nucleotides (9-11). The selective changes in protein structural elements that extend to the nucleotide binding site support this hypothesis. The interactions of $PIP_2$ with hexyl-ARF1 (4.8d) are again more modest, being largely confined to the positive patch and N-terminal helix. It appears that membrane anchoring through the hexyl chain in some way occludes sites that are filled by $PIP_2$ in the absence of a membrane.

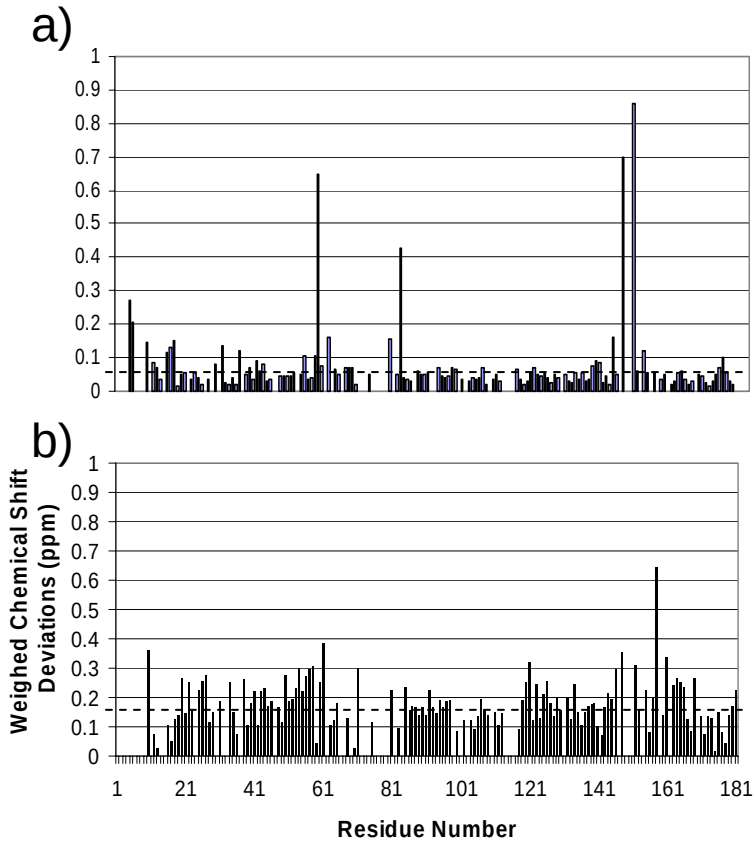


Figure 4.9. $^{15}N$-$^{1}H$ chemical shift deviations in ARF1 bound to a) dibutyryl $PIP_2$ and b) diacyl $PIP_2$ plotted as a function of residue number. All values are shown as the overall magnitude of the deviation observed. The horizontal dotted lines represent the standard shift deviation for each experiment.

### 4.5.2 THE INFLUENCE OF $PIP_2$ ON MEMBRANE ASSOCIATION OF ARF1

Evaluating the effect of $PIP_2$ on membrane association is most easily done by analysis of RDCs. The program REDCAT (33) was used to analyze RDCs to calculate an order tensor for ARF1 using coordinates from a structurally invariant region of the crystal structure (4). Previous studies of ARF1-GDP have identified residues 90-165 as a region that is structurally conserved even upon truncation of the N-terminal helix and nucleotide exchange (6). Order tensors were calculated both when aligned with and

without $PIP_2$. Diagonalization of the resulting tensor provided information on the orientation of the principal alignment frame as seen from the point of view of the protein. In Table 4.2 order parameters and Euler angles that describe the orientation of ARF1 relative to the alignment frame in different alignment media are summarized. Rotating the molecular frame of ARF1 into the REDCAT-calculated alignment frames was accomplished using the Euler angles $\alpha$, $\beta$, and $\gamma$ given in Table 4.2. Euler angles appear to change upon addition of either dibutyryl or diacyl $PIP_2$. Unfortunately, because RDCs are insensitive to axis inversion, there are four degenerate solutions for these orientations. These can be generated by 180º rotations about each of the x, y, and z axes (27-28). One orientation was chosen for ARF1 alone and each of the four solutions for diacyl $PIP_2$-bound ARF1 was compared to find the pair with minimum deviations. This pair is plotted in Figure 4.10. While diacyl $PIP_2$ did indeed change ARF1's orientation for ARF1 ordered by 4.6% $C_{12}E_5$, it is difficult to know if the change in orientation is due to a specific interaction with membrane-anchored $PIP_2$ or simply due to electrostatic interactions between ARF1 and the membrane charged by the presence of an acidic lipid.

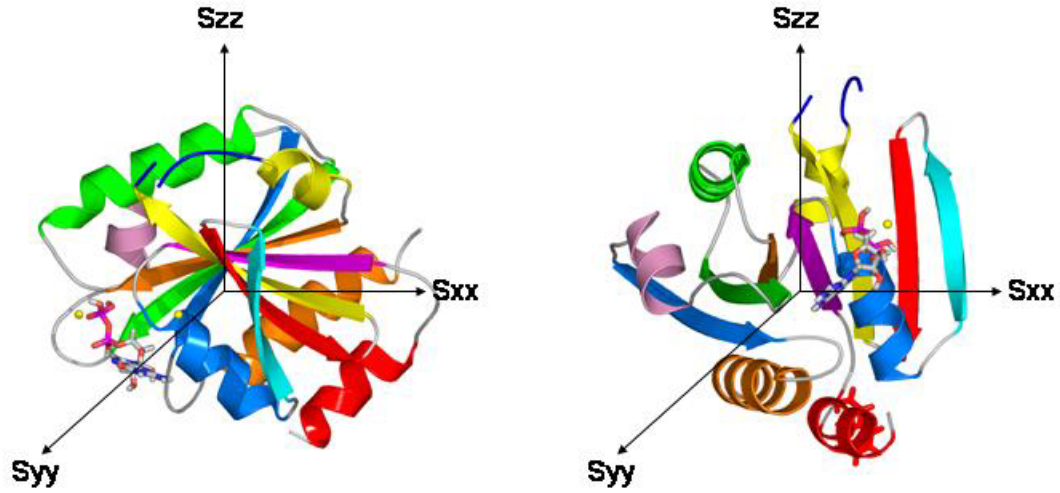


Figure 4.10. ARF1 changes orientation in the magnetic field upon addition of $PIP_2$. a) ARF1 rotated into the alignment frame in the absence of $PIP_2$ and b) upon addition of $PIP_2$.

Based on prior evidence that 1) $PIP_2$ binds ARF1 (above and (9-11)) and 2) diacyl-$PIP_2$ is ordered in a bilayer (chapter 2 and (20)), we expected the level of order of ARF1 to increase upon addition of diacyl $PIP_2$ to the membrane. However, contrary to our expectations, order parameters calculated using a singular value decomposition approach did not show significant changes in the level of order. While there are differences in RDCs between the membrane-ordered ($C_{12}E_5$ only) and $PIP_2$-membrane ordered ARF1, the resulting order parameters do not indicate increased levels of order (Table 4.2). It is possible that changes in chemical shift ascribed to association of $PIP_2$ with ARF1 could arise from other effects such as a change in pH. Therefore, the absence of a $PIP_2$ interaction could explain the lack of membrane association; however, this seems unlikely. First, the changes observed in $^{15}N$-$^{1}H$ HSQC spectra (Figures 4.2a & 4.2b) do not correlate with pH-induced changes and are specific enough to indicate $PIP_2$ does indeed bind ARF1. Second, radioactive binding assays (10) and NMR evidence (11)

strongly suggest a highly specific interaction between $PIP_2$ and ARF1 that is unique not only to phosphatidylinositides (compared to other phospholipids) (9,10), but specifically to the phosphate headgroup pattern of $PIP_2$ (11). The shift changes clearly involve the residues of the positive patch that have been previously suggested as influencing $PIP_2$ binding. Additional chemical shift perturbations occur throughout the structure extending all the way to the guanine nucleotide binding pocket, but these more extensive changes have also been rationalized in terms of known influences of $PIP_2$ on nucleotide binding affinities. Third, micromolar dissociation constants have previously been determined for ARF1-$PIP_2$ complexes, but exact experimental conditions differ from those described in this model system. A $K_d$ of 42 μM was determined for ARF1-GTP-$PIP_2$ complex in the presence of detergent micelles and phospholipids (34), and an upper limit of 10 μM was established for ARF1-GDP in the presence of dibutyryl $PIP_2$.

Since we know $PIP_2$ interacts with ARF1, this leaves three possibilities for the lack of a strong membrane interaction: 1) the ARF1-$PIP_2$ complex does not associate with the membrane at all (in other words, ARF1 removes $PIP_2$ from the membrane), 2) the complex forms a nearly isotropic, micellar as opposed to bilayer, structure from membrane components, and hence does not strongly orient, or 3) there is some mixed mode of interaction in which signals from a true membrane-binding component are too broad to observe and we selectively observe only a freely soluble form of the complex.

The minimal loss of signal intensity in HSQC spectra between the isotropic and $PIP_2$-bound spectra easily eliminates the third possibility as a significant option. Tight binding, *i.e.*, micromolar or nanomolar binding, decreases the off rate resulting in longer periods of time where the ligand remains bound. In principle, two sets of resonances

would arise with intensities distributed proportionately between them. For the membrane bound set, spin diffusion can cause excessive line broadening to the extent that only the resonance from the soluble form is observed, but it would only represent its proportion of intensity. We estimate that no more than 15% of the resonance intensity could be missing.

The remaining possibilities are hard to distinguish, but both require removal of $PIP_2$ from a bilayer-like environment. This removal is plausible and is consistent with HSQC spectra, RDC-determined order parameters, and $^{31}P$ NMR spectra. The extent of $PIP_2$ ordering can be established *via* $^{31}P$ NMR. In solution, dibutyryl $PIP_2$ and diacyl $PIP_2$ (solubilized with octylglucoside) give identical $^{31}P$ spectra (data not shown). In the presence of a low percentage of $C_{12}E_5$, dibutyryl $PIP_2$ spectra resemble those seen in solution (Figure 4.4b). At higher levels membrane-like particles form and oriented $^{31}P$ chemical shifts for dibutyryl $PIP_2$ move, but they still remain near those in isotropic solution. This suggests that either dibutyryl $PIP_2$ is not strongly associated with the membrane or that the short chain phospholipid exhibits very small shift differences between isotropic and aligned states. Short chain phospholipids such as dihexanoylphosphtidylcholine tend to accumulate on the edges of discoidal phospholipid bicelles, producing only small chemical shift offsets between isotropic and aligned samples. We may be observing the nearly isotropic diester chemical shift of dibutyryl $PIP_2$ due its small chemical shift anisotropy, as is the case with dihexanoylphosphatidylcholine aligned in a bicelle. In Figure 4.5b where ARF1 is added to dibutyryl $PIP_2$ in the presence of the bilayer, $^{31}P$ NMR spectra suggest two populations of $PIP_2$ where dibutyryl $PIP_2$ appears to be in both isotropic and membrane-anchored

states. The shifts of the membrane anchored state are small and similar to unperturbed $PIP_2$ in oriented $C_{12}E_5$ in the absence of ARF1. The other population is near isotropic with the small perturbations possibly being the result of ARF1 binding. It is estimated that 10-13% of $PIP_2$ is bound to ARF1 based on the integration of $^{31}P$ resonances. This amount is apparently enough to promote chemical shift changes in $^{15}N$-$^{1}H$ HSQC spectra. Integration of ARF1-bound $PIP_2$ peaks relative to ARF1-bound GDP peaks indicates binding is approximately stoichiometric, or all ARF1 carries a bound dibutyryl $PIP_2$. This is consistent with a 10 μM dissociation constant.

The changes in the diacyl $PIP_2$ are more dramatic. The phosphorus chemical shifts indicate the $PIP_2$ is well-ordered in the bilayer (Figure 4.4a). In Figure 4.5a, diacyl $PIP_2$ is also found in two distinct forms, where one appears to be isotropic in solution and the other is aligned. Strongly ordered $PIP_2$ shows distinctly different chemical shifts for each of its phosphomono- and diesters due to their different chemical shift anisotropy. A strongly ordered phosphodiester, such as the one in $PIP_2$ or dimyristoylphosphatidylcholine in a phospholipid bilayer or bicelle, typically displays a $^{31}P$ chemical shift of around -15 ppm at neutral pH but at ±1 ppm when isotropic (20). The resonances observed near these values in the presence of ARF1 appear unperturbed, and observation is consistent with ARF1 not binding to membrane associated diacyl $PIP_2$. The other resonances are near isotropic, but perturbed in a manner consistent with a soluble $PIP_2$ carrying ARF1. Integration of diacyl $PIP_2$ phosphomonoester resonances and GDP $^{31}P$ resonances suggests, however, that $PIP_2$-bound-ARF1 is substoichiometric. It may be that the binding affinity of our particular form of ARF1 for a long chain PIP is greater than indicated by a 10 μM dissociation constant when a membrane is present.

However, the affinity is clearly enough to pull some $PIP_2$ out of the bilayer and into isotropic solution. The extensive chemical shift perturbations in the HSQC also include changes in the cleft between the N- and C-terminal helices. This region is thought to protect the myristoyl chain in ARF1's cytosolic form. Additional selective shifts in this region in diacyl $PIP_2$-ARF1 suggest a change in local electronic environment that could result from burying the fatty acid chains of $PIP_2$.

The question remains as to how ARF1 could overcome the estimated 27.2 kcal/mol required to withdraw the acyl chains from the membrane, where each methylene group contributes 0.8 kcal/mol (35). In its native myristoylated form, ARF1 is capable of burying its myristoyl group within the protein, possibly in the cleft between the N-terminal and C-terminal helices (36,37). It may be possible for ARF1 to bury the exposed chains of $PIP_2$ in between these helices, partially aided by the inositol phosphate head group bound to ARF1's neighboring patch of positively charged residues. The 27.2 kcal pertains only to an acyl chain exposed in solution, and a binding site within ARF1 could compensate for this energy difference. There also remains the possibility mentioned in option 3 that the ARF1-$PIP_2$ complex causes the bilayer to deform to a more micellar structure involving other lipids, possibly mimicking events in vesicle budding (38).

### 4.5.3 HEXYL-ARF1, A STEP TOWARD MYRARF1

A possible model for some of the properties of myrARF1, hexyl-ARF1, has recently become available (39). Hexyl-ARF1 in a $C_{12}E_5$ model membrane was also studied by $^{15}N$-$^{1}H$ HSQC, N-H RDCs, and $^{31}P$ NMR experiments. Diacyl $PIP_2$ was added to this sample and the same experiments were repeated. Chemical shift

perturbations were substantially less extensive than non-myrARF1 (Figure 4.8d). In addition, RDCs indicated some enhanced alignment, and therefore membrane association, but not as much as expected for even a hexyl chain. Moreover, this alignment was not substantially different with and without $PIP_2$ in the membrane. This suggests hexyl-ARF1 may not interact with $PIP_2$ to the same extent as non-myrARF1. In addition, $^{31}P$ NMR spectra of hexyl-ARF1 doped with diacyl $PIP_2$ showed only a single population of $PIP_2$ (Figure 4.6b). These data suggest that ARF1 may have an acyl chain binding site, but this site is at least partially occupied by the hexyl chain in hexyl-ARF1.

### 4.5.4 MODELS VERSUS MYRARF1-TRUE MEMBRANE SPECIES

It is important to realize that the model studies are still a long way from the natural ARF1 system. Hexyl-ARF1 is not identical to myr-ARF1, and it may be that the GTP form and not the GDP form, is the primary species that associates with $PIP_2$ and the membrane. The choice of alignment medium may also be relevant. ARF1 naturally associates with phospholipid membranes, and most biological studies of ARF1 include phospholipids. The phospholipid bicelle as alignment medium (DMPC:DHPC) is one possible alternate choice for an alignment medium, but its high phosphorus content overwhelms crucial $^{31}P$ signals from the GDP and $PIP_2$, rendering phosphorus analysis nearly impossible. We did, in fact, orient isotopically labeled ARF1 in phospholipid bicelles and observed chemical shift perturbations with dibutyryl $PIP_2$ similar to those seen in $C_{12}E_5$ (data not shown). In addition, order parameters calculated from $^{15}N$-$^{1}H$ RDCs were not substantially different from those determined in $C_{12}E_5$-oriented ARF1 (Table 4.2). Although we were not able to use chemical shift anisotropy offsets of $^{31}P$ resonances to analyze geometry without strong ordering of the ARF1- $PIP_2$ complexes,

we expect these will be useful as better ARF1 models evolve. The $C_{12}E_5$ medium appears to remain a useful membrane model option. Furthermore, even without perfect models the results are interesting. The evidence presented here for an acyl-chain binding site in ARF1 is new and has implications for an interplay among myr-binding, $PIP_2$ binding and membrane association that may be significant. Previous models for membrane association have suggested that $PIP_2$ may act as an ARF1 effector that destabilizes the N-terminal helix and other structural elements, possibly altering the GDP binding affinity (11), stabilizing an apo structure (10), or providing the conformational change and energy necessary to bind GTP. Here, it has been shown that $PIP_2$ binding may effect interesting conformational changes in the presence of a model membrane that may position ARF1 for activation and membrane association, all important steps toward the goal of characterizing myrARF1 activation and membrane association.

REFERENCES


1. Losonczi, J.A., Tian, F. and Prestegard, J.H. (2000) Nuclear magnetic resonance studies of the N-terminal fragment of adenosine diphosphate ribosylation factor 1 in micelles and bicelles: Influence of N-myristoylation. *Biochemistry*, **39,** 3804-3816.
2. Losonczi, J.A. and Prestegard, J.H. (1998) NMR characterization of the myristoylated, N-terminal fragment of ADP-Ribosylation factor 1 in a magnetically oriented membrane array. *Biochemistry*, **37,** 706-716.
3. Kishore, A.I. and Prestegard, J.H. (2003) Spectral assignments and molecular geometry of membrane-associated Phosphoinositides using variable angle sample spinning (VASS). *Biophys J*, **84,** 276A-276A.
4. Amor, J.C., Harrison, D.H., Kahn, R.A. and Ringe, D. (1994) Structure of the human ADP-ribosylation factor 1 complexed wtih GDP. *Nature*, **372,** 704-708.
5. Goldberg, J. (1998) Structural Basis for activation of ARF GTPase: mechanisms of guanine nucleotide exchange and GTP-myristoyl switching. *Cell*, **95,** 237-248.
6. Seidel, R.D., Amor, J.C., Kahn, R.A. and Prestegard, J.H. (2004) Conformational changes in human Arf1 on nucleotide exchange and deletion of membrane-binding elements. *J Biol Chem*, **279,** 48307-48318.

7. Donaldson, J.G. and Jackson, C.L. (2000) Regulators and effectors of the ARF GTPases. *Curr Opin Cell Biol*, **12,** 475-482.
8. Czech, M.P. (2000) PIP2 and PIP3: Complex roles at the cell surface. *Cell*, **100,** 603-606.
9. Terui, T., Kahn, R.A. and Randazzo, P.A. (1994) Effects of acid phospholipids on nucleotide exchange properties of ADP-Ribosylation Factor-1 - evidence for specific interaction with phosphatidylinositol 4,5-bisphosphate. *J Biol Chem*, **269,** 28130-28135.
10. Randazzo, P.A. (1997) Functional interaction of ADP-ribosylation factor 1 with phosphatidylinositol 4,5-bisphosphate. *J Biol Chem*, **272,** 7688-7692.
11. Seidel, R.D., Amor, J.C., Kahn, R.A. and Prestegard, J.H. (2004) Structural perturbations in human ADP ribosylation factor-1 accompanying the binding of phosphatidylinositides. *Biochemistry*, **43,** 15393-15403.
12. Saupe, A. and Englert, G. (1963) High-resolution nuclear magnetic resonance spectra of orientated molecules. *Phys Rev Lett*, **11,** 462-464.
13. Saupe, A. (1968) Recent results in the field of liquid crystals. *Angew Chem Internat Edit*, **7,** 97-&.
14. Losonczi, J.A., Andrec, M., Fischer, M.W.F. and Prestegard, J.H. (1999) Order matrix analysis of residual dipolar couplings using singular value decomposition. *J Magn Reson*, **138,** 334-342.
15. Koenig, B.W., Mitchell, D.C., Konig, S., Grzesiek, S., Litman, B.J. and Bax, A. (2000) Measurement of dipolar couplings in a transducin peptide fragment weakly bound to oriented photo-activated rhodopsin. *J Biomol NMR*, **16,** 121-125.
16. Koenig, B.W., Kontaxis, G., Mitchell, D.C., Louis, J.M., Litman, B.J. and Bax, A. (2002) Structure and orientation of a G protein fragment in the receptor bound state from residual dipolar couplings. *J Mol Biol*, **322,** 441-461.
17. Shimizu, H., Donohue-Rolfe, A. and Homans, S.W. (1999) Derivation of the bound-state conformation of a ligand in a weakly aligned ligand-protein complex. *J Am Chem Soc*, **121,** 5815-5816.
18. Randazzo, P.A. and Kahn, R.A. (1995) Myristoylation and ADP-ribosylation factor function. *Methods Enzymol*, Vol. 250, pp. 394-405.
19. Kenyon, G.L. and Bruice, T.W. (1977) Novel Sulfhydryl Reagents. *Methods: A Companion to Methods in Enzymology*, Vol. 47, pp. 407-430.
20. Kishore, A.I. and Prestegard, J.H. (2003) Molecular orientation and conformation of phosphatidylinositides in membrane mimetics using variable angle sample spinning (VASS) NMR. *Biophys J*, **85,** 3848-3857.
21. Freyssingeas, E., Nallet, F. and Roux, D. (1996) Measurement of the membrane flexibility in lamellar and "sponge" phases of the C12E5/hexanol/water system. *Langmuir*, **12,** 6028-6035.
22. Jonstromer, M. and Strey, R. (1992) Nonionic bilayers in dilute solutions: effect of additives. *J Phys Chem*, **96,** 5993-6000.
23. Ruckert, M. and Otting, G. (2000) Alignment of biological macromolecules in novel nonionic liquid crystalline media for NMR experiments. *J Am Chem Soc*, **122,** 7793-7797.

24. Ottiger, M., Delaglio, F. and Bax, A. (1998) Measurement of J and dipolar couplings from simplified two-dimensional NMR spectra. *J Magn Reson*, **131,** 373-378.
25. Pervushin, K., Riek, R., Wider, G. and Wuthrich, K. (1997) Attenuated T-2 relaxation by mutual cancellation of dipole-dipole coupling and chemical shift anisotropy indicates an avenue to NMR structures of very large biological macromolecules in solution. *Proc Natl Acad Sci U S A*, **94,** 12366-12371.
26. Riek, R., Wider, G., Pervushin, K. and Wuthrich, K. (1999) Polarization transfer by cross-correlated relaxation in solution NMR with very large molecules. *Proc Natl Acad Sci U S A*, **96,** 4918-4923.
27. Kontaxis, G., Clore, G.M. and Bax, A. (2000) Evaluation of cross-correlation effects and measurement of one-bond couplings in proteins with short transverse relaxation times. *J Magn Reson*, **143,** 184-196.
28. Delaglio, F., Grzesiek, S., Vuister, G.W., Zhu, G., Pfeifer, J. and Bax, A. (1995) Nmrpipe - a Multidimensional Spectral Processing System Based on Unix Pipes. *J Biomol NMR*, **6,** 277-293.
29. van Paridon, P.A., de Kruijff, B., Ouwerkerk, R. and Wirtz, K.W.A. (1986) Polyphosphoinositides undergo charge neutralization in the physiological pH range: a $^{31}$P-NMR study. *Biochim Biophys Acta*, **877,** 216-219.
30. Weybright, P., Millis, K., Campbell, N., Cory, D.G. and Singer, S. (1998) Gradient, high-resolution, magic angle spinning H-1 nuclear magnetic resonance spectroscopy of intact cells. *Magn Reson Med*, **39,** 337-345.
31. Geyer, M., Schweins, T., Herrmann, C., Prisner, T., Wittinghofer, A. and Kalbitzer, H.R. (1996) Conformational transitions in p21(ras) and in its complexes with the effector protein Raf-RBD and the GTPase activating protein GAP. *Biochemistry*, **35,** 10308-10320.
32. Kraulis, P.J., Domaille, P.J., Campbellburk, S.L., Vanaken, T. and Laue, E.D. (1994) Solution Structure and Dynamics of Ras P21-Center-Dot-Gdp Determined by Heteronuclear 3-Dimensional and 4-Dimensional Nmr-Spectroscopy. *Biochemistry*, **33,** 3515-3531.
33. Valafar, H. and Prestegard, J.H. (2004) REDCAT: a residual dipolar coupling analysis tool. *J Magn Reson*, **167,** 228-241.
34. Randazzo, P.A., Miura, K. and Jackson, T.R. (2001) Assay and purification of phosphoinositide-dependent ADP- ribosylation factor (ARF) GTPase activating proteins. *Regulators and Effectors of Small Gtpases, Pt E*, Vol. 329, pp. 343-354.
35. Murray, D., BenTal, N., Honig, B. and McLaughlin, S. (1997) Electrostatic interaction of myristoylated proteins with membranes: simple physics, complicated biology. *Structure*, **5,** 985-989.
36. Franco, M., Chardin, P., Chabre, M. and Paris, S. (1996) Myristoylation-facilitated binding of the G protein ARF1(GDP) to membrane phospholipids is required for its activation by a soluble nucleotide exchange factor. *J Biol Chem*, **271,** 1573-1578.
37. Franco, M., Chardin, P., Chabre, M. and Paris, S. (1995) Myristoylation of Adp-Ribosylation Factor-1 Facilitates Nucleotide Exchange at Physiological Mg2+ Levels. *J Biol Chem*, **270,** 1337-1341.

38. Schekman, R. and Orci, L. (1996) Coat proteins and vesicle budding. *Science*, **271,** 1526-1533.
39. Seidel, R.D., Zhuang, T. and Prestegard, J.H. (2005) Preparation of acylated protein mutants: cysteine-mediated acylation.
40. Amor, J.C., Seidel, R.D., Tian, F., Kahn, R.A. and Prestegard, J.H. (2002) Letter to the Editor: H-1, N-15 and C-13 assignments of full length human ADP Ribosylation Factor 1 (ARF1) using triple resonance connectivities and dipolar couplings. *J Biomol NMR*, **23,** 253-254.

TABLES

Table 4.1. Amino acid resonances of non-myrARF1 with significant chemical shift perturbations upon addition of $PIP_2$ in a $C_{12}E_5$ model membrane.

| **Dibutyryl $PIP_2$** | | **Diacyl $PIP_2$** | |
|---|---|---|---|
| **Amino Acid** | **Secondary Structure** | **Amino Acid** | **Secondary Structure** |
| F5 | NTH[a] | F5 | NTH[**] |
| A6 | NTH | A6 | NTH[**] |
| F9 | NTH[**] | K10 | NTH, + |
| K10 | NTH, +[b] | L12 | L1 [c*] |
| L12 | L1[c] | F13 | L1[*] |
| F13 | L1 | K15 | L1, +[**] |
| K15 | L1, +[**] | E17 | L1, +[*] |
| K16 | L1, + | R19 | B1[*] |
| E17 | L1, + | L25 | Ploop[k] |
| M18 | B1[d] | D26 | Ploop |
| K30 | Helix A, NBP[e] | G29 | Helix A, Ploop[*] |
| T31 | Helix A, NBP[**] | T31 | Helix A, NBP |
| T32 | Helix A, NBP | L34 | Helix A, NBP |
| G40 | L2 | Y35 | Helix A, NBP[*] |
| I42 | SW1[f] | K36 | Helix A, NBP[*] |
| T44 | SW1 | I49 | Loop, ISW[*] |
| E54 | B2, NBP[**] | G50 | Loop, ISW |
| V56 | B2, ISW[g] | N52 | B2, ISW |
| K59 | L3, ISW | V53 | B2, ISW |
| N60 | L3, ISW | E54 | B2, ISW |
| I61 | B3, ISW | T55 | B2, ISW |
| F63 | B3, ISW | V56 | B2, ISW |
| G69 | SW2[h] | E57 | B2, ISW |
| | | Y58 | L3, ISW |
| K73 | SW2[**] | N60 | L3, ISW |
| Y81 | Helix | I61 | B3, ISW |
| N84 | Loop | F63 | B3, ISW[*] |
| N126 | Beta strand, GBM[i], NBP | Q71 | SW2 |
| T140 | Helix | D72 | SW2[*] |
| D141 | Helix | R75 | SW2[*] |
| L142 | Helix | Y81 | Helix |
| H146 | Loop, pH? | N84 | Loop |
| R149 | Loop | T85 | Loop |
| N152 | Loop | N86 | Beta strand[*] |
| I155 | Beta strand | V92 | Beta strand |
| R178 | CTH[j] | N95 | Loop |

| Amino Acid | Secondary Structure | Amino Acid | Secondary Structure |
|---|---|---|---|
| Q180 | CTH, +* | S94 | Loop* |
| K181 | CTH, +* | L121 | Beta strand |
| | | N126 | GBM,NBP |
| | | D129 | GBM,NBP |
| | | M134 | GBM,NBP |
| | | T140 | Helix |
| | | G144 | Loop |
| | | L145 | Loop |
| | | H146 | Loop, pH |
| | | L148 | Loop |
| | | R149 | Loop* |
| | | N152 | Beta strand |
| | | N153 | Beta strand* |
| | | I155 | Beta strand |
| | | A157 | Beta strand |
| | | T158 | TCAT[l] |
| | | T161 | TCAT |
| | | G163 | Loop |
| | | D164 | Loop |
| | | G165 | CTH |
| | | G169 | CTH |
| | | N172 | CTH |

** missing from spectrum due to line broadening
* broadened
[a] N-terminal helix
[b] Positive patch
[c] Loop 1, 2, 3, etc.
[d] Beta sheet 1, 2, 3, etc.
[e] Nucleotide binding pocket
[f] Switch 1
[g] Interswitch region
[h] Switch 2
[i] Guanine-binding motif
[j] C-terminal helix
[k] Phosphate-binding loop
[l] T-C-A-T box, Thr158-Cys159-Ala160-Thr161 box, binds guanine

Table 4.2. Alignment tensor and order parameters for ARF1 oriented in different alignment media.

| Sample | $C_{12}E_5$ (w/w%) | $PIP_2$ (mM) | $S_{xx}$ | $S_{yy}$ | $S_{zz}$ | α | β | γ | $R^{2\,a}$ | $Q^{a}$ |
|---|---|---|---|---|---|---|---|---|---|---|
| 0.77 mM $^{15}N,^{2}H$ | 4.25 | - | -8.24E-04 | -3.07E-05 | 8.54E-04 | 32.4 | 113.6 | 81.2 | 0.71 | 0.48 |
| 0.77 mM $^{15}N,^{2}H$ | 4.25 | 1.4 [b] | 4.64E-04 | 3.75E-04 | -8.39E-04 | -41.0 | 63.7 | 134.8 | 0.60 | 0.60 |
| 0.77-1.65 $^{15}N,^{13}C$ | 2.17 | - | 1.10E-04 | 1.54E-05 | -1.25E-04 | -49.9 | 73.2 | 80.9 | 0.46 | - |
| 0.77-1.65 $^{15}N,^{13}C$ | 2.17 | 2.0 [c] | 2.67E-04 | 3.13E-05 | -2.98E-04 | -56.3 | 92.6 | 77.7 | 0.79 | - |
| 0.6 mM $^{15}N,^{2}H$ | [d] | - | 2.17E-04 | 8.84E-05 | -3.05E-04 | -50.0 | 94.5 | 115.8 | 0.51 | - |
| 0.6 mM $^{15}N,^{2}H$ | [d] | 2.0 [c] | -1.24E-04 | -4.01E-05 | 1.64E-04 | 32.7 | 65.6 | 72.5 | 0.40 | - |
| 1.0 mM $^{15}N$ | 4.60 | 1.4 [b] | 2.28E-04 | 6.59E-05 | -2.94E-04 | -54.8 | 54.1 | 103.5 | 0.61 | 0.79 |
| 1.4 mM $^{15}N$ | 4.60 | 1.4 [b] | 2.13E-04 | 8.01E-05 | -2.93E-04 | -64.5 | 220.5 | 15.8 | 0.35 | 0.76 |

[a] Calculated based on experimental RDCs and back-calculated RDCs. Q is defined as $\{\sum_{i=1,\ldots N} (D_{NHi}^{meas} - D_{NHi}^{calc})^2/N\}^{1/2}/\mathrm{rms}\,(D_{NHi}^{meas})$ where $D_{NH}$ is the N-H residual dipolar coupling.
[b] diacyl $PIP_2$
[c] dibutyryl $PIP_2$
[d] 13.5% DMPC:DHPC bicelle used as alignment medium

Table 4.3 $^{15}N$-$^{1}H$ RDCs of ARF1 oriented in 4.6% $C_{12}E_5$ and 1.4 mM diacyl $PIP_2$ measured using the HSQC-TROSY approach

| Amino Acid[a] | J[b] | Error[c] | J+D[d] | RDCs[e] |
|---|---|---|---|---|
| F5 | 36.552 | 34.297 | 73.104 | -18.902 |
| A6 | | | | |
| F9 | | | | |
| K10 | 46.777 | 2.764 | 93.554 | 0.688 |
| L12 | 40.838 | 3.233 | 81.676 | -8.706 |
| F13 | 41.927 | 7.26 | 83.854 | -7.68 |
| G14 | 41.557 | 2.912 | 83.114 | |
| K15 | 42.294 | 1.722 | 84.588 | |
| K16 | 45.03 | 1.017 | 90.06 | -1.812 |
| E17 | 40.599 | 2.443 | 81.198 | -9.912 |
| M18 | 48.739 | 2.243 | 97.478 | 4.472 |
| R19 | 43.652 | 3.896 | 87.304 | -2.01 |
| I20 | 47.82 | 1.224 | 95.64 | 5.082 |
| L21 | 46.956 | 2.847 | 93.912 | 1.51 |
| V23 | 47.127 | 3.475 | 94.254 | 2.142 |
| G24 | | | | |
| L25 | 47.21 | 7.184 | 94.42 | 3.486 |
| D26 | 50.109 | 3.103 | 100.218 | 10.324 |
| A27 | 46.12 | 2.984 | 92.24 | 3.608 |
| A28 | 47.91 | 1.902 | 95.82 | 2.91 |
| G29 | 45.759 | 4.633 | 91.518 | -2.408 |
| K30 | | | | |
| T31 | 49.757 | 3.79 | 99.514 | 7.502 |

| Amino Acid[a] | J[b] | Error[c] | J+D[d] | RDCs[e] |
|---|---|---|---|---|
| T32 | | | | |
| I33 | 48.466 | 2.151 | 96.932 | 5.864 |
| L34 | 50.052 | 6.655 | 100.104 | 7.772 |
| Y35 | 46.867 | 1.897 | 93.734 | 2.002 |
| K36 | 48.269 | 2.12 | 96.538 | 3.07 |
| L37 | | | | |
| K38 | 50.657 | 3.224 | 101.314 | 11.014 |
| L39 | 42.638 | 2.332 | 85.276 | -5.554 |
| G40 | 44.232 | 1.099 | 88.464 | -1.812 |
| E41 | 46.792 | 0.817 | 93.584 | 2.95 |
| I42 | 44.851 | 1.476 | 89.702 | -1.728 |
| V43 | 46.447 | 2.677 | 92.894 | 0.422 |
| T44 | 49.288 | 1.275 | 98.576 | 8.634 |
| T45 | 46.779 | 2.033 | 93.558 | 1.156 |
| I46 | 48.035 | 1.332 | 96.07 | 6.182 |
| T48 | 40.317 | 1.431 | 80.634 | -8.08 |
| I49 | 42.584 | 0.713 | 85.168 | -7.886 |
| G50 | 50.59 | 1.794 | 101.18 | 9.208 |
| F51 | 43.808 | 1.081 | 87.616 | -4.562 |
| N52 | 47.248 | 2.101 | 94.496 | 3.29 |
| V53 | 45.661 | 1.468 | 91.322 | 0.16 |
| E54 | 52.226 | 1.913 | 104.452 | 14.456 |
| T55 | 48.054 | 2.227 | 96.108 | 5.146 |
| V56 | 48.618 | 3.794 | 97.236 | 6.492 |
| E57 | 46.642 | 1.436 | 93.284 | 2.598 |
| Y58 | 48.891 | 1.326 | 97.782 | 5.964 |
| K59 | 45.895 | 1.09 | 91.79 | -0.948 |
| N60 | 48.183 | 3.832 | 96.366 | 4.954 |
| I61 | | | | |
| S62 | | | | |
| F63 | 49.321 | 5.484 | 98.642 | 7.822 |
| T64 | 40.558 | 1.104 | 81.116 | -10.874 |
| V65 | 48.044 | 1.162 | 96.088 | 5.954 |
| N66 | 41.845 | 1.315 | 83.69 | -8.342 |
| V68 | 43.822 | 2.823 | 87.644 | -1.528 |
| G69 | 40.789 | 4.704 | 81.578 | |
| G70 | 46.058 | 0.409 | 92.116 | 0.58 |
| N71 | 47.277 | 0.298 | 94.554 | 11.534 |
| K73 | | | | |
| R75 | 48.644 | 2.588 | 97.288 | 6.654 |
| Y81 | 44.039 | 3.253 | 88.078 | -4.144 |
| Q83 | 45.083 | 0.735 | 90.166 | -2.232 |
| N84 | 49.894 | 3.001 | 99.788 | |
| T85 | 49.433 | 0.802 | 98.866 | 6.92 |
| N86 | 48.099 | 1.879 | 96.198 | 4.402 |
| G87 | 45.915 | 1.714 | 91.83 | 0.912 |
| L88 | 46.772 | 1.402 | 93.544 | 1.926 |
| I89 | 46.13 | 1.671 | 92.26 | 1.216 |

| Amino Acid[a] | J[b] | Error[c] | J+D[d] | RDCs[e] |
|---|---|---|---|---|
| F90 | 48.723 | 1.734 | 97.446 | 6.568 |
| V91 | 46.288 | 2.011 | 92.576 | 0.826 |
| V92 | 49.528 | 1.775 | 99.056 | 6.55 |
| D93 | 48.565 | 2.041 | 97.13 | 5.522 |
| S94 | 46.834 | 5.364 | 93.668 | -0.474 |
| N95 | 47.123 | 1.657 | 94.246 | 3.036 |
| D96 | 46.123 | 1.721 | 92.246 | 0.718 |
| R97 | 41.877 | 1.777 | 83.754 | -8.04 |
| E98 | 47.373 | 0.847 | 94.746 | 3.026 |
| R99 | 47.209 | 2.035 | 94.418 | 4.196 |
| V100 | 40.895 | 0.671 | 81.79 | -10.194 |
| E102 | 42.161 | 1.151 | 84.322 | -7.262 |
| R104 | 42.261 | 1.334 | 84.522 | -7.546 |
| E105 | 45.077 | 1.405 | 90.154 | -2.294 |
| E106 | 43.172 | 1.358 | 86.344 | -5.89 |
| L107 | 42.765 | 2.309 | 85.53 | -7.384 |
| M108 | 46.732 | 2.414 | 93.464 | 1.192 |
| R109 | 41.318 | 1.031 | 82.636 | -10.232 |
| L111 | 41.81 | 1.1 | 83.62 | -7.98 |
| A112 | 45.545 | 1.321 | 91.09 | -0.73 |
| E113 | 42.694 | 1.192 | 85.388 | -6.634 |
| R117 | | | | |
| D118 | 42.205 | 0.939 | 84.41 | -8.542 |
| A119 | 49.267 | 0.963 | 98.534 | 4.402 |
| V120 | 48.408 | 1.685 | 96.816 | 6.194 |
| L121 | 50.735 | 3.99 | 101.47 | 10.294 |
| L122 | 45.891 | 1.838 | 91.782 | -0.028 |
| V123 | 48.259 | 2.328 | 96.518 | 1.792 |
| F124 | 45.963 | 1.176 | 91.926 | 0.156 |
| A125 | 50.318 | 1.983 | 100.636 | 8.334 |
| N126 | 48.223 | 1.266 | 96.446 | 3.096 |
| K127 | 49.526 | 2.817 | 99.052 | 7.968 |
| Q128 | 45.232 | 1.876 | 90.464 | -0.61 |
| D129 | 44.494 | 2.572 | 88.988 | -0.942 |
| L130 | 47.976 | 1.646 | 95.952 | 2.318 |
| N132 | 46.943 | 0.935 | 93.886 | 1.436 |
| A133 | | | | |
| M134 | 45.944 | 2.17 | 91.888 | -0.106 |
| N135 | 48.179 | 2.101 | 96.358 | 3.81 |
| A136 | 46.565 | 0.9 | 93.13 | 1.058 |
| A137 | 44.273 | 1.024 | 88.546 | -4.22 |
| E138 | 44.063 | 0.855 | 88.126 | -4.83 |
| I139 | 49.247 | 1.26 | 98.494 | 5.39 |
| T140 | 42.158 | 2.236 | 84.316 | -7.862 |
| D141 | 44.082 | 1.241 | 88.164 | -4.004 |
| L142 | 42.623 | 0.935 | 85.246 | -7.268 |
| L143 | 46.907 | 1.657 | 93.814 | 3.108 |
| G144 | 41.615 | 1.165 | 83.23 | -9.41 |

| Amino Acid[a] | J[b] | Error[c] | J+D[d] | RDCs[e] |
|---|---|---|---|---|
| L145 | 44.318 | 2.054 | 88.636 | -2.776 |
| H146 | 43.372 | 1.069 | 86.744 | -5.044 |
| S147 | | | | |
| L148 | | | | |
| R149 | 44.716 | 4.397 | 89.432 | |
| N152 | 43.595 | 2.523 | 87.19 | -3.184 |
| N153 | 46.936 | 1.053 | 93.872 | 1.55 |
| I155 | 46.13 | 1.003 | 92.26 | 0.622 |
| Q156 | 43.377 | 1.866 | 86.754 | -8.406 |
| A157 | 47.649 | 1.369 | 95.298 | 2.464 |
| T158 | 48.009 | 2.436 | 96.018 | 3.782 |
| A160 | 48.515 | 1.729 | 97.03 | 2.424 |
| T161 | | | | |
| G163 | 49.065 | 2.156 | 98.13 | 6.384 |
| D164 | 44.886 | 1.129 | 89.772 | -3.378 |
| G165 | 49.502 | 1.523 | 99.004 | 6.97 |
| L166 | 45.996 | 1.92 | 91.992 | -0.122 |
| Y167 | 44.063 | 1.504 | 88.126 | -3.016 |
| E168 | 41.88 | 1.677 | 83.76 | -6.99 |
| G169 | 45.044 | 2.383 | 90.088 | |
| D171 | 41.667 | 1.356 | 83.334 | -8.776 |
| N172 | 41.098 | 1.191 | 82.196 | -9.556 |
| L173 | 43.334 | 1.469 | 86.668 | -4.66 |
| S174 | 42.671 | 0.996 | 85.342 | -6.356 |
| N175 | | | | |
| N176 | 45.273 | 1.571 | 90.546 | -1.764 |
| L177 | 41.632 | 1.688 | 83.264 | -9.08 |
| R178 | 35.71 | 1.841 | 71.42 | -20.574 |
| N179 | 45.534 | 1.192 | 91.068 | -0.628 |
| Q180 | 44.754 | 0.212 | 89.508 | -0.596 |
| K181 | 50.443 | 0.131 | 100.886 | 8.46 |
| Y154/A103 | | | | |
| L170/L159 | | | | |
| D67/L116 | 45.78 | 1.857 | 91.56 | 0.818 |
| F82/S162 | 48.931 | 1.716 | 97.862 | 6.47 |
| | | | | |
| | | | MAX | 14.456 |
| | | | MIN | -20.574 |
| | | | RANGE | 35.03 |

[a] Amino acid assignment (40)
[b] Half the $^{15}N$-$^{1}H$ scalar coupling (Hz) determined from an isotropic sample
[c] Error to scalar coupling (Hz)
[d] Total (scalar + dipolar) coupling (Hz)
[e] RDC (Hz)

# CHAPTER 5

# PARTIAL $^{13}C$ ISOTOPIC ENRICHMENT OF ARF1'S LIGAND GUANOSINE DIPHOSPHATE (GDP): A USEFUL REPORTER ON MEMBRANE-ASSOCIATED ARF1[1]

[1] Kishore, A.I., M.R. Mayer, & J.H. Prestegard. *Nucleic Acids Research.* 33(18):p.e164-1-10. (2005). Reprinted here with permission of publisher.

ABSTRACT

Analysis of the $^{13}C$ isotopic labeling patterns of nucleoside monophosphates (NMPs) extracted from *E.coli* grown in a mixture of C-1 and C-2 glucose is presented. By comparing our results to previous observations on amino acids grown in similar media, we have been able to rationalize the labeling pattern based on the well-known biochemistry of nucleotide biosynthesis. Except for a few notable absences of label (C4 and C3') and one highly enriched site (C1'), most carbons are randomly enriched at a low level (an average of 13%). These sparsely labeled NMPs give less complex NMR spectra than their fully isotopically labeled analogs due to the elimination of most $^{13}C$-$^{13}C$ scalar couplings. The spectral simplicity is particularly advantageous when working in ordered systems, as illustrated with GDP bound to ADP Ribosylation Factor 1 (ARF1) aligned in a liquid crystalline medium. In this system, the absence of scalar couplings and additional long-range dipolar couplings significantly enhances signal to noise and resolution.

## 5.1 INTRODUCTION TO BIOMOLECULAR ISOTOPIC LABELING

Strongly ordered, membrane-associated molecules are typically out of reach for $^{1}$H-based solution NMR experiments due to fast relaxing nuclei that broaden lines in these high molecular weight systems. Solid-state NMR (SSNMR) methods suitable for characterizing such molecules usually rely on direct detection of nuclei other than $^{1}$H due to their longer relaxation times and narrower linewidths. In the case of non-myristoylated (non-myr) GDP-bound ARF1, the attempt to increase membrane association through the membrane-anchored lipid $PIP_2$ was monitored using residual dipolar coupling (RDC) experiments based on $^{1}$H direct detection (Chapter 4). However, a more reliable method for characterizing membrane association may involve the direct observation of other more slowly relaxing nuclei such as $^{13}$C. The introduction of $^{13}$C labeling into ARF1 offers this possibility, but the large number of $^{13}$C resonances in a uniformly labeled sample would relegate study to indirect detection such as through an HSQC experiment. ARF1's natural ligand guanosine diphosphate (GDP), however, binds with nanomolar affinity through a coordinated $Mg^{2+}$; and when isotopically labeled, GDP can be used to characterize membrane-anchored ARF1's geometry.

The use of uniform, isotopic enrichment in biological molecules has been indispensable to the advancement of biomolecular NMR. Resonance assignment of $^{13}$C and $^{15}$N nuclei in proteins up to 40 kDa and nucleic acids up to 15 kDa is now routine in high resolution NMR (1-3). In solid-state NMR and in NMR of partially ordered systems, isotope labeling methods are also advantageous. Uniform isotopic labeling has, in general, facilitated assignment but has introduced some unique spectroscopic problems as well. Abundant scalar and dipolar couplings of adjacent $^{13}$C nuclei, for example,

actually degrade resolution and can lead to dilution of signal by transfer of magnetization through multiple pathways. Selective labeling reduces the probability of adjacent $^{13}C$ groups, improving spectral resolution and simplifying resonance assignment.

Selective labeling is often achieved through exploitation of known metabolic pathways in organisms such as *E. coli.* Such procedures have primarily been applied to protein systems (4,5); however, some selective labeling has also been done in nucleic acids (6,7), primarily for applications to dynamics. The high cost of selectively labeled late-stage intermediates has, nevertheless, limited applicability. Labeling with random fractionally labeled basic substrates can be a more cost-effective alternative (8-10), but such randomly labeled metabolic substrates are not always available. Here a procedure is presented for nucleotide labeling that relies on a combination of fully, but site-specifically, labeled substrates that may facilitate NMR structural application to RNAs and systems that use nucleotides as cofactors; my particular interest is in production of labeled guanosine diphosphate (GDP) for the study of ARF1. The anticipated structural data are from chemical shift anisotropy (CSA) offsets and residual dipolar couplings (RDCs). As an illustration, some preliminary data is presented on GDP-ARF1 ordered in a liquid crystalline model membrane.

$^{13}C$ labeling of proteins using site specifically labeled substrates has been documented previously in protein systems. For example, substitution of site-specifically labeled substrates, such as glucose (C1, C2), glycerol (C1/C3, C2), or pyruvate (C1, C3), for uniformly labeled substrates leads to enhanced labeling at a subset of sites throughout expressed proteins (4,5,11-13). There can, of course, be some sacrifice in sensitivity by a reduction in percentage of labeling at certain sites, but as suggested above this is partially

compensated by more efficient magnetization transfer and simpler spectra. Pulse sequences developed for magnetization transfer in uniformly enriched molecules typically require only minor modifications to take advantage of the spectral simplification seen in specifically labeled systems.

Nucleic acid structure determination has also benefited from isotopic labeling. Protocols to extract intact RNA from cells grown on uniformly isotopically labeled media and to isolate nucleoside monophosphates (NMPs) from the RNA have been described (6,14), but the use of specifically labeled precursors is less common (7,15). Isolating deoxyNMPs (dNMPs) is more difficult since cells contain 7-10 times more RNA than DNA (16), but this, too, has been described (17,18). Most protocols to extract NMPs from cell lysate call for the growth of *E.coli* in labeled minimal media to the late log phase for optimum ribosome production. Simple organic extractions easily separate proteins and lipids from the polymeric nucleic acids found in these structures (19).

The initial motivation for the work described here included an attempt to take advantage of by-products from protein labeling efforts at the SECSG (20). Proteins expressed for the NMR core of the SECSG were grown in 98% $^{15}$N ammonium chloride and a mixture of $^{13}$C-1 and $^{13}$C-2 glucose instead of uniformly labeled glucose; this yielded carbon enrichment at the 16-20% level in targeted proteins. The primary justification for this method initially was to reduce costs in large scale expression, but additional spectroscopic benefits have also been described (21). As discussed below, isolation of dNMPs and NMPs from cell debris proved difficult. In cells that have already been harvested and extracted of proteins, the lysate is frequently treated with deoxyribonuclease (DNAse I) to hydrolyze DNA and reduce the viscosity of the solution.

In addition, most protein preparation protocols do not use RNAse-free techniques to preserve the ribosome and other readily isolatable sources of RNA. The mononucleosidephosphates (dNMPs and NMPs) that result from DNAse and RNAse hydrolysis are more difficult to isolate and extract than intact nucleic acids. Hence, *E. coli* was grown to late log phase with the isolation of labeled nucleotides specifically in mind.

The use of $^{13}$C-1 and $^{13}$C-2 glucose for partial labeling remains an important aspect in the studies described here. The low percentage $^{13}$C enriched nucleotides isolated from *E.coli* grown with C-1 and C-2 labeled glucose should enjoy the same dilute spin advantages described for proteins. These nucleotides are particularly desirable over uniformly enriched nucleotides for measuring $^{13}$C CSA offsets and RDCs in aligned systems. The alignment of biomolecules in the magnetic field has produced a wealth of information on their structures and orientations. RDCs induced by low levels of order have been measured in a variety of molecules and alignment media (22-25). Chemical shift offsets can provide orientational constraints in a manner quite analogous to those provided by RDCs. They are particularly advantageous in providing constraints on nucleotide bases where all RDCs are in the plane of the base and the out-of-plane contributions of CSA offsets are highly complementary. CSA offsets have been measured for a number of biological systems where ordering is weak and long range dipolar couplings cause minimal degradation of resolution (26-31). In the case of a more strongly aligned sample, (in membrane-associated systems, for example) expected changes in chemical shift between isotropic and aligned resonances of aromatic carbons could reach tens of ppms, (32-35). However, under such strong alignment, multiple

through-space dipolar couplings present in uniformly labeled samples produce coupled spectra with many poorly resolved splittings. Even $^{13}C$-$^{13}C$ one-bond scalar couplings in uniformly labeled samples contribute an additional 40 Hz, and two and three-bond couplings produce an additional 7-11 Hz (36). When through-space dipolar couplings are present, the splittings are even more numerous. Hence, improved resolution is expected for partially labeled nucleotides, particularly if labels are nearly randomly distributed. One example of the potential use of partially labeled nucleotides is to measure $^{13}C$ chemical shift offsets for nucleotide cofactors bound to membrane-associated GDP/GTP-binding GTPases, or G proteins (37,38). RDCs have been used in combination with other NMR data to determine geometries of bound ligands in weakly aligned proteins (39-43), and it should be possible to use CSA offset information in a similar way when systems are more strongly ordered. It is in these latter applications that partial labeling can be particularly advantageous.

## 5.2 CHEMICAL SHIFT OFFSET THEORY

The chemical shift offset, $\delta_i^{csa}$, can be expressed as shown in equation 1 where the $\delta_{kk}$ are the principal elements of the anisotropic part of the chemical shift tensor, $\theta_{ik}$ and $\theta_{jk}$ are the angles between the principal axes of the shift tensor and an arbitrary molecular frame, and $S_{ij}$ are the elements of the order tensor in the molecular frame. The values of $\delta_{kk}$ are assumed to be well defined in a frame oriented in an individual molecular group. In practice, the principal frame chemical shift values and directions of the axes are usually taken from suitable model compounds collected in the solid state or from *ab initio* calculations of chemical shielding tensors (44,45).

$$\delta_i^{csa} = \delta_{align} - \delta_{iso} = 2/3 \, \Sigma_{i=x,y,z} \, \Sigma_{j=x,y,z} \, \Sigma_{k=x,y,z} \, S_{ij} \cos(\theta_{ik}) \cos(\theta_{jk}) \, \delta_{kk} \qquad (1)$$

### 5.2.1 PROTEIN GEOMETRY THROUGH LIGAND RESTRAINTS

In my approach, I would like to use chemical shift offsets from an isotopically labeled ligand bound to a weakly ordered, membrane-associated protein, ARF1, to determine ligand orientation. In the case where ARF1 is weakly ordered, N-H RDCs from the protein alone can provide enough geometrical restraints for structural applications. When ARF1 is strongly anchored to the membrane, for example in the presence of a high percentage of lipid bilayer or through a covalently attached acyl chain, protein RDCs become more difficult to measure, and CSA offsets from the isotopically labeled ligand are essential to determining molecular geometry. Since the level of order and alignment frame of the ligand will be the same for the bound protein, the membrane-associated orientation can be inferred using available crystal structures. One assumption is that the membrane-associated geometry of the ligand and protein is the same as in solution.

RDCs from the protein itself have already been used to determine the molecular geometry of the membrane-associating GTPase ADP Ribosylation Factor 1 (ARF1) (46) and its orientation in weakly aligned systems (47). When more strongly aligned through association with a membrane, the CSA offsets from ARF1's isotopically labeled nucleotide cofactor GDP or GTP may be more accessible and may prove a more useful probe of protein orientation relative to the membrane surface. To pursue such studies, it is important to have methods for producing partially labeled nucleotides and to know the details of labeling patterns for such molecules. Here we offer a fundamental analysis of isotopic labels in nucleotides extracted from *E.coli* grown on a mixture of C-1 and C-2 labeled glucose. We also present spectra demonstrating the enhanced signal to noise and

improved resolution of partially $^{13}$C-labeled GDP over uniformly labeled GDP when bound to ARF1, both in solution and in the presence of a model membrane. Although the extent of ordering in our particular system is less than in many membrane-anchored protein systems, it provides a stepping-stone to future studies of more strongly ordered systems with bound nucleotide cofactors.

## 5.3 MATERIALS & METHODS

### 5.3.1 CELL GROWTH & NMP ISOLATION

All isotopes were purchased from Cambridge Isotope Laboratories, Inc (Andover, MA). M9 media for growth of cells was prepared by adding per liter: 6 g $NaHPO_4$, 3 g $KH_2PO_4$, 0.5 g NaCl, and 1 g $NH_4Cl$ to $_{dd}H_2O$ and the solution was autoclaved. In addition, filter-sterilized solutions of the following were added to each liter: 15 mL 20% glucose, 1 mL 2.0 M $MgSO_4$, 1 mL metal mix (0.1 M $CaCl_2$, 0.1 M $MnCl_2$-$4H_2O$, 0.1 M $ZnSO_4$-$7H_2O$, 0.02 M $CoCl_2$-$6H_2O$, 0.02 M $CuCl_2$-$2H_2O$ and 0.02 M $NiCl_2$-$6H_2O$). A pET14 plasmid with no insert was transformed into *E. coli* BL21(DE3) Gold (Stratagene, La Jolla, CA) and plated onto M9 agar plates containing 100 μg/mL ampicillin. A single colony was used to inoculate 50 mL of M9 media containing 100 μg/mL ampicillin in a 250 mL baffled flask and grown overnight (~16 hours) at 37ºC while shaking at 250 rpm. One liter of M9 containing 100 μg/mL ampicillin, 1 g $^{15}$N-$NH_4Cl$, 2 g 1-$^{13}$C-glucose and 1 g 2-$^{13}$C-glucose in a 2.5 L baffled flask was inoculated with 20 mL (1:50 dilution) of the overnight culture. The flask was grown at 37ºC while shaking at 250 rpm until $OD_{600}$ = 0.7 (approximately 3-4 hours), moved to 22ºC and the cells were harvested 16 hours later. The cell pellets (~15 g) were immediately frozen at -70ºC. Ribosomal RNA was extracted from thawed cells *via* French press, centrifugation, and organic phase extraction

according to Nikonowicz et al. (14). RNA was hydrolyzed to NMPs using P1 Nuclease (Roche), and the NMPs were eluted from a Vydac 3021.10C ion exchange HPLC column (Grace Vydac, Hesperia, CA) with 50 mM ammonium formate, adjusted to pH 3.2 with formic acid (both from Aldrich, St. Louis, MO). Peaks corresponding to CMP, UMP, AMP and GMP were collected separately, lyophilized, redissolved in water, and lyophilized an additional two times to facilitate removal of volatile ammonium formate. Approximately 12 mg of each partially labeled NMP was recovered.

### 5.3.2 GDP SYNTHESIS

Since our target application is a GDP/GTP binding switch protein (ARF1), GMP was converted to GDP, and for comparison purposes, this was done with both partially labeled and fully labeled starting materials. Fully labeled GDP was synthesized from >98% $^{13}C$, $^{15}N$ GMP (Spectra Stable Isotopes, Columbia, MD), and partially labeled GDP was synthesized from the GMP described above, both using a modified protocol from Niconowicz et al (14). Guanylate Kinase (Sigma) was used to phosphorylate GMP and excess ATP (Sigma) was added as the phosphate donor. The reaction was maintained at 37ºC for 44-48 hours and then quenched by addition of 100 μL of 50 mM EDTA. The volume was reduced to half by lyophilization, and absolute ethanol was added to three times the volume with overnight storage at -20ºC to effect precipitation of nucleotides. The precipitated nucleotides were dried in air, dissolved in water, and purified by HPLC using the Vydac 3021.10C ion exchange column and a 35 mL step gradient of 50, 100, and 200 mM ammonium formate (pH 3.2). Fractions were lyophilized, redissolved in water and lyophilized again to facilitate removal of formate. The yield from this separation was 50-65%.

### 5.3.3 NUCLEOTIDE EXCHANGE

$^{15}$N-labeled ARF1 was prepared according to previously described methods (46). $^{13}$C, $^{15}$N GDP was exchanged into ARF1 by an EDTA-mediated exchange. A 25-fold excess of EDTA over ARF1 was added to a solution of 0.5 mM ARF1 to remove magnesium and facilitate turnover of native nucleotide. This was followed by addition of a 10-fold excess of $^{13}$C, $^{15}$N GDP in buffer containing 20 mM Tris-HCl (pH 7.6), 100 mM NaCl, 5 mM $MgCl_2$, and 2 mM $NaN_3$. The exchange took place for 48 hours at 4ºC. EDTA was removed from the solution by several serial dilutions with the above buffer minus GDP until the final estimated concentration of EDTA was less than 30 nM.

### 5.3.4 ALIGNMENT MEDIUM PREPARATION

$C_{12}E_5$/hexanol has previously been identified as a suitable alignment medium for both ARF1 (47) and a lipid that interacts with ARF1 at a membrane surface, $PIP_2$ (48). This medium was prepared as follows: Pentaethylene glycol monododecyl ether $C_{12}E_5$ (Sigma, St. Louis, MO) was combined with hexanol in the ratio 0.88:1 to make a solution of 4.6% (w/w) $C_{12}E_5$ (49-51). Pure $PIP_2$ (phosphatidylinositol 4,5-bisphosphate, Avanti Polar Lipids, (Alabaster, AL)), was dried under a stream of nitrogen and added directly to the $C_{12}E_5$ bilayers at a relatively low molar ratio of $PIP_2$ to $C_{12}E_5$ (1:80) so that bilayer order is not disrupted. ARF1 was added to the medium to produce a final solution of ~0.7-1.0 mM protein at a 2:1 $PIP_2$ to ARF1 ratio.

### 5.3.5 NMP NMR ANALYSIS

NMP fractions were analyzed by $^{1}$H, $^{13}$C, and $^{31}$P NMR on a 500 MHz Varian (Palo Alto, CA) Inova spectrometer using a triple resonance Varian probe for $^{1}$H, a 5 mm Nalorac $^{13}$C/$^{15}$N broadband observe probe (operating at 125.6 MHz) for $^{13}$C, and a 5 mm

Varian broadband observe probe (operating at 202.6 MHz) for $^{31}P$ spectra. $^{13}C$ spectra were collected with a 45° tip angle, rapid recycling (0.5 sec recycle delay), and Waltz-16 $^{1}H$ decoupling for NOE enhancement. These spectra were used to determine chemical shifts (and $^{13}C$-$^{1}H$ scalar couplings by turning off the proton decoupling during acquisition). Relative peak intensities were determined by integrating peaks observed with decoupling during acquisition only and a long recycle delay (5 sec) to allow sufficient magnetization recovery. $^{31}P$ observe and 1D $^{1}H$-$^{31}P$ HMQC spectra were collected to confirm ribose phosphorylation (Data not shown). The pH of each sample was recorded, and free phosphate was added to 0.85-1.65 mM to each HPLC fraction as a reference signal for determination of $^{31}P$ chemical shift and nucleotide concentration. $^{13}C$ chemical shifts were referenced indirectly by referencing to added DSS and using appropriate ratios for properly referenced $^{13}C$ spectra (52,53).

### 5.3.6 GDP-BOUND ARF1 NMR ANALYSIS

$^{13}C$ direct observe data on an ARF1 complex containing labeled GDP were collected at 25° C on an 800 MHz Varian Inova spectrometer using the normal $^{13}C$ decoupling input on a triple resonance Varian Chili Probe in a 4mM $D_2O$ susceptibility-matched Shigemi (Alison Park, PA) tube. $^{13}C$ spectra were collected with a 33-45° tip angle and Waltz-16 $^{1}H$ decoupling at a $B_1$ field of 12000 Hz during acquisition. For 98%-$^{13}C$ GDP isotropic samples, 30000-40000 scans were acquired, and for aligned samples 83,000 scans were acquired, both with a 1.6 sec recycle time. For 13%-$^{13}C$ GDP isotropic samples, 300000 scans were acquired, and for aligned samples 630000 scans were acquired, both with rapid recycling (0.3 sec recycle time). $^{15}N$-$^{1}H$ heteronuclear single quantum coherence spectra (HSQC) were also collected before and after each $^{13}C$

experiment (data not shown) to confirm protein integrity. Liquid crystal alignment was also confirmed by monitoring the $^{2}H$ NMR quadrupolar splitting of water deuterons (18-21 Hz). Protein alignment was independently determined by measuring $^{15}N$-$^{1}H$ RDCs on the lipid-doped $C_{12}E_5$ model membrane sample (data not shown). $^{13}C$ spectra were processed using nmrPipe (54), applying backwards linear prediction and an exponential apodization function with a 30 Hz line broadening constant. The automated lineshape fitting routine within nmrPipe (nlinLS) was used in order to accurately extract resonance positions. $^{13}C$ and $^{15}N$ chemical shifts in the protein samples were referenced indirectly by referencing to added DSS and using appropriate ratios for properly referenced $^{13}C$ or $^{15}N$ spectra, respectively.

## 5.4 RESULTS

NMPs were easily separated by HPLC (Figure 5.1) and analyzed by NMR. Resolution of the four bases was facilitated by reversed-phase interactions with the column resin. In Figure 5.2 the $^{13}C$ NMR spectrum of both the base and ribose regions for UMP is shown as a representative of other nucleotide spectra. Chemical shift assignments are based on previously reported data (36). Note, that the C1' carbon shows the highest level of carbon labeling. Peak intensities vary due to the differing levels of enrichment, as dictated by their origin in biosynthetic pathways. Other ribose carbons show moderate levels of labeling as evidenced by $^{13}C$ spectra, but the lack of ribose $^{13}C$-$^{13}C$ couplings (except at the bases of peaks) suggests low levels of incorporation.

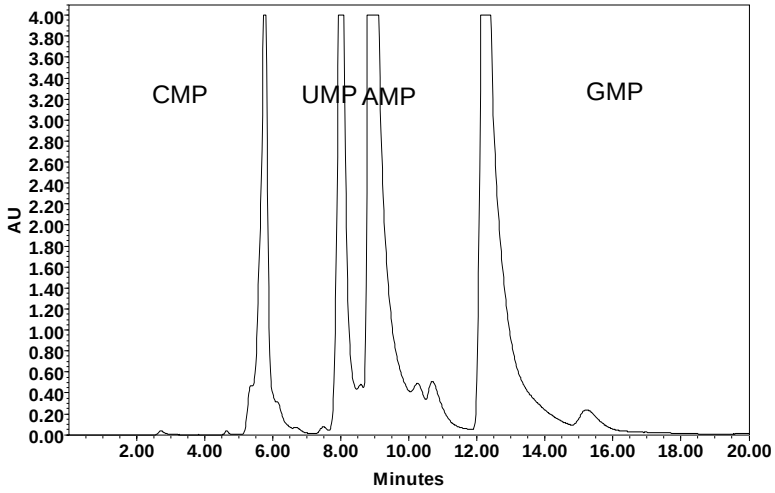


Figure 5.1 HPLC chromatogram of NMPs in 50 mM ammonium formate, pH 3.2.

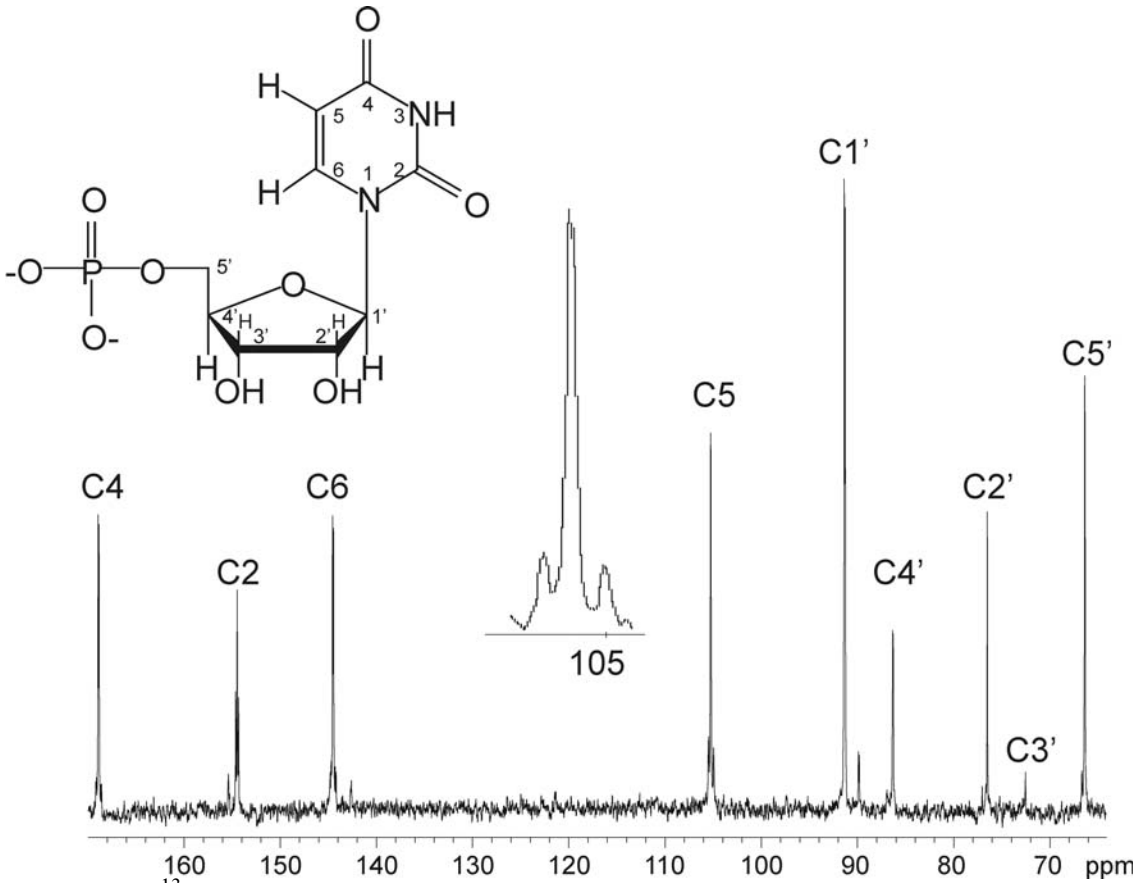


Figure 5.2 . $^{13}C$ NMR spectrum of base and ribose regions of UMP. Short tip angles and long recycle delay times were used to promote uniform carbon relaxation. Assignments were based on published spectra. (36)

In Figure 5.3 expansions of the base region in $^{13}C$ NMR spectra of each of the NMPs are shown. C5 and C6 of pyrimidines (3a for CMP, 3b for UMP) appear to get labeled at approximately the same percentage, and C2 and C4 show significantly lower intensities. These differing intensities are due, in part, to the nuclear Overhauser enhancement (NOE) for protonated carbons, C5 and C6. A small amount of AMP was present in the UMP spectrum, as noted by asterisks. In purine (3c for AMP, 3d for GMP) spectra, we observed $^{13}C$ labeling of C2, C5, C6, and C8, and almost no $^{13}C$ labeling of C4 (Figure 5.3c,d). C2 and C8 show similar labeling levels in both AMP and GMP. C5 and C6 exhibit lower, but approximately equal levels of isotopic labels. The AMP fraction was contaminated with about 10% UMP, represented in Figure 5.3c by asterisks. Several one bond $^{13}C$-$^{15}N$ scalar couplings are observed in $^{13}C$ spectra, for example, the barely observable splittings seen at the top of the peaks for C4 and C6 of UMP and CMP (Figures 3a and 3b).

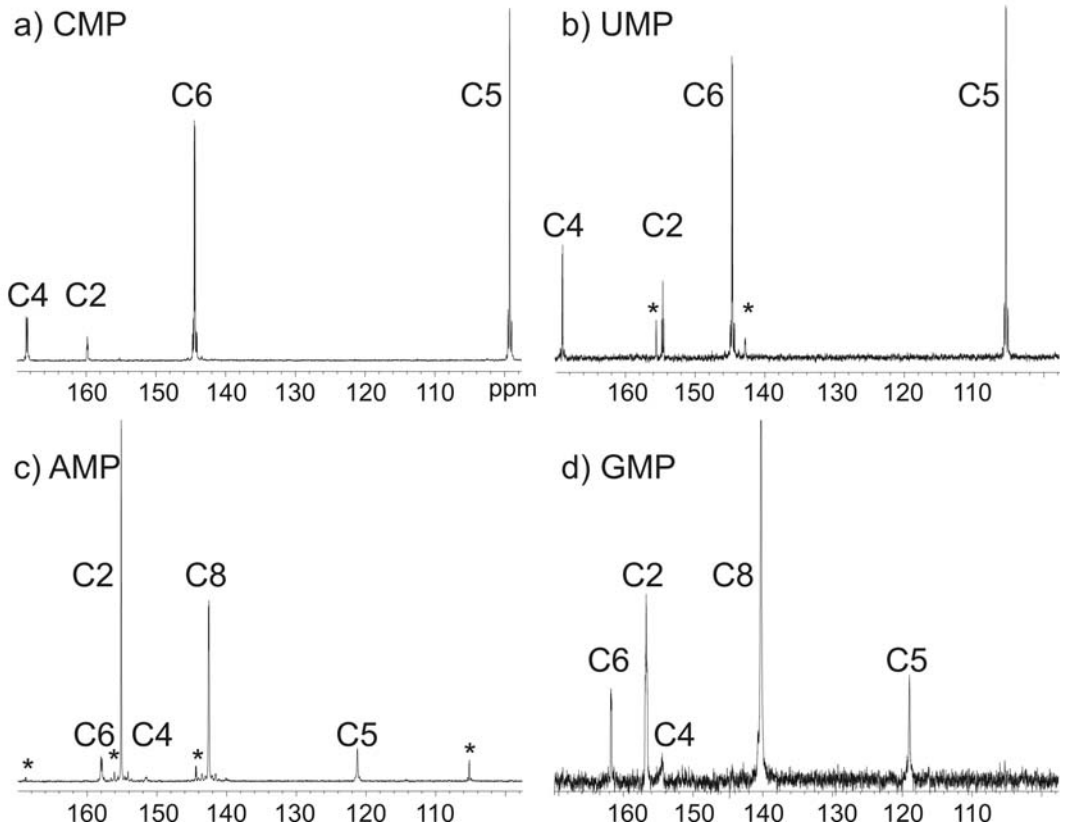


Figure 5.3. $^{13}C$ ($^{1}H$-decoupled) NMR spectra of the base region of NMPs: a) CMP b) UMP c) AMP d) GMP. Assignments were based on published spectra. (36) Asterisks represent contaminating peaks from other nucleotides.

In Table 5.1 the chemical shifts are summarized for the four NMPs as well as estimates of isotopic enrichment. The level of carbon enrichment is estimated based on $^{13}C$ resonance intensities collected with long recycle delays (data not shown) and on $^{13}C$ satellites in $^{1}H$ spectra (Figure 5.4). The H6 proton signal from CMP (Figure 5.4a), for example, shows $^{13}C$ satellites that represent 29% of the total incorporation. H1' is the only ribose sugar proton resonance with appreciable $^{13}C$ satellites. Satellites for H5 and H1' resonances (Figure 5.4b) of CMP show about 31% $^{13}C$ incorporation for H5 and 45% for H1'.

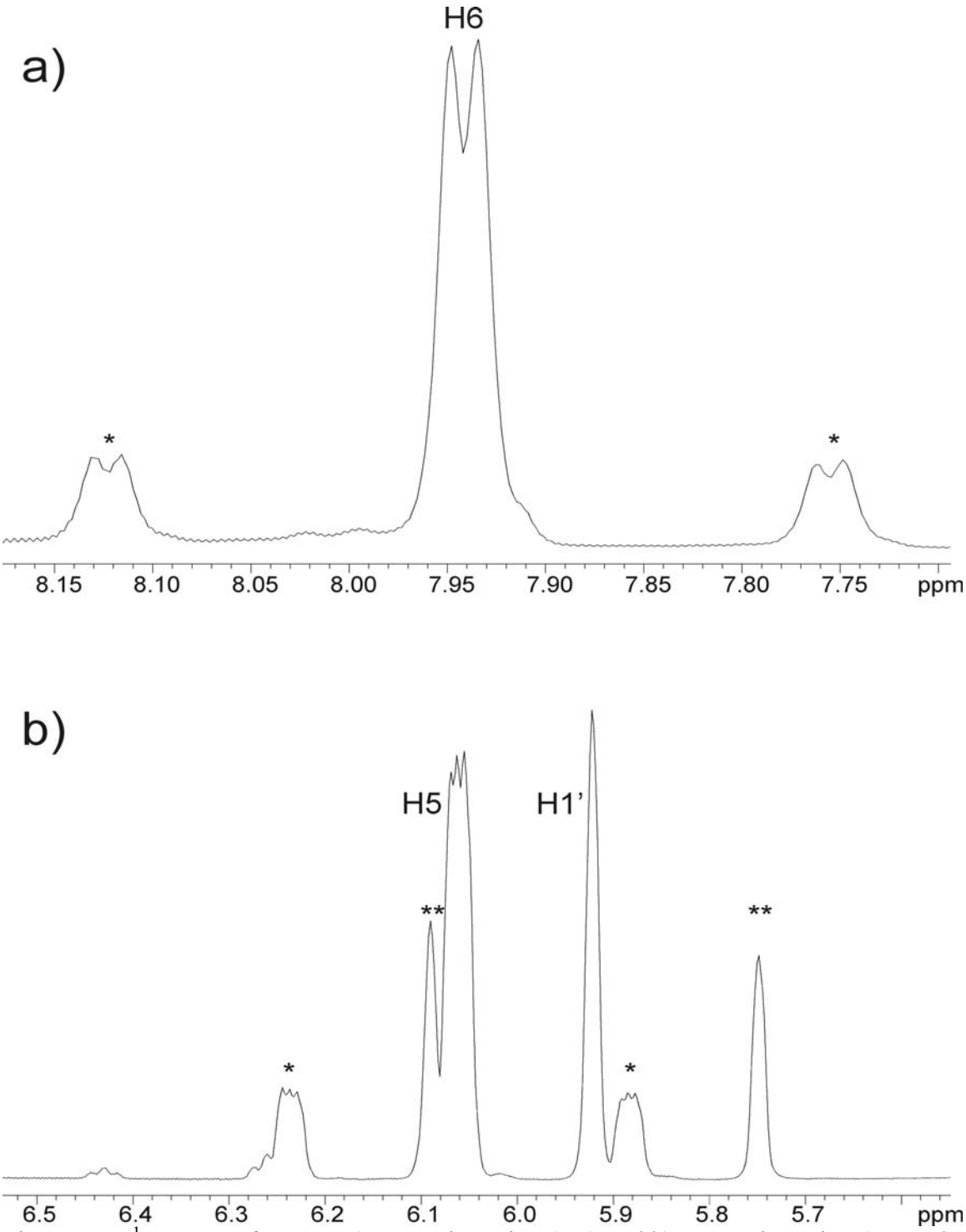


Figure 5.4. $^{1}H$ NMR of CMP's a) aromatic region (H6) and b) anomeric region (H5 and H1'). $^{13}C$ satellites are observed for all three $^{1}H$ peaks and are represented by a single asterisk for H5 and H6 and a double asterisk for H1'. Assignments were based on published spectra. (36)

Table 5.1. $^{13}C$ chemical shifts (ppm) of labeled NMPs and site-specific percentage of isotopic incorporation.

| $^{13}C$ | CMP | | | UMP | | | AMP | | | GMP | | |
|---|---|---|---|---|---|---|---|---|---|---|---|---|
| | Chemical shift (ppm) | Relative %Label[a] | Absolute %Label[b] | Chemical shift (ppm) | Relative %Label[a] | Absolute %Label[b] | Chemical shift (ppm) | Relative %Label[a] | Absolute %Label[b] | Chemical shift (ppm) | Relative %Label[a] | Absolute %Label[b] |
| C2 | 159.8 | 32 | 14 | 154.5 | 39 | 16 | 155.1 | 73 | 38 | 156.8 | 66 | 22 |
| C4 | 168.5 | 46 | 21 | 168.9 | 41 | 61 | 151.5 | 7 | 4 | 154 | - | < 2 |
| C5 | 99.3 | 68 | 31 | 105.2 | 72 | 29 | 121.2 | 40 | 21 | 118.9 | 37 | 12 |
| C6 | 144.5 | 64 | 29 | 157.9 | 61 | 24 | 157.9 | 31 | 16 | 161.8 | 28 | 9 |
| C8 | - | - | - | - | - | - | 142.6 | 70 | 36 | 140.3 | 57 | 19 |
| C1’ | 92.1 | 100 | 45 | 91.3 | 100 | 40 | 89.9 | 100 | 52 | 89.6 | 100 | 33 |
| C2’ | 77.0 | 26 | 12 | 76.5 | 30 | 12 | 77.0 | 26 | 14 | 76.6 | 26 | 9 |
| C3’ | 72.3 | 8 | 4 | 72.4 | 11 | 4 | 73.1 | 5 | 2 | 73.2 | 7 | 2 |
| C4’ | 85.8 | 29 | 13 | 86.3 | 35 | 14 | 86.7 | 24 | 12 | 86.7 | 35 | 12 |
| C5’ | 66.3 | 63 | 28 | 66.4 | 58 | 23 | 66.8 | 52 | 27 | 67.2 | 42 | 14 |

[a] Percentage labeling determined relative to C1’ peak intensity by integrating $^{13}C$ peak intensities in fully relaxed $^{13}C$ spectra.
[b] Percentage determined by integrating $^{13}C$ satellites to H1’ in $^{1}H$ spectra and using relative $^{13}C$ percentage labels.

In Figures 5.5a and 5.5b we present $^{13}C$ spectra from the aromatic region of 13% $^{13}C$-labeled GDP bound to ARF1 when aligned (5a) and in isotropic buffer solution (5b), respectively. The aligned sample is oriented in a 4.6% (w/w) $C_{12}E_5$ bilayered liquid crystal doped with $PIP_2$, a signaling lipid that is suggested to interact with ARF1 (55-57). Aromatic base carbon frequencies are labeled for easily observed resonances; C4 and C6 are not observed to due lower levels of isotopic incorporation. Unlabeled regions of high spectral intensity represent natural abundance $^{13}C$ protein signals from aromatic (~130 ppm) resonances; these are marked with double asterisks. Some free GDP (denoted by a single asterisk) is also observed in isotropic solution, and resonances from this free GDP are readily identified based on distinct chemical shifts between free and bound forms. Chemical shift offsets between isotropic and aligned spectra, though small, are observed for the aromatic carbons, with C2 and C5 displaying differential shifts with C2 moving downfield (54 Hz). These differences are likely to arise from orientational dependences of CSAs, and they can be structurally useful.

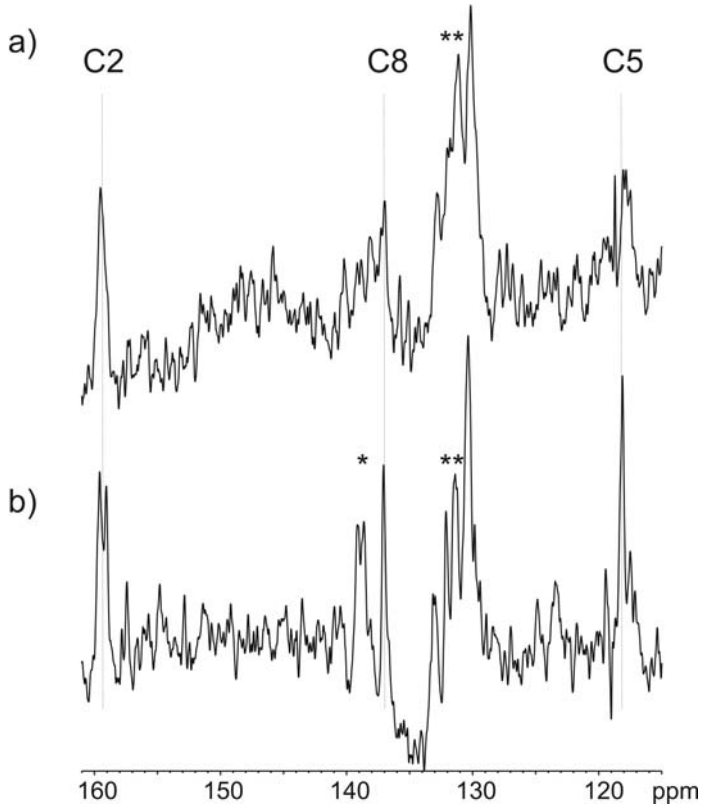


Figure 5.5. $^{13}C$ ($^{1}H$-decoupled) NMR spectra of the aromatic region of 13%-$^{13}C$ GDP-ARF1: a) when aligned in $C_{12}E_5$-$PIP_2$ model-membranes (1.0 mM ARF1) and b) isotropic buffer solution (1.4 mM ARF1). A single asterisk represents free GDP in solution, and a double asterisk represents unlabeled aromatic carbons from ARF1. Vertical lines indicate observed shift offsets between isotropic and aligned carbons.

Figure 5.6 shows a similar comparison between isotropic and aligned 98%-$^{13}C$ labeled GDP-ARF1. All five aromatic carbons of GDP are observed in this case. The lower resolution compared to Figure 5.5 is due, in large part, to fewer collected scans but also to numerous scalar and dipolar couplings that broaden line widths.

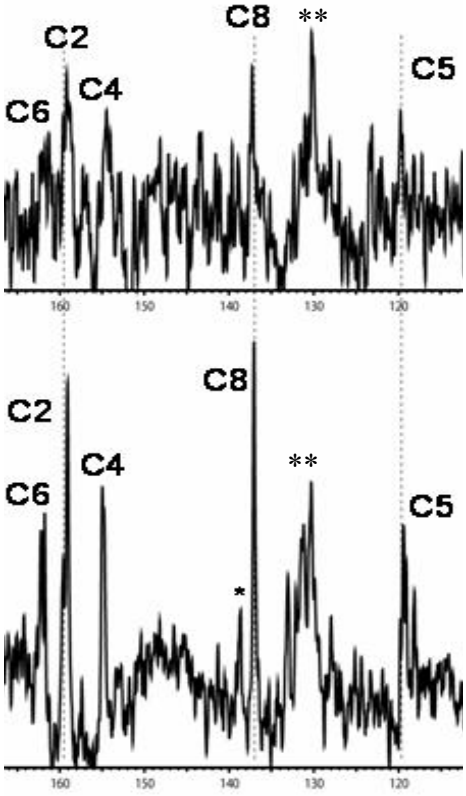


Figure 5.6. $^{13}C$ NMR spectral comparison of 98% GDP-ARF1 when a) aligned in 4.6% $C_{12}E_5$ + $PIP_2$ and b) isotropic in buffer solution. * represents free GDP and ** represents unlabeled aromatic carbons from protein background.

The resolution and quality of some signals, for example C2, in 13% carbon-labeled GDP is significantly better than what can be obtained under comparable conditions with a 98% carbon-labeled sample. Figures 5.7a-5.7d show expansions of the C2 and C5 regions of the spectrum for similarly aligned (C2) and isotropic (C5) samples using a 13% carbon-labeled sample (5.7a, 5.7c) and a 98% carbon-labeled sample (5.7b, 5.7d). The resonances are considerably broader for the 98% sample, and the signal to noise ratio appears less despite the fact that the additional scans for the 13% sample (a factor of 8) are not nearly enough to compensate for the decrease in $^{13}C$ content by a

factor of 7.5. Even if the repetition time were the same in both acquisitions (it was shorter for the 13% sample), this factor would need to be squared to fully compensate for decreased label content.

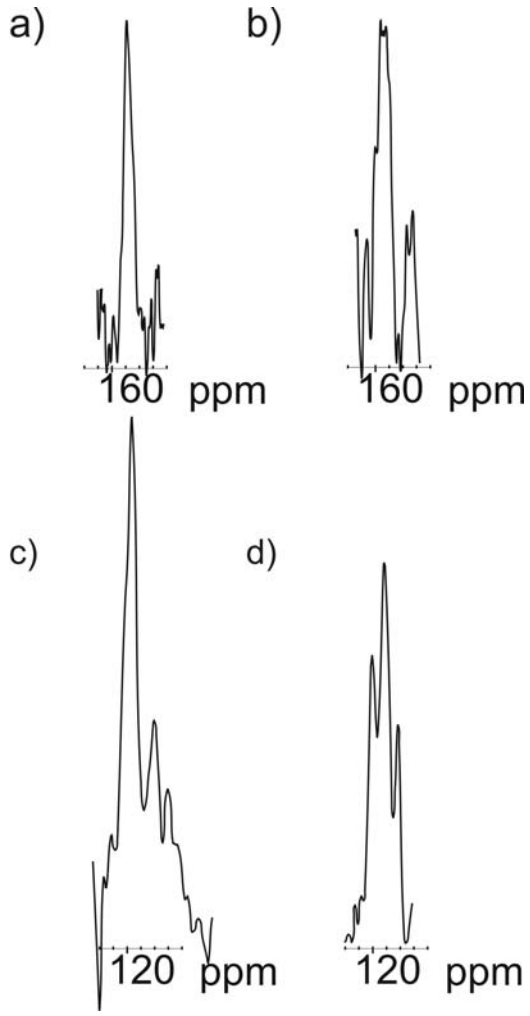


Figure 5.7. Expansion of $^{13}C$ NMR spectral regions for the C2 and C5 carbons of GDP in GDP-bound ARF1: C2 in aligned in 4.6% $C_{12}E_5$-$PIP_2$ model-membranes a) 13%-$^{13}C$ GDP (630,000 scans, 0.3 s recycle time) b) 98%-$^{13}C$ GDP (83,000 scans, 1.6 s recycle time). C5 is in isotropic buffer solution c) 13%-$^{13}C$ GDP d) 98%-$^{13}C$ GDP. Resolution is improved for 13% $^{13}C$-GDP-ARF1 compared to 98% $^{13}C$-GDP-ARF1.

## 5.5 DISCUSSION

### 5.5.1 IMPROVED RESOLUTION IN SPECTRA OF PARTIALLY LABELED NMPS

There is little doubt that reduction of percent labeling, when done approximately randomly, results in an improvement in signal quality despite somewhat lower overall sensitivity. We suggest that the absence of significant $^{13}C$-$^{13}C$ splittings from both scalar and long-range dipolar couplings is the origin of this improvement. One would expect broadening of resonances and loss of signal due to unresolved splittings of resonances when enrichment is high or if labeled pairs were incorporated as intact units. We do not see scalar couplings at 13% enrichment under high resolution, non-protein-bound, conditions (Figures 5.2 and 5.3), and we would expect fewer dipolar couplings under aligned conditions as well. Resonance intensity, even if reduced by partial labeling, would be largely concentrated into a single resonance resulting in an improvement in resonance quality.

### 5.5.2 BIOSYNTHETIC PATHWAYS LEAD TO DESIRABLE LABELING: PENTOSE PHOSPHATE PATHWAY YIELDS LABELED RIBOSE

Near random labeling, or labeling only of select sites, is essential to the gains from the absence of scalar or dipolar coupling described above. The labeling patterns observed for the systems studied here can be understood based on well known biosynthetic pathways for ribose and the nucleotide bases. The use of $^{13}C$ NMR has long been important in the elucidation of metabolic pathways (58-60) as well as in the introduction of $^{13}C$ isotopic labels into proteins of interest. Less discussion exists for isotopic labeling of nucleotides, and none exists specifically for the use of C-1, C-2

glucose mixture in *E. coli* growth. Here we attempt to rationalize the isotopic labeling pattern of nucleic acids grown with $^{13}C$ labeling from C-1 and C-2 glucose.

Unlike most amino acids of proteins, where $^{13}C$ labels from C-1, C-2 glucose mixtures are nearly uniformly distributed across alpha, carbonyl, and other carbons, ribose carbons are highly enriched at the C-1 position. Ribose-5-phosphate, the precursor to ribose in all nucleotides is produced directly from glucose and glucose-6-phosphate in the pentose phosphate pathway (PPP) by the elimination of C-1 from glucose (Figure 5.8). Depending on the cell's metabolic needs, glucose-6-phosphate (G6P) can either undergo isomerization to fructose 6-phosphate (F6P) by phosphoglucose isomerase or oxidation and hydrolysis to 6-phosphogluconate (6PG) by 6GP dehydrogenase and 6-phosphoglucono lactonase, respectively. The subsequent oxidative decarboxylation of 6PG by phosphogluconate dehydrogenase to ribulose-5-phosphate (Ru5P) is the final step in the oxidative portion of the pentose phosphate pathway. Isomerization of Ru5P to ribose-5-phosphate (R5P) by ribulose-5-phosphate isomerase is controlled by the cell's metabolic needs. R5P is then utilized in nucleotide biosynthesis (61). Hence, the enriched carbon of the C-2 glucose used in our minimal media for *E.coli* growth has a direct route to the C1 of ribose, and nucleotides thus become highly enriched at C1', as shown in Table 5.1.

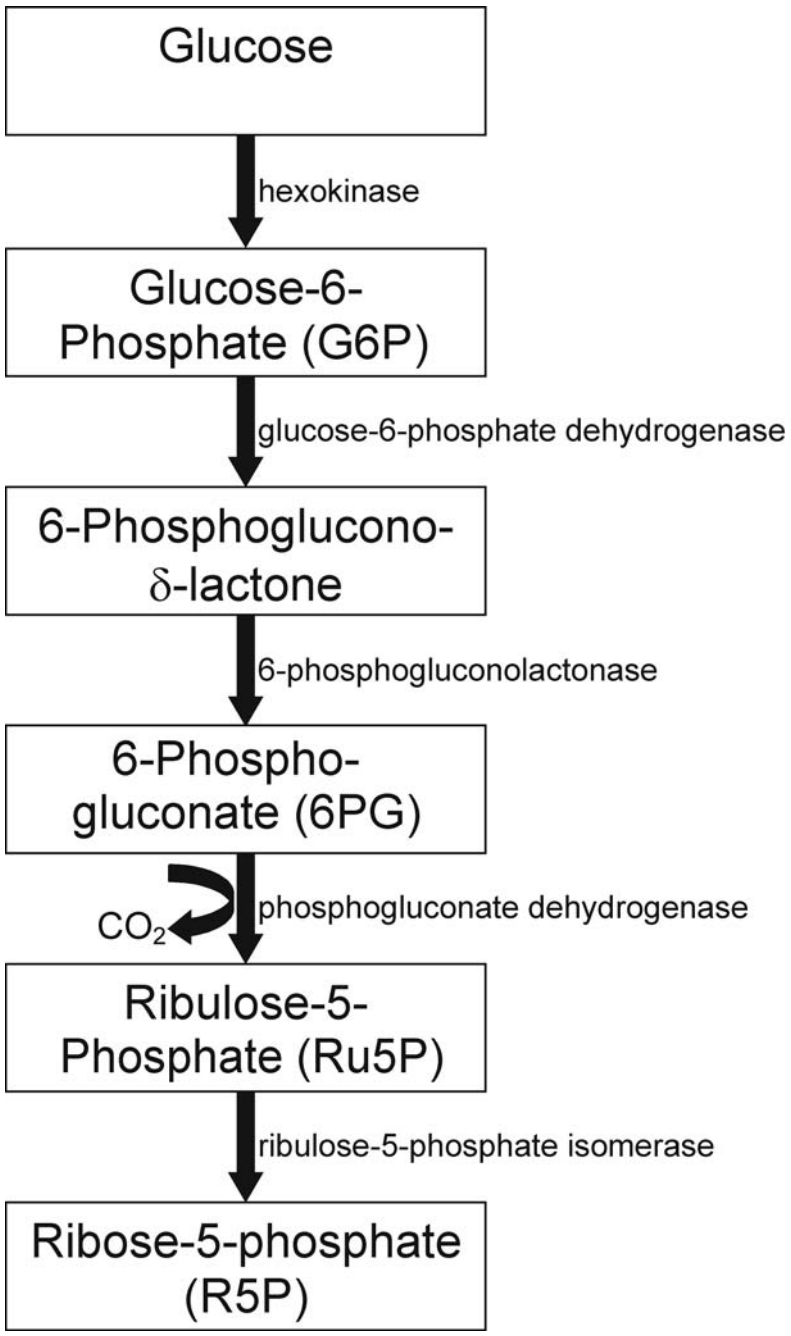


Figure 5.8. The pentose phosphate pathway, the predominant pathway for ribose-5-phosphate synthesis.(61)

Some labeling of ribose carbons C2', C4', and C5' is also observed (Figure 5.2), but C3' shows almost no $^{13}C$ enrichment (Table 5.1). The labeling pattern can be rationalized as follows. The recycling of cellular components with near random levels of

isotopic incorporation results in low labeling levels for most ribose carbons. Specifically, glycolysis and gluconeogenesis scramble the C-1 and C-2 labels such that C1', C2', C5', and C6' of glucose all become labeled. In addition, the pentose phosphate pathway regenerates glucose with C1' and C3' labels (62-64). However, C4' does not become labeled through any of the above pathways. The final labeling scheme results in isotopic labels everywhere except C4' of glucose. Due to the decarboxylation discussed above, C4' of glucose becomes C3' of ribose, and little labeling of ribose C3' is observed.

### 5.5.3 PURINE BASE BIOSYNTHESIS.

Labeling patterns in nucleotide base biosynthesis can be understood by considering isotopic labeling of their precursors. In the case of purines, labeling can be rationalized by considering the origin from constitutive amino acids, formate, and bicarbonate (Figure 5.9a). C2 and C8 are derived from a formyl group transferred by N10-formyl-tetrahydrofurate. C6 is derived from bicarbonate. These one carbon sources are labeled by metabolic degradation of glucose. The single carbon pool is diluted by $^{12}C$ carbons, hence labeling of these groups is at a lower level and essentially random. C4 and C5 are derived from the C' and Cα carbons, respectively, from glycine. Glycine, synthesized in the linear part of amino acid biosynthesis from serine, should incorporate an isotopic label at Cα, but the carbonyl carbon is not predicted to be labeled in *E.coli* grown on C-1 glucose or C-2 glycerol (12). In our purine (AMP, GMP) spectra, we observed significant $^{13}C$ labeling of C2, C5, C6, and C8, and almost no $^{13}C$ labeling of C4 (Figure 5.3c,d). As C4 comes from the carbonyl carbon of glycine, the lack of labeling in our system is consistent with previous predictions for amino acids in similar growth media (12).

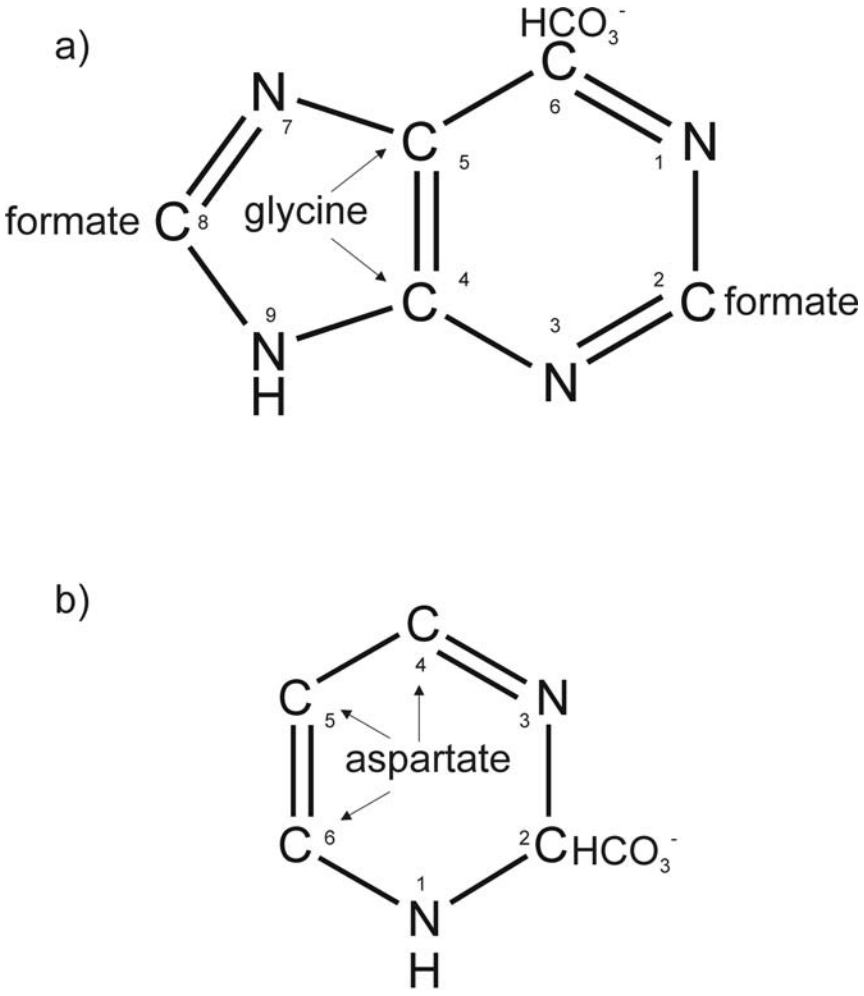


Figure 5.9. Predicted biosynthetic carbon sources for a) purines and b) pyrimidines (61).

### 5.5.4 PYRIMIDINE BASE BIOSYNTHESIS.

Pyrimidines differ from purines in that they are almost entirely synthesized from aspartate. (Figure 5.9b) Biochemical pathways indicate aspartic acid carbons form pyrimidines as follows: Cα forms C6, Cβ forms C5, Cγ forms C4. The C2 originates from bicarbonate. Theoretical and experimental analysis of a selectively, but extensively, labeled protein indicates all aspartate carbons should eventually become labeled with $^{13}$C-1 and $^{13}$C-2 glucose through the citric acid cycle, but at lower levels for Cγ and C' (12,13,65). Aspartic acid is generated from oxaloacetate, which in turn can arise from

direct carboxylation of pyruvate or from the citric acid cycle. Aspartate formed from pyruvate carboxylation lacks both the Cγ and C' label; whereas, aspartate synthesized from oxaloacetate derived from the citric acid cycle has highly enriched labels at Cα and Cβ and lower levels of labeling at Cγ and C'. C5 and C6 of CMP and UMP appear to get labeled at approximately the same percentage, consistent with Cα and Cβ of aspartic acid being labeled. The lower level of enrichment for C4 is consistent with the predicted low level of labeling at Cγ in similar media (12). In all cases the precursors start with glucose molecules containing a single $^{13}C$, and these single sites are diluted with $^{12}C$ in metabolic intermediates. Hence, there is little possibility of having directly bonded $^{13}C$'s.

### 5.5.5 ISOLATION OF NMPS AS BY-PRODUCTS FROM PROTEIN EXPRESSION

While we found it advantageous to grow cells explicitly for the purpose of isolating RNA and subsequently NMPs, the prospect of recovering these as by-products of protein synthesis remains appealing. A one liter growth of cells for protein expression requiring 3 g $^{13}C$ glucose and 1 g $^{15}N$ ammonium chloride typically leaves a significant amount of isotopically labeled biological waste. Given that a typical *E.coli* cell is composed of about 55% protein, 20% RNA, 9% lipid, and 3% DNA by weight (16), this represents a significant source of RNA and NMPs. The reasons for our lack of success in isolation are not entirely clear. However, cells grown to the mid-log phase for IPTG induction and protein overexpression either may produce much less RNA than cells grown to the late log phase, as is typically done for RNA preps, or RNA in these preps may be degraded during protein isolation, yielding mononucleotides that are difficult to

recover. In either case, minor modifications of protein production protocols may facilitate recovery of NMPs.

### 5.5.6 CHEMICAL SHIFT OFFSETS ARE SMALL, BUT STILL MEASURABLE, WITHOUT A MEMBRANE ANCHOR

While we do not have a highly ordered system to demonstrate the full utility of the partially labeled systems we have produced, it is possible to see some of this utility in the effects of chemical shift anisotropy (CSA) offsets on even weakly ordered systems. The distribution of electrons in some molecular groups such as aromatic carbons gives rise to a large CSA which contributes significantly to chemical shift offsets. This CSA does not contribute to an isotropic spectrum, but it can be interpreted in solid-state or liquid crystalline NMR through the use of chemical shielding tensors. A comparison of experimental and calculated chemical shift offsets could, for example, be used to screen models with different orientations of GDP relative to a membrane system for consistency with data.

Chemical shift offsets were measured for the aromatic carbons with the best defined resonances seen in Figure 5.5. The C1' resonance of the ribose ring was used as a chemical shift reference; this site has the smallest CSA of the resonances detected (26-40 ppm (66,67)) as was assumed not to move between oriented and isotropic states. The differences between aligned and isotropic resonance positions are reported in Table 5.2 as observed CSA offsets. Errors are estimated to be approximately half the observed line width.

Chemical shift anisotropies for carbons in the rings of nucleotide bases are large (*i.e.* 108 ppm for C2 and 114 ppm for C8 of guanine) (67) with the most shielded

component ($\delta_{33}$) perpendicular to the base ring, for example. If the protein were to orient with the GDP ring plane preferentially perpendicular to the magnetic field, the C2 and C8 resonances would move downfield relative to resonances with lower chemical shift anisotropies such as C5 (66 ppm) and the ribose C1' carbon. This is roughly consistent with observed shifts, and the GDP (bound to ARF1) is depicted in this perpendicular orientation in Figure 5.10a, where the normal to the GDP ring plane is parallel to the magnetic field. This GDP orientation, however, differs from the orientation of GDP-ARF1 in the presence of diacyl $PIP_2$, as determined from singular value decomposition of equations relating $^{15}N$-$^{1}H$ RDCs measured in ARF1 to order tensor elements (Chapter 4) (Figure 5.10b). Some difference in observed and predicted orientation can be accounted for by the addition of $PIP_2$ which is known to propagate conformational differences to the nucleotide-binding region (Chapter 4). The GDP-ARF1 crystal structure (46) used to generate the models in Figure 5.10 does not take into account these conformational changes.

Table 5.2. $^{13}C$ Chemical shift offsets for GDP aromatic carbons.

| **Guanine carbon ($C_n$)** | **Observed Δδ Hz [a]** | **Calculated Δδ Hz [b]** |
|---|---|---|
| C2 | 39 | 48 |
| C8 | 15 | 47 |
| C5 | -60 | 42 |

[a] {(Aligned)$C_n$ – (isotropic)}$C_n$ – (C1' shift offset)
[b] With order parameters $10^{-3}$

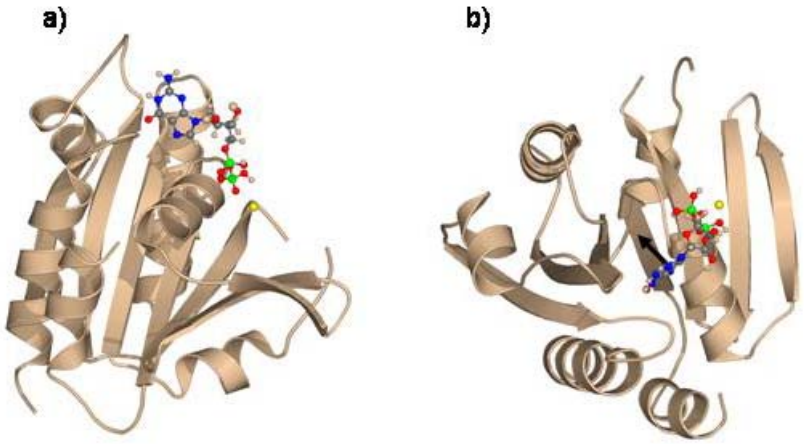


Figure 5.10 GDP-ARF1 crystal structure orientations used in data interpretation. a) The GDP ring plane was rotated perpendicular to the direction of the magnetic field $B_o$, and the normal to the plane is along $B_o$. b) The rotation was calculated from Euler angles previously determined in Chapter 4; the black arrow represents the normal to the GDP plane. The magnetic field direction comes out of the plane in both figures.

In anticipation of characterizing more strongly aligned molecules, a program was written in Maple (68) to calculate shift offsets using shift tensor principal values and orientations taken from those experimentally determined and calculated for nucleosides reported in the literature (66,67). In calculations performed here, GDP was positioned using the orientation previously deduced in Chapter 4. Details of the programs (Maple scripts) used for these calculations are included in Appendix C. There can be some error, of course, in accounting for the extrapolation of shift tensors derived from the model compound guanosine compared to guanosine diphosphate, and there are substantial errors in measurement compared to the experimentally observed shift offsets (Table 5.2). These differences may be attributed to small shifts due to the presence of $PIP_2$ or simply from error in measurement where signal-to-noise is low. In addition, the lack of an accurate chemical shift reference between isotropic and aligned data sets introduces some uncertainty to observed offsets. This case may be an application for the magic-angle

spinning/static approach (Chapter 3) to collecting shift offsets, particularly in a more strongly ordered case such as membrane-associated myrARF1. In Table 5.2, both experimentally measured and calculated offsets are small, given the weak ordering of ARF1; however, an increase in the level of ordering by a factor of ten is likely to increase shift offsets by a similar number, providing us with a new tool to assess GDP, and in turn ARF1 geometry at the membrane surface.

### 5.5.7 USE OF PARTIALLY LABELED NMPS IN STRUCTURAL NMR STUDIES

It is clear from spectra on ordered ARF1 (Figure 5.5) that partially labeled nucleotide samples can give useable spectra in complex biochemical systems. This opens opportunities for monitoring both co-factor and protein behavior in many systems. While shift offsets in our system, which is not strongly associated with the membrane-like bicelles of the alignment medium (ordering just a few parts in 10000), are small, offsets calculated with order parameters on the order of $10^{-3}$ give large enough shift offsets (a tenth of a ppm) to measure accurately and interpret quantitatively. The myristoylated form of GDP-bound ARF1, for example, would be expected to orient more strongly (perhaps $10^{-2}$) through myristoyl chain – $C_{12}E_5$ bilayer interactions and display much larger shift offsets. This would give a picture of membrane-protein interaction geometry through the nucleotide-cofactor reporter. We expect the partially labeled material and the approach to its production described here to be useful in such studies.

### 5.5.8 CONCLUSIONS

The $^{13}C$ isotopic labeling patterns of NMPs extracted from *E.coli* grown on a less commonly used mixture of C-1 and C-2 glucose have been presented here. By

comparing results to previously observed data on amino acids grown in similar media and relying on the well-known biochemistry of nucleotide biosynthesis, the labeling pattern has been rationalized. Despite a few notable absences (C4 and C3') and one more highly labeled site (C1'), most carbons are randomly labeled at a low level. With the low level of labeling, scalar couplings and additional splitting from long-range dipolar couplings are minimized, affording greater spectral quality than seen in fully labeled materials. This should allow high resolution measurement of structurally useful parameters such as chemical shift anisotropy offsets in weakly aligned liquid crystals. Application to studies of proteins with nucleotide cofactors, particularly in their membrane-associated states where direct observation of $^{13}C$ is preferred to observation of more strongly relaxing proton signals, should soon be possible.

REFERENCES


1. Clore, G.M. and Gronenborn, A.M. (1994) Multidimensional Heteronuclear Nuclear-Magnetic-Resonance of Proteins. *Nuclear Magnetic Resonance, Pt C*, Vol. 239, pp. 349-363.
2. Bax, A. (1994) Multidimensional Nuclear-Magnetic-Resonance Methods for Protein Studies. *Curr Opin Struct Biol*, **4,** 738-744.
3. Mollova, E.T. and Pardi, A. (2000) NMR solution structure determination of RNAs. *Curr Opin Struct Biol*, **10,** 298-302.
4. LeMaster, D.M. and Kushlan, D.M. (1996) Dynamical mapping of E-coli thioredoxin via C-13 NMR relaxation analysis. *J Am Chem Soc*, **118,** 9255-9264.
5. Lian, L.Y. and Middleton, D.A. (2001) Labelling approaches for protein structural studies by solution-state and solid-state NMR. *Prog Nucl Magn Reson Spectrosc*, **39,** 171-190.
6. Batey, R.T., Battiste, J.L. and Williamson, J.R. (1995) Preparation of isotopically enriched RNAs for heteronuclear NMR. *Nuclear Magnetic Resonance and Nucleic Acids*, Vol. 261, pp. 300-322.
7. Scott, L.G., Tolbert, T.J. and Williamson, J.R. (2000) Preparation of specifically H-2- and C-13-labeled ribonucleotides. *Rna-Ligand Interactions Pt A*, Vol. 317, pp. 18-38.
8. Wand, A.J., Bieber, R.J., Urbauer, J.L., McEvoy, R.P. and Gan, Z.H. (1995) Carbon Relaxation in Randomly Fractionally C-13-Enriched Proteins. *J Magn Reson Ser B*, **108,** 173-175.
9. Boisbouvier, J., Brutscher, B., Simorre, J.P. and Marion, D. (1999) C-13 spin relaxation measurements in RNA: Sensitivity and resolution improvement using spin-state selective correlation experiments. *J Biomol NMR*, **14,** 241-252.
10. Kojima, C., Ono, A., Kainosho, M. and James, T.L. (1998) DNA duplex dynamics: NMR relaxation studies of a decamer with uniformly C-13-labeled purine nucleotides. *J Magn Reson*, **135,** 310-333.
11. Gardner, K.H. and Kay, L.E. (1998) The use of H-2, C-13, N-15 multidimensional NMR to study the structure and dynamics of proteins. *Annu Rev Biophys Biomolec Struct*, **27,** 357-406.
12. Hong, M. (1999) Determination of multiple phi-torsion angles in proteins by selective and extensive C-13 labeling and two-dimensional solid-state NMR. *J Magn Reson*, **139,** 389-401.
13. Castellani, F., van Rossum, B., Diehl, A., Schubert, M., Rehbein, K. and Oschkinat, H. (2002) Structure of a protein determined by solid-state magic-angle-spinning NMR spectroscopy. *Nature*, **420,** 98-102.
14. Nikonowicz, E.P., Sirr, A., Legault, P., Jucker, F.M., Baer, L.M. and Pardi, A. (1992) Preparation of C-13 and N-15 Labeled Rnas for Heteronuclear Multidimensional Nmr-Studies. *Nucleic Acids Res*, **20,** 4507-4513.
15. Tolbert, T.J. and Williamson, J.R. (1997) Preparation of specifically deuterated and C-13-labeled RNA for NMR studies using enzymatic synthesis. *J Am Chem Soc*, **119,** 12100-12108.

16. Neidhardt, F.C. and Umbarger, H.E. (1996) Chemical Composition of Escherichia coli. In Neidhardt, F. C. (ed.), *Escherichia coli and Salmonella: Cellular and Molecular Biology*. 2nd Edition ed. ASM Press, Washington, DC, Vol. 1.
17. Zimmer, D.P. and Crothers, D.M. (1995) NMR of Enzymatically Synthesized Uniformly (Cn)-C-13-N-15-Labeled DNA Oligonucleotides. *Proc Natl Acad Sci U S A*, **92,** 3091-3095.
18. Smith, D.E., Su, J.Y. and Jucker, F.M. (1997) Efficient enzymatic synthesis of C-13,N-15-labeled DNA for NMR studies. *J Biomol NMR*, **10,** 245-253.
19. Sambrook, J., Fritsch, E.F. and Maniatis, T. (1989) *Molecular cloning : a laboratory manual*. 2nd ed. Cold Spring Harbor Laboratory, Cold Spring Harbor, N.Y.
20. Adams, M.W.W., Dailey, H.A., Delucas, L.J., Luo, M., Prestegard, J.H., Rose, J.P. and Wang, B.C. (2003) The Southeast Collaboratory for Structural Genomics: A high-throughput gene to structure factory. *Acc Chem Res*, **36,** 191-198.
21. Tian, F., Valafar, H. and Prestegard, J.H. (2001) A dipolar coupling based strategy for simultaneous assignment and structure determination of protein backbones. *J Am Chem Soc*, **123,** 11791-11796.
22. Hansen, M.R., Hanson, P. and Pardi, A. (2000) Filamentous bacteriophage for aligning RNA, DNA, and proteins for measurement of nuclear magnetic resonance dipolar coupling interactions. *Methods Enzymol*, **317,** 220-240.
23. Bax, A. (2003) Weak alignment offers new NMR opportunities to study protein structure and dynamics. *Protein Sci*, **12,** 1-16.
24. Prestegard, J.H. and Kishore, A.I. (2001) Partial alignment of biomolecules: an aid to NMR characterization. *Curr Opin Chem Biol*, **5,** 584-590.
25. Prestegard, J.H., Bougault, C.M. and Kishore, A.I. (2004) Residual dipolar couplings in structure determination of biomolecules. *Chem Rev*, **104,** 3519-3540.
26. Sanders, C.R. (1993) Solid-state 13C NMR of unlabeled phosphatidylcholine bilayers: spectral assignments and measurement of carbon-phosphorus dipolar couplings and 13C chemical shift anisotropies. *Biophys J*, **64,** 171-181.
27. Lipsitz, R.S. and Tjandra, N. (2001) Carbonyl CSA restraints from solution NMR for protein structure refinement. *J Am Chem Soc*, **123,** 11065-11066.
28. Lipsitz, R.S. and Tjandra, N. (2003) N-15 chemical shift anisotropy in protein structure refinement and comparison with NH residual dipolar couplings. *J Magn Reson*, **164,** 171-176.
29. Choy, W.Y., Tollinger, M., Mueller, G.A. and Kay, L.E. (2001) Direct structure refinement of high molecular weight proteins against residual dipolar couplings and carbonyl chemical shift changes upon alignment: an application to maltose binding protein. *J Biomol NMR*, **21,** 31-40.
30. Wu, Z.R., Tjandra, N. and Bax, A. (2001) P-31 chemical shift anisotropy as an aid in determining nucleic acid structure in liquid crystals. *J Am Chem Soc*, **123,** 3617-3618.
31. Boyd, J. and Redfield, C. (1999) Characterization of N-15 chemical shift anisotropy from orientation-dependent changes to N-15 chemical shifts in dilute bicelle solutions. *J Am Chem Soc*, **121,** 7441-7442.

32. Losonczi, J.A. and Prestegard, J.H. (1998) NMR characterization of the myristoylated, N-terminal fragment of ADP-Ribosylation factor 1 in a magnetically oriented membrane array. *Biochemistry*, **37,** 706-716.
33. Gu, Z.T.T. and Opella, S.J. (1999) Two- and three-dimensional H-1/C-13 PISEMA experiments and their application to backbone and side chain sites of amino acids and peptides. *J Magn Reson*, **140,** 340-346.
34. Valentine, K.G., Mesleh, M.F., Opella, S.J., Ikura, M. and Ames, J.B. (2003) Structure, topology, and dynamics of myristoylated recoverin bound to phospholipid bilayers. *Biochemistry*, **42,** 6333-6340.
35. Wang, J., Denny, J., Tian, C., Kim, S., Mo, Y., Kovacs, F., Song, Z., Nishimura, K., Gan, Z., Fu, R. *et al.* (2000) Imaging membrane protein helical wheels. *J Magn Reson*, **114,** 162-167.
36. Ippel, J.H., Wijmenga, S.S., deJong, R., Heus, H.A., Hilbers, C.W., deVroom, E., vanderMarel, G.A. and vanBoom, J.H. (1996) Heteronuclear scalar couplings in the bases and sugar rings of nucleic acids: Their determination and application in assignment and conformational analysis. *Magn Reson Chem*, **34,** S156-S176.
37. Nuoffer, C. and Balch, W.E. (1994) Gtpases - Multifunctional Molecular Switches Regulating Vesicular Traffic. *Annu Rev Biochem*, **63,** 949-990.
38. Takai, Y., Sasaki, T. and Matozaki, T. (2001) Small GTP-binding proteins. *Physiol Rev*, **81,** 153-208.
39. Shimizu, H., Donohue-Rolfe, A. and Homans, S.W. (1999) Derivation of the bound-state conformation of a ligand in a weakly aligned ligand-protein complex. *J Am Chem Soc*, **121,** 5815-5816.
40. Bolon, P.J., Al-Hashimi, H.M. and Prestegard, J.H. (1999) Residual dipolar coupling derived orientational constraints on geometry in a 53kDa protein-ligand complex. *J Mol Biol*, **293,** 107-115.
41. Al-Hashimi, H.M., Bolon, P.J. and Prestegard, J.H. (2000) Molecular symmetry as an aid to geometry determination in ligand protein complexes. *J Magn Reson*, **142,** 153-158.
42. Jain, N.U., Noble, S. and Prestegard, J.H. (2003) Structural characterization of a mannose-binding protein-trimannoside complex using residual dipolar couplings. *J Biomol NMR*, **328,** 451-462.
43. Umemoto, K., Leffler, H., Venot, A., Valafar, H. and Prestegard, J.H. (2003) Conformational differences in liganded and unliganded states of Galectin-3. *Biochemistry*, **42,** 3688-3695.
44. Case, D.A. (1998) The use of chemical shifts and their anisotropies in biomolecular structure determination. *Curr Opin Struct Biol*, **8,** 624-630.
45. Czerneky, J. (2001) An ab initio study of hydrogen bonding effects on the N-15 and H-1 chemical shielding tensors in the Watson-Crick base pairs. *J Phys Chem A*, **105,** 1357-1365.
46. Amor, J.C., Harrison, D.H., Kahn, R.A. and Ringe, D. (1994) Structure of the human ADP-ribosylation factor 1 complexed wtih GDP. *Nature*, **372,** 704-708.
47. Seidel, R.D., Amor, J.C., Kahn, R.A. and Prestegard, J.H. (2004) Conformational changes in human Arf1 on nucleotide exchange and deletion of membrane-binding elements. *J Biol Chem*, **279,** 48307-48318.

48. Kishore, A.I. and Prestegard, J.H. (2003) Molecular orientation and conformation of phosphatidylinositides in membrane mimetics using variable angle sample spinning (VASS) NMR. *Biophys J*, **85,** 3848-3857.
49. Freyssingeas, E., Nallet, F. and Roux, D. (1996) Measurement of the membrane flexibility in lamellar and "sponge" phases of the C12E5/hexanol/water system. *Langmuir*, **12,** 6028-6035.
50. Jonstromer, M. and Strey, R. (1992) Nonionic bilayers in dilute solutions: effect of additives. *J Phys Chem*, **96,** 5993-6000.
51. Ruckert, M. and Otting, G. (2000) Alignment of biological macromolecules in novel nonionic liquid crystalline media for NMR experiments. *J Am Chem Soc*, **122,** 7793-7797.
52. Maurer, T. and Kalbitzer, H.R. (1996) Indirect referencing of $^{31}$P and $^{19}$F NMR Spectra. *J Magn Res, Ser B*, **113,** 177-178.
53. Wishart, D.S., Bigam, C.G., Yao, J., Abildgaard, F., Dyson, H.J., Oldfield, E., Markley, J.L. and Sykes, B.D. (1995) H-1, C-13 and N-15 Chemical-Shift Referencing in Biomolecular Nmr. *J Biomol NMR*, **6,** 135-140.
54. Delaglio, F., Grzesiek, S., Vuister, G.W., Zhu, G., Pfeifer, J. and Bax, A. (1995) Nmrpipe - a Multidimensional Spectral Processing System Based on Unix Pipes. *J Biomol NMR*, **6,** 277-293.
55. Seidel, R.D., Amor, J.C., Kahn, R.A. and Prestegard, J.H. (2004) Structural perturbations in human ADP ribosylation factor-1 accompanying the binding of phosphatidylinositides. *Biochemistry*, **43,** 15393-15403.
56. Randazzo, P.A. (1997) Functional interaction of ADP-ribosylation factor 1 with phosphatidylinositol 4,5-bisphosphate. *J Biol Chem*, **272,** 7688-7692.
57. Terui, T., Kahn, R.A. and Randazzo, P.A. (1994) Effects of acid phospholipids on nucleotide exchange properties of ADP-Ribosylation Factor-1 - evidence for specific interaction with phosphatidylinositol 4,5-bisphosphate. *J Biol Chem*, **269,** 28130-28135.
58. Lundberg, P., Harmsen, E., Ho, C. and Vogel, H.J. (1990) Nuclear-Magnetic-Resonance Studies of Cellular-Metabolism. *Anal Biochem*, **191,** 193-222.
59. Rothman, D.L., Magnusson, I., Katz, L.D., Shulman, R.G. and Shulman, G.I. (1991) Quantitation of Hepatic Glycogenolysis and Gluconeogenesis in Fasting Humans with C-13 Nmr. *Science*, **254,** 573-576.
60. Szyperski, T. (1998) C-13-NMR, MS and metabolic flux balancing in biotechnology research. *Q Rev Biophys*, **31,** 41-106.
61. Voet, D. and Voet, J.G. (1995) *Biochemistry*. 2nd ed. John Wiley & Sons, Inc., New York.
62. Wood, T. (1985) *The Pentose Phosphate Pathway*. Academic Press, Inc., Orlando.
63. Magnusson, I., Chandramouli, V., Schumann, W.C., Kumaran, K., Wahren, J. and Landau, B.R. (1988) Pentose Pathway in Human-Liver. *Proc Natl Acad Sci USA*, **85,** 4682-4685.
64. Kunnecke, B. and Seelig, J. (1991) Glycogen-Metabolism as Detected by Invivo and Invitro C-13-Nmr Spectroscopy Using 1,2-C-2(13) Glucose as Substrate. *Biochim Biophys Acta*, **1095,** 103-113.

65. Castellani, F., van Rossum, B.J., Diehl, A., Rehbein, K. and Oschkinat, H. (2003) Determination of solid-state NMR structures of proteins by means of three-dimensional N-15-C-13-C-13 dipolar correlation spectroscopy and chemical shift analysis. *Biochemistry*, **42,** 11476-11483.
66. Bryce, D.L., Grishaev, A. and Bax, A. (2005) Measurement of ribose carbon chemical shift tensors for A-form RNA by liquid crystal NMR spectroscopy. *J Am Chem Soc*, **127,** 7387-7396.
67. Stueber, D. and Grant, D.M. (2002) C-13 and N-15 chemical shift tensors in adenosine, guanosine dihydrate, 2 '-deoxythymidine, and cytidine. *J Am Chem Soc*, **124,** 10539-10551.
68. (1999) Maple. 7.0 ed. Waterloo Maple Inc., Waterloo, Ontario.

# CHAPTER 6

# CONCLUDING REMARKS

## 6.1 NMR & MEMBRANE-ASSOCIATED SYSTEMS

The structural characterization of membrane proteins and membrane-associated proteins represents a major challenge in structural biology for both X-ray crystallography and NMR approaches. The techniques developed within this dissertation have provided a step toward making NMR more applicable to these systems. The techniques rely on biomolecules associating with, and orienting with respect to, elements of a liquid crystalline model membrane system. The NMR experiments rely on the measurement of anisotropic parameters such as chemical shift anisotropy offsets and residual dipolar couplings. I have introduced variable angle and magic angle spinning methods that should facilitate anisotropic data measurement, I have introduced some nucleotide co-factor labeling schemes that should improve resolution and sensitivity, and I have made preliminary application to an important biological system, ADP Ribosylation Factor 1. However, there are clearly improvements that can be made to the methods. The experiments have for the most part been based on simple experiments, many times with collection of only one-dimensional spectra. Expansion to additional dimensions is imperative for the techniques to be of greater utility. A number of multidimensional pulse sequences designed specifically for large proteins (1) may be applicable to membrane-associated systems. One likely aspect is a necessary shift away from the more commonly used INEPT-based experiments. The usual reason is the severe sensitivity loss during the fixed time (1/2J) delay for INEPT transfers; this loss increases as molecular weight increases. CRIPT (cross relaxation-induced polarization transfer) (2) and CRINEPT (cross relaxation-enhanced polarization transfer) (3) experiments offer alternatives that can be combined with higher resolution TROSY detection. In CRIPT,

magnetization transfer is accomplished through cross-correlation relaxation; the rates of this transfer increase with molecular weight and transfer times can be reduced well below those used in INEPT experiments. An added benefit is that the transfers are independent of the extent of total coupling (J+D) and hence will be applicable to membrane-associated proteins where the distributions of such couplings will be large. The myristoylated form of ARF1 (myrARF1) may be an interesting target for CRIPT as it is expected to associate strongly with membranes. In fact, ordering of non-myrARF1 in a concentrated model membrane (16% $C_{12}E_5$) was attempted with normal INEPT transfer HSQC experiments, but nearly all $^{15}N$-$^{1}H$ HSQC resonances were broadened beyond observation. The application of the VASS tool, combined with multidimensional experiments such as the CRIPT-TROSY and appropriate isotopic labeling schemes, may prove to be quite useful.

## 6.2 CHALLENGES TO THE STUDY OF MYRARF1

An ideal target for the methods developed here remains myrARF1. However, its production has presented significant biochemical challenges. First, *E.coli*, the expression host commonly used in the production of most proteins including ARF1, does not naturally contain the N-myristoyl transferase (NMT) required for myristoylation; plasmids carrying NMT have been included in expression protocols, but so far have produced only very low levels of myristoylation. Second, the efficient separation of myristoylated and non-myristoylated ARF1 has proven difficult. Efforts to increase the yield of myrARF1 are currently under development in our lab, but to date, only a 10% yield has resulted. Another potential target for NMR structural studies is GTP-bound-non-myrARF1. This is believed to interact more strongly with a membrane, but in

solution the protein has proven to be highly unstable. However, there is reason to believe that the stability of GTP-non-myrARF1 will improve in the presence of phospholipids (4), and perhaps in the presence of our lipid-bilayer like orientation medium.

## 6.3 PROSPECTS FOR OTHER MEMBRANE-ASSOCIATED MOLECULES

The experimental and computational methods developed here will provide tools not only to study myrARF1 on a membrane but may also be applied to a large number of proteins such other acyl-modified, membrane-associated proteins. In fact at least 100 different myristoylated proteins have been experimentally identified in eukaryotes, playing roles as diverse as cellular signaling, oncogenesis, and retrovirus infectivity (5). The number of predicted myristoylated proteins is even higher. Nearly 2000 proteins have been predicted to be myristoylated according to estimates from MYRbase, a program that uses an N-terminal glycine and a unique amino acid sequence as indicators to predict myristoylation (6). A number of these proteins are signal-dependent myristoyl switches that bind to a membrane in response to a signal, similar to the ARF1 mechanism, but much like ARF1, lack structural data.

Finally, the results described here for the headgroup geometry of phosphoinositides such as $PIP_2$ when membrane-bound provide the groundwork for future structural studies of protein-lipid interactions. Over 250 different domains that show homology to the pleckstrin domain (pleckstrin homology, or PH, domains) (7) bind specific phosphatidylinositol phosphates (8), and phosphoinositide geometry provided here should assist in generating more structural data on PH domains and other proteins that bind phosphoinositides. The future for structural information on these biologically intriguing systems is bright.

REFERENCES

1. Fernandez, C. and Wider, G. (2003) TROSY in NMR studies of the structure and function of large biological macromolecules. *Curr Opin Struct Biol*, **13,** 570-580.
2. Riek, R., Wider, G., Pervushin, K. and Wuthrich, K. (1999) Polarization transfer by cross-correlated relaxation in solution NMR with very large molecules. *Proc Natl Acad Sci U S A*, **96,** 4918-4923.
3. Riek, R., Fiaux, J., Bertelsen, E.B., Horwich, A.L. and Wuthrich, K. (2002) Solution NMR techniques for large molecular and supramolecular structures. *J Am Chem Soc*, **124,** 12144-12153.
4. Randazzo, P.A. (1997) Functional interaction of ADP-ribosylation factor 1 with phosphatidylinositol 4,5-bisphosphate. *J Biol Chem*, **272,** 7688-7692.
5. Boutin, J.A. (1997) Myristoylation. *Cell Signal*, **9,** 15-35.
6. Maurer-Stroh, S., Gouda, M., Novatchkova, M., Schleiffer, A., Schneider, G., Sirota, F.L., Wildpaner, M., Hayashi, N. and Eisenhaber, F. (2004) MYRbase: analysis of genome-wide glycine myristoylation enlarges the functional spectrum of eukaryotic myristoylated proteins. *Genome Biology*, **5**.
7. Lemmon, M.A. and Ferguson, K.M. (2000) Signal-dependent membrane targeting by pleckstrin homology (PH) domains. *Biochem J*, **350,** 1-18.
8. Hyvonen, M., Macias, M.J., Nilges, M., Oschkinat, H., Saraste, M. and Wilmanns, M. (1995) Structure of the Binding-Site for Inositol Phosphates in a Ph Domain. *EMBO J*, **14,** 4676-4685.

# APPENDIX A: ALIGNMENT MEDIA PROTOCOL

## A.1 COMMONLY USED MEDIA

Described herein are protocols to prepare two of the most commonly used alignment media, phospholipids bicelles and polyethylene glycol ether bilayers. Both bicelles and PEG* have no overall charge. Bicelles are zwitterionic molecules, and PEG is uncharged. These two media are the simplest to prepare, and starting materials are readily available from Avanti Polar Lipids (Birmingham, AL) for bicelles and from Sigma (St. Louis, MO) for PEG. One of the key differences between bicelle and PEG alignment mechanisms is that bicelles require elevated temperatures to align (28-40ºC, depending on concentration); whereas, PEG is usually aligned at room temperature.

## A.2 ALIGNMENT OF $D_2O$ ONLY

The majority of liquid crystal samples described in Tables 1 and 2 (Excel spreadsheet) were not prepared for proteins; therefore, information on optimum liquid crystal conditions for useful protein alignment is not readily available. However, it is generally agreed that a liquid crystal alignment giving 12-20 Hz $^2H$ quadrupolar splitting (of $D_2O$) yields N-H RDCs on the order of 6-15 Hz. It is important to keep in mind that the $^2H$ splitting is from $D_2O$ and not the macromolecule being aligned; therefore, the only way to know the presence and degree of alignment is by collecting and measuring RDCs for the molecule of interest.

*Note, we refer to the polyethylene glycol ether bilayer media as PEG, but this media is not the same as the high molecular weight polyethylene glycol, also known as PEG*x*, where *x* is the number of repeating ethylene units.

## A.3 BICELLE PROTOCOLS

The following bicelle protocols are intended for the preparation of stock solutions. Stock solutions not only save time in aligning future samples, but also ensure similar alignment conditions will apply. These high percentage lipid solutions (15-25% w/v) typically align at slightly lower temperatures (28-33ºC); whereas, the more dilute solutions (6-8% w/v) align at 35ºC. Phospholipid bicelles can be prepared from either ester-linked or ether-linked lipids. Slow hydrolysis of ester-linked bicelles has been observed even at neutral pH and -80ºC storage over time. Samples can last from a few days to several months. Improved bicelles can be prepared from ether-linked lipids.

In the following protocols, q stands for the ratio of long chain phospholipids to short chain. In phospholipid preparations of only DMPC, the extended bilayers that form are not magnetically aligned.

### A.3.1 DMPC/DHPC ESTER LINKAGE BICELLES:

q=3:1
25% w/v lipid
25 g/100mL solvent. To make 1mL bicelles, need 250mg lipid.

| | |
|---|---|
| DMPC = 687g/mol | DHPC =453.3g/mol |
| 3*687 = 2061 | 1*453.3=453.3 |

2062/453.3=4.55
4.55+1=5.55
0.25/5.55=0.0450721 mol fraction
0.045*4.55 = 205 mg DMPC
0.045*1 = 45 mg DHPC

Each lipid is mixed separately in 500µL buffer containing $D_2O$ by vortexing for 15 sec or until thoroughly mixed. DHPC* is a short-chain lipid and dissolves quickly. DMPC forms a white, chalky suspension. When both solutions are homogeneous, DHPC is added to DMPC and vortexed vigorously for 30 sec – 1 min. Small, white chunks may form. The mixture is rapidly frozen with liquid $N_2$ or a pre-prepared acetone/dry ice

mixture and thawed to RT. Upon thawing, the mixture is vortexed for 1-2 min. The mixture is then sonicated 30 min. This freeze-thaw-sonicate cycle is repeated at least 3 times until sample is clear at RT (no visible white chunks). If chunks remain, bicelles are stored at –80ºC for 1-2 hours, thawed, and vortexed. If chunks are still present, try to siphon only clear, dissolved materials for bicelle use.

*Note: DHPC is hygroscopic. Powder samples should be allowed to equilibrate to room temperature before weighing. Drying in the lyophilizer before use is recommended. Alternatively, DHPC can be stored in chloroform/methanol, pipetted when needed, and dried over $N_2$ and vacuum pump.

The following bicelle protocol is to prepare deuterated bicelles for solid-state NMR applications. Fully deuterated lipids are much more expensive than protonated ones, and care should be taken to avoid their accidental use.

### A.3.2 d-DMPC/d-DHPC ESTER BICELLES (FOR SOLIDS)

Deuterated to investigate biaxial condition and VASS
q=3:1
25% w/v lipid
25 g/100mL solvent. To make 1mL bicelles, need 250mg lipid.
DMPC d-54 (chain, not headgroup) = 732.37g/mol DHPC d-22 (chain, not HG) =497.82g/mol
3*732.37 = 2197.11 1*497.82=497.82
2197.11/497.82=4.4134627
4.41+1=5.41
0.25/5.41=0.0461811 mol fraction
0.046*4.41 = 204 mg DMPC
0.046*1 = 46 mg DHPC

The following bicelle protocol is to prepare bicelles from phospholipids with an ether linkage to the phosphate. Ether-linked phospholipids are only available from Avanti Polar Lipids (Birmingham, AL).

### A.3.3 DMPC/DHPC ETHER BICELLES (HYDROLYSIS RESISTANT):

q=3:1
15% w/v lipid
15 g/100mL solvent. To make 1mL bicelles, need 150 mg lipid.
DMPC = 649.97 g/mol DHPC = 425.54 g/mol
3*649.97 = 1949.91 1*425.54 = 425.54
1949.91/425.54 = 4.58
4.58+1 = 5.58
0.15/5.58 = 0.02687, mole fraction
0.02687*4.58 = 123 mg DMPC
0.02687*1 = 26.9 mg DHPC
15 g/100mL = 90 mg/ 600 μL Want to make only 600 μL of 15% bicelles
123*60% = 62.2 mg DMPC
26.8*60% = 12.7 mg DHPC
(*This protocol was used for a real sample at pH 5.0. Aligned from 25-30ºC, isotropic above and below this temperature range).*

## A.4 MONITORING ALIGNMENT IN THE MAGNETIC FIELD

Upon successful preparation of bicelles, a temperature-dependent phase change should be obvious, but alignment must be confirmed by NMR. Some amount of temperature variation may be required to induce alignment of bicelles, particularly after the macromolecule to be aligned has been added. The following instructions are specific to a Varian Inova spectrometer with older model pre-amplifiers. Both hardware and software need to be adjusted to observe $^{2}H$.

To check alignment in the magnet, the $^{2}H$ quadrupolar splitting should be observed. Aligned samples are difficult to shim due to their inherent inhomogeneity. Isotropic samples of exact or nearly exact volume should always be shimmed before attempting to shim aligned samples. Isotropic samples should be locked and shimmed on

the proton channel at 25c. After shimming, the lock power should be turned off and the spectrometer recabled for $^2H$ observe through the lock channel. In the software window, the transmitter nucleus (tn) should be set to $^2H$, with a power (tpwr) of 45 dB and a pulse width (pw) of 10 μs. The pw is actually much longer than this, (~200-300 μs), but calibrating an accurate 90º pulse width is not important for these experiments. A spectrum is collected and saved. Alignment is then induced by increasing the temperature to 35ºC, (settemp(35)). A quick way to check for alignment is to monitor the lock level after recabling from $^2H$ observe channel to the lock channel. When the sample is aligned, the lock level should decrease and may show increased periodicity. The presence of two $^2H$ frequencies now makes locking very difficult. Note, do not bother locking and shimming on the aligned sample unless you have a lot of time: $B_o$ inhomogeneity should not prevent you from seeing if your sample is aligned or not. However, collecting too few points in the FID will decrease resolution and skew results. The spectrum should be collected with the smallest spectral width and greatest number of points to digitally improve resolution with a minimum of resolution-enhancing functions.

To monitor the alignment your sample as temp increases (and a fun way to kill time), array the parameter number of transients (nt) 100 times with 1 scan each. You should see the phase transition in the $^2H$ quadrupolar splittings. To measure the splittings in Hz, display the x-axis in Hz (axis='h') and record.

To check the temperature range of alignment, set vttype=2 and array the temperature as you would array any other parameter. Also array the parameter pad to give the sample time to equilibrate btwn each temp. Set up the temp array and the pad

array separately. Then type array='(pad,temp)' and the two parameters will be arrayed simultaneously.

## A.5 PEG PROTOCOLS

In the following protocols, r stands for the molar ratio of $C_{12}E_5$ to hexanol. Chemicals are readily available from Sigma. PEG samples are stable over a wide pH (but not necessarily temperature) range. It is highly recommended to prepare a test PEG sample before adding in your macromolecule for alignment. Prepare a high percentage of PEG, check the alignment by $^2H$ splitting, dilute with buffer, and check the $^2H$ splitting again. If the $^2H$ splitting is between 10 and 15 Hz, it is probably OK to proceed to aligning the macromolecule. A word of caution, the $^2H$ splitting does not always behave linearly with buffer vs. protein or carbohydrate. In other words, what worked for buffer may not work exactly the same with your precious sample. Table 1 contains data on the >150 $C_{12}E_5$ PEG samples I have prepared for myself and my colleagues.

### A.5.1 $C_{12}E_5$

(pentaethylene glycol monododecyl ether), Ruckert and Otting, JACS 122:7793 (2000).
4.25% w/w (includes mass of solvent, lipid, NOT hexanol)
r = 0.87
25 μL $C_{12}E_5$
9 μL hexanol
50 μL $D_2O$
550 μL buffer

Mix in this order: lipid, water/$D_2O$, vortex very well. Add hexanol in 3 or 4 μL increments, vortexing well after each addition. Solution goes from clear to milky, turbid. Then to translucent and viscous w/ lots of bubbles (upon vortexing). This phase aligns in the magnet but it may be biphasic and heterogeneous. Continue adding in 4 μL aliquots. If the solution becomes cloudy or milky again and very fluid, you have gone past the nematic phase. It is usually easier to prepare a new sample.

It is not advised to deviate from the typical concentrations of PEG prepared in Table 1. The phase diagram of $C_{12}E_5$ has a very narrow region of the nematic phase of the liquid crystal. Concentrations of PEG, hexanol, and water have been highly optimized in these experiments. If you choose to prepare PEG samples at concentrations higher than those given in Table 1, you may have to use more hexanol. You will then have to experimentally determine the correct ratio of $C_{12}E_5$:hexanol.

PEG liquid crystals can also be prepared from $C_8E_5$ (also available from Sigma). Table 2 contains data on the 32 $C_8E_5$ samples I prepared or helped others prepare.

A.5.2 $C_8E_5$

**(**Pentaethylene glycol octylether)
4.83% w/w (includes mass of solvent, lipid, NOT octanol)
r = molar ratio $C_8E_5$:octanol, r = 1.35
$C_8E_5$ more soluble in water than $C_{12}E_5$.
*e.g.* 5% $C_8E_5$ w/ r=0.84 aligns at 25c to 24-26Hz $^2$H quad splitting
51 μL $C_8E_5$
16 μL octanol
100 μL $D_2O$ (or if $D_2O$ already in buffer ignore this step and add 100 μL to buffer amount)
825 μL buffer
This sample gives a $^2$H splitting of 32 Hz.

# APPENDIX B: MAPLE CSA CALCULATION SCRIPTS

The following scripts were written to calculate chemical shift offsets of a particular molecular system, PI(4)P or PI(4,5)$P_2$ (phosphatidylinositol phosphates) and GDP bound to ARF1. These scripts are NOT generally applicable, meaning these scripts have been written specifically for their intended molecules, but the principles they demonstrate are. These scripts explain how to:

1) read in the coordinates of a pdb file
2) rotate those coordinates into a desired frame
3) rotate a select group of those coordinates (headgroup) 360 degrees about a particular torsion angle
4) save each of those new sets of coordinates
5) rotate a select group of coordinates 360 about another torsion angle.
6) calculate anisotropic contributions to the chemical shift.
7) plots the results of the calculation in a 3D point plot.

Comments specific to Maple programming are explained in the file **csacalc_comment.mws**. Step 6 is better demonstrated in csacalc_comment.mws and is also well-commented. This script illustrates how to define vectors and matrices and use these to calculate chemical shifts. The plotting section is not commented. An RMSD between calculated and observed chemical shift differences is also in this program but is not commented.

In the second script, **13CCSAcalc_GDP_arbframe**, the chemical shift offset of GDP given a unique molecular geometry is calculated.

```
> #Calculating diester CSA.
> #Chemical shift tensor from model diester, anhydrous powder DPPC,
  Herzfeld et al, Biochemistry 17:271(1978).
> restart: #clears the memory
  with(LinearAlgebra); #library containing definitions for calculations
  cstensor:=<34|-134|98>; #chemical shielding tensor of phosphodiester in its principal
  axis frame
  csdiest:=Matrix(1..3,1..3,cstensor,shape=diagonal); #make cstensor a
  diagonal matrix
> diest_iso:=(sum('cstensor[i]','i'=1..3))/3; #calculate the isotropic
  chemical shift of phosphodiester

> for i to 3 do
  cstensor[i]:=cstensor[i]-diest_iso
  end do; #subtract the isotropic chem. shift from the anisotropic component
  csdiest2:=Matrix(1..3,1..3,cstensor,shape=diagonal); #make a new
  matrix from above elements
```

[*Add*, *Adjoint*, *BackwardSubstitute*, *BandMatrix*, *Basis*, *BezoutMatrix*, *BidiagonalForm*, *BilinearForm*, *CharacteristicMatrix*, *CharacteristicPolynomial*, *Column*, *ColumnDimension*, *ColumnOperation*, *ColumnSpace*, *CompanionMatrix*, *ConditionNumber*, *ConstantMatrix*, *ConstantVector*, *CreatePermutation*, *CrossProduct*, *DeleteColumn*, *DeleteRow*, *Determinant*, *DiagonalMatrix*, *Dimension*, *Dimensions*, *DotProduct*, *Eigenvalues*, *Eigenvectors*, *Equal*, *ForwardSubstitute*, *FrobeniusForm*, *GaussianElimination*, *GenerateEquations*, *GenerateMatrix*, *GetResultDataType*, *GetResultShape*, *GivensRotationMatrix*, *GramSchmidt*, *HankelMatrix*, *HermiteForm*, *HermitianTranspose*, *HessenbergForm*, *HilbertMatrix*, *HouseholderMatrix*, *IdentityMatrix*, *IntersectionBasis*, *IsDefinite*, *IsOrthogonal*, *IsSimilar*, *IsUnitary*, *JordanBlockMatrix*, *JordanForm*, *LA_Main*, *LUDecomposition*, *LeastSquares*, *LinearSolve*, *Map*, *Map2*, *MatrixAdd*, *MatrixInverse*, *MatrixMatrixMultiply*, *MatrixNorm*, *MatrixScalarMultiply*, *MatrixVectorMultiply*, *MinimalPolynomial*, *Minor*, *Multiply*, *NoUserValue*, *Norm*, *Normalize*, *NullSpace*, *OuterProductMatrix*, *Permanent*, *Pivot*, *QRDecomposition*, *RandomMatrix*, *RandomVector*, *Rank*, *ReducedRowEchelonForm*, *Row*, *RowDimension*, *RowOperation*, *RowSpace*, *ScalarMatrix*, *ScalarMultiply*, *ScalarVector*, *SchurForm*, *SingularValues*, *SmithForm*, *SubMatrix*, *SubVector*, *SumBasis*, *SylvesterMatrix*, *ToeplitzMatrix*, *Trace*, *Transpose*, *TridiagonalForm*, *UnitVector*, *VandermondeMatrix*, *VectorAdd*, *VectorAngle*, *VectorMatrixMultiply*, *VectorNorm*, *VectorScalarMultiply*, *ZeroMatrix*, *ZeroVector*, *Zip*]

$$cstensor := [34, -134, 98]$$

$$csdiest := \begin{bmatrix} 34 & 0 & 0 \\ 0 & -134 & 0 \\ 0 & 0 & 98 \end{bmatrix}$$

$$diest\_iso := \frac{-2}{3}$$

$$cstensor_1 := \frac{104}{3}$$

$$cstensor_2 := \frac{-400}{3}$$

$$cstensor_3 := \frac{296}{3}$$

$$csdiest2 := \begin{bmatrix} \frac{104}{3} & 0 & 0 \\ 0 & \frac{-400}{3} & 0 \\ 0 & 0 & \frac{296}{3} \end{bmatrix}$$

```
> sigma:=<2|-51|48>;
```
# Define phosphomonoester chemical shielding tensor in the principal axis frame. (from serine monophosphate, Kohler & Klein, 1977)

$$\sigma := [2, -51, 48]$$

```
> sig1:=Matrix(1..3,1..3,sigma,shape=diagonal);
```
# make this vector a diagonal matrix

```
sigma_iso:=(sum('sigma[i]','i'=1..3))/3;
```
#calculate the isotropic chemical shift

$$sig1 := \begin{bmatrix} 2 & 0 & 0 \\ 0 & -51 & 0 \\ 0 & 0 & 48 \end{bmatrix}$$

$$sigma\_iso := \frac{-1}{3}$$

```
> for i to 3 do
sigma[i]:=sigma[i]-sigma_iso
end do;
```
#subtract the isotropic chem. shift. from the anisotropic components

```
sig1:=Matrix(1..3,1..3,sigma,shape=diagonal);
```
#redefine the phosphomonoester matrix in terms of above

$$\sigma_1 := \frac{7}{3}$$

$$\sigma_2 := \frac{-152}{3}$$

$$\sigma_3 := \frac{145}{3}$$

$$sig1 := \begin{bmatrix} \frac{7}{3} & 0 & 0 \\ 0 & \frac{-152}{3} & 0 \\ 0 & 0 & \frac{145}{3} \end{bmatrix}$$

```
> sig4:=<4.7381|4.7381|-9.4762>;
```
#defines monoester 4 as sigma perp, perp, parallel, calculated elsewhere

```
sig4:=Matrix(1..3,1..3,sig4,shape=diagonal);
```
#make above vector a diagonalized matrix

```
sig5:=<4.5531|4.5531|-9.1062>;
```
#defines monoester 5 as sigma perp, perp, parallel, calculated elsewhere

```
sig5:=Matrix(1..3,1..3,sig5,shape=diagonal);
```
#make above vector a diagonalized matrix

$$sig4 := [4.7381, 4.7381, -9.4762]$$

$$sig4 := \begin{bmatrix} 4.7381 & 0 & 0 \\ 0 & 4.7381 & 0 \\ 0 & 0 & -9.4762 \end{bmatrix}$$

$$sig5 := [4.5531, 4.5531, -9.1062]$$

$$sig5 := \begin{bmatrix} 4.5531 & 0 & 0 \\ 0 & 4.5531 & 0 \\ 0 & 0 & -9.1062 \end{bmatrix}$$

```
> #Define phosphodiester coords from pdb in PO frame.
> with(linalg);
```
#this library allows you to open up text files

```
N:=readdata("p2145bi1010",float,3);
```
#read in 3 columns of this coordinate file, a text file "p2145bi1010" with no extension name

```
with(LinearAlgebra);
```
#need this library to define rows and columns

```
N:=convert(N,Matrix);
```
#convert these coordinates into a Matrix

```
C34:=Transpose(Row(N,24));
```
#Define the atomic coordinates for C34, the origin of the bilayer normal vector

```
C32:=Transpose(Row(N,21));
```
#Define the atomic coordinates for C32, the end of the bilayer normal vector

```
binorm:=Normalize((C34-C32),Euclidean);
```
#Define the bilayer normal vector and normalize to length 1.

```
with(linalg):
```
#need this library to read text files

```
printlevel:=2:
```
#print the output of each line, level 2 b/c two for loops

```
for i from 10 to 10 by 10 do
for j from 10 to 10 by 10 do
M[i,j]:=readdata(cat("p2145bi",(i,j)),float,3):
```
#read in all the data files one by one

```
with(LinearAlgebra):
```
#need this library to operate on Matrices

```
M[i,j]:=convert(M[i,j],Matrix):
```
#convert each set of coordinates into a Matrix

```
P[i,j]:=Transpose(Row(M[i,j],65)):
```
#Define the atomic coordinates for P, the diester phosphorus atom

```
O1[i,j]:=Transpose(Row(M[i,j],68)):
```
#Define the atomic coordinates for O12, the diester oxygen connecting P to the headgroup

```
O2[i,j]:=Transpose(Row(M[i,j],4)):
```
#Define the atomic coordinates for O11, the diester oxygen connecting P to the diacylglycerol moiety

```
O3[i,j]:=Transpose(Row(M[i,j],66)):
```
#Define the atomic coordinates for O13, the unesterified diester oxygen, in front of the plane

```
O4[i,j]:=Transpose(Row(M[i,j],67)):
```
#Define the atomic coordinates for O14, the other unesterified diester oxygen, behind the plane

```
PO1[i,j]:=Normalize((P[i,j]-O1[i,j]),Euclidean):
```
#Define bond vectors

```
PO2[i,j]:=Normalize((P[i,j]-O2[i,j]),Euclidean):
PO3[i,j]:=Normalize((P[i,j]-O3[i,j]),Euclidean):
PO4[i,j]:=Normalize((P[i,j]-O4[i,j]),Euclidean):
zP[i,j]:=Normalize(CrossProduct(PO4[i,j],PO3[i,j]),Euclidean):
```
#Define the z-axis within the molecular frame

```
xP[i,j]:=Normalize((PO4[i,j]+PO3[i,j]),Euclidean):
```
#Define the x-axis within the molecule frame

```
yP[i,j]:=CrossProduct(zP[i,j],xP[i,j]):
```
#Define the y-axis within the molecular frame

```
mf2crys[i,j]:=Transpose(<<xP[i,j]>|<yP[i,j]>|<zP[i,j]>>):
```
#"shorthand" notation: direction cosines that define the transformation from the principal axis frame to the molecular frame

```
csad[i,j]:=-0.5*(Transpose(binorm).Transpose(mf2crys[i,j]).csdiest
2.mf2crys[i,j].binorm):
```
#calculating the chemical shift offset: -0.5 * B(-1).MF(-1).A.MF.B. Starting from the PAF, rotate into MF, project onto z-axis, or bilayer normal for observation, scale by -0.5 b/c of liquid crystal order parameter - bilayer normal is perpendicular to magnetic field.

```
> P[i,j]:=Transpose(Row(M[i,j],97)):
```
# Define the atomic coordinates for P, the monoester phosphorus atom

```
O1[i,j]:=Transpose(Row(M[i,j],83)):
```
# Define the atomic coordinates for O1, the monoester oxygen connecting P to the proton

```
O2[i,j]:=Transpose(Row(M[i,j],75)):
```
#Define the atomic coordinates for O2, the monoester oxygen connect P to the headgroup

```
O3[i,j]:=Transpose(Row(M[i,j],80)):
```
#Define the atomic coordinates for O3, the out-of-plane (front) monoester oxygen

```
> O4[i,j]:=Transpose(Row(M[i,j],84)):
```
#Define the atomic coordinates for O4, the out-of-plane (back) monoester oxygen

```
PO1[i,j]:=Normalize((P[i,j]-O1[i,j]),Euclidean):
```
#Define bond vectors

```
PO2[i,j]:=Normalize((P[i,j]-O2[i,j]),Euclidean):
PO3[i,j]:=Normalize((P[i,j]-O3[i,j]),Euclidean):
```

```
  PO4[i,j]:=Normalize((P[i,j]-O4[i,j]),Euclidean):
  zP[i,j]:=Normalize((O2[i,j]-P[i,j]),Euclidean): #Define the z-axis as the
  axis of rotation of the phosphomonoester to mimic rapid axially symmetric motion
  xP[i,j]:=Normalize((CrossProduct(zP[i,j],PO3[i,j])),Euclidean):
  #Define the x-axis perpendicular
  yP[i,j]:=CrossProduct(zP[i,j],xP[i,j]):
  mf2crys[i,j]:=Transpose(<<xP[i,j]>|<yP[i,j]>|<zP[i,j]>>):
  csam4[i,j]:=-0.5*(Transpose(binorm).Transpose(mf2crys[i,j]).sig4.m
  f2crys[i,j].binorm):
> P[i,j]:=Transpose(Row(M[i,j],98)):
  O1[i,j]:=Transpose(Row(M[i,j],82)):
  O2[i,j]:=Transpose(Row(M[i,j],78)):
  O3[i,j]:=Transpose(Row(M[i,j],81)):
  O4[i,j]:=Transpose(Row(M[i,j],76)):
  PO1[i,j]:=Normalize((P[i,j]-O1[i,j]),Euclidean):
  PO2[i,j]:=Normalize((P[i,j]-O2[i,j]),Euclidean):
  PO3[i,j]:=Normalize((P[i,j]-O3[i,j]),Euclidean):
  PO4[i,j]:=Normalize((P[i,j]-O4[i,j]),Euclidean):
  zP[i,j]:=Normalize((O2[i,j]-P[i,j]),Euclidean):
  xP[i,j]:=Normalize((CrossProduct(zP[i,j],PO3[i,j])),Euclidean):
  yP[i,j]:=CrossProduct(zP[i,j],xP[i,j]):
  mf2crys[i,j]:=Transpose(<<xP[i,j]>|<yP[i,j]>|<zP[i,j]>>):
  csam5[i,j]:=-0.5*(Transpose(binorm).Transpose(mf2crys[i,j]).sig5.m
  f2crys[i,j].binorm): #calculate the chem shift offset for monoester 5
  expm4:=6.76:
  expdi:=28.94:
  expm5:=5.25:
  jhp4[i,j]:=(expdi/csad[i,j])*csam4[i,j]:
  jhper4[i,j]:=jhp4[i,j]-expm4:
  jhper42[i,j]:=(jhper4[i,j])^2:
  jhp5[i,j]:=(expdi/csad[i,j])*csam5[i,j]:
  jhper5[i,j]:=jhp5[i,j]-expm5:
  jhper52[i,j]:=(jhper5[i,j])^2:
  jhptoter[i,j]:=sqrt((jhper42[i,j]+jhper52[i,j])/2):
  end do;
  end do;
>
>
Warning, the previous binding of the name GramSchmidt has been removed and it now
has an assigned value

Warning, the protected names norm and trace have been redefined and unprotected

[BlockDiagonal, GramSchmidt, JordanBlock, LUdecomp, QRdecomp, Wronskian, addcol,
```

*addrow*, *adj*, *adjoint*, *angle*, *augment*, *backsub*, *band*, *basis*, *bezout*, *blockmatrix*, *charmat*, *charpoly*, *cholesky*, *col*, *coldim*, *colspace*, *colspan*, *companion*, *concat*, *cond*, *copyinto*, *crossprod*, *curl*, *definite*, *delcols*, *delrows*, *det*, *diag*, *diverge*, *dotprod*, *eigenvals*, *eigenvalues*, *eigenvectors*, *eigenvects*, *entermatrix*, *equal*, *exponential*, *extend*, *ffgausselim*, *fibonacci*, *forwardsub*, *frobenius*, *gausselim*, *gaussjord*, *geneqns*, *genmatrix*, *grad*, *hadamard*, *hermite*, *hessian*, *hilbert*, *htranspose*, *ihermite*, *indexfunc*, *innerprod*, *intbasis*, *inverse*, *ismith*, *issimilar*, *iszero*, *jacobian*, *jordan*, *kernel*, *laplacian*, *leastsqrs*, *linsolve*, *matadd*, *matrix*, *minor*, *minpoly*, *mulcol*, *mulrow*, *multiply*, *norm*, *normalize*, *nullspace*, *orthog*, *permanent*, *pivot*, *potential*, *randmatrix*, *randvector*, *rank*, *ratform*, *row*, *rowdim*, *rowspace*, *rowspan*, *rref*, *scalarmul*, *singularvals*, *smith*, *stackmatrix*, *submatrix*, *subvector*, *sumbasis*, *swapcol*, *swaprow*, *sylvester*, *toeplitz*, *trace*, *transpose*, *vandermonde*, *vecpotent*, *vectdim*, *vector*, *wronskian* ]

$N$ := [ [ -0.663938824, 7.733385941, -1.091402807 ],
[ -0.8451888219, 8.111729053, 0.2460073508 ], [ -0.8598516, 7.027573057, 1.256899422 ],
[ -1.768571321, 6.755722582, -1.470719832 ], [ -2.102034104, 6.398286029, 11.42566536 ],
[ 0.1944106637, 7.844289406, 12.46614585 ], [ -0.0805195760, 7.843921047, 9.874638141 ],
[ 0.4444427179, 10.17001436, 0.247053887 ], [ 0.3735775782, 8.893665342, 0.6945729573 ],
[ 1.759325871, 10.78972153, 0.8070613217 ], [ -0.2320002892, 10.84356750, -0.3609633936 ],
[ 1.636164521, 11.33378426, 2.039154267 ], [ 1.348204193, 10.69375250, 3.301122251 ],
[ 1.636621906, 11.42038135, 4.656004804 ], [ 1.276353799, 10.80109150, 5.839249486 ],
[ 1.682925189, 11.51893327, 7.089592590 ], [ 1.311501780, 10.98591782, 8.333913356 ],
[ 1.797734786, 11.53521018, 9.634556797 ], [ -1.008717129, 6.921112301, 3.600143788 ],
[ -1.099361429, 7.696943164, 2.462570896 ], [ -1.226349327, 7.591885451, 4.914794162 ],
[ -1.242023019, 5.775471620, 3.523712161 ], [ -1.226349326, 6.703118814, 6.206016400 ],
[ -1.226349326, 7.591885452, 7.437401744 ], [ -1.194177885, 6.718933100, 8.654462626 ],
[ -1.094054165, 7.448200051, 9.929951148 ], [ -1.074556999, 6.745111188, 11.30335382 ],
[ -0.8419683514, 7.502108559, 12.48322818 ], [ -1.039125848, 6.688413083, 13.71105292 ],
[ -0.311460926, 5.877710200, 13.73895620 ], [ 0.3084141348, 7.257317852, -1.209020387 ],
[ -1.809889553, 8.618649988, 0.2188473592 ], [ 0.0995900601, 6.509292589, 1.283508793 ],
[ 2.089915614, 11.56911477, 0.1184964367 ], [ 0.8449745483, 12.07596823, 1.928481881 ],
[ 1.924449474, 9.767261218, 3.313822203 ], [ 1.115535361, 12.37751212, 4.624900086 ],
[ 1.735533410, 9.813562300, 5.851983927 ], [ 1.261870594, 12.51975580, 7.034164230 ],
[ 1.617366772, 9.940241204, 8.315446759 ], [ 1.446741913, 12.56813653, 9.676937945 ],
[ 0.0737495757, 6.827748015, 3.627031442 ], [ -2.195266306, 8.092906793, 4.868002105 ],
[ -0.3355011523, 6.072371746, 6.213204199 ], [ -2.124746672, 8.204518244, 7.447415192 ],
[ -0.3340910379, 6.054028179, 8.574100536 ], [ -1.943629043, 8.130871968, 9.953816923 ],
[ -0.296808812, 5.981909950, 11.25681744 ], [ -1.528802059, 8.345310919, 12.50270207 ],

[-2.040284411, 6.258066338, 13.71777691], [-0.7056327877, 8.612475075, -1.733896318],
[-1.605044288, 6.262559556, 1.044806981], [2.476782049, 9.975630115, 0.895224856],
[2.690061267, 11.54815863, 2.215844055], [0.2619956046, 10.62139395, 3.290966092],
[2.724089758, 11.46146226, 4.703712583], [0.1898164316, 10.78053793, 5.845890233],
[2.772406223, 11.44000257, 7.091331267], [0.2524506726, 11.24694808, 8.369225631],
[2.867290699, 11.33185466, 9.573085881], [-0.3629820601, 8.245256906, 5.033742509],
[-2.117412700, 6.074857552, 6.214952391], [-0.3541901388, 8.248896594, 7.422714560],
[-2.143038081, 6.187341480, 8.677629124], [-1.810671942, 6.191608546, -2.859185492],
[-1.835665910, 7.287338761, -3.719057341], [-0.8185162012, 5.026506900, -3.084587670],
[-3.180147157, 5.464305366, -2.955043326], [-4.663115924, 4.735454219, -4.678974199],
[-2.791255169, 3.261165347, -3.860928579], [-4.437339798, 2.337225014, -5.477960321],
[-4.913549004, 3.745448709, -5.803482698], [-3.227930676, 4.691859470, -4.158234532],
[-2.968276875, 2.332690619, -5.058332435], [-4.628793115, 1.518416345, -6.627509361],
[-1.548763293, 0.6015650256, -7.006399779], [-5.566403185, 4.429971683, -3.615671070],
[-2.552616657, 1.028328206, -4.655552993], [-6.323227052, 3.690661748, -6.058622247],
[-7.104364962, 0.8842617018, -6.496158933], [-0.5069810681, -0.4533260526, -4.961833419],
[-2.699780492, -1.331800505, -5.755939413], [-5.535063426, -0.500839331, -7.922721173],
[-5.269071745, -0.5943989579, -5.397855034], [-1.405798584, 3.268941579, -3.498549521],
[-2.328043288, 2.717201491, -5.885755751], [-3.353522788, 2.860639905, -2.985392459],
[-4.409157965, 4.100231861, -6.734308458], [-4.936585152, 5.752882300, -5.039856011],
[-6.393372683, -0.3871106764, -8.294114512], [-5.038120566, 1.962118419, -4.613361276],
[-3.472119582, -1.158490708, -5.256121400], [-2.536292749, 5.107610204, -4.929030425],
[-1.133042737, 2.373871539, -3.385935711], [-5.544584330, 5.155946872, -3.018697902],
[-6.748566561, 4.068990704, -5.306789485], [-5.634928433, 0.2781497822, -6.538427512],
[-1.856874128, 0.0164725601, -5.688867797]]

```
Warning, the assigned name GramSchmidt now has a global binding
```

[*Add*, *Adjoint*, *BackwardSubstitute*, *BandMatrix*, *Basis*, *BezoutMatrix*, *BidiagonalForm*, *BilinearForm*, *CharacteristicMatrix*, *CharacteristicPolynomial*, *Column*, *ColumnDimension*, *ColumnOperation*, *ColumnSpace*, *CompanionMatrix*, *ConditionNumber*, *ConstantMatrix*, *ConstantVector*, *CreatePermutation*, *CrossProduct*, *DeleteColumn*, *DeleteRow*, *Determinant*, *DiagonalMatrix*, *Dimension*, *Dimensions*, *DotProduct*, *Eigenvalues*, *Eigenvectors*, *Equal*, *ForwardSubstitute*, *FrobeniusForm*, *GaussianElimination*, *GenerateEquations*, *GenerateMatrix*, *GetResultDataType*, *GetResultShape*, *GivensRotationMatrix*, *GramSchmidt*, *HankelMatrix*, *HermiteForm*, *HermitianTranspose*, *HessenbergForm*, *HilbertMatrix*, *HouseholderMatrix*, *IdentityMatrix*, *IntersectionBasis*, *IsDefinite*, *IsOrthogonal*, *IsSimilar*, *IsUnitary*, *JordanBlockMatrix*, *JordanForm*, *LA_Main*, *LUDecomposition*, *LeastSquares*, *LinearSolve*, *Map*,

*Map2*, *MatrixAdd*, *MatrixInverse*, *MatrixMatrixMultiply*, *MatrixNorm*, *MatrixScalarMultiply*, *MatrixVectorMultiply*, *MinimalPolynomial*, *Minor*, *Multiply*, *NoUserValue*, *Norm*, *Normalize*, *NullSpace*, *OuterProductMatrix*, *Permanent*, *Pivot*, *QRDecomposition*, *RandomMatrix*, *RandomVector*, *Rank*, *ReducedRowEchelonForm*, *Row*, *RowDimension*, *RowOperation*, *RowSpace*, *ScalarMatrix*, *ScalarMultiply*, *ScalarVector*, *SchurForm*, *SingularValues*, *SmithForm*, *SubMatrix*, *SubVector*, *SumBasis*, *SylvesterMatrix*, *ToeplitzMatrix*, *Trace*, *Transpose*, *TridiagonalForm*, *UnitVector*, *VandermondeMatrix*, *VectorAdd*, *VectorAngle*, *VectorMatrixMultiply*, *VectorNorm*, *VectorScalarMultiply*, *ZeroMatrix*, *ZeroVector*, *Zip* ]

$$N := \begin{bmatrix} 98 \text{ x } 3 \text{ Matrix} \\ \text{Data Type: anything} \\ \text{Storage: rectangular} \\ \text{Order: Fortran\_order} \end{bmatrix}$$

$$C34 := \begin{bmatrix} -1.226349326 \\ 7.591885452 \\ 7.437401744 \end{bmatrix}$$

$$C32 := \begin{bmatrix} -1.226349327 \\ 7.591885451 \\ 4.914794162 \end{bmatrix}$$

$$binorm := \begin{bmatrix} 0.396415237099541076\ 10^{-9} \\ 0.396415237099541076\ 10^{-9} \\ 0.99999999998725896 \end{bmatrix}$$

```
Warning, the previous binding of the name GramSchmidt has been removed and it now
has an assigned value
```

$M_{10,\,10} :=$ [ [ -0.663938824, 7.733385941, -1.091402807 ],
[ -0.8451888219, 8.111729053, 0.2460073508 ], [ -0.8598516, 7.027573057, 1.256899422 ],
[ -1.768571321, 6.755722582, -1.470719832 ], [ -2.102034104, 6.398286029, 11.42566536 ],
[ 0.1944106637, 7.844289406, 12.46614585 ], [ -0.0805195760, 7.843921047, 9.874638141 ],
[ 0.4444427179, 10.17001436, 0.247053887 ], [ 0.3735775782, 8.893665342, 0.6945729573 ],
[ 1.759325871, 10.78972153, 0.8070613217 ], [ -0.2320002892, 10.84356750, -0.3609633936 ],
[ 1.636164521, 11.33378426, 2.039154267 ], [ 1.348204193, 10.69375250, 3.301122251 ],
[ 1.636621906, 11.42038135, 4.656004804 ], [ 1.276353799, 10.80109150, 5.839249486 ],
[ 1.682925189, 11.51893327, 7.089592590 ], [ 1.311501780, 10.98591782, 8.333913356 ],
[ 1.797734786, 11.53521018, 9.634556797 ], [ -1.008717129, 6.921112301, 3.600143788 ],
[ -1.099361429, 7.696943164, 2.462570896 ], [ -1.226349327, 7.591885451, 4.914794162 ],
[ -1.242023019, 5.775471620, 3.523712161 ], [ -1.226349326, 6.703118814, 6.206016400 ],
[ -1.226349326, 7.591885452, 7.437401744 ], [ -1.194177885, 6.718933100, 8.654462626 ],
[ -1.094054165, 7.448200051, 9.929951148 ], [ -1.074556999, 6.745111188, 11.30335382 ],
[ -0.8419683514, 7.502108559, 12.48322818 ], [ -1.039125848, 6.688413083, 13.71105292 ],

```
    [-0.311460926, 5.877710200, 13.73895620], [0.3084141348, 7.257317852, -1.209020387],
    [-1.809889553, 8.618649988, 0.2188473592], [0.0995900601, 6.509292589, 1.283508793],
    [2.089915614, 11.56911477, 0.1184964367], [0.8449745483, 12.07596823, 1.928481881],
    [1.924449474, 9.767261218, 3.313822203], [1.115535361, 12.37751212, 4.624900086],
    [1.735533410, 9.813562300, 5.851983927], [1.261870594, 12.51975580, 7.034164230],
    [1.617366772, 9.940241204, 8.315446759], [1.446741913, 12.56813653, 9.676937945],
    [0.0737495757, 6.827748015, 3.627031442], [-2.195266306, 8.092906793, 4.868002105],
    [-0.3355011523, 6.072371746, 6.213204199], [-2.124746672, 8.204518244, 7.447415192],
    [-0.3340910379, 6.054028179, 8.574100536], [-1.943629043, 8.130871968, 9.953816923],
    [-0.296808812, 5.981909950, 11.25681744], [-1.528802059, 8.345310919, 12.50270207],
    [-2.040284411, 6.258066338, 13.71777691], [-0.7056327877, 8.612475075, -1.733896318],
    [-1.605044288, 6.262559556, 1.044806981], [2.476782049, 9.975630115, 0.895224856],
    [2.690061267, 11.54815863, 2.215844055], [0.2619956046, 10.62139395, 3.290966092],
    [2.724089758, 11.46146226, 4.703712583], [0.1898164316, 10.78053793, 5.845890233],
    [2.772406223, 11.44000257, 7.091331267], [0.2524506726, 11.24694808, 8.369225631],
    [2.867290699, 11.33185466, 9.573085881], [-0.3629820601, 8.245256906, 5.033742509],
    [-2.117412700, 6.074857552, 6.214952391], [-0.3541901388, 8.248896594, 7.422714560],
    [-2.143038081, 6.187341480, 8.677629124], [-1.810671942, 6.191608546, -2.859185492],
    [-1.835665910, 7.287338761, -3.719057341], [-0.8185162012, 5.026506900, -3.084587670],
    [-3.180147157, 5.464305366, -2.955043326], [-4.663115924, 4.735454219, -4.678974199],
    [-2.791255169, 3.261165347, -3.860928579], [-4.437339798, 2.337225014, -5.477960321],
    [-4.913549004, 3.745448709, -5.803482698], [-3.227930676, 4.691859470, -4.158234532],
    [-2.968276875, 2.332690619, -5.058332435], [-4.628793115, 1.518416345, -6.627509361],
    [-1.548763293, 0.6015650256, -7.006399779], [-5.566403185, 4.429971683, -3.615671070],
    [-2.552616657, 1.028328206, -4.655552993], [-6.323227052, 3.690661748, -6.058622247],
    [-7.104364962, 0.8842617018, -6.496158933], [-0.5069810681, -0.4533260526, -4.961833419],
    [-2.699780492, -1.331800505, -5.755939413], [-5.535063426, -0.500839331, -7.922721173],
    [-5.269071745, -0.5943989579, -5.397855034], [-1.405798584, 3.268941579, -3.498549521],
    [-2.328043288, 2.717201491, -5.885755751], [-3.353522788, 2.860639905, -2.985392459],
    [-4.409157965, 4.100231861, -6.734308458], [-4.936585152, 5.752882300, -5.039856011],
    [-6.393372683, -0.3871106764, -8.294114512], [-5.038120566, 1.962118419, -4.613361276],
    [-3.472119582, -1.158490708, -5.256121400], [-2.536292749, 5.107610204, -4.929030425],
    [-1.133042737, 2.373871539, -3.385935711], [-5.544584330, 5.155946872, -3.018697902],
    [-6.748566561, 4.068990704, -5.306789485], [-5.634928433, 0.2781497822, -6.538427512],
    [-1.856874128, 0.0164725601, -5.688867797]]
Warning, the assigned name GramSchmidt now has a global binding
```

[*Add*, *Adjoint*, *BackwardSubstitute*, *BandMatrix*, *Basis*, *BezoutMatrix*, *BidiagonalForm*, *BilinearForm*, *CharacteristicMatrix*, *CharacteristicPolynomial*, *Column*, *ColumnDimension*, *ColumnOperation*, *ColumnSpace*, *CompanionMatrix*, *ConditionNumber*, *ConstantMatrix*, *ConstantVector*, *CreatePermutation*, *CrossProduct*, *DeleteColumn*, *DeleteRow*, *Determinant*, *DiagonalMatrix*, *Dimension*, *Dimensions*, *DotProduct*, *Eigenvalues*, *Eigenvectors*, *Equal*, *ForwardSubstitute*, *FrobeniusForm*, *GaussianElimination*, *GenerateEquations*, *GenerateMatrix*, *GetResultDataType*, *GetResultShape*, *GivensRotationMatrix*, *GramSchmidt*, *HankelMatrix*, *HermiteForm*, *HermitianTranspose*, *HessenbergForm*, *HilbertMatrix*, *HouseholderMatrix*, *IdentityMatrix*, *IntersectionBasis*, *IsDefinite*, *IsOrthogonal*, *IsSimilar*, *IsUnitary*, *JordanBlockMatrix*, *JordanForm*, *LA_Main*, *LUDecomposition*, *LeastSquares*, *LinearSolve*, *Map*, *Map2*, *MatrixAdd*, *MatrixInverse*, *MatrixMatrixMultiply*, *MatrixNorm*, *MatrixScalarMultiply*, *MatrixVectorMultiply*, *MinimalPolynomial*, *Minor*, *Multiply*, *NoUserValue*, *Norm*, *Normalize*, *NullSpace*, *OuterProductMatrix*, *Permanent*, *Pivot*, *QRDecomposition*, *RandomMatrix*, *RandomVector*, *Rank*, *ReducedRowEchelonForm*, *Row*, *RowDimension*, *RowOperation*, *RowSpace*, *ScalarMatrix*, *ScalarMultiply*, *ScalarVector*, *SchurForm*, *SingularValues*, *SmithForm*, *SubMatrix*, *SubVector*, *SumBasis*, *SylvesterMatrix*, *ToeplitzMatrix*, *Trace*, *Transpose*, *TridiagonalForm*, *UnitVector*, *VandermondeMatrix*, *VectorAdd*, *VectorAngle*, *VectorMatrixMultiply*, *VectorNorm*, *VectorScalarMultiply*, *ZeroMatrix*, *ZeroVector*, *Zip*]

$$M_{10,\,10} := \begin{bmatrix} \text{98 x 3 Matrix} \\ \text{Data Type: anything} \\ \text{Storage: rectangular} \\ \text{Order: Fortran\_order} \end{bmatrix}$$

$$P_{10,\,10} := \begin{bmatrix} -1.810671942 \\ 6.191608546 \\ -2.859185492 \end{bmatrix}$$

$$O1_{10,\,10} := \begin{bmatrix} -3.180147157 \\ 5.464305366 \\ -2.955043326 \end{bmatrix}$$

$$O2_{10,\,10} := \begin{bmatrix} -1.768571321 \\ 6.755722582 \\ -1.470719832 \end{bmatrix}$$

$$O3_{10,\,10} := \begin{bmatrix} -1.835665910 \\ 7.287338761 \\ -3.719057341 \end{bmatrix}$$

$$O4_{10,\,10} := \begin{bmatrix} -0.8185162012 \\ 5.026506900 \\ -3.084587670 \end{bmatrix}$$

$$PO1_{10,\,10} := \begin{bmatrix} 0.881494563939921427 \\ 0.468145602405968920 \\ 0.0617011236541842730 \end{bmatrix}$$

$$PO2_{10,\,10} := \begin{bmatrix} -0.0280806000700062168 \\ -0.376257172994980572 \\ -0.926089639138513610 \end{bmatrix}$$

$$PO3_{10,\,10} := \begin{bmatrix} 0.0179417148882841000 \\ -0.786560945905357966 \\ 0.617251952759949596 \end{bmatrix}$$

$$PO4_{10,\,10} := \begin{bmatrix} -0.641417905662920340 \\ 0.753225554144514642 \\ 0.145720058856933814 \end{bmatrix}$$

$$zP_{10,\,10} := \begin{bmatrix} 0.675638098206670756 \\ 0.464608344018312192 \\ 0.572409160860990696 \end{bmatrix}$$

$$xP_{10,\,10} := \begin{bmatrix} -0.632405524504434324 \\ -0.0338128163080041386 \\ 0.773899183847402639 \end{bmatrix}$$

$$yP_{10,\,10} := \begin{bmatrix} 0.378914784000000004 \\ -0.884870488300000036 \\ 0.270975656600000003 \end{bmatrix}$$

$$mf2crys_{10,\,10} := \begin{bmatrix} -0.632405524504434324 & -0.0338128163080041386 & 0.773899183847402639 \\ 0.378914784000000004 & -0.884870488300000036 & 0.270975656600000003 \\ 0.675638098206670756 & 0.464608344018312192 & 0.572409160860990696 \end{bmatrix}$$

$$csad_{10,\,10} := -21.65026954$$

$$P_{10,\,10} := \begin{bmatrix} -5.634928433 \\ 0.2781497822 \\ -6.538427512 \end{bmatrix}$$

$$O1_{10,\,10} := \begin{bmatrix} -5.535063426 \\ -0.500839331 \\ -7.922721173 \end{bmatrix}$$

$$O2_{10,\,10} := \begin{bmatrix} -4.628793115 \\ 1.518416345 \\ -6.627509361 \end{bmatrix}$$

$$O3_{10,\,10} := \begin{bmatrix} -7.104364962 \\ 0.8842617018 \\ -6.496158933 \end{bmatrix}$$

$$O4_{10,\,10} := \begin{bmatrix} -5.269071745 \\ -0.5943989579 \\ -5.397855034 \end{bmatrix}$$

$$PO1_{10,\,10} := \begin{bmatrix} -0.0627465835660921124 \\ 0.489449777823374954 \\ 0.869771108912535172 \end{bmatrix}$$

$$PO2_{10,\,10} := \begin{bmatrix} -0.629018268704456760 \\ -0.775393043169649854 \\ 0.0556924197257649690 \end{bmatrix}$$

$$PO3_{10,\,10} := \begin{bmatrix} 0.924118722179542940 \\ -0.381179698193375827 \\ -0.0265824242442151658 \end{bmatrix}$$

$$PO4_{10,\,10} := \begin{bmatrix} -0.246879563301915822 \\ 0.588794626368904340 \\ -0.769656656605452016 \end{bmatrix}$$

$$zP_{10,\,10} := \begin{bmatrix} 0.629018268704456760 \\ 0.775393043169649854 \\ -0.0556924197257649690 \end{bmatrix}$$

$$xP_{10,\,10} := \begin{bmatrix} -0.0436809482885478496 \\ -0.0362738124115999442 \\ -0.998386791722942756 \end{bmatrix}$$

$$yP_{10,\,10} := \begin{bmatrix} -0.776162349100000038 \\ 0.630436228899999951 \\ 0.0110530127399999997 \end{bmatrix}$$

$$mf2crys_{10,\,10} := \begin{bmatrix} -0.0436809482885478496 & -0.0362738124115999442 & -0.998386791722942756 \\ -0.776162349100000038 & 0.630436228899999951 & 0.0110530127399999997 \\ 0.629018268704456760 & 0.775393043169649854 & -0.0556924197257649690 \end{bmatrix}$$

$$csam4_{10,\,10} := -2.347006141$$

$$P_{10,\,10} := \begin{bmatrix} -1.856874128 \\ 0.0164725601 \\ -5.688867797 \end{bmatrix}$$

$$O1_{10,\,10} := \begin{bmatrix} -2.699780492 \\ -1.331800505 \\ -5.755939413 \end{bmatrix}$$

$$O2_{10,\,10} := \begin{bmatrix} -2.552616657 \\ 1.028328206 \\ -4.655552993 \end{bmatrix}$$

$$O3_{10,\,10} := \begin{bmatrix} -0.5069810681 \\ -0.4533260526 \\ -4.961833419 \end{bmatrix}$$

$$O4_{10,\,10} := \begin{bmatrix} -1.548763293 \\ 0.6015650256 \\ -7.006399779 \end{bmatrix}$$

$$PO1_{10,\,10} := \begin{bmatrix} 0.529634555051815890 \\ 0.847178328959189764 \\ 0.0421439996350130089 \end{bmatrix}$$

$$PO2_{10,\,10} := \begin{bmatrix} 0.433516081400287690 \\ -0.630485670013317567 \\ -0.643856837854721031 \end{bmatrix}$$

$$PO3_{10,\,10} := \begin{bmatrix} -0.841794368444959362 \\ 0.292966782497134370 \\ -0.453379207025200681 \end{bmatrix}$$

$$PO4_{10,\,10} := \begin{bmatrix} -0.209007330869095618 \\ -0.396898130913745262 \\ 0.893749299314608892 \end{bmatrix}$$

$$zP_{10,\,10} := \begin{bmatrix} -0.433516081400287690 \\ 0.630485670013317567 \\ 0.643856837854721031 \end{bmatrix}$$

$$xP_{10,\,10} := \begin{bmatrix} -0.491067700495064652 \\ -0.764365096424232226 \\ 0.417849868083426724 \end{bmatrix}$$

$$yP_{10,\,10} := \begin{bmatrix} 0.755590047999999958 \\ -0.135032659400000004 \\ 0.640975709600000054 \end{bmatrix}$$

$$mf2crys_{10,\,10} := \begin{bmatrix} -0.491067700495064652 & -0.764365096424232226 & 0.417849868083426724 \\ 0.755590047999999958 & -0.135032659400000004 & 0.640975709600000054 \\ -0.433516081400287690 & 0.630485670013317567 & 0.643856837854721031 \end{bmatrix}$$

$$csam5_{10,\,10} := 0.5546925240$$

$$expm4 := 6.76$$

$$expdi := 28.94$$

$$expm5 := 5.25$$

$$jhp4_{10,\,10} := 3.137252290$$

$$jhper4_{10,\,10} := -3.622747710$$

$$jhper42_{10,\,10} := 13.12430097$$

$$jhp5_{10,\,10} := -0.7414596668$$

$$jhper5_{10,\,10} := -5.991459667$$

$$jhper52_{10,\,10} := 35.89758894$$

$$jhptoter_{10,\,10} := 4.950852953$$

```
>
> #fd:=fopen("nM4.txt",WRITE);
> #for i from 10 to 360 by 10 do for j from 10 to 360 by 10 do
  B:=fprintf(fd,"% 3d % 3d %+10.6f\n",i,j,csam4[i,j]): end do: end
  do:fclose(fd):
> #with(plots):B:=readdata("nM4.txt",float,3):
  pointplot3d(B,axes=BOXED,color=red,symbol=circle,symbolsize=14,lab
  els=[a1,a1p,diff]);

> #fd:=fopen("nM5.txt",WRITE);
> #for i from 10 to 360 by 10 do for j from 10 to 360 by 10 do
  B:=fprintf(fd,"% 3d % 3d %+10.6f\n",i,j,csam5[i,j]): end do: end
  do:fclose(fd):
> #with(plots):B:=readdata("nM5.txt",float,3):
  pointplot3d(B,axes=BOXED,color=red,symbol=circle,symbolsize=14,lab
  els=[a1,a1p,diff]);
> #fd:=fopen("p2m145diest.txt",WRITE);for i from 10 to 360 by 10 do
  for j from 10 to 360 by 10 do #B:=fprintf(fd,"% 3d % 3d
  %+10.6f\n",i,j,csad[i,j]): end do: end do:fclose(fd):
> #with(plots):B:=readdata("p2m145diest.txt",float,3):
> #pointplot3d(B,axes=BOXED,color=red,symbol=circle,symbolsize=14,la
  bels=[a1,a1p,csad]);


> #fd:=fopen("p2145g.txt",WRITE);for i from 10 to 360 by 10 do for j
  from 10 to 360 by 10 do #B:=fprintf(fd,"% 3d % 3d
  %+10.6f\n",i,j,jhper4[i,j]): end do: end do:fclose(fd):
> #with(plots):B:=readdata("p2145g.txt",float,3):
> #pointplot3d(B,axes=BOXED,color=red,symbol=circle,symbolsize=14,la
  bels=[a1,a1p,"diff(calc-exp)^2"]);
> #fd:=fopen("p2145h.txt",WRITE);for i from 10 to 360 by 10 do for j
  from 10 to 360 by 10 do #B:=fprintf(fd,"% 3d % 3d
  %+10.6f\n",i,j,jhper5[i,j]): end do: end do:fclose(fd):
> #with(plots):B:=readdata("p2145h.txt",float,3):
> #pointplot3d(B,axes=BOXED,color=red,symbol=circle,symbolsize=14,la
  bels=[a1,a1p,"diff(calc-exp)^2"]);
> #fd:=fopen("p2145k.txt",WRITE);for i from 10 to 360 by 10 do for j
  from 10 to 360 by 10 do #B:=fprintf(fd,"% 3d % 3d
  %+10.6f\n",i,j,jhper42[i,j]): end do: end do:fclose(fd):
> #with(plots):B:=readdata("p2145k.txt",float,3):
> #pointplot3d(B,axes=BOXED,color=red,symbol=circle,symbolsize=14,la
  bels=[a1,a1p,"diff(calc-exp)^2"]);
> #fd:=fopen("p2145l.txt",WRITE);for i from 10 to 360 by 10 do for j
```

```
  from 10 to 360 by 10 do #B:=fprintf(fd,"% 3d % 3d
  %+10.6f\n",i,j,jhper52[i,j]): end do: end do:fclose(fd):
> #with(plots):B:=readdata("p2145l.txt",float,3):
> #pointplot3d(B,axes=BOXED,color=red,symbol=circle,symbolsize=14,la
  bels=[a1,a1p,"diff(calc-exp)^2"]);
> #fd:=fopen("p2m145_0701.txt",WRITE);for i from 10 to 360 by 10 do
  for j from 10 to 360 by 10 do #B:=fprintf(fd,"% 3d % 3d
  %+10.6f\n",i,j,jhptoter[i,j]): end do: end do:fclose(fd):
> #with(plots):B:=readdata("p2m145_0701.txt",float,3):
> #pointplot3d(B,axes=BOXED,color=red,symbol=circle,symbolsize=14,la
  bels=[a1,a1p,"diff(calc-exp)^2"]);
> #fd:=fopen("p2145n.txt",WRITE);for i from 10 to 360 by 10 do for j
  from 10 to 360 by 10 do #B:=fprintf(fd,"% 3d % 3d
  %+10.6f\n",i,j,jhp4[i,j]): end do: end do:fclose(fd):
> #with(plots):B:=readdata("p2145n.txt",float,3):
> #pointplot3d(B,axes=BOXED,color=red,symbol=circle,symbolsize=14,la
  bels=[a1,a1p,"diff(calc-exp)^2"]);
> #fd:=fopen("p2145p.txt",WRITE);for i from 10 to 360 by 10 do for j
  from 10 to 360 by 10 do #B:=fprintf(fd,"% 3d % 3d
  %+10.6f\n",i,j,jhp5[i,j]): end do: end do:fclose(fd):
> #with(plots):B:=readdata("p2145p.txt",float,3):
> #pointplot3d(B,axes=BOXED,color=red,symbol=circle,symbolsize=14,la
  bels=[a1,a1p,"diff(calc-exp)^2"]);
>
>
>
>
>
>
>
>
>
>
>
```

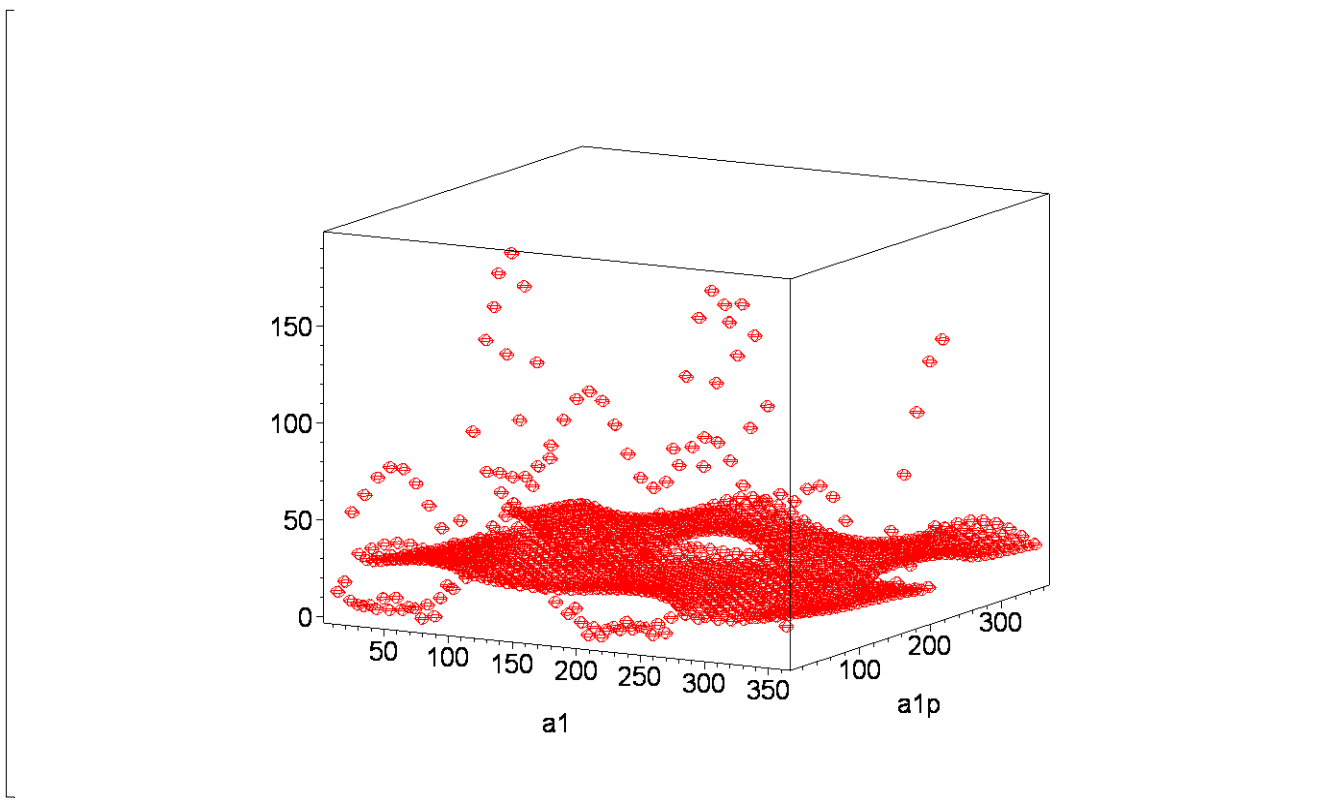
150
100
50
0
50
100
150
200
250
300
350
a1
100
200
300
a1p

# #13C CSA calculation of GDP in arbitrary frame.

#Defined rotation matrix that put molecule into PAF, then matrix multiplied that rotation matrix by chemical shielding tensor.

[ Anita I. Kishore, April 29, 2005, JHP Lab. akishore@chem.uga.edu. Time: 3.2 sec

## #Rotate pdb frame into C8-H8 frame, where C8H8 is y-axis.

### Read in molecular coordinates in pdb frame. pdb taken from 1hur.pdb (ARF1) and protonated using reduce.

```
> restart:
  with(linalg):
  M := readdata(gdp7,float,3): fclose(gdp7):
  with(LinearAlgebra):
  M := convert(M,Matrix);
```

```
Warning, the protected names norm and trace have been redefined and
unprotected

Warning, the assigned name GramSchmidt now has a global binding
```

$$M := \begin{bmatrix} 50 \text{ x } 3 \text{ Matrix} \\ \text{Data Type: anything} \\ \text{Storage: rectangular} \\ \text{Order: Fortran\_order} \end{bmatrix}$$

*#Define C8 vector of GDP (y) in pdb frame.*

```
> C8 := Transpose(Row(M,19)):
> H8 := Transpose(Row(M,47)):
> y := Normalize((C8-H8),Euclidean):
```

*#Define arbitrary vector of GDP (arb) in pdb frame.*

```
> N9 := Transpose(Row(M,18)):
> arb:=Normalize((C8-N9),Euclidean):
```

*#Define (x) vector of GDP in pdb frame.*

```
> z:=CrossProduct(y,arb): z=Normalize(z,Euclidean):
> x:=CrossProduct(y,z):
```

*#Define rotation matrix to rotate GDP into C8H8 frame.*

```
> new_axes:=<<x>|<y>|<z>>: R:=Transpose(new_axes):
```

*#Rotate coordinates M into C8H8 frame.*

```
> B:= R.Transpose(M): B_T:=Transpose(B):
```

*#Save coordinates in C8H8 frame as c8fr.*

```
> B1:=convert(B_T,matrix):
  writedata(c8fr,B1,float):fclose(c8fr):
```

# #Rotate c8fr into PAF.

## #Read in molecular coordinates in C8H8 frame.

```
> restart:
  with(linalg):
  M := readdata(c8fr,float,3): fclose(c8fr):
  with(LinearAlgebra):
  M := convert(M,Matrix); C8 := Transpose(Row(M,19));H8 :=
  Transpose(Row(M,47));y := Normalize((C8-H8),Euclidean);
```

```
Warning, the protected names norm and trace have been redefined and
unprotected

Warning, the assigned name GramSchmidt now has a global binding
```

$$M := \begin{bmatrix} 50 \text{ x } 3 \text{ Matrix} \\ \text{Data Type: anything} \\ \text{Storage: rectangular} \\ \text{Order: Fortran\_order} \end{bmatrix}$$

$$C8 := \begin{bmatrix} -41.83426498 \\ 19.62015851 \\ -27.40585932 \end{bmatrix}$$

$$H8 := \begin{bmatrix} -41.83426498 \\ 18.52087738 \\ -27.40585932 \end{bmatrix}$$

$$y := \begin{bmatrix} 0. \\ 0.99999999995290566 \\ 0. \end{bmatrix}$$

## #Define rotation matrices about z-axis for all angles.

```
> j := 21.6:
> Rz[j] := Matrix([[cos(j*(Pi/180)),sin(j*(Pi/180)),0],
  [-sin(j*(Pi/180)), cos(j*(Pi/180)), 0],[0,0,1]]);
```

$$Rz_{21.6} := \begin{bmatrix} \cos(0.1200000000\,\pi) & \sin(0.1200000000\,\pi) & 0 \\ -\sin(0.1200000000\,\pi) & \cos(0.1200000000\,\pi) & 0 \\ 0 & 0 & 1 \end{bmatrix}$$

## #Rotate C8H8 frame by j degrees into PAF.

```
> rotfr := (Rz[j].Transpose(M)):
  rotfr:=Transpose(rotfr):
  rotfra:= evalf(evalm(rotfr)):
```

## #Save coordinates in rotated frame as rofr.

```
> B1:=convert(rotfra,matrix):
  writedata(rofr,B1,float):
  fclose(rofr):
  B1:=convert(rotfra,Matrix):
```

# #Define direction cosines from PAF.

## #Define C8 vector of GDP (y) in PAF frame.

```
> C8 := Transpose(Row(B1,19)):H8 := Transpose(Row(B1,47)):y :=
  Normalize((C8-H8),Euclidean);
```

$$y := \begin{bmatrix} 0.368124559268497630 \\ 0.929776483811717512 \\ 0. \end{bmatrix}$$

## #Define (x) vector of GDP in PAF frame.

```
> N9 := Transpose(Row(B1,18)):
  C8N9:=Normalize((C8-N9),Euclidean):
  z := CrossProduct(y,C8N9); z := Normalize(z,Euclidean);
```

$$z := \begin{bmatrix} 0. \\ 0. \\ 0.780225032299999954 \end{bmatrix}$$

$$z := \begin{bmatrix} 0. \\ 0. \\ 0.99999999987873788 \end{bmatrix}$$

## #Define (z) vector of GDP in PAF frame.

```
> x := CrossProduct(y,z);
```

$$x := \begin{bmatrix} 0.929776483699999988 \\ -0.368124559299999986 \\ 0. \end{bmatrix}$$

## #Define direction cosines that relate orientation of frag frame to PAF frame.

```
> CS2MF := Transpose((<<x>|<y>|<z>>)):
> CS2MF2 := evalf(evalm(CS2MF));
```

$$CS2MF2 := \begin{bmatrix} 0.9297764837 & -0.3681245593 & 0. \\ 0.3681245593 & 0.9297764838 & 0. \\ 0. & 0. & 0.9999999999 \end{bmatrix}$$

# # Frame transformation: MF to PAF?

**Ref: Sitkoff & Case, Prog. Nucl. Magn. Res. Spec. 32:165-190 (1998). (another ref, not used, is: Fiala et al, JBNMR, 16:291-302 (2000)). Sigmapar is nearly along s11. H8/H1': s33 is nearly**

**along C-H bond vector. Subtract isotropic (trace) to look at chemical shift offset only.---NO! Finally used SHIFT TENSOR from Stueber and Grant, JACS 124:105339-10551(2002).**

**#Define 13C chemical shielding tensor of guanine C8.**

```
> with(LinearAlgebra):
  cstensor := <214|141|59>;
  dummy := Matrix(1..3,1..3,cstensor,shape=diagonal);
> #Note chemical shift tensor used so isotropic shift not
  subtracted.
```

$$cstensor := [214, 141, 59]$$

$$dummy := \begin{bmatrix} 214 & 0 & 0 \\ 0 & 141 & 0 \\ 0 & 0 & 59 \end{bmatrix}$$

```
> iso := (sum('cstensor[i]','i'=1..3))/3;
  for i to 3 do cstensor[i] := cstensor[i]-iso end do:
  cstens := Matrix(1..3,1..3,cstensor,shape=diagonal);
```

$$iso := 138$$

$$cstens := \begin{bmatrix} 76 & 0 & 0 \\ 0 & 3 & 0 \\ 0 & 0 & -79 \end{bmatrix}$$

**#Rotate into MF**

```
> csaC8 := (Transpose(CS2MF).dummy.CS2MF);
  csaC8a := evalf(evalm(csaC8));
```

$$csaC8 := \begin{bmatrix} 204.107354713552979 & -24.9859697549294780 & 0. \\ -24.9859697549294780 & 150.892645596949933 & 0. \\ 0. & 0. & 58.9999999856910762 \end{bmatrix}$$

$$csaC8a := \begin{bmatrix} 204.1073547 & -24.98596975 & 0. \\ -24.98596975 & 150.8926456 & 0. \\ 0. & 0. & 58.99999999 \end{bmatrix}$$

# #C8 Frame transformation. Rotate diagonalized chemical shielding tensor in principal axis frame to the alignment frame.

**#Define the alignment tensor. Alignment tensor determined by experimentally collected RDCs in 4.6% C12E5 + PIP2 from AIK, Sxx = 0.002276314, Syy = 0.0006593687 Szz = -0.002935683.**

```
> AT := <0.002276314|  0.0006593687 | -0.002935683>:
  AT := Matrix(1..3,1..3,AT,shape=diagonal);
```

$$AT := \begin{bmatrix} 0.002276314 & 0 & 0 \\ 0 & 0.0006593687 & 0 \\ 0 & 0 & -0.002935683 \end{bmatrix}$$

**#Calculate offset to chemical shift (daniso) using daniso = 2/3 (sum(AT*CSA2AF)), takes into account fully diagonalized alignment tensor b/c molecule not uniformly oriented along one axis, i.e. Sxx. Eqn comes from Judit's SVD-Order Matrix paper JMR 1999.**

```
> daniso := 2/3 * trace(AT.Transpose(csaC8));
  daniso2 := evalf(evalm(daniso));
  daniso3 := evalf(evalm(2/3 *
  (AT[1,1]*csaC8[1,1]+AT[1,1]*csaC8[1,2]+AT[1,1]*csaC8[1,3]+AT[
  2,2]*csaC8[2,1]+AT[2,2]*csaC8[2,2]+AT[2,2]*csaC8[2,3]+AT[3,3]
  *csaC8[3,1]+AT[3,3]*csaC8[3,2]+AT[3,3]*csaC8[3,3])));
```

$$daniso := 0.2606006797$$

$$daniso2 := 0.2606006797$$

$$daniso3 := 0.2117000936$$

**#Expected chemical shift offset (at 800MHz) for C8 in this weakly aligned system.**

```
> Hz2 := daniso2*201;Hz3 := daniso3*201;
```

$$Hz2 := 52.38073662$$

$$Hz3 := 42.55171881$$